Organometallic anticancer and antimicrobial complexes

A thesis submitted for the degree of

Doctor of Philosophy

by

Feng Chen

University of Warwick

Department of Chemistry

Contents

Acknowledgements

I would like to thank my Ph.D supervisor Professor Peter J. Sadler. Many thanks to him for giving me the opportunity to work with his eminent research group. I really appreciate all the instructions for the last three and half years. I am nothing if without his academic assistant. I will never forget the mysterious 'Christmas Secret Santa' and the happy times of the PJS group summer BBQ every year.

I am thankful to Professor Christopher Dowson, from School of Life Sciences, University of Warwick for allowing me to work with his research group.

I would also like to thank Dr.Abraha Habtemariam, a true friend of both my personal and academic life in UK. I really appreciate your time and will miss all the chat happened between us and will never forget the Birch reduction you guided me in my first year.

Especially, I would like to thank Dr. Guy Clarkson for his great assistance with the determination of x-ray crystal structures in each chapter, and Dr. Lijiang Song, Philip Aston and Dr. Ivan Prokes for their their excellent assistance with the NMR and MS measurements.

I also thank Professor Martin Wills very much, for his guidance on the synthesis of tethered complexes and opinions for Chapter 5.

I thank Dr. Joan Josep Soldevila Barreda for his excellent guidance in some my initial experiments during my first year of Ph.D.

A big thank you to Dr. Isolda Romero and Ji-Inn Song for their assistance in biological experiments.

I also thank Dr. James Coverdale for helping with the ICP-OES and ICP-MS samples. And many thanks to Dr. Samya Benerjee for his assistance in paper and thesis written up.

Especially, I am thankful to Daniel McFeely from Professor Christopher Dowson group, his great assistance and guidance on starting my project in School of Life Sciences is much appreciated.

Many thanks to my good friend Mr. John Moat, because of you, I have acquired the microbiological skills in antibacterial study. Without you, all the contents and data cannot be achieved in Chapter 6. Thanks so much for all the assistance and academic guidance.

I would also like to thank Professor Viktor Brabec and Dr. Jana Kasparkova, for their great assistance in DNA related study, and thank Dr. Juliuzs Wolny and Professor Volker Schünemann for their great help in DFT calculations.

I am very grateful to 'The Community for Antimicrobial Drug Discovery' (CO-ADD, funded by the Wellcome Trust (UK) and The University of Queensland (Australia)) for their excellent assistance in the broad antimicrobial screening in Chapter 6.

I want to take this opportunity to thank all of my Chinese friends like Hongke Liu, Yanqing Wang, Huayun Shi, Xin (Star) Zhang, Yaqiong Kong, Hualong Song, Huayun Shi, Wenying (Wendy) Zhang, Pingyu Zhang and Huaiyi Huang, *etc*; and India friends Samya Benerjee and Venkate Venkatesh. Without their help in my daily life, I cannot live a life like now. I will never forget the scene that we have meal together, especially in COSMO's restaurant.

I am thankful to my parents, living an overseas life is never as easy as it looks, thanks for being with me and supporting me all the time from my birth.

Declaration

I hereby declare that except where specific reference is made to other sources, the work contained in this thesis is the original work of the author. It has been composed by myself and has not been submitted, in the whole or in part, for any other degree, diploma or other qualification.

Some of the work presented in this thesis has been published:

1. Effect of Sulfonamidoethylenediamine Substituents on Ru^{II} Arene Anticancer Catalysts on Transfer Hydrogenation of Coenzyme NAD^+ by Formate. Chen, F.; Soldevila-Barreda, J. J.; Romero-Canelón, I.; Coverdale, J. P. C.; Song, J. I.; Clarkson, G. J.; Kasparkova, J.; Habtemariam, A.; Brabec, V.; Wolny, J. A.; Schünemann, V.; Sadler, P. J. *Dalton Trans.* **2018**, *47*, 7178–7189.

2. Transfer Hydrogenation and Antiproliferative Activity of Tethered Half-Sandwich Organoruthenium Catalysts. Chen, F.; Romero-Canelón, I.; Soldevila-Barreda, J. J.; Song, J.-I.; Coverdale, J. P. C.; Clarkson, G. J.; Kasparkova, J.; Habtemariam, A.; Wills, M.; Brabec, V.; Sadler, P. J. *Organometallics* **2018**, *37*, 1555−1566.

Abstract

Platinum complexes, *e.g.* cisplatin, oxaliplatin, carboplatin, have been used for near 40 years in clinic as potent anticancer drugs. However, these drugs can cause severe side effects, and hence there is an urgent need to develop other metal based antiproliferative agents. For example, organometallic $Ru^{II/III}$complexes possess potent anticancer activity but low cytotoxicity towards normal cells, which makes them promising alternatives to currently used anticancer drugs.

In this thesis, a series of neutral *pseudo*-octahedral Ru^{II}-sulfonamidoethylenediamine complexes [(η^6-arene)Ru(*N*,*N'*)X] where η^6-arene is *p*-cym, biph and benzene, *N*,*N'* is ethylenediamine chelating ligands with sulfonyl substituents (*e.g.* Ts or Nb) on one terminal N and various functional groups (*e.g.* Me, Me_2, Et, benzyl, 4-fluorobenzyl or naphthalen-2-ylmethyl) on the other terminal N were synthesized and fully characterized, including X-ray crystal structures. These complexes catalyse the reduction of NAD^+ regioselectively to 1, 4-NADH using sodium formate as hydride source under biologically relevant conditions. The catalytic efficiency depends markedly on the steric and electronic effects of the N-substituent, with turnover frequencies (TOFs) increasing with the enhancement of bulkiness and electron withdrawing of the substituents, achieving a highest TOF of 12.9 h^{-1} for complex **10** [(η^6-biph)Os(TsEnBz)Cl]. These complexes exhibited antiproliferative activity against A2780 human ovarian cancer cells. Co-administration with sodium formate (2 mM) increased their potency significantly towards A2780 cells. Substituted Ru^{II} sulfonylethylenediamine complexes can also interact rapidly with glutathione (GSH) and N-acetyl-L-cysteine (NAC) to form S-bridged $[(\eta^6\text{-arene})_2Ru_2(GS)_3]^{2+}$ or $[(\eta^6\text{-arene})_2Ru_2(NAC)_3]^+$ dimers, and the presence of GSH can effectively hamper the catalytic reduction of NAD^+ to NADH.

Next, a series of neutral organometallic tethered [Ru(η^6-benzene-N-R-ethylenediamine)Cl] complexes was synthesized and characterized, where R = methylsulfonyl (Ms), toluenesulfonyl (Ts), trifluorobenzenesulfonyl (Tf) and 4-nitrobenzenesulfonyl (Nb), including their X-ray crystal structures. In general, these complexes also exhibited potent catalytic activity in the transfer hydrogenation of NAD^+ to NADH with formate as hydride donor (310 K, pH 7), but with moderate antiproliferative activity towards human ovarian, lung, liver and breast cancer cell lines. Tethered Ru^{II} complexes showed preferential binding to 9-ethylguanine (9-EG) over adenosine 5'-monophosphate (5'-AMP). However, DNA appears not to be the target, as little binding of complex **17** [Ru(η^6-benzene-N-Ts-ethylenediamine)Cl] to ct-DNA or bacterial plasmid DNA was observed. Also, the tethered complexes bind rapidly to GSH, which might again hamper the transfer hydrogenation reactions in cells. Interestingly, these tethered Ru^{II} complexes can induce a dose-dependent G1 cell cycle arrest and high level of reactive oxygen species (ROS) generation, which is likely to contribute to their antiproliferative activity.

Diseases caused by bacterial infections, especially by multidrug-resistance bacteria, are the major cause of deaths worldwide. Traditional clinical drugs cannot cope with the rapid rise of drug resistance.

In this thesis, a new class of organometallic antimicrobial complexes of the type [(arene/Cp^x)Ir(Big)Z]Z (where arene is *para*-cymene or biphenyl, Cp^x = Cp* (tetramethylcyclopentadienyl), Cp^{*ph} or Cp^{*biph}, Big = biguanide ligands and functional sulfonyl substituted biguanide ligands, Z = Cl, Br and I) were synthesized and characterized by NMR, ESI-MS, elemental analysis and X-ray crystallography. These complexes not only have promising antibacterial activity against Gram-negative bacteria and excellent potency against Gram-positive bacteria, but also exhibit high antifungal potency towards *C. albicans* and *C. neoformans*. Most of the complexes have low cytotoxicity towards mammalian cells (*HEK-293* human red blood cells and *HaCaT* keratinocyte cells), indicating a high selectivity.

These Ir^{III} complexes have a high stability in both medium even at high temperature (315 K). A mutant generation study suggests that *S. aureus* exhibits a low tendency to generate mutants in response to these complexes. Ir biguanide complexes **27** [(η^5-Cp^{Xbiph})Ir(PhBig)]Cl, **30** [(η^5-Cp^{Xbiph})Ir(TolBig)Cl]Cl and **33** [(η^5-Cp^{Xbiph})Ir(TsTolBig)Cl] exhibited synergy with clinical drug vancomycin when co-administered in vancomycin-resistant Enterococci (VRE), with the MIC 256× lower at sub-MIC complex concentration. These complexes also exhibited potent anti-biofilm activity against biofilms generated by *S. aureus*. Potent antimicrobial activity against various microbes might provide an alternative pathway to treat drug resistant nosocomial pathogens.

Abbreviations

9-EtG	9-Ethylguanine
9-EtA	9-Ethyladenine
A. baumannii	*Acinetobacter baumannii*
bip	Biphenyl
B. subtilis	*Bacillus subtilis*
Cp*	Pentamethylcyclopentadienyl
Cp^{xph}	3-Phenyl-1,2,4,5-tetramethyl-1,3-cyclopentandienyl
Cp^{xbiph}	3-Biphenyl-1,2,4,5-tetramethyl-1,3-cyclopentandienyl
C. albicans	*Candida albicans*
C. neoformans	*Cryptococcus neoformans*
CD	Circular dichroism
ct	Calf Thymus
ddw	doubly distilled water
DFT	Density functional theory
DMSO	Dimethyl sulfoxide
EDTA	Ethylenediamine tetraacetate
en	Ethylenediamine
E. coli	*Escherichia coli*

E. faecalis	*Enterococcus faecalis*
ESI-MS	Electrospray ionisation mass spectrometry
GSH	Glutathione
GSSG	Glutathione disulphide
HPLC	High performance liquid chromatography
HR-MS	High resolution mass spectrometry
IC_{50}	50% inhibitory concentration
ICP-OES	Inductively coupled plasma optical emission spectroscopy
ICP-MS	Inductively coupled plasma mass spectrometry
J	Coupling constant
K. pneumoniae	*Klebsiella pneumoniae*
K_M	Michaelis-Menten constant
L-BSO	L-Buthionine sulfoximine
LC-MS	Liquid chromatography-mass spectrometry
MBC	Minimum bactericidal concentration
MIC	Minimum inhibitory concentration
MRSA	Methicillin resistant *Staphylococcus aureus*
NAD^+	Nicotinamide adenine dinucleotide
NADH	Nicotinamide adenine dinucleotide reduced

NAC	N-acetyl-L-cysteine
Nb	4-nitrobenzenesulfonyl
p-cym	*para*-cymene
P. aeruginosa	*Pseudomonas aeruginosa*
PBS	Phosphate buffered saline
ROS	Reactive oxygen species
RBC	Red blood cells
SRB	Sulforhodamine B
S. aureus	*Staphylococcus aureus*
S. pyogenes	*Streptococcus pyogenes*
S. epidermidis	*Staphylococcus epidermidis*
TsEn	Toluenesulfonyl ethylenediamine
TFA	Trifluoroacetic acid
Tf	Trifluorobenzenesulfonyl
TON	Turnover number
TOF	Turnover frequency
VRE	Vancomycin resistant *Enterococci*

Chapter 1

Introduction

1.1 Cancer Chemotherapy

What is cancer? Cancer is a collection of diseases with common features of uncontrolled cell proliferation.[1] Cancer now has been one of the worldwide leading fatal diseases and estimated to cause approximately 13.1 million deaths in 2030.[2] Until now, over 100 types of cancers in the human body have been diagnosed. Treatment of cancers is generally divided into three ways: initially, the benign tumours can be removed by physical surgery; however, when tumours are becoming malignant and metastasised, radio-therapy or chemotherapy must be introduced.[1] Undoubtedly, treatment of cancer with chemotherapy (chemodrugs are taken orally or intravenously) is one of the biggest challenges for biochemical science.

Over the last few decades, metallodrugs are routinely used in chemotherapy for the treatment of cancers. The frontline anticancer drug, cisplatin (CDDP) was synthesized over a century ago, however, its potent antiproliferative activity was not observed until the 1960s by Rosenberg and co-workers in their course of investigation of the effect of electric current on *Escherichia coli* (**Figure 1.1**).[3] CDDP was approved soon by FDA (Food and Drug Administration of U.S.A) as anticancer drug in 1978. Since then, a series of platinum based anticancer drugs were developed and approved by FDA, *e.g.* Carboplatin (1986), Oxaliplatin (1996) and Nedaplatin (1994), *etc* (**Figure 1.1**). Encouragingly, over 95% cure rate for the treatment of testicular cancers has made CDDP the most prevailing chemodrug.[4] The mechanism of cancer killing for CDDP is complex, numerous related reports have been revealed over the last few decades, briefly, the most widely accepted routes are the following. CDDP enters cancer cells by passive diffusion,[5] and undergoes one chloride hydrolysis prior to DNA nucleobase binding, then the aqua CDDP species enter the nucleus and bind to N7 of DNA nucleobase guanine,[6] until then after a second Cl hydrolysis, to guanine or adenine nucleobase, to form an intrastrand DNA cross-linked adduct, which subsequently induces cancer cell apoptosis.[7] However, the severe side effects of CDDP, *e.g.* nephrotoxicity,

neurotoxicity and vomiting, and have limited its use. Also, with the emergence of cisplatin resistant cancers, for instance cisplatin resistant A2780 human ovarian cancer, which now has made platinum based anticancer drugs much less effective.

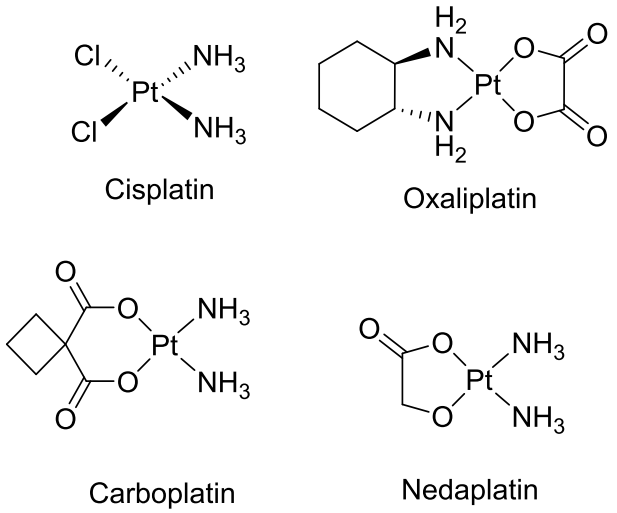

Figure 1.1 Examples of current clinical platinum anticancer drugs.

The success of platinum based antiproliferative agents has greatly stimulated the development of new generations of anticancer drugs. Metallocene compounds being considered as promising CDDP alternatives. The study of metallocenes began with the discovery of ferrocene in 1952, and the ferrocene structure was identified as having *C5*-symmetrical sandwich geometry with iron covered with two π–bonded Cp rings.[8] The Nobel Prize in chemistry was awarded to Wilkinson, Woodward and Fisher for their contribution to the elucidation of the sandwich complex of ferrocene in 1973. Ferrocene itself is relatively non toxic to human beings; but by modification of the ferrocene structure, Jaouen *et al.* have developed a series of ferrocifens based on the anticancer drug tamoxifen (**Figure 1.2**).[9,10] Tamoxifen is one of the frontline chemotherapy agents for treating hormone-dependent breast cancer (breast cancers are mainly divided into two types: estrogen receptor presence (ER+) or absence (ER-), tamoxifen acts as a (ER+) modulator which is an active drug for (ER+) patients).[11] Ferrocifen was believed to show similar antiproliferative behaviour to tamoxifen. Unexpectedly, ferrocifen when n = 4

(**Figure 1.2**) was found to be active against (ER-) type tumour cells (MDA-MB231) and hormone-dependent MRC-7 breast cancer cell lines, probably indicating a different mode of action. Another ferrocene-related complex, ferroquine exhibits strong antimalarial activity (**Figure 1.2**), and now has entered phase III clinical trials and may become a next generation antimalarial drug in the near future.[12]

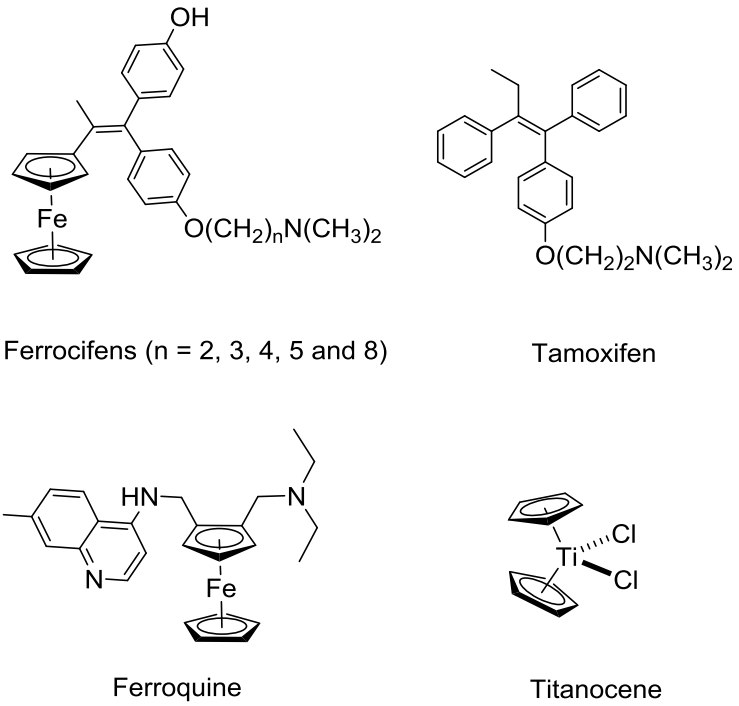

Figure 1.2 Examples of anticancer and antimalarial metallocene agents.

Titanocene is, structurally similar to ferrocene, but a 'non-classical' metallocene complex with two 'bent' Cp rings (**Figure 1.2**). As a representative 'bent' metallocene, titanocene dichloride has poor *in vitro* but good *in vivo* anticancer activity.[13,14] However, the poor physiochemical behaviour of titanocene dichloride prevented it from proceeding further than phase II clinical trials. It has very poor aqueous solubility but can hydrolyse readily. This hydrolysis leads to deprotonation of bound water to form hydroxido-oligomers, which generate the biologically nontoxic and insoluble TiO_2.[15-17]

In recent years, organometallic half-sandwich complexes have become of particular interest as next generation anticancer agents.[18,19] η^5-Cyclopentadienyls and η^6-arenes can stabilize the

metal centre occupying three binding sites, with three unoccupied coordination sites. The biological activity of organometallic complexes can be tuned by subtle chemical modification.[20] The azopyrididine Os^{II} complexes of the type $[(\eta^6\text{-}p\text{-cym})Os(Impy\text{-}NMe_2)X]$ where Impy is *p*-dimethyl aminophenylazopyridine and X is halide (Cl or I), were synthesized by Fu and coworkers.[20, 21] Complexes **FY25** (X = Cl) and **FY26** (X = I) are water soluble (**Figure 1.3**), and have shown high antiproliferative potency towards A2780 human ovarian cancer cells (IC_{50} as low as 140 nM), but low cytotoxicity against normal MRC 5 human fibroblasts. Active azopyridine complex **FY26** can induce a dramatic increase in the levels of reactive oxygen species (ROS) in A549 lung cancer cells. Liu *et al.* have reported a series of Ir complexes of the type $[(Cp^{*X})Ir(phpy)(py)]PF_6$, X = phenyl or biphenyl (**Figure 1.3**).[22, 23] These novel complexes showed potent antiproliferative activity towards A2780 human ovarian cancer cells (IC_{50} = 120 nm), about 10 times more effective than CDDP. Furthermore, this complex exhibited relatively low cytotoxicity against MRC 5 normal cell lines, with a similar selectivity to that of CDDP (approximately 13 times less toxic). $[(Cp^{Xbiph})Ir(phpy)(py)]PF_6$ can oxidise cellular coenzyme NADH (reduced form of nicotinamide adenine dinucleotide (NAD^+); discussed in following section) to generate hydrogen peroxide (H_2O_2), and induce high levels of reactive oxidative species (ROS) in A2780 cancer cells (92.5%) but low ROS and superoxide levels in the MRC 5 normal cell (only 3.6%), such complexes can also change the cell mitochondrial membrane potential, which leads to apoptosis.[23]

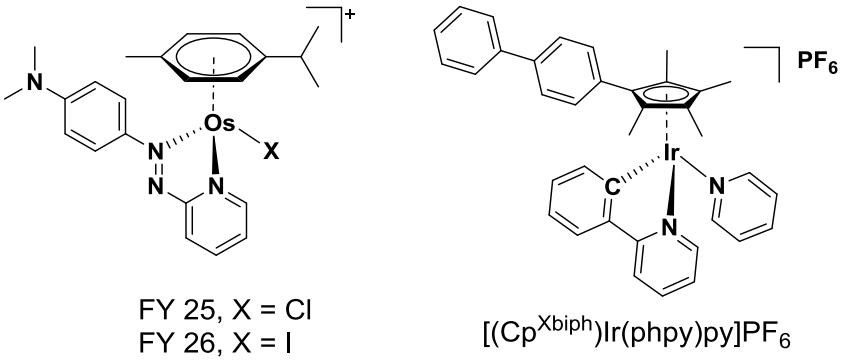

FY 25, X = Cl
FY 26, X = I

$[(Cp^{Xbiph})Ir(phpy)py]PF_6$

Figure 1.3 Azopyridine Os^{II} complexes and phenyl-pyridine Ir^{III} anticancer complexes.

1.2 Organo-Ruthenium Anticancer Agents

Two sets of ruthenium^{III} complexes have exhibited significant antitumor activity and have attracted wide attention since the 1990s.[24] Two of these have reached phase II clinical trials: **NAMI-A** ((imidazoleH)[trans-$RuCl_4$-(imidazole)(DMSO)], **Figure 1.4**),[25] the first ruthenium^{III} anticancer agent developed by Alessio *et al.*; and **KP1019** ((indazoleH)[trans-$RuCl_4$-(indazole)$_2$], **Figure 1.4**), studied by Keppler and co-workers from the end of 1980s. The latter is effective against resistant CDDP resistant tumours, especially active against autochthonous colorectal tumors.[26] **NAMI-A** and **KP-1019** exhibit structural resemblance. Unlike CDDP, **NAMI-A** has very low cytotoxicity against the NCI 60 panel of cell lines *in vitro* (on average over 1000 times less cytotoxic than CDDP).[27] However, **NAMI-A** manifested excellent *in vivo* activity and selectivity against lung metastases of a variety of solid metastasizing tumours in nude mice.[28] To date, the mechanism of action of **NAMI-A** and **KP-1019** is not yet very clear, with activation of reduction of Ru^{III} to Ru^{II} as a plausible pathway which is responsible for the *in vivo* potency.[26a]

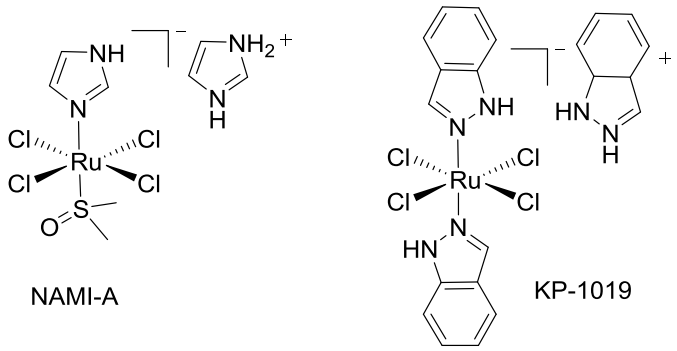

Figure 1.4 Ru^{III} anticancer agents, **NAMI-A** and **KP-1019**.

The success of **NAMI-A** and **KP-1019** has inspired intensive antiproliferative studies on various organo-ruthenium complexes. **RAPTA** ([Ru^{II}-(η^6-*p*-cym)(PTA)Cl_2], PTA is 1,3,5-triaza-7-phosphatricyclo [3.3.1.1]-decane) and its derivatives, developed by Dyson *et al.* (**Figure 1.5**),[29] have also added extra value in the family of Ru based anticancer agents.

Structurally, RAPTA-Ru^{II} complexes have a 'piano-stool' geometry, with aromatic arene on the top and three monodentate ligands (two chlorides and one PTA) on the bottom. Similarly to **NAMI-A** and **KP-1019**, RAPTA series complexes also show good aqueous solubility. *In vitro* anticancer studies with these complexes revealed that such complexes are much less toxic than the clinical drug cisplatin towards various cancer cell lines (IC_{50} > 200 μM),[29] however, **RAPTA-C** Ru^{II} complexes can effectively reduce the mice lung cancer cells metastasis without affecting the primary tumour size,[30,31] and have shown promising antiangiogenic activity against chicken chorioallantoic membrane.[32] According to a molecular docking experiment, the Ru-PTA complex is initially hydrolysed with one Cl^- replaced by a H_2O molecule; next, other than binding to DNA, aqueous species coordinate to the important cell enzymes, *e.g.* cathepsin B. Cathepsin B is a lysosomal cysteine protease important for cellular metabolism processes, tumour progression and metastasis, is a prognostic marker for several types of cancer.[33] Thioredoxin reductase (TrXR, a selenoenzyme that can regulate intracellular oxidative stress and is overexpressed in many human cancer cells) is also a potential target that can induce cell apoptosis.[34]

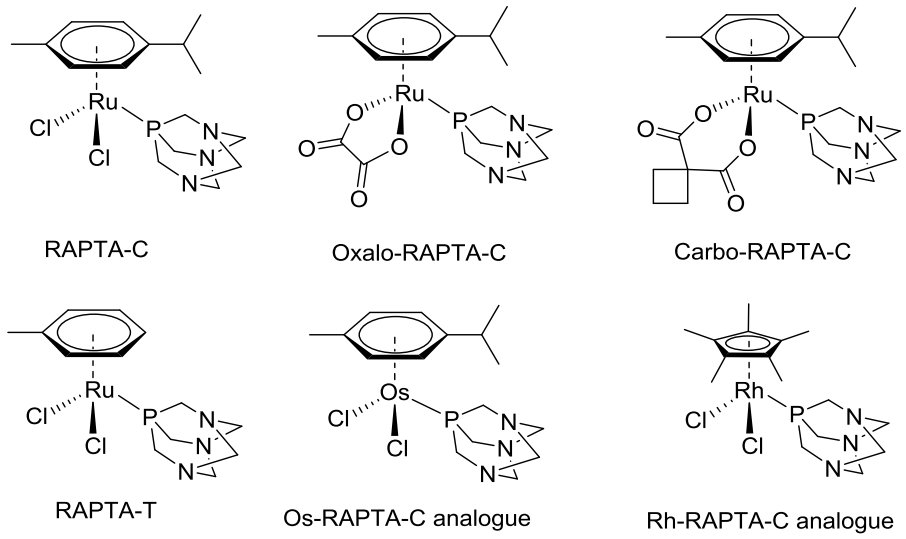

Figure 1.5 RAPTA-C and its derivatives and Os^{II} and Rh^{III} analogues.

Combinations of biologically active organic molecules with organometallic complexes may have synergistic effects to improve the cytotoxicity against cancer cells *via* different mechanism of actions.[35] Inspired by Jaouen's work, Dyson *et al.* decorated the RAPTA complex by introducing naphthalimide (a strong DNA intercalator, **Figure 1.6**) to the aromatic arene. The new complex is known to show moderate anticancer activity towards A2780 human ovarian cancer cells, with IC_{50} value as low as 6.1 μM when compared to RAPTA Ru^{II} complexes (IC_{50} over 100 μM). Interestingly, the new napthalimide-tagged Ru^{II} complex prefers to bind to proteins rather than targeting DNA.[36]

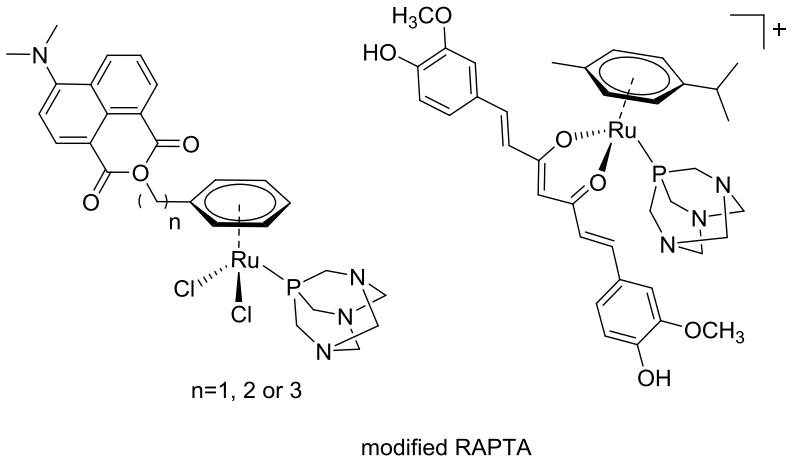

Figure 1.6 Modified RAPTA with functional groups: naphthalimide and curcumin.

Curcumin is a low molecular weight polyphenol with multiple biological activity, *e.g.* anti-inflammatory and anti-tumor activity.[37] The curcumin based RAPTA Ru^{II} complex, RAPTA-curc (**Figure 1.16**) exhibited potent antiproliferative activity against A2780 human ovarian cancer cells (IC_{50} values as low as 0.14 μM) and cisplatin-resistant A2780 cells (A2780 cisR IC_{50} as low as 0.27 μM), but low cytotoxicity towards human embryonic kidney cells (*HEK-293*, IC_{50}, 30 μM).[38]

Ang and Gaiddon *et al.* have reported a library of water-soluble Ru^{II}-arene Schiff-base (RAS) complexes synthesized *via* a water-stimulated multicomponent reaction (**RAS-1H** and **RAS-1T** in **Figure 1.7**).[39] RAS complexes are stable in aqueous medium and unlikely to target

DNA, some of these complexes exhibit potent cell killing efficacy towards A2780 human ovarian cancer cells, making them comparable to cisplatin; and importantly the complexes did not show any cross-resistance against A2780cisR (Resistant Factors (RFs) *ca.* 1, approximately 10 times lower than that of cisplatin) and colorectal cancer cell lines (RFs are 4.5 and 2.8, respectively).[39,40] A suitable modification may cause a drastic change in the mode of action. The subsequent mechanism of actions study revealed that Ru^{II} complexes **RAS-1H** and **RAS-1T** did not change the p53 level in cancer cells, but could induce endoplasmic reticulum (ER) stress through ROS-independent and ROS-mediated pathways, to induce a non-apoptotic programmed cell death. p53 is an important tumour suppressor gene, mutations of p53 in cancer cells are associated with DNA repair, and cell apoptosis.[41]

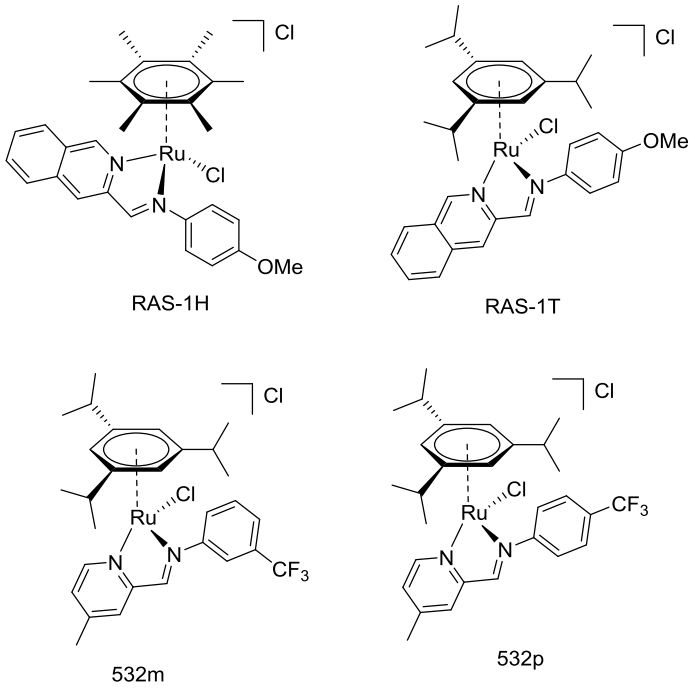

Figure 1.7 Ruthenium−arene Schiff-base complexes.

Very recently, Ang and Gaiddon *et al.* developed a phenotypic screening protocol against colorectal cancer cell lines to identify the apoptosis-independent RAS Ru^{II} complexes. By screening anticancer activity of over 100 RAS Ru^{II} complexes, two RAS complexes **532m** and **532p** with RFs of 0.9 and 0.8, respectively, were selected (**Figure 1.7**).[42] Anticancer activity

for both the RAS Ru^{II} complexes is through a non-apoptotic pathway without activating p53 tumour suppressor genes.

Sadler and co-workers have reported a series of Ru^{II} complexes of the type [(η^6-arene)Ru(en)X]PF_6 where arene is benzene, η^6-*p*-cymene, η^6-biphenyl, dihydroanthracene or tetrahydroanthracene, en is ethylenediamine and X is halide (Cl, Br and I), pyridine ligands and thiol-containing molecules,[43] and have also built up the relationship between hydrolysis and functional substitutions, which are associated with the antiproliferative activity against various cancer cells (**Figure 1.8**).[43] Ru^{II}-en complexes exhibited antiproliferative activity in the range of 0.5-100 μM, such potency has made some complexes comparable to clinical drug cisplatin (0.6 μM) against A2780 human ovarian cancer cells without any cross resistance against cisplatin resistant ovarian cancer cells A2780 cisR.[44] The complexes, **RM-175** and **HC27** of this series have been studied intensively (**Figure 1.8**).[45] Ru^{II}-arene(en) complexes are believed to target DNA in cancer cells to induce apoptosis, *e.g.* Ru^{II}-en complex **RM-175**, proved to be highly selective in binding to the N7 of DNA nucleobase guanine to form the [Ru(en)-(9EtG-N7)]PF_6 adduct.[45, 46, 47]

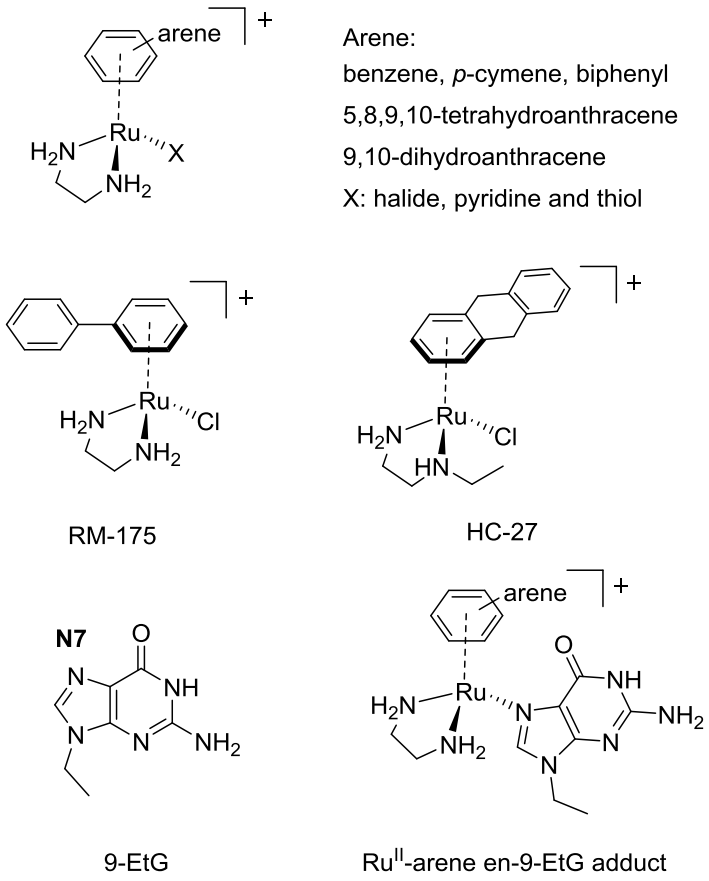

Figure 1.8 Structures of Ru^{II}-arene ethylenediamine complexes, guanine and Ru-9-EtG adduct.

1.3 Reactive Oxygen Species (ROS)

Reactive oxygen species describe a series of oxygen-contained molecules and free radicals, including peroxide (O_2^{2-}), superoxide ($O_2^{\bullet-}$), hydroxyl radical ($OH^{\bullet-}$) and singlet oxygen ($^1O_2$).[48] The process of conversion of O_2 to water and carbon dioxide during aerobic respiration starts from the reduction of oxygen; by accepting one electron, O_2 can be reduced to generate superoxide anions ($O_2^{\bullet-}$), followed by the dismutation of superoxide by superoxide dismutase (SOD) produces hydrogen peroxide (H_2O_2), and further reduction of H_2O_2 generates H_2O (fully reduced) and hydroxyl radicals (partially reduced through Fenton Reaction, $OH^{\bullet}$ is one of the highly reactive oxygen species, can directly react with DNA, *e.g.* guanine can react with hydroxyl to form 8-oxoguanine to induce the degradation or mutation,[49] **Figure 1.9**).[48]

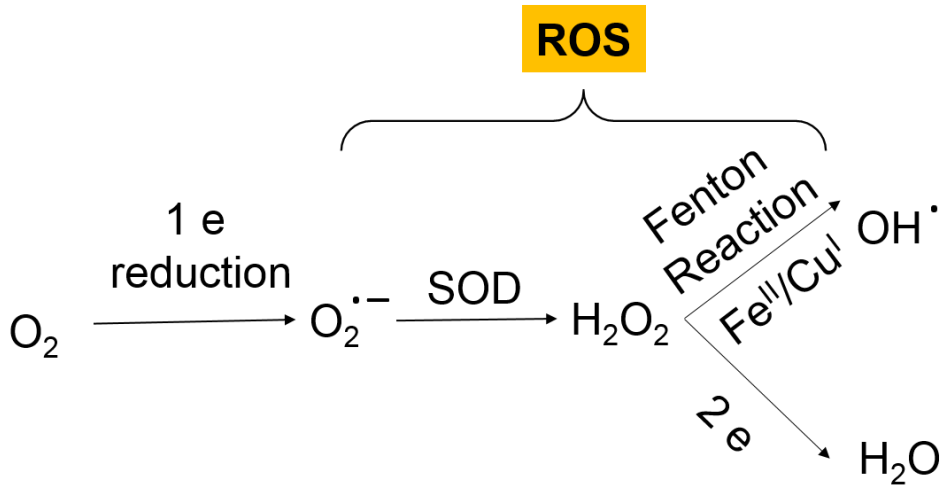

Figure 1.9 ROS generation and damaging level of ROS in mammalian cells and bacteria.

ROS can be produced enzymatically and non-enzymatically, mitochondria are the main organelle of ROS generation,[50] basal levels of ROS are important for cell progression and signaling.[51] However, excessive ROS can damage cell membrane lipid, nucleic acid and proteins.[52] Most importantly, enhanced ROS levels can potentially induce tumor progression and cancer cells metastasis.[53] Cancer cells and microorganisms are exposed to high oxidative stress due to the continuous cell proliferation and metabolism. To cope with such severe situation, cancer cells are normally equipped with over-expressed thiol-containing tripeptide, glutathione or amino acid cysteine, to attenuate ROS levels and maintain the cellular redox homeostasis;[54] while bacteria such as *Bacillus subtilis* (*B. subtilis*, Gram-positive bacteria) and *Staphylococcus aureus* (*S. aureus*, Gram-positive bacteria) contain unique small thiol-containing molecules, *e.g.* Mycothiol and Bacillithiol (**Figure 1.10**), to deal with the metabolized byproduct.[55]

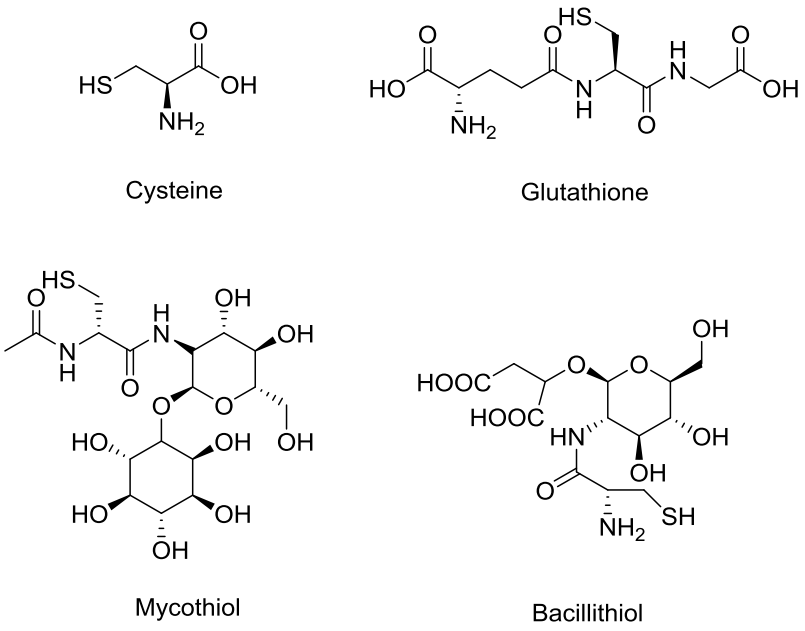

Figure 1.10 Thiol-containing peptides of mammalian cells and bacteria.

Taking the advantage of the upregulated ROS levels in cancer cells, development of ROS induced antiproliferative or antibacterial agents may provide an effective and alternative chemotherapy for treating malignant cancers and severe antibiotic resistance.[56]

1.4 Transfer Hydrogenation

Transfer hydrogenation (TH) of unsaturated substrates catalysed by organometallic complexes has been studied for decades. In the 1950s, the first TH reduction report of hydrogen transferred from cyclohexene to organic acceptors catalysed by palladium black was revealed.[57]

As one of the most powerful catalytic tools for the asymmetric synthesis of amines and alcohols, with an aim of constructing important natural product scaffolds and satisfying the higher demand of industry, chemists have been in pursuit of developing novel and effective catalysts.[58] A variety of half-sandwich transition-metal complexes have been developed and studied as transfer hydrogenation catalysts towards the asymmetric transfer hydrogenation of ketones and amines.[59]

Noyori and co-workers have reported the chiral half-sandwich ruthenium complexes of the type [(η^6-arene)Ru(TsDPEN)Cl] (arene: η^6-*p*-cym or biph; TsDPEN: N-((1S,2S)-2-amino-1,2-diphenylethyl)-4-methylbenzenesulfon amide, **Figure 1.11**).[60] Up to 97% ee and 95% yield was achieved when the Noyori-type Ru^{II} complexes were used in asymmetric transfer hydrogenation of aromatic ketones.

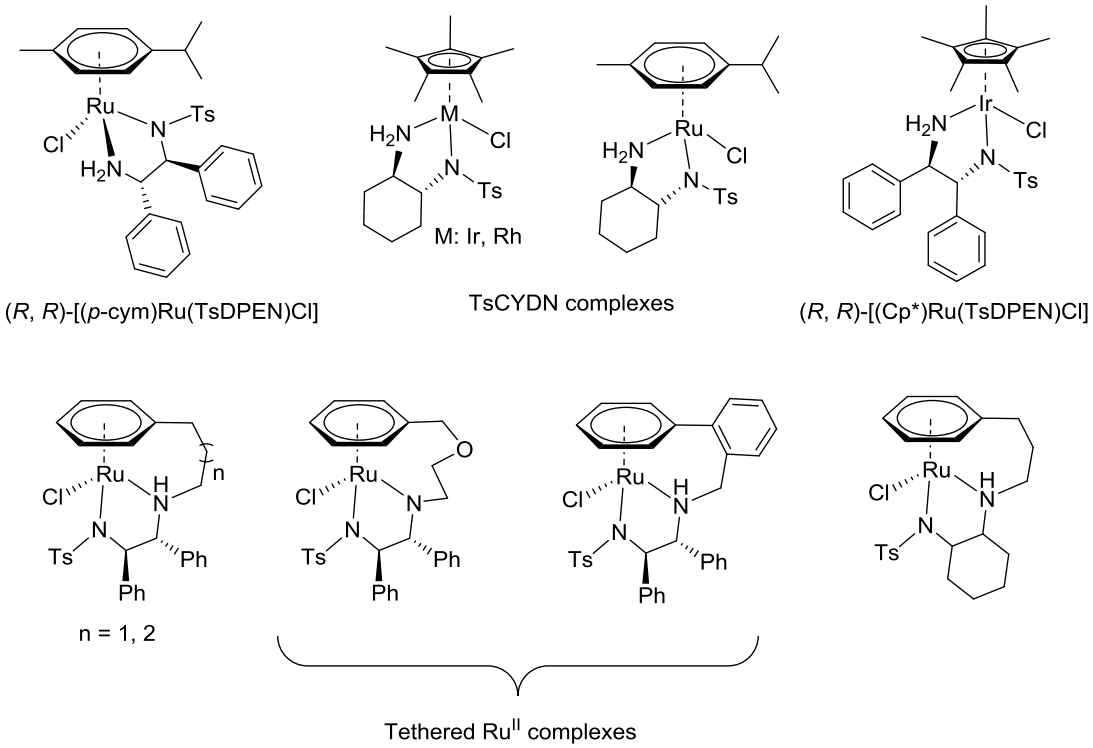

Figure 1.11 Noyori-type organometallic transition metal complexes for asymmetric transfer hydrogenation (ATH) reactions.

A wider series of Noyori-type complexes have now been reported for the same application. Xiao and co-workers have utilized a series of Noyori-type organometallic transition metal (*i.e.* Rh^{III}, Ir^{III} and Ru^{II}, TSCYDN complexes in **Figure 1.11**) complexes in the asymmetric transfer hydrogenation of aromatic ketones, *e.g.* acetophenone and methyl beta-naphthyl ketone and imines in aqueous solution with good yield and excellent ee values (up to 99%, **Figure 1.11**).[61] To further improve the stability and catalytic activity of Noyori-type complexes, Wills *et al.* have reported a series of Ru η^6-arene tethered Ru^{II} complexes by introducing a "tethering"

chain between the η^6-arene and the diamine.[62] Such modification allowed lower catalysts loading, and up to 99% yield and ee values were obtained for the asymmetric transfer hydrogenation of acetophenone, and some other reduction challenging ketones, such as α-chloroketones and alkynyl ketones (**Figure 1.11**).[63]

1.5 Important Roles of NAD^+ and NADH

Nicotinamide adenine dinucleotide (NAD^+) and its reduced form (NADH) play an essential role in biological metabolic systems. As an important coenzyme, NAD^+ exists ubiquitously in both prokaryotic and eukaryotic cells.[64] NAD^+ can bind to approximately 500 human cell proteins,[65] for example, nucleophilic amino acid residues (*e.g.* Arg, Asn, Glu, Asp and Cys) can react with NAD^+ to yield ADP-ribosylated proteins,[66] poly(ADP-ribose) polymerases (PARPs) and Sirtuins (SIRTs) require NAD^+ for covalent modifications during group transfer reactions.[67] In cell metabolism, over 400 enzymatic redox reactions rely on the action of nicotinamide enzymes, in which transformation of $NAD(P)^+$ to NAD(P)H is involved.[68]

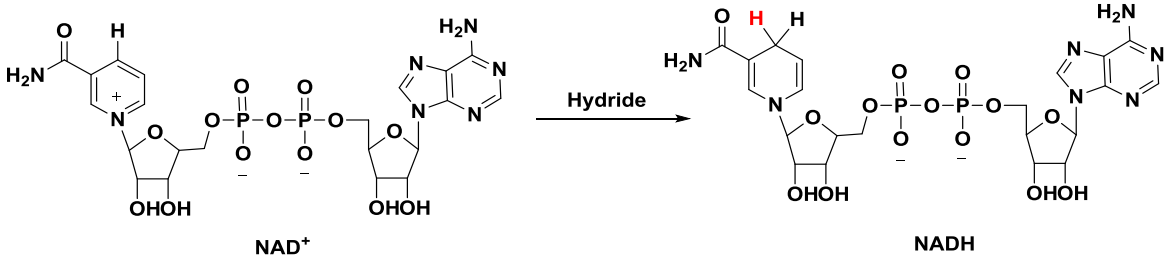

Figure 1.12 Transformation between coenzyme pair NAD^+ and NADH.

Originally, according a popular synthesis route: the Preiss-Handler pathway,[69] NAD^+ was synthesized by consecutive addition of ribose-P (ribosephosphate), AMP (from ATP) and an amino group (from ammonium or glutamine) to nicotinic acid.[70] NAD^+ and NADH are structurally similar to each other, NAD^+ is the oxidized form of the NAD^+/NADH pair.[71] By accepting hydride on the C18 active site, NAD^+ is reduced to NADH (**Figure 1.12**).

Cancer cells rely more on lactate than normal tissues to survive; this feature has led cancer cells toward more glucose uptake. Lactate is generated through an aerobic glycolysis catalysed by lactate dehydrogenase A (LDH-A), an important NADH dependent enzyme, which can regenerate and build-up large amount of NAD^+ in cancer cells.[72] Nicotinamide phosphoribosyl transferase mediated biosynthesis of NAD^+ in cancer cells can play a significant role, as it is involved in many physiological processes, *e.g.* cell metabolism, survival, apoptosis, DNA repair and inflammation, *etc*.[73] Cancer cells are constantly exposed to high levels of oxidative stress, partially due to the built-up of NAD^+; a suitable ratio change to the NAD^+/NADH can modify the oxidative homeostasis and potentially cause apoptosis of cancer cells.[74] Research on the interconversion between NAD^+ and NADH is likely to have great significance in terms of strategy for the next generation anticancer therapy.

1.6 Transformation between NAD^+ and NADH

The catalytic transformation between NAD^+ and NADH usually involves two pathways: enzymatic and non-enzymatic. The non-enzymatic catalytic pathway often possesses significant advantages: cheaper, reaction conditions are less complicated and the catalysts used are more stable than enzymes.[75] The first TH reduction of NAD^+ model compounds was introduced by Steckhan *et al.* by utilizing Rh^{III} complex $[(Cp^*)Rh(bpy)Cl]PF_6$ as catalyst either using formate as hydride donor, or electrochemically, to achieve a regioselective product 1, 4-NADH (**Figure 1.13**).[76,77] In 1999, Fish and co-workers used Rh^{III} complex $[(Cp^*)Rh(bpy)Cl]PF_6$ as catalyst in the TH reaction of NAD^+ type substrate $BNAD^+$ to its reduced form with sodium formate as hydride source.[78] Later, Fish *et al.* used horse liver alcohol dehydrogenase (HLADH) to fulfil the catalytic reduction cycle of ketones enantioselectively (**Figure 1.13**), giving asymmetric alcohols with ee values up to 99%.[79]

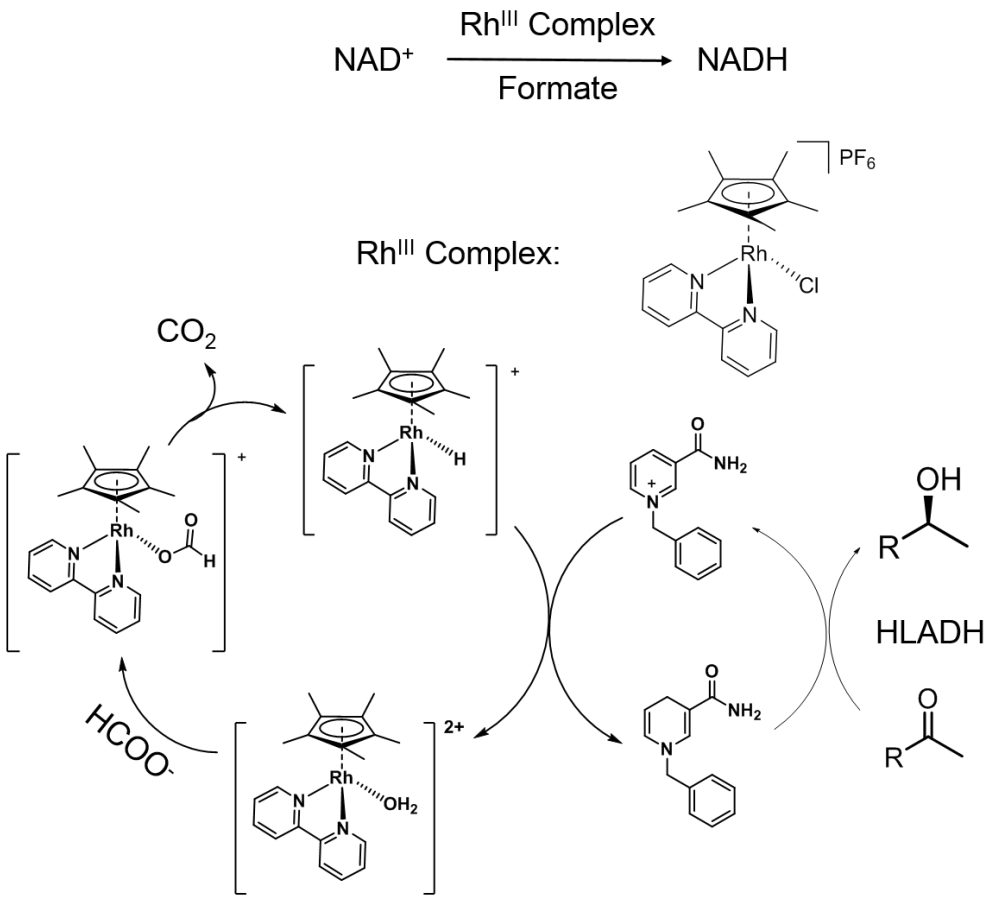

Figure 1.13 Organometallic Rh^{III} catalysts for transfer hydrogenation of NAD^+ to NADH. HLADH is horse liver alcohol dehydrogenase.

Betanzos-Lara *et al.* have demonstrated the conversion of NADH to NAD^+ using organo-ruthenium and organoiridium as double action catalysts (**Figure 1.14**).[80] Interestingly, these complexes can reduce NAD^+ to NADH using formate as hydride source, once the hydride is fully transferred to NADH, a reverse hydride transfer between NADH and organo-ruthenium or iridium catalysts is reported to occur, with a sharp ^1H NMR singlet for Ru-H observed at -7.44 ppm. They also utilized the reversible reaction to reduce pyruvate to lactate to mimic the action of enzyme lactate dehydrogenase *in vitro* (**Figure 1.1**). Liu *et al.* in the Sadler group suggested a straightforward catalytic reduction of quinones using organoiridium complex $[(Cp^*)Ir(phen)Cl]PF_6$ (Ir complex in **Figure 1.14**) as catalyst and NADH as hydride source.[81]

however such reductions can provide only semiquinones rather than dihydroquinones, which may involve a novel mechanism of action.

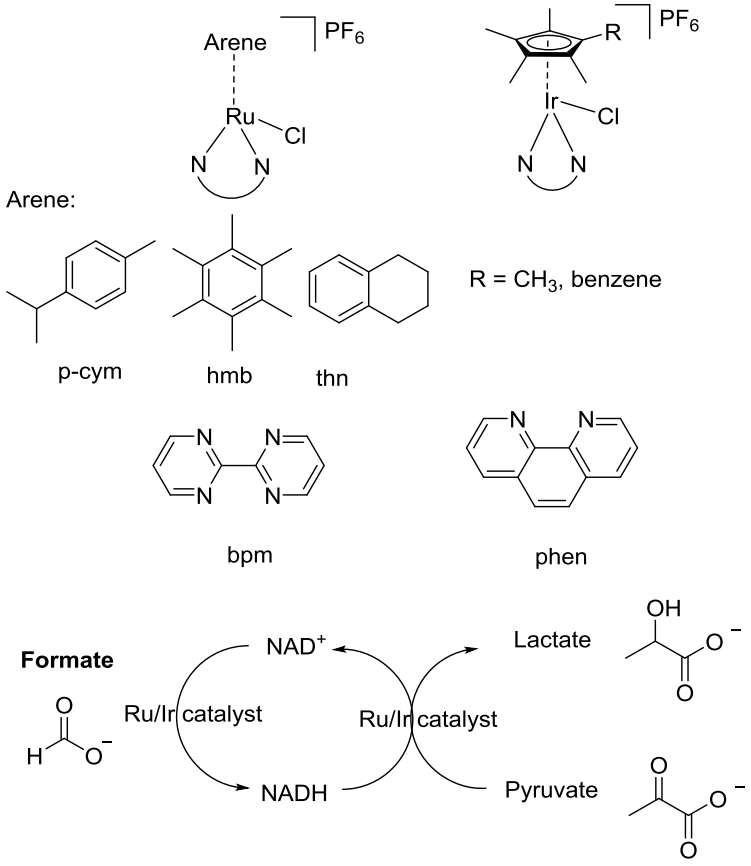

Figure 1.14 Reversible hydride transfer between NAD^+ and NADH catalysed by organoruthenium and iridium complexes.

1.7 Mechanistic Study

In recent years, much effort has been devoted to the development of transition metal complexes capable of reducing unsaturated compounds *via* transfer hydrogenation.[82]

In 2000, Noyori *et al.* reported the reversible hydrogen transfer between alcohols and carbonyl compounds by using $[(benzene)RuCl_2]_2$, N-tosylethylenediamine or ethanolamine (Noyori-type) as catalysts and KOH as base.[83] The results from his work reveal that the carbonyl oxygen atom interacts with the terminal N-H on the Ru^{II} complexes and the hydroxyl moiety with the amido nitrogen via hydrogen bonding; the protons of NH or NH_2 in the ethylenediamine are

crucial for TH reaction between alcohols and ketones. A simple and different mechanism in which a 16-e intermediate is involved was proposed by Noyori (**Figure 1.15**).

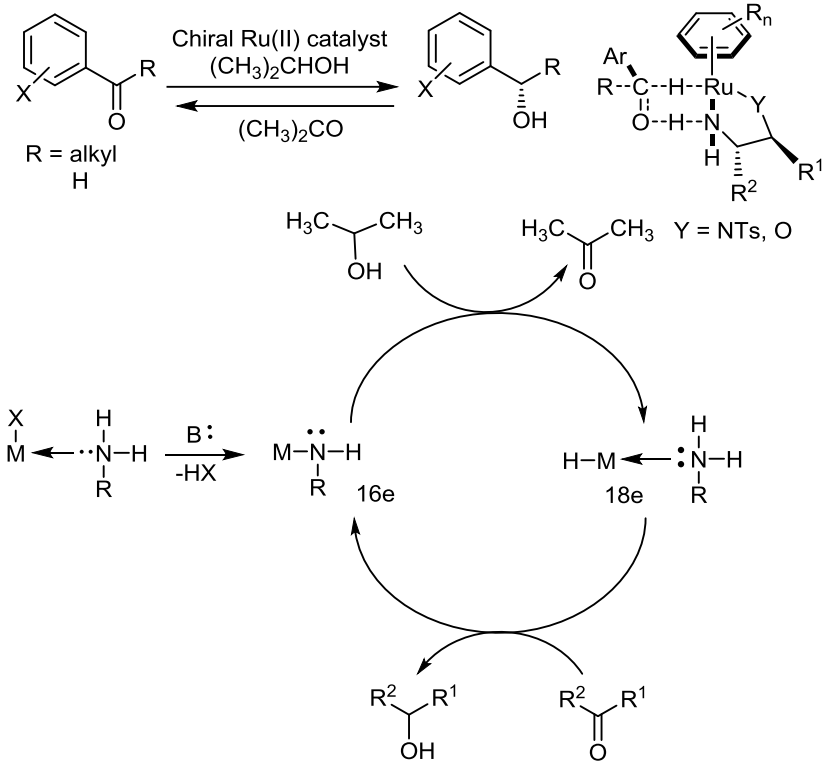

Figure 1.15 A mechanism for asymmetric transfer hydrogenation of aromatic ketones to alcohol involving the 16-e intermediate proposed by Noyori *et al.*[83]

In 2011, Wills *et al.* demonstrated the important role of the N-H proton in the asymmetric reduction of ketones and amines through hydrogen transfer reactions by using Noyori type Ru^{II} TsDPEN complexes as catalysts.[84] In Wills' work, it was observed that Ru^{II} complexes with two alkyl groups on the terminal nitrogen atom are poor catalysts for transfer hydrogenation of ketones and imines. The TH reaction of ketones and amines probably underwent a six-membered ring transition state, and involvement of N-H indicates that proton on terminal nitrogen atom of the TsDPEN ligand is a necessity for the TH reaction of ketones and imines to occur (**Figure 1.16**).

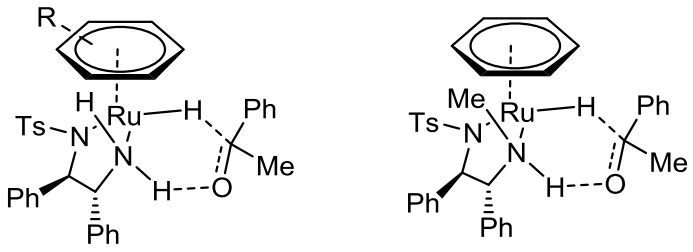

Figure 1.16 Involvement of N–H in the transition state for reduction.

The proton of the terminal N-H on the chelating ligand appears to play an essential role in the transfer hydrogenation of ketones and amines. The modified Noyori type complexes such as [(η^6-*p*-cym)Ru(TsEn)Cl] have also been shown to perform the TH reaction of NAD^+ in cells successfully.[74] The mechanism of action of such compounds have been proposed recently by Sadler *el al.* (**Figure 1.17**). In this proposal, the aqua Ru^{II} species can bind to formate ions to form arene-Ru formate transition states, then the formate twists to form the Ru-H species, followed by the terminal N H-interaction with NAD^+ to effect hydride transfer.

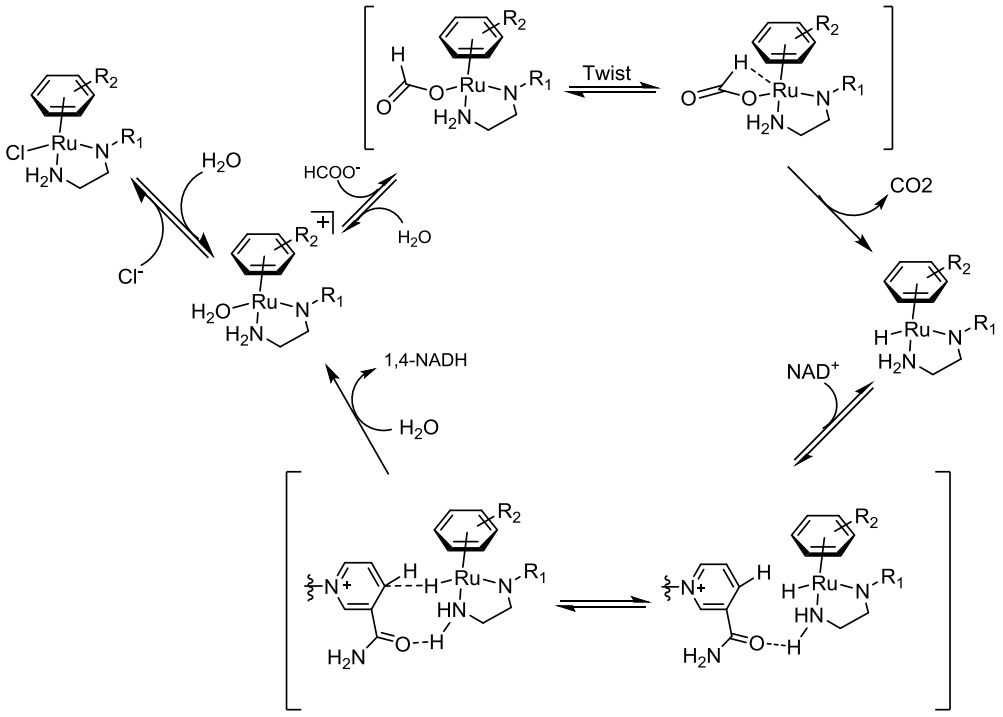

Figure 1.17 Proposed mechanism of TH reduction from NAD^+ to NADH.

In 1999, Fish *et al.* reported a mechanistic study of transfer hydrogenation of BNA^+ (NAD^+ type compound **a** in **Figure 1.18**) to BNAH using $[(Cp^*)Rh(bpy)H]^+$ as catalyst and sodium formate as hydride source,[78] in which a Cp* ring slipped intermediate containing Rh coordinated to the amide of the pyridine ring is involved. Fish and coworkers used different substituents to the C3 position of pyridine ring as substrates to assess the electronic and steric effects of the TH reaction as well, in which a Cp* ring-slipped intermediate with Rh coordinated to the amide of the pyridine ring was proposed (**Figure 1.18**).

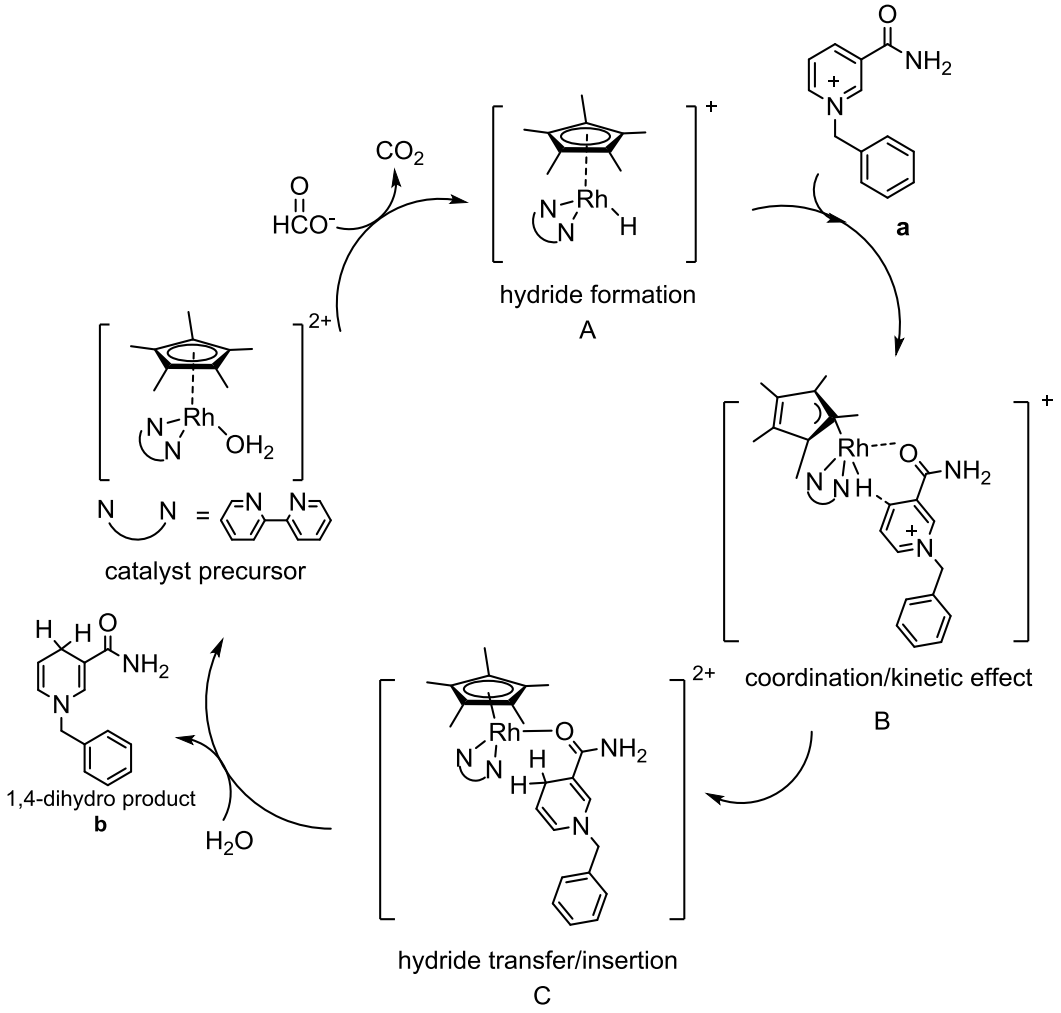

Figure 1.18 Proposed mechanism for catalytic reduction of NAD^+ type substrate.

In 2000, Ishitani *et al.* reported a mechanistic study of the regio-specific transfer hydrogenation of a NAD^+ model to its reduced form using *cis*-$[Ru(bpy)_2(CO)(CHO)]^+$ as catalyst and hydride

source.[85] To mimic the enzymatic reactions catalysed by aldehyde dehydrogenases in cells, Ishitani and coworkers applied the ruthenium formyl complex to transfer hydrogenation of NAD^+ model compounds without using any auxiliary hydride source. It is worth mentioning that among all the substrates, the strong electron-withdrawing group CF_3 at 3-position of the pyridine which is totally different from the amide group of the NAD^+ was used, and exceptional conversion was obtained in TH reactions (**Figure 1.19**).

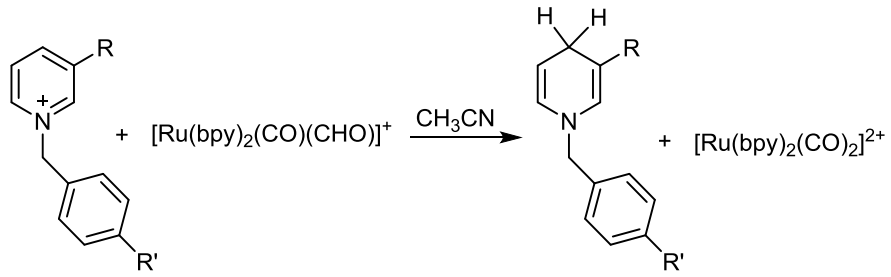

R:	$CONH_2$	CF_3	$COCH_3$	$CONH_2$	$COEt_2$
R':	H	H	H	CH_3	H
conversion:	100%	100%	100%	100%	100% longer time

Figure 1.19 Reduction of NAD^+ models catalysed by Ru^{II} formyl complexes.

1.8 Current Antibacterial Study

Infectious diseases are currently the second main cause of death worldwide and the third leading cause of death in developed countries.[86] According to the latest survey, over 20000 deaths were caused by bacterial and bacterial resistant infections per year in America alone.[87] And 1.4 million people are affected in other developed countries, this number is increased by 200-2000% in developing countries.[88]

Bacteria normally have a rigid cell wall as outer cell membrane, to guard the cell from changes in osmotic pressure, chemical or enzymatic lysis and mechanical damage. Bacteria are mainly classified into two groups: Gram-positive and Gram-negative.[89] The cell wall of Gram-positive

bacteria (which stains with purple Crystal Violet) is composed of a thick layer of peptidoglycan with a group of inlaid molecules called teichoic acids. While the Gram-negative cell wall consists of a thin layer of peptidoglycan but it is covered by an outer membrane. Compared to eukaryotic cells (without cell wall), bacteria usually can survive in very extreme conditions (**Scheme 1.1**).[89]

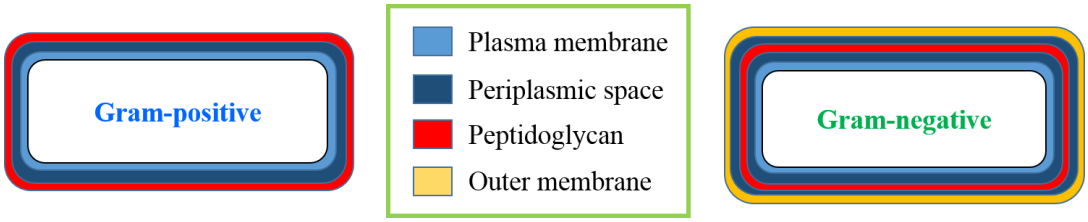

Scheme 1.1 The biological composition of Gram-positive and Gram-negative bacteria.

Multidrug resistant bacteria, including the notorious *Enterococcus faecium*, *Staphylococcus* aureus, *Klebsiella pneumoniae*, *Acetinobacter baumanii*, *Pseudomonas aeruginosa*, and *Enterobacteriaceae* species, abbreviated as 'ESKAPE' (underlined letters of each bacteria name), are now a huge threat to human health and a major cause of bacterial infectious diseases.[90]

The antibacterial chemotherapy was developed in late 19th century, when microbiologists observed the antagonistic activity between microbial populations.[91] In the mid-20th century, the sulfonamides were introduced as therapies and β-lactams was used as natural product therapies, and antibiotics have been used widely since then.[91,92] Currently, the approved antimicrobial drugs are mainly organic molecules. However, only 1% of these are natural products and over 95% are artificially synthesized.[93]

The abuse of clinically approved drugs make the growth of pathogens resistant to the existing agents surprisingly fast, and in many cases, the current antibiotics are not effective enough to kill them. For example, methicillin-resistant *Staphylococcus aureus* (*MRSA*) is resistant to β-lactam antibiotics,[90b] and about 59.5% of hospital-acquired infections caused by *S. aureus* have

shown resistance to methicillin. Options for chemotherapic drugs for certain microorganisms have become increasingly scarce. Thus, novel, effective, and safe antibiotics are urgently needed.[92]

Over the last few decades, the antibacterial activity of organo-transition-metals have attracted particular attention. Noble metals like gold and silver as potent antibacterial agents have been well studied.[94] The application of silver by mankind dates back about 7000 years, and people used silver as containers to conserve food and water in ancient times thereby preventing bacterial infections.[95]

Some other transition metal complexes have also been reported to exhibit antibacterial properties.[96] Among those, the platinum group metals have aroused significant interest, as the intensive studies based on these metals are related to their anticancer activities.[97] Reports of antimicrobial activity of the platinum group complexes has been relatively rare in the literature.

1.9 Antibacterial Study with Organometallic Complexes

A series of inert polypyridyl ruthenium^{II} [98] and iridium^{III} [99] complexes with bridging alkene chain has been synthesized by Collins and Keene and coworkers (**Figure 1.20**), the MICs of these complexes against both Gram positive (MRSA and *S. aureus*) and negative (*E. coli* and *P. aeruginosa*) bacteria were determined. The dinuclear Ru^{II} complexes of the type $[(Ru(phen)_2)_2(m\text{-}bb_n)]^{4+}$ (where phen = 1,10-phenanthroline; bb = bis[4(4'-methyl-2, 2'-bipyridyl)]$^{-1}$) showed very potent activity towards both *S. aureus* and MRSA with MICs value of 1 µg/mL.[98] The HC_{50} (obtained by incubation of dinuclear Ru^{II} complexes with red blood cells) and IC_{50} (dinuclear Ru^{II} drugs against THP-1 cells lines) values were over 100-fold higher than the MIC values from antibacterial activity. The high selectivity between mammalian cells and bacteria make Ru^{II} complexes potential antibiotics for clinical trial.

The inert Ir^{III} complexes of the type $[(Ir(phen)_2)_2(\mu\text{-}bb_{12})]^{6+}$ also showed significant activity against bacteria with MIC value as low as 2 μg/mL. The MBC/MIC ratios of dinuclear Ir^{III} complexes are over 2, which indicate that the inhibition of bacteria is bacteriostatic rather than bactericidal. Interestingly, the determination of pK_a values of the Ir^{III} complexes suggested that the dinuclear complexes deprotonate rapidly and enter bacteria as 4^+ charged species.

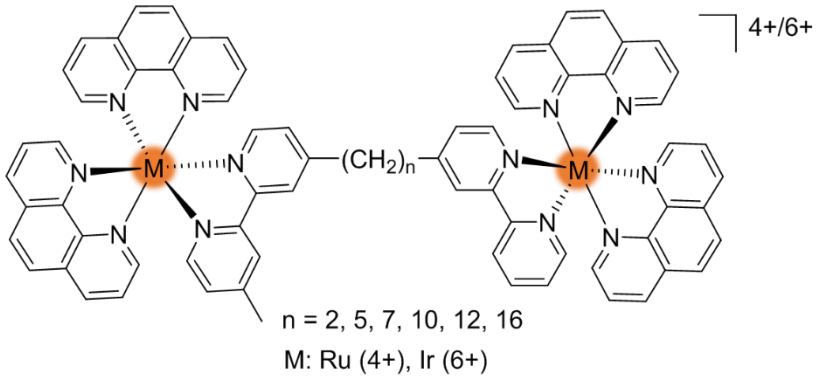

Figure 1.20 Structures of Ru^{II} and Ir^{III} antibiotic agents.

Aggregation-induced phosphorescence (AIP) of active Ir^{III} complexes attracts significant research interest.[100] Panwar *et al.* reported a series of phosphorescent Ir^{III} complexes (**Figure 1.21a**), and the antibacterial activity of these complexes was determined.[101] These complexes can penetrate the bacteria cell wall, and a DNA cleavage study suggested that DNA was the direct target of Ir^{III} complexes for their bactericidal activity (MBC as low as 4 μg/mL).

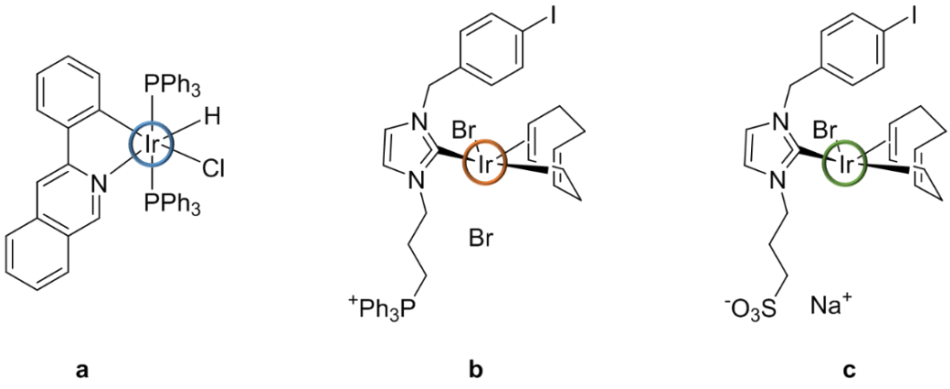

Figure 1.21 Structures of Ir^{III} complexes as antibiotics.

Another series of iridium–NHC complexes bearing anionic and cationic substituents were synthesised and the antibacterial, antiparasitic and anticancer activities were evaluated by Schatzschneider and coworkers.[102] Ir^{III} complexes bearing a NHC-phosphonium ligand (**Figure 1.21b**) showed better antibacterial activity (both Gram positive and negative) than Ir^{III} complexes bearing NHC-sulfonate ligand (**Figure 1.21c**) in terms of MIC and MBC; Also, Ir^{III}-NHC-phosphonium complexes exhibited a better activity against Gram positive bacteria (2.5-20 µg/mL) than Gram negative bacteria (> 20 µg/mL).

1.10 Aims

The general aim of this thesis is to design and synthesize a library of organoruthenium ethylenediamine complexes containing various arene and functional substituents on the terminal N of ethylenediamine ligands, which can effectively reduce the cell coenzyme NAD^+ to NADH via transfer hydrogenation using sodium formate as hydride source; and a series of organoiridium, ruthenium and osmium biguanide complexes as novel antibacterial agents. The details are summarized as follows:

- Study the catalytic efficacy of Ru^{II} ethylenediamine monosulfonyl complexes containing different substituents and tethered Ru^{II} monosulfonyl ethylenediamine complexes towards the TH reduction of NAD^+ to NADH using sodium formate as hydride source.
- Investigate the antiproliferative activity of Ru^{II} ethylenediamine monosulfonyl and tethered Ru^{II} complexes.
- Investigate the potential targets for Ru^{II} ethylenediamine monosulfonyl complexes (including non-tethered and tethered), *e.g.* DNA or GSH/cysteine.
- Synthesize and study the antimicrobial activity of novel Ir^{III} biguanide complexes against Gram-positive and Gram-negative bacteria, and fungi; and compare with Ru^{II} and Os^{II} analogue complexes.
- Explore the antimicrobial mechanism of action of novel biguanide complexes (Ir^{III}, Ru^{II} or Os^{II}).

1.11 References

(1) King, R. J. B.; Robins, M. W. *Cancer Biology*, 3rd Ed., Pearson Education Limited, England, **2006**.

(2) Mjos, K. D.; Orvig, C. *Chem. Rev.* **2014**, *114*, 4540−4563.

(3) Rosenberg, B.; Camp, L. V.; Krigas, T. *Nature*, **1965**, *205*, 698–699.

(4) Johnstone, T. C.; Suntharalingam, K.; Lippard, S. J. *Chem. Rev.* **2016**, *116*, 3436−3486.

(5) Gately, D. P.; Howell, S. B. *Br. J. Cancer* **1993**, *67*, 1171−1176.

(6) Frey, U.; Ranford, J. D.; Sadler, P. J. *Inorg. Chem.* **1993**, *32*, 1333−1340.

(7) Fichtinger-Schepman, A. M. J.; van der Veer, J. L.; den Hartog, J. H. J.; Lohman, P. H. M.; Reedijk, J. *Biochemistry* **1985**, *24*, 707−713.

(8) Gasser, G.; Ott, I.; Metzler-Nolte, N. *J. Med. Chem.* **2011**, *54*, 3–25.

(9) Nguyen, A.; Vessieres, A.; Hillard, E. A.; Top, S.; Pigeon, P.; Jaouen, G. *Chimia* **2007**, *61*, 716–724.

(10) Jaouen, G.; Top, S.; Vessieres, A.; Leclercq, G.; McGlinchey, M. J. *Curr. Med. Chem.* **2004**, *11*, 2505–2517.

(11) Schatzschneider, U.; Metzler-Nolte, N. *Angew. Chem., Int. Ed.* **2006**, *45*, 1504–1507.

(12) Dive, D.; Biot, C. *ChemMedChem* **2008**, *3*, 383–391.

(13) Melendez, E. *Crit. Rev. Oncol. Hematol.* **2002**, *42*, 309–315.

(14) Caruso, F.; Rossi, M. *Met. Ions Biol. Syst.* **2004**, *42*, 353–384.

(15) Toney, J. H.; Marks, T. J. *J. Am. Chem. Soc.* **1985**, *107*, 947–953.

(16) Erxleben, A.; Claffey, J.; Tacke, M. *J. Inorg. Biochem.* **2010**, *104*, 390–396.

(17) Noffke, A. L.; Habtemariam, A.; Pizarro, A. M.; Sadler, P. J. *Chem. Commun.* **2012**, *48*, 5219–5246.

(18) Novakova, O.; Kasparkova, J.; Vrana, O.; van Vliet, P. M.; Reedijk, J.; Brabec, V. *Biochemistry* **1995**, *34*, 12369–12378.

(19) Allen, O. R.; Croll, L.; Gott, A. L.; Knox, R. J.; McGowan, P. C. *Organometallics* **2003**, *23*, 288–292.

(20) Fu, Y.; Romero, M. J.; Habtemariam, A.; Snowden, M. E.; Song, L.; Clarkson, G. J.; Qamar, B.; Pizarro, A. M.; Unwin, P. R.; Sadler, P. J. *Chem. Sci.* **2012**, *3*, 2485–2494.

(21) Fu, Y.; Habtemariam, A.; Pizarro, A. M.; van Rijt, S. H.; Healey, D. J.; Cooper, P. A.; Shnyder, S. D.; Clarkson, G. J.; Sadler, P. J. *J. Med. Chem.* **2010**, *53*, 8192–8196.

(22) Liu, Z.; Romero-Canelon, I.; Qamar, B.; Hearn, J. M.; Habtemariam, A.; Barry, N. P. E.; Pizarro, A. M.; Clarkson, G. J.; Sadler, P. J. *Angew. Chem. Int. Ed.* **2014**, *53*, 3941 –3946.

(23) Liu, Z.; Romero-Canelón, I.; Habtemariam, A.; Clarkson, G. J.; Sadler, P. J. *Organometallics* **2014**, *33*, 5324−5333.

(24) Alessio, E. *Eur. J. Inorg. Chem.* **2017**, 1549–1560.

(25) a) Sava, G.; Pacor, S.; Mestroni, G.; Alessio, E. *Clin. Exp. Metastasis* **1992**, 10, 273–280. b) Sava, G.; Pacor, S.; Mestroni, G.; Alessio, E. *Anti-Cancer Drugs* **1992**, *3*, 25–31.

(26) a) Chiorescu, I.; Deubel, D. V.; Arion, V. B.; Keppler, B. K. *J. Chem. Theory Comput.* **2008**, *4*, 499–506; b) Reisner, E.; Arion, V. B.; Guedes da Silva, M. F. C.; Lichtenecker, R.; Eichinger, A.; Keppler, B. K.; Kukushkin, V. Y.; Pombeiro, A. J. L. *Inorg. Chem.* **2004**, *43*, 7083–7093; c) Reisner, E.; Arion, V. B.; Eichinger, A.; Kandler, N.; Giester, G.; Pombeiro, A. J. L.; Keppler, B. K. *Inorg. Chem.* **2005**, *44*, 6704–6716. d) Keppler, B. K.; Wehe, D.; Endres, H.; Rupp, W. *Inorg. Chem.* **1987**, *26*, 844–846; e) Keppler, B. K.; Rupp, W.; Juhl, U. M.; Endres, H.; Niebl, R.; Balzer, W. *Inorg. Chem.* **1987**, *26*, 4366–4370.

(27) Pluim, D.; van Waardenburg, R. C. A. M.; Beijnen, J. H.; Schellens, J. H. M. *Cancer Chemother. Pharmacol.* **2004**, *54*, 71–78.

(28) Coluccia, M.; Sava, G.; Salerno, G.; Bergamo, A.; Pacor, S.; Mestroni, G.; Alessio, E. *Met. Based Drugs* **1995**, *2*, 195–199.

(29) Casini, A.; Gabbiani, C.; Sorrentino, F.; Rigobello, M. P.; Bindoli, A.; Geldbach, T. J.; Marrone, A.; Re, N.; Hartinger, C. G.; Dyson, P. J.; Messori, L. *J. Med. Chem.* **2008**, *51*, 6773–6781.

(30) Scolaro, C.; Bergamo, A.; Brescacin, L.; Delfino, R.; Cocchietto, M.; Laurenczy, G.; Geldbach, T. J.; Sava, G.; Dyson, P. J. *J. Med. Chem.* **2005**, *48*, 4161–4171.

(31) Ang, W. H.; Daldini, E.; Scolaro, C.; Scopelliti, R.; Juillerat-Jeannerat, L.; Dyson, P. J. *Inorg. Chem.* **2006**, *45*, 9006–9013.

(32) Nowak-Sliwinska, P.; van Beijnum, J. R.; Casini, A.; Nazarov, A. A.; Wagnieres, G.; van den Bergh, H.; Dyson, P. J.; Griffioen, A. W. *J. Med. Chem.* **2011**, *54*, 3895–3902.

(33) Koblinski, J. E.; Ahram, M.; Sloane, B. F. *Clin. Chim. Acta* **2000**, *291*, 113–135.

(34) Xie, L.; Luo, Z.; Zhao, Z.; Chen, T. *J. Med. Chem.* **2017**, *60*, 202−214.

(35) Hillard, E. A.; Vessières, A.; Jaouen, G. *Top. Organomet. Chem.* **2010**, *32*, 81−117.

(36) Kilpin, K. J.; Clavel, C. M.; Edafe, F.; Dyson P. J. *Organometallics* **2012**, *31*, 7031−7039.

(37) Banerjee, S.; Prasad, P.; Hussain, A.; Khan, I.; Kondaiah, P.; Chakravarty, A. R. *Chem. Commun.* **2012**, *48*, 7702−7704.

(38) Pettinari, R.; Marchetti, F.; Condello, F.; Pettinari, C.; Lupidi, G.; Scopelliti, R.; Mukhopadhyay, S.; Riedel, T.; Dyson P. J. *Organometallics* **2014**, *33*, 3709−3715.

(39) Chow, M. J.; Licona, C.; Wong, D. Y. Q.; Pastorin, G.; Gaiddon, C.; Ang W. H. *J. Med. Chem.* **2014**, *57*, 6043−6059.

(40) Chow, M. J.; Licona, C.; Pastorin, G.; Mellitzer, G.; Ang, W. H.; Gaiddon, C. *Chem. Sci.* **2016**, *7*, 4117–4124.

(41) Meulmeester, E.; Jochemsen, A. G. *Curr. Cancer Drug Targets* **2008**, *8*, 87−97.

(42) Chow, M. J.; Alfiean, M.; Pastorin, G.; Gaiddon, C.; Ang, W. H. *Chem. Sci.* **2017**, *8*, 3641–3649.

(43) Wang, F.; Habtemariam, A.; van der Geer, E. P. L.; Fernández, R.; Melchart, M.; Deeth, R. J.; Aird, R.; Guichard, S.; Fabbiani, F. P. A.; Lozano-Casal, P.; Oswald, I. D. H.; Jodrell, D. I.; Parsons, S.; Sadler, P. J. *Proc. Natl. Acad. Sci. U.S.A.* **2005**, *102*, 18269–18274.

(44) Aird, R. E.; Cummings, J.; Ritchie, A. A.; Muir, M.; Morris, R. E.; Chen, H.; Sadler, P. J.; Jodrell, D. I. *Br. J. Cancer* **2002**, *86*, 1652–1657.

(45) Chen, H.; Parkinson, J. A.; Parsons, S.; Coxall, R. A.; Gould, R. O.; Sadler, P. J. *J. Am. Chem. Soc.* **2002**, *124*, 3064–3082.

(46) Chen, H.; Parkinson, J. A.; Morris, R. E.; Sadler, P. J. *J. Am. Chem. Soc.* **2003**, *125*, 173–186.

(47) Wang, F.; Xu, J.; Habtemariam, A.; Bella, J.; Sadler, P. J. *J. Am. Chem. Soc.* **2005**, *127*, 17734–17743.

(48) Turrens, J. F. *J. Physiol.* **2003**, *552*, 335–344.

(49) Imlay, J. A. *Nat. Rev. Microbiol.* **2013**, *11*, 443−454.

(50) Murphy, M. P. *Biochem. J.* **2009**, *417*, 1–13.

(51) Balaban, R. S.; Nemoto, S.; Finkel, T. *Cell* **2005**, *120*, 483–495.

(52) Stringfellow, H. M.; Jones, M. R.; Green, M. C.; Wilson, A. K.; Francisco, J. S. *J. Phys. Chem. A* **2014**, *118*, 11399−11404.

(53) Sabharwal, S. S.; Schumacker, P. T. *Nat. Rev. Cancer* **2014**, *14*, 709−721.

(54) Imlay, J. A. *Annu. Rev. Biochem.* **2008**, *77*, 755−776.

(55) Newton, G. L.; Rawat, M.; La Clair, J. J.; Jothivasan, V. K.; Budiarto, T.; Hamilton, C. J.; Claiborne, A.; Helmann, J. D.; Fahey, R. C. *Nat. Chem. Biol.* **2009**, *5*, 625−627.

(56) Dharmaraja, A. T. *J. Med. Chem.* **2017**, *60*, 3221−3240.

(57) Linstead, R. P.; Braude, F. A.; Mitchell, P. W. D.; Wooldridge, K. R. H.; Jackman, L. M. *Nature* **1952**, *169*, 100–103.

(58) Gladiali, S.; Alberico, E. *Chem. Soc. Rev.* **2006**, *35*, 226–236.

(59) Robertson, A.; Matsumoto, T.; Ogo, S. *Dalton Trans.* **2011**, *40*, 10304–10310.

(60) Hashiguchi, S.; Fujii, A.; Takehara, J.; Ikariya, T.; Noyori, R. *J. Am. Chem. Soc.* **1995**, *117*, 7562–7563.

(61) a) Wu, X.; Li, X.; King, F.; Xiao, J. *Angew. Chem. Int. Ed.* **2005**, *44*, 3407–3411; b) Wu, X.; Vinci, D.; Ikariya, T.; Xiao, J. *Chem. Commun.* **2005**, 4447–4449; c) Wu, X.; Li, X.; Hems, W.; King, F.; Xiao, J. *Org. Biomol. Chem.* **2004**, *2*, 1818–1821; d) Tang, W.; Johnston, S.; Li, C.; Iggo, J. A.; Bacsa, J.; Xiao, J. *Chem. Eur. J.* **2013**, *19*, 14187–14193; e) Tang, W.; Johnston, S.; Iggo, J. A.; Berry, N. G.; Phelan, M.; Lian, L.; Bacsa, J.; Xiao, J. *Angew. Chem. Int. Ed.* **2013**, 52, 1668 –1672; f) Li, X.; Wu, X.; Chen, W.; Hancock, F. E.; King, F.; Xiao, J. *Org. Lett.* **2004**, *6*, 3321–3324.

(62) a) Hannedouche, J.; Clarkson, G. J.; Wills, M. *J. Am. Chem. Soc.* **2004**, *126*, 986–987; b) Hayes, A. M.; Morris, D. J.; Clarkson, G. J.; Wills, M. *J. Am. Chem. Soc.* **2005**, *127*, 7318–7319; c) Martins, J. E. D.; Clarkson, G. J.; Wills, M. *Org. Lett.* **2009**, *11*, 847–850; d) Soni, R.; Cheung, F. K.; Clarkson, G. C.; Martins, J. E. D.; Graham, M. A.; Wills, M. *Org. Biomol. Chem.* **2011**, *9*, 3290-3294; e) Wu, X.; Li, X.; Hems, W.; King, F.; Xiao, J. *Org. Biomol. Chem.* **2004**, *2*, 1818–1821.

(63) a) Morris, D. J.; Hayes, A. M.; Wills, M. *J. Org. Chem.* **2006**, *71*, 7035−7044; b) Fang, Z.; Wills, M. *Org. Lett.* **2014**, *16*, 374−377.

(64) Deore, B. A.; Freund, M. S. *Chem. Mater.* **2005**, *17*, 2918–2923.

(65) Giangreco, I.; Packer, M. J. *J. Med. Chem.* **2013**, *56*, 6175−6189

(66) Szczepankiewicz, B. G.; Dai, H.; Koppetsch, K. J.; Qian, D.; Jiang, F.; Mao, C.; Perni, R. B. *J. Org. Chem.* **2012**, *77*, 7319−7329.

(67) Pesnot, T.; Kempter, J.; Schemies, J.; Pergolizzi, G.; Uciechowska, U.; Rumpf, T.; Sippl, W.; Jung, M.; Wagner, G. K. *J. Med. Chem.* **2011**, *54*, 3492–3499.

(68) Gębicki, J.; Marcinek, A.; Zielonka, J. *Acc. Chem. Res.* **2004**, *37*, 379–386.

(69) Preiss, J.; Handler, P. *J. Biol. Chem.* **1958**, *233*, 488–492.

(70) de Figueiredo, L. F.; Gossmann, T. I.; Ziegler, M.; Schuster, S. *Biochem. J.* **2011**, *439*, 341–348.

(71) Guillot, B.; Muzet, N.; Artacho, E.; Lecomte, C.; Jelsch, C. *J. Phys. Chem. B* **2003**, *107*, 9109–9121.

(72) Fan, J.; Hitosugi, T.; Chung, T. W.; Xie, J.; Ge, Q.; Gu, T. L.; Polakiewicz, R. D.; Chen, G. Z.; Boggon, T. J.; Lonial, S.; Khuri, F. R.; Kang, S.; Chen, J. *Mol. Cell. Biol.* **2011**, *31*, 4938–4950.

(73) Tan, B.; Young, D. A.; Lu, Z. H.; Wang, T.; Meier, T. I.; Shepard, R. L.; Roth, K.; Zhai, Y.; Huss, K.; Kuo, M. S.; Gillig, J.; Parthasarathy, S.; Burkholder, T. P.; Smith, M. C.; Geeganage, S.; Zhao, G. *J. Biol. Chem.* **2013**, *288*, 3500–3511.

(74) Soldevila-Barreda, J. J.; Bruijnincx, P. C. A.; Habtemariam, A.; Clarkson, G. J.; Deeth, R. J.; Sadler, P. J. *Organometallics* **2012**, *31*, 5958–5967.

(75) Steckhan, E.; Herrmann, S.; Ruppert, R.; Thommes, J.; Wandrey, C. *Angew Chem. Int. Ed.* **1990**, *29*, 388–390.

(76) Ruppert, R.; Herrmann, S.; Steckhan, E. *Tetrahedron Lett.* **1987**, 28, 6582–6586.

(77) Steckhan, E.; Herrmann, S.; Ruppert, R.; Dietz, E.; Frede, M.; Spika, E. *Organometallics* **1991**, *10*, 1568–1577.

(78) Lo, H. C.; Buriez, O.; Kerr, J. B.; Fish, R. H. *Angew. Chem. Int. Ed.* **1999**, *38*, 1429–1432.

(79) Lo, H. C.; Fish, R. H. *Angew. Chem. Int. Ed.* **2002**, *41*, 478–481.

(80) Betanzos-Lara, S.; Liu, Z.; Habtemariam, A.; Pizarro, A. M.; Qamar, B.; Sadler, P. J. *Angew. Chem. Int. Ed.* **2012**, *51*, 3897–3900.

(81) Liu, Z.; Deeth, R. J.; Butler, J. S.; Habtemariam, A.; Newton, M. E.; Sadler, P. J. *Angew. Chem. Int. Ed.* **2013**, *52*, 4194–4197.

(82) a) Barrett, S. M.; Pitman, C. L.; Walden, A. G.; Miller, A. J. M. *J. Am. Chem. Soc.* **2014**, *136*, 14718–14721; b) Kobayashi, A.; Sakamoto, K.; Ishitani, O. *Inorg. Chem. Commun.* **2005**, *8*, 365–367; c) Kobayashi, A.; Takatori, R.; Kikuchi, I.; Konno, H.; Sakamoto, K.; Ishitani, O.; *Organometallics* **2001**, *20*, 3361–3363; e) Maenaka, Y.; Suenobu, T.; Fukuzumi, S. *J. Am. Chem. Soc.* **2012**, *134*, 9417–9427; f) Matsubara, Y.; Koga, K.; Kobayashi, A.; Konno, H.; Sakamoto, K.; Morimoto, T.; Ishitani, O. *J. Am. Chem. Soc.* **2010**, *132*, 10547–10552.

(83) Yamakawa, M.; Ito, H.; Noyori, R. *J. Am. Chem. Soc.* **2000**, *122*, 1466–1478.

(84) Soni, R.; Cheung, F. K.; Clarkson, G. C.; Martins, J. E. D.; Graham, M. A.; Wills, M. *Org. Biomol. Chem.* **2011**, *9*, 3290–3294.

(85) Konno, H.; Sakamoto, K.; Ishitani, O. *Angew. Chem. Int. Ed.* **2000**, *39*, 4061–4063.

(86) Nathan, C. *Nature* **2004**, *431*, 899–902.

(87) Dennis, M. L.; Pitcher, N. P.; Lee, M. D.; DeBono, A. J.; Wang, Z.; Harjani, J. R.; Rahmani, R.; Cleary, B.; Peat, T. S.; Baell, J. B.; Swarbrick, J. D. *J. Med. Chem.* **2016**, *59*, 5248–5263.

(88) Ng, N. S.; Leverett, P.; Hibbs, D. E.; Yang, Q.; Bulanadi, J. C.; Wu, M. J.; Aldrich-Wright, J. R. *Dalton Trans.* **2013**, *42*, 3196–3209.

(89) Li, F.; Collins, J. G.; Keene, F. R. *Chem. Soc. Rev.* **2015**, 44, 2529–2542.

(90) a) Zhao, Y.; Chen, Z.; Chen, Y.; Xu, J.; Li, J.; Jiang, X. *J. Am. Chem. Soc.* **2013**, *135*, 12940−12943; b) Bouley, R.; Ding, D.; Peng, Z.; Bastian, M.; Lastochkin, E.; Song, W.; Suckow, M. A.; Schroeder, V. A.; Wolter, W. R.; Mobashery, S.; Chang, M. *J. Med. Chem.* **2016**, *59*, 5011−5021.

(91) Lloyd, N. C.; Morgan, H.W.; Nicholson, B. K.; Ronimus, R. S. *Angew. Chem. Int. Ed.* **2005**, *44*, 941–944.

(92) O'Connell, K. M. G.; Hodgkinson, J. T.; Sore, H. F.; Welch, M.; Salmond, G. P. C.; Spring, D. R. *Angew. Chem. Int. Ed.* **2013**, *52*, 10706–10733.

(93) von Nussbaum, F.; Brands, M.; Hinzen, B.; Weigand, S.; Häbich, D. *Angew. Chem. Int. Ed.* **2006**, *45*, 5072–5129.

(94) a) Jo, Y. K.; Seo, J. H.; Choi, B.; Kim, B. J.; Shin, H. H.; Hwang, B. H.; Cha, H. J. *ACS Appl. Mater. Interfaces* **2014**, *6*, 20242−20253; b) Regiel-Futyra, A.; Kus-Liśkiewicz, M.; Sebastian, V.; Irusta, S.; Arruebo, M.; Stochel, G.; Kyzioł, A. *ACS Appl. Mater. Interfaces* **2015**, *7*, 1087−1099.

(95) Chernousova, S.; Epple, M. *Angew. Chem. Int. Ed.* **2013**, *52*, 1636–1653.

(96) Li, Y.; Zhang, W.; Niu, J.; Chen, Y. *ACS Nano* **2012**, *6*, 5164–5173.

(97) Noffke, A. L.; Habtemariam, A.; Pizarro, A. M.; Sadler, P. J. *Chem. Commun.* **2012**, *48*, 5219–5246.

(98) Li, F.; Mulyana, Y.; Feterl, M.; Warner, J. M.; Collins, J. G.; Keene, F. R. *Dalton Trans.* **2011**, *40*, 5032–5038.

(99) Pandrala, M.; Li, F.; Feterl, M.; Mulyana, Y.; Warner, J. M.; Wallace, L.; Keene, F. R.; Collins, J. G. *Dalton Trans.* **2013**, *42*, 4686–4694.

(100) Alam, P.; Karanam, M.; Choudhury, A. R.; Laskar, I. R. *Dalton Trans.* **2012**, *41*, 9276–9279.

(101) Jain, N.; Alam, P.; Laskar, I. R.; Panwar, J. *RSC Advances* **2015**, *5*, 61983–61988.

(102) Simpson, P. V.; Schmidt, C.; Ott, I.; Bruhn, H.; Schatzschneider, U. *Eur. J. Inorg. Chem.* **2013**, *2013*, 5547–5554.

Chapter 2

Materials, Methods & Experimental

2.1 Materials

2.1.1 Chemicals

Ruthenium(III) trichloride, iridium(III) trichloride and osmium(III) trichloride were purchased from Precious Metals Online (PMO Pty Ltd.) and used as received. 4-nitrobenzenesulfonyl chloride, 4-fluorobenzenesulfonyl chloride, 2,3,4,5-tetramethyl-2-cyclopentanone, 1,2,3,4,5-pentamethylcyclopentadiene, ethylenediamine, 1-(bromomethyl) naphthalene, N-benzyl-ethylenediamine, 4-bromo-biphenyl, bromobenzene, n-butyllithium in hexane 1.6 M, benzenesulfonyl chloride, sodium formate and *β*-nicotinamide adenine dinucleotide hydrate (NAD^+) were obtained from Sigma-Aldrich. Metformin was purchased from Cayman chemical company, and all other biguanide chelating ligands (ligands without any sulfonyl substitution) used in Chapter 4 were also obtained from Sigma-Aldrich. Methanesulfonyl chloride and toluenesulfonyl chloride were purchased from Fluka. Magnesium sulphate, potassium hydroxide, sodium chloride, sodium iodide, potassium bromide and hydrochloric acid were obtained from Fisher Scientific. *α*-Phellandrene was purchased from SAFC. The solvents used for NMR spectroscopy were purchased from Sigma-Aldrich and Cambridge Isotope Laboratories Inc. Non-dried solvents used in syntheses were obtained from Fisher Scientific and Prolabo. Solvents (including HPLC solvents, *e.g.* H_2O and Acetonitrile) were used as obtained, except in the case of ethanol and 2-propanol, which were refluxed and degassed with nitrogen, respectively, prior to use.

2.1.2 Bio-materials

2.1.2.1 Cell Culture

A2780 human ovarian carcinoma cells were obtained from the European Collection of Cell Cultures. The cell line was grown in Roswell Park Memorial Institute medium (RPMI-1640) supplemented with 10% of fetal calf serum, 1% of 2 mM glutamine and 1% penicillin /streptomycin (1000 units). All cells were grown as adherent monolayers at 310 K in a 5% CO_2-humidified atmosphere and passaged at *ca.* 70–80% confluency. All bio-materials were purchased and handled by Dr. Isolda Romero-Canelon and Ji-Inn Song.

2.1.2.2 Antimicrobial Study Related Materials

Staphylococcus aureus (*S. aureus*, strain type: R 34), *Bacillus subtilis* (*B. subtilis*, strain type: DSM 10) and *Streptococcus pyogenes* (*S. pyogenes*, strain type: 151112), *Staphylococcus epidermidis* (*S. epidermidis*, strain type: 12228), *Enterococcus faecalis* (*E. faecalis*, strain type: 29212) were obtained from the culture collection of Professor Christopher G. Dowson and Mr John Moat (School of Life Sciences, University of Warwick). Antimicrobial activity against methillicin-resistant *S. aureus* (*MRSA*, strain type: ATCC 43300), FDA control *Escherichia coli* (*E. coli*, strain type: ATCC 25922), multi-drug resistant *Klebsiella pneumoniae* (MDR *K. pneumoniae*, strain type: ATCC 700603), *Pseudomonas aeruginosa* (*P. aeruginosa*, strain type: ATCC 27853), *Acinetobacter baumannii* (*A. baumannii*, strain type: ATCC 19606), and antifungal activity against *Candida albicans* (*A. albicans*, strain type: ATCC 90028) and *Cryptococcus neoformans* (*C. neoformans*, strain type: ATCC 208821), as well as cytotoxicity towards human embryonic kidney cells (*HEK-293*, strain type: ATCC CRL-1573) and *RBC* (human red blood cells) were screened by Community for Open Antimicrobial Drug Discovery (CO-ADD) at the University of Queensland, Australia.

2.2 Preparation of Precursors

2.2.1 Synthesis of Arene Ligands[1]

3-Phenyl-1,2,4,5-tetramethyl-1,3-cyclopentandiene (Cp^{XPh})[1a,b]

To a solution of phenyllithium (50 mL, 1.9 M in dibutyl ether) was added 2,3,4,5-tetramethyl-2-cyclopentenone (12 mL) at 273 K under N_2. The reaction was allowed to warm slowly to 298 K with stirring overnight. The yellow solution was cooled down by addition of ice and then acidified with HCl (36% in water, v/v). The aqueous solution was extracted with diethyl ether (3 × 50 mL). The combined organic portions were dried over anhydrous magnesium sulphate and filtered, and the solvent was removed on a rotary evaporator to obtain a yellow oil. The product was purified by distillation under vacuum (fraction at 410 K, 0.5 mbar). Yield = 12.87 g (82%). The ligand purity was confirmed by comparison of ^{1}H NMR spectrum with reported literature.[1b]

3-Biphenyl-1, 2, 4, 5-tetramethyl-1, 3-cyclopentandiene (Cp^{Xbiph})[1b,c]

A solution of 4-bromobiphenyl (16 g, 68.6 mmol) in dried tetrahydrofuran (400 mL) was treated with a solution of n-BuLi in hexane (50 mL, 1.6 M) at 195 K under nitrogen. After 3 h reaction, 2,3,4,5-tetramethyl-2-cyclopentenone (12 mL) was added. The solution was allowed to warm slowly to 298 K with stirring overnight. The orange solution was acidified with HCl (36% in water, v/v) and the organic phase was removed. The aqueous layer was extracted with diethyl ether (3 × 50 mL). The combined organic portions were dried over anhydrous $MgSO_4$ and filtered, and the solvent was removed on a rotary evaporator to obtain a dark yellow powder. The product was washed in methanol (3 × 20 mL) to give a light yellow powder. Yield = 21 g (94.4%). ^{1}H NMR (400 MHz, $CDCl_3$): δ_H 7.64 (m, 4H), 7.44 (m, 2H), 7.33 (m, 3H), 3.25 (m, 1H), 2.08 (s, 3H), 1.95 (s, 3H), 1.88 (s, 3H), 1.00 (d, J = 7.5 Hz, 3H).

2.2.2 Preparation of Dimers

2.2.2.1 Synthesis of Ru(II) Dimers[2]

$[(\eta^6$-*p*-cym)$RuCl_2]_2$ - Method 1[2a,b]

$RuCl_3 \cdot 3H_2O$ (1.02 g, 4.01 mol) and *α*-phellandrene (6.15 mL, 5.06 mol) were dissolved in freshly distilled ethanol (75 mL) and the reaction mixture heated to reflux (353 K) under a nitrogen atmosphere for 18 h. The red precipitate formed was filtered and washed with ice cold ethanol (3 × 20 mL) and diethyl ether (3 × 20 mL) and dried under vacuum. Yield = 1.1 g (88 %). ^{1}H NMR (400 MHz, DMSO-d_6): δ_H 5.82 (d, *J* = 6.4 Hz, 2H), 5.76 (d, *J* = 6.4 Hz, 2H), 2.84 (m, 1H), 2.09 (s, 3H), 1.20 (d, *J* = 6.9 Hz, 6H).

Method 2[2c]

$RuCl_3 \cdot 3H_2O$ (1.00 g, 4.00 mol) and *α*-phellandrene (6.15 mL, 5.06 mol) were dissolved in anhydrous MeOH (10 mL) in a microwave vial. The solution was sonicated in water bath at 313 K for 10 min. Then the mixture was irradiated with microwave irradiation at 413 K for 5 min. Next, the solution was placed in a freezer at 255 K for 2 h and the resulting precipitate was washed with ice-cold MeOH (3 × 20 mL) and diethyl ether (3 × 20 mL), to give a red solid. The product was dried overnight in air. Yield = 1 g (77%).

$[(\eta^6$-biph)$RuCl_2]_2$[2a,b]

3-Phenyl-1,4-cyclohexadiene (1.77 g, 11.36 mmol) was added to a solution of $RuCl_3 \cdot 3H_2O$ (1.00 g, 3.79 mmol) in anhydrous MeOH (10 mL) in microwave vial. The solution was sonicated in water bath at 313 K for 10 min. Then the mixture was irradiated with microwave irradiation at 413 K for 5 min. Next, the solution was placed in a freezer at 255 K for 2 h and the resulting precipitate was washed with ice-cold MeOH (3 × 20 mL) and diethyl ether (3 ×

20 mL), to give a brown solid. The product was dried under vacuum overnight. Yield = 1 g (81%). ^{1}H NMR (400 MHz, DMSO-d_6): δ_H 6.07 (m, 3H), 6.42 (d, *J* = 6.1 Hz, 2H), 7.50 (m, 3H), 7.82 (m, 2H).

[(η^6-HO(CH_2)$_2$OPh)$RuCl_2$]$_2$[2b]

2-(Cyclohexa-1,4-dien-1-yloxy)ethan-1-ol (1.60 g, 11.40 mmol) was added to a solution of $RuCl_3 \cdot 3H_2O$ (1.00 g, 3.79 mmol) in freshly distilled ethanol (100 mL). The reaction mixture was heated to reflux (363 K) under nitrogen atmosphere for 18 h. The red precipitate formed was filtered and washed with ice-cold ethanol (3 × 20 mL) and ether (3 × 20 mL) dried under vacuum overnight. Yield = 892 mg (76%). ^{1}H NMR (400 MHz, DMSO-d_6): δ_H 3.72 (t, *J* = 4.5 Hz, 2H), 4.21 (t, *J* = 4.5 Hz, 2H), 4.94 (s, broad, 1H), 5.37 (t, *J* = 5.3 Hz, 1H), 5.54 (d, *J* = 6.3 Hz, 2H), 6.15 (t, *J* = 5.8 Hz, 2H).

2.2.2.2 Synthesis of Os(II) Dimers[3]

[(η^6-biph)$OsCl_2$]$_2$

$OsCl_3 \cdot 3H_2O$ (1.00 g, 2.85 mmol) and 3-phenyl-1,4-cyclohexa diene (1.58 g, 10.12 mmol) were dissolved in anhydrous MeOH (10 mL) in a microwave reaction vial, the solution was sonicated in water bath at 313 K for 10 min. Then the mixture was irradiated with microwave irradiation at 393 K for 10 min. After cooling down to ambient temperature, an orange precipitate was collected through filtration, and the solid was washed with ice-cold EtOH (3 × 20 mL) and diethyl ether (3 × 20 mL). The product was dried overnight *in vacuo*. Yield = 1.06 g (80%). ^{1}H NMR (400 MHz, DMSO-d_6): δ_H 6.31-6.38 (m, 6H), 6.68 (d, *J* = 5.6 Hz, 4H), 7.44-7.49 (m, 6H), 7.71 (dd, *J* = 1.4 Hz, 8.1 Hz, 4H).

2.2.2.3 Synthesis of Ir(III) Dimers[1b, 4]

$[(\eta^5\text{-Cp*})IrCl_2]_2$[1b]

$IrCl_3 \cdot 3H_2O$ (1.00 g, 2.84 mmol) and 1,2,3,4,5-pentamethylcyclo pentadiene (1.34 mL, 8.56 mmol) were placed in a microwave vial, to which anhydrous MeOH (10 mL) was added, and the solution was sonicated in a water bath for 10 min. Then the solution was irradiated with microwave irradiation at 413 K for 5 min. After cooling to room temperature, the vial was placed in the freezer for 2 h, and the reddish orange precipitate was collected by filtration. The solid was washed with pentane (3 × 20 mL) and diethyl ether (3 × 20 mL), and the product was dried in air overnight. Yield = 900 mg (80%). ^{1}H NMR (400 MHz, $CDCl_3$): δ_H 1.59 (s, 15H).

$[(\eta^5\text{-Cp}^{Xph})IrCl_2]_2$[1b, 4]

$[(\eta^5\text{-Cp}^{Xph})IrCl_2]_2$ was synthesized following the procedure described for $[(\eta^5\text{-Cp*})IrCl_2]_2$ using $IrCl_3 \cdot 3H_2O$ (1.00 g, 2.84 mmol) and 3-phenyl-1,2,4,5-tetramethyl-1,3-cyclopentadiene (1.00 g, 5.00 mmol). An orange solid was obtained. Yield = 600 mg (46%). ^{1}H NMR (400 MHz, $CDCl_3$): δ_H 1.63 (s, 6H), 1.72 (s, 6H), 7.35-7.36 (m, 3H), 7.56-7.57 (m, 2H).

$[(\eta^5\text{-Cp}^{Xbiph})IrCl_2]_2$[1b, 4]

$[(\eta^5\text{-Cp}^{Xbiph})IrCl_2]_2$ was synthesized following the procedure depicted for $[(\eta^5\text{-Cp*})IrCl_2]_2$ using $IrCl_3 \cdot 3H_2O$ (814 mg, 2.31 mmol) and 3-biphenyl-1,2,4,5-tetramethyl-1,3-cyclopentadiene (1.5 g, 5.47 mmol). An orange solid was obtained. Yield = 796 mg (64%). ^{1}H NMR (400 MHz, $CDCl_3$): δ_H 1.69 (s, 6H), 1.75 (s, 6H), 7.32-7.37 (m, 1H), 7.41-7.45 (m, 2H), 7.56-7.60 (m, 4H), 7.64-7.67 (m, 2H).

2.2.3 Preparation of Bidentate Chelating Ligands[5-7]

2.2.3.1 Synthesis of Ethylenediamine Ligands in Chapters 3 and 4

The ethylenediamine chelating ligands were synthesized according to the literature with the guidance of Dr. Joan Joseph Soldevila Barreda at the University of Warwick.

N-(2-Aminoethyl)-4-toluensulfonamide (**TsEn**)

This ligand was obtained following the method described in the literature.[5] A solution of ethylenediamine (17 mL, 0.26 mol) in dichloromethane (150 mL) was placed in a round bottom flask. A solution of toluenesulfonyl chloride (5.0 g, 26 mmol) in dichloromethane (50 mL) was added slowly via a dropping funnel, and the mixture stirred vigorously for 1 h. The solution was then washed with water (3 × 25 mL), and dried over $MgSO_4$. Solvent was removed on a rotary evaporator to give a white solid which was purified by column chromatography (MeOH: DCM, 1: 9 (v/v)). Yield = 3 g (54%). ^{1}H NMR (400 MHz, $CDCl_3$): δ_H 2.43 (s, 3H), 2.78 (t, *J* = 5.6 Hz, 2H), 2.95 (t, *J* = 5.6 Hz, 2H), 7.30 (d, *J* = 8.1 Hz, 2H), 7.75 (d, *J* = 8.1 Hz, 2H). ESI-MS: *Calcd* for $[C_9H_{14}N_2O_2S + H]^+$ 215.0 *m/z*, found: 215.1 *m/z*.

Methyl-(2-((4-methylphenyl)sulfonamido)ethyl)carbamate

This ligand was synthesized as precursor of 4-methyl-N-(2-(methylamino)ethyl)benzene sulfonamide (TsEnMe) and obtained following the method described in the literature.[6] TsEn (428 mg, 2.0 mmol) was dissolved in dichloromethane (20 mL) and then methyl chloroformate (0.185 mL, 2.4 mmol) and triethylamine (0.306 mL, 2.2 mmol) were added and the reaction mixture left stirring at ambient temperature overnight. The mixture was washed with water (20 mL), extracted with chloroform (3 × 30 mL) and then dried over anhydrous $MgSO_4$. The solvent was removed under rotary evaporator to give white solid. Yield = 494 mg (89%). ^{1}H

NMR (400 MHz, $CDCl_3$): δ_H 2.43 (s, 3H), 3.06-3.10 (m, 2H), 3.26-3.29 (m, 2H), 3.65 (s, 3H), 4.97 (d, *J* = 23.4 Hz, 2H), 7.31 (d, *J* = 8.1 Hz, 2H), 7.74 (d, *J* = 8.2 Hz, 2H).

4-Methyl-N-(2-(methylamino)ethyl)benzenesulfonamide (**TsEnMe**)[6]

To a stirred solution of amide precursor (408 mg, 1.5 mmol, methyl-(2-((4-methylphenyl) sulfonamido)ethyl)carbamate above) in dry THF (20 mL), a 2 M solution of $LiAlH_4$ in THF (3.2 mL, 6 mmol) was added dropwise under nitrogen. The reaction was heated under reflux for 4 h and then 1 mL water was added and left the reaction mixture stirred for another 2 h. The product was extracted with chloroform (3 × 30 mL) and the combined organic fractions were washed with brine (2 × 30 mL) and dried over $MgSO_4$, concentrated by rotary evaporation to give a crude product which was further purified on a silica gel column to give white solid. Yield = 226 mg (66%). ^{1}H NMR (400 MHz, $CDCl_3$): δ_H 2.29 (s, 3H), 2.42 (s, 3H), 2.66 (t, *J* = 5.6 Hz, 2H), 2.99 (t, *J* = 5.4 Hz, 2H), 7.30 (d, *J* = 8.0 Hz, 2H), 7.75 (d, *J* = 8.1 Hz, 2H). ESI-MS: *Calcd* for $[C_{10}H_{16}N_2O_2S + H]^+$ 229.0 *m/z*, found: 229.1 *m/z*.

N-(2-(Dimethylamino)ethyl)-4-methylbenzenesulfonamide (**TsEnMe$_2$**)

This was obtained following the protocol described in the literature.[5c] A solution of N, N-dimethylethane-1,2-diamine (0.42 mL, 4.5 mmol) in dichloromethane (80 mL) was placed in a round-bottom flask. A solution of toluenesulfonyl chloride (572 mg, 4.5 mmol) in DCM (50 mL) was added slowly via a dropping funnel, and the mixture was stirred vigorously for another 4 h in the ice bath. The solution was then washed with water (3 × 25 mL), and dried over $MgSO_4$. The solvent was removed on a rotary evaporator to give a white solid. Yield = 490 mg (45%). ^{1}H NMR (400 MHz, $CDCl_3$): δ_H 2.56 (s, 6H), 2.44 (s, 3H), 2.48 (t, *J* = 6.9 Hz, 2H), 2.97 (t, *J* = 6.8 Hz, 2H), 7.40 (d, *J* = 8.0 Hz, 2H), 7.75 (d, *J* = 8.2 Hz, 2H). ESI-MS: *Calcd* for $[C_{11}H_{18}N_2O_2S + H]^+$ 243.1 *m/z*, found: 243.1 *m/z*.

N-(2-(Ethylamino)ethyl)-4-methylbenzenesulfonamide (**TsEnEt**)

This was obtained following the method described in the literature.[5c] A solution of N-ethylethylenediamine (0.737 mL, 7 mmol) in dichloromethane (100 mL) was placed in a round-bottom flask. A solution of toluenesulfonyl chloride (1 g, 5.2 mmol) in DCM (50 mL) was added slowly via a dropping funnel, and the mixture was stirred vigorously for 12 h. The product was washed with brine (2 × 30 mL) and dried over $MgSO_4$, and concentrated by rotary evaporation to give a crude product which was further purified on a silica gel column (MeOH: DCM, 1: 9 (v/v)) to give white solid. Yield = 667 mg (53%). ^{1}H NMR (300 MHz, MeOD-d_4): δ_H 1.29 (t, *J* = 7.2 Hz, 3H), 2.43 (s, 3H), 3.02 (q, *J* = 7.4 Hz, 14.6 Hz, 2H), 3.08–3.12 (m, 4H), 7.41 (d, *J* = 7.6 Hz, 2H), 7.77 (d, *J* = 7.7 Hz, 2H). ESI-MS: *Calcd* for $[C_{11}H_{18}N_2O_2S + H]^+$ 243.1 *m/z*, found: 243.1 *m/z*.

N-(2-(Benzylamino)ethyl)-4-methylbenzenesulfonamide (**TsEnBz**)

This was obtained following the method described in the literature.[5c] A solution of N-benzylethylenediamine (0.94 mL, 6.24 mmol) in dichloromethane (100 mL) was placed in a round-bottom flask. A solution of toluenesulfonyl chloride (1 g, 5.2 mmol) in DCM (50 mL) was added slowly via a dropping funnel, and the mixture was stirred vigorously for 12 h. The product was washed with brine (2 × 30 mL) and dried over $MgSO_4$, and concentrated by rotary evaporation to give a crude product which was further purified on a silica gel column (MeOH: DCM, 1: 9 (v/v)) to give white solid. Yield = 696 mg (44%). ^{1}H NMR (300 MHz, MeOD-d_4): δ_H 2.44 (s, 3H), 3.07 (t, *J* = 5.3 Hz, 2H), 3.14 (t, *J* = 5.2 Hz, 2H), 4.15 (s, 2H), 7.40–7.47 (m, 7H), 7.77 (d, *J* = 7.6 Hz, 2H). ESI-MS: *Calcd* for $[C_{16}H_{20}N_2O_2S + H]^+$ 305.1 *m/z*, found: 305.1*m/z*.

N-(2-((4-Fluorobenzyl)amino)ethyl)-4-methylbenzenesulfonamide (**4-F-BzEnTs**)

This was obtained following the method described in the literature.[7] A solution of N-(2-aminoethyl)-4-methylbenzenesulfonamide (TsEn) (500 mg, 2.33 mmol) and triethylamine (1.63 mL, 11 mmol) in dichloromethane (100 mL) was placed in a round-bottom flask. A solution of 1-(bromomethyl)-4-fluorobenzene (0.29 mL, 2.3 mmol) in DCM (50 mL) was added slowly via a dropping funnel, and the mixture was stirred vigorously for 12 h. The product was washed with brine (2 × 30 mL) and dried over $MgSO_4$, and concentrated by rotary evaporation to give a crude product which was further purified by silica gel column (MeOH: DCM, 1: 9 (v/v)) to give white solid. Yield = 400 mg (54%). ^{1}H NMR (300 MHz, MeOD-d_4): δ_H 2.41 (s, 3H), 2.63 (t, *J* = 6.2 Hz, 2H), 2.97 (t, *J* = 6.2 Hz, 2H), 3.67 (s, 2H), 7.03 (t, *J* = 8.1 Hz, 2H), 7.29 (t, *J* = 6.7 Hz, 2H), 7.35 (d, *J* = 7.7 Hz, 2H), 7.71 (d, *J* = 7.4 Hz, 2H). ESI-MS: *Calcd* for $[C_{16}H_{19}FN_2O_2S + H]^+$ 323.1 *m/z*, found: 323.1 *m/z*.

4-Methyl-N-(2-((naphthalen-2-ylmethyl)amino)ethyl)benzenesulfonamide (**TsEnNaph**)

This was obtained following the method described in the literature.[7] A solution of TsEn (500 mg, 2.33 mmol) and triethylamine (1.63 mL, 11 mmol) in dichloromethane (100 mL) was placed in a round-bottom flask. A solution of 2-(bromomethyl)naphthalene (500 mg, 2.33 mmol) in DCM (50 mL) was added slowly via a dropping funnel, and the mixture was stirred vigorously for 12 h. The product was washed with brine (2 × 30 mL) and dried over $MgSO_4$, and concentrated by rotary evaporation to get crude product and further purified on a silica gel column (MeOH: DCM, 1: 9 (v/v)) to give white solid. Yield = 355 mg (54%). ^{1}H NMR (300 MHz, MeOD-d_4): δ_H 2.34 (s, 3H), 2.65 (t, *J* = 6.2 Hz, 2H), 3.00 (t, *J* = 6.2 Hz, 2H), 3.83 (s, 2H), 7.26 (d, *J* = 7.7 Hz, 2H), 7.40-7.47 (m, 3H), 7.67-7.71 (m, 3H), 7.79-7.84 (m, 3H). ESI-MS: *Calcd* for $[C_{20}H_{22}N_2O_2S + H]^+$ 355.1 *m/z*, found: 355.1 *m/z*.

N-(*t*-Boc)-ethylenediamine[5c]

A solution of *t*-Boc-anhydride (6.1 g, 28 mmol) in dichloromethane (250 mL) was added drop-wise over 2 h to a solution of ethylenediamine (11.2 mL, 166.7 mmol) in dichloromethane (50 mL) during which the mixture slowly turned cloudy. The mixture was stirred overnight at ambient temperature. The solvent was removed on a rotary evaporator to obtain a yellow oil which was redissolved in aqueous sodium carbonate (500 mL) and extracted with dichloromethane. The organic layer was dried over Na_2SO_4, filtered and concentrated in vacuum to afford a yellow oil. Yield = 3.63 g (81%). ^{1}H NMR (300 MHz, $CDCl_3$): δ_H 1.44 (s, 9H), 2.80 (t, J = 5.9 Hz, 2H), 3.17 (m, 2H), 4.85 (s, 1H).

N-(*t*-Boc)-N'-(2-aminoethyl)methylensulfonamid[5c]

A solution of methane sulfonyl chloride (1.85 mL, 25.8 mmol) in dichloromethane (25 mL) was added drop-wise over 45 min to a solution of *t*-Boc-protected ethylenediamine prepared above (3.6 g, 22.7 mmol) and triethylamine (5 mL). The reaction mixture was stirred overnight at ambient temperature. The solution was washed with water, dried over $MgSO_4$ and filtered. After removal of the solvent on a rotary evaporator, a yellow oil was obtained. A white powder precipitated after washing with diethyl ether. Yield = 2.83 mg (52.3%). ^{1}H NMR (300 MHz, $CDCl_3$): δ_H 1.44 (s, 9H), 2.97 (s, 3H), 3.29-3.31 (m, 4H), 4.89 (s, 1H).

N-(2-Aminoethyl)methylensulfonamide (**MsEn**)[5c]

To a cooled solution (273 K) of *t*-Boc protected N-(2-aminoethyl)methylenesulfonamide (2.83 g, 11.87 mmol) in dry dichloromethane (50 mL) was added 3.11 mL of triflic acid (5 mol equiv) under a N_2 atmosphere. The reaction mixture was stirred for 5 h at room temperature during which a white precipitate gradually formed. The solvent was removed on a rotary evaporator to give an orange oil which was washed with diethyl ether to precipitate an orange powder.

After filtration, the orange product was washed with ether to remove the triflic acid and a white powder was collected by filtration. Yield = 1.56 g (95%). ^{1}H NMR (400 MHz, D_2O): δ_H 3.10 (s, 3H), 3.16 (t, *J* = 5.7 Hz, 2H), 3.42 (t, *J* = 5.7 Hz, 2H).

N-(2-(Benzylamino)ethyl)-4-nitrobenzenesulfonamide (4-NO_2-PhEnBz)[5c]

A solution of N-benzylethylenediamine (0.214 mL, 1.43 mmol) in dichloromethane (100 mL) was placed in a round-bottom flask. A solution of 4-nitrobenzenesulfonyl chloride (0.3 g, 1.36 mmol) in DCM (50 mL) was added slowly via a dropping funnel, and the mixture was stirred vigorously for 12 h. The solvent was removed on a rotary evaporator and further purified by silica gel column (MeOH: DCM, 1: 9 (v/v)) to give white solid. Yield = 246 mg (54%). ^{1}H NMR (400 MHz, $CDCl_3$): δ_H 2.73 (t, *J* = 5.8 Hz, 2H), 3.05 (t, *J* = 5.8 Hz, 2H), 3.67 (s, 2H), 7.21 (d, *J* = 6.8 Hz, 2H), 7.28-7.33 (m, 3H), 7.99 (d, *J* = 8.9 Hz, 2H), 8.30 (d, *J* = 8.6 Hz, 2H); ESI-MS: *Calcd* for $[C_{15}H_{17}N_3O_4S + H]^+$ 336.1 *m/z*, found: 335.9 *m/z*.

N-(2-(Benzylamino)ethyl)-4-fluorobenzenesulfonamide(4-F-PhSulEnBz)[5c]

A solution of N-benzylethylenediamine (0.278 mL, 1.85 mmol) in dichloromethane (100 mL) was placed in a round-bottom flask. A solution of 4-fluorobenzenesulfonyl chloride (0.3 g, 1.54 mmol) in DCM (50 mL) was added slowly via a dropping funnel, and the mixture was stirred vigorously for 12 h. The solvent was removed on a rotary evaporator and further purified by silica gel column (MeOH: DCM, 1: 9 (v/v)) to get white solid. Yield = 270 mg (57%). ^{1}H NMR (400 MHz, $CDCl_3$): δ_H 2.71 (t, *J* = 5.8 Hz, 2H), 3.00 (t, *J* = 5.8 Hz, 2H), 3.66 (s, 2H), 7.15 (t, *J* = 8.6 Hz, 2H), 7.22 (d, *J* = 6.9 Hz, 2H), 7.28-7.33 (m, 3H), 7.83-7.86 (m, 2H); ESI-MS: *Calcd* for $[C_{15}H_{17}FN_2O_2S + H]^+$ 309.1 *m/z*, found: 308.8 *m/z*.

N-(2-(Benzylamino)ethyl)benzenesulfonamide (**PhSulEnBz**)[5c]

A solution of N-benzylethylenediamine (0.50 mL, 3.33 mmol) in dichloromethane (100 mL) was placed in a round-bottom flask. A solution of 4-fluorobenzenesulfonyl chloride (0.212 mL, 1.664 mmol) in DCM (50 mL) was added slowly via a dropping funnel, and the mixture was stirred vigorously for 12 h. The solvent was removed on a rotary evaporator and further purified by silica gel column (MeOH: DCM, 1: 9 (v/v)) to give a white solid. Yield = 323 mg (67%). ^{1}H NMR (400 MHz, $CDCl_3$): δ_H 2.67 (t, *J* = 5.8 Hz, 2H), 3.00 (t, *J* = 5.8 Hz, 2H), 3.62 (s, 2H), 7.19-7.21 (m, 2H), 7.22-7.24 (m, 1H), 7.28-7.31 (m, 2H), 7.45-7.48 (m, 2H), 7.52-7.56 (m, 1H), 7.82-7.85 (m, 2H); ESI-MS: *Calcd* for $[C_{15}H_{18}N_2O_2S + H]^+$ 291.1 *m/z*, found: 290.8 *m/z*.

N-(2-(Benzylamino)ethyl)-5-(dimethylamino)naphthalene-1-sulfonamide (**DanEnBz**).[5c]

A solution of N-benzylethylenediamine (0.267 mL, 1.78 mmol) in dichloromethane (100 mL) was placed in a round-bottom flask. A solution of dansyl chloride (400 mg, 1.483 mmol) in DCM (50 mL) was added slowly via a dropping funnel, and the mixture was stirred vigorously for 12 h. The solvent was removed on a rotary evaporator and further purified by silica gel column (MeOH: DCM, 4: 96 (v/v)) to get white solid. Yield = 324 mg (57%). ^{1}H NMR (400 MHz, MeOD-d_4): δ_H 2.51 (t, *J* = 6.2 Hz, 2H), 2.87 (s, 6H), 2.99 (t, *J* = 6.2 Hz, 2H), 3.46 (s, 2H), 7.09 (d, *J* = 6.6 Hz, 2H), 7.20-7.28 (m, 4H), 7.55-7.60 (m, 2H), 8.21 (dd, *J* = 0.9 Hz, 7.2 Hz, 1H), 8.33 (d, *J* = 8.6 Hz, 1H), 8.56 (d, *J* = 8.5 Hz, 1H); ESI-MS: *Calcd* for $[C_{21}H_{26}N_3O_2S + H]^+$ 384.1 *m/z*, found: 384.2 *m/z*.

2.2.3.2 Synthesis of Biguanide Related Ligands in Chapter 6[5c]

4-Methyl-N-(N-(N-(o-tolyl)carbamimidoyl)carbamimidoyl)benzenesulfonamide (TsTolBig)

A solution of 1-(o-tolyl)biguanide (360 mg, 1.88 mmol) in dichloromethane (150 mL) was placed in a round bottom flask. A solution of toluenesulfonyl chloride (300 g, 1.58 mmol) in dichloromethane (50 mL) was added slowly via a dropping funnel, and the mixture stirred vigorously for 12 h. Solvent was removed on a rotary evaporator to give a white solid which was purified by chromatography column (MeOH: DCM, 7: 93 (v/v)). Yield = 294 mg (54 %). ^{1}H NMR (400 MHz, MeOD-d_4): δ_H 2.23 (s, 3H), 2.40 (s, 3H), 7.19-7.23 (m, 3H), 7.28 (d, *J* = 6.8 Hz, 1H), 7.32 (d, *J* = 8.0 Hz, 2H), 7.76 (d, *J* = 8.2 Hz, 2H). ESI-MS: *Calcd* for $[C_{16}H_{19}N_5O_2S + Na]^+$ 368.1 *m/z*, found: 368.1 *m/z*.

4-(Bromomethyl)-N-(N-(N-(o-tolyl)carbamimidoyl)carbamimidoyl) benzenesulphonamide (4-BrCH$_2$-PhSulTolBig)

This ligand was obtained following the method described above using 400 mg of 1-(o-tolyl)biguanide and 470 mg of 4-(bromomethyl)benzene sulfonyl chloride. Yield = 252 mg (34%). ^{1}H NMR (400 MHz, DMSO-d_6): δ_H 2.15 (s, 3H), 4.73 (s, 2H), 7.17 (d, *J* = 7.3 Hz, 2H), 7.24 (d, *J* = 7.0 Hz, 2H), 7.59 (d, *J* = 8.2 Hz, 2H), 7.80 (d, *J* = 8.4 Hz, 2H). ESI-MS: *Calcd* for $[C_{16}H_{18}BrN_5O_2S + H]^+$ 446.0 *m/z*, found: 446.2 *m/z*.

4-Fluoro-N-(N-(N-(o-tolyl)carbamimidoyl)carbamimidoyl)benzenesulfonamide (4-F-PhSulTolBig)

This ligand was obtained following the method described above using 400 mg of 1-(o-tolyl)biguanide and 340 mg of 4-fluoro-benzenesulfonyl chloride. Yield = 390 mg (64%). ^{1}H

NMR (400 MHz, MeOD-d_4): δ_H 2.24 (s, 3H), 7.19-7.26 (m, 5H), 7.28 (d, *J* = 6.6 Hz, 1H), 7.91-7.94 (m, 2H). ESI-MS: *Calcd* for $[C_{15}H_{16}FN_5O_2S + Na]^+$ 372.0 *m/z*, found: 371.9 *m/z*.

4-Nitro-N-(N-(N-(o-tolyl)carbamimidoyl)carbamimidoyl)benzenesulfonamide (4-NO_2-PhSulTolBig)

This ligand was obtained following the method described above using 360 mg of 1-(o-tolyl)biguanide and 300 mg of 4-nitro-benzenesulfonyl chloride. Yield = 240 mg (47%). ^{1}H NMR (400 MHz, DMSO-d_6): δ_H 2.17 (s, 3H), 7.01 (t, *J* = 6.8 Hz, 1H), 7.26 (dd, *J* = 7.6 Hz, 22 Hz, 3H), 8.05 (d, *J* = 8.4 Hz, 2H), 8.34 (d, *J* = 3.4 Hz, 2H). ESI-MS: *Calc* for $[C_{15}H_{16}N_6O_4S + H]^+$ 377.1 *m/z*, found: 376.9 *m/z*.

5-(Dimethylamino)-N-(N-(N-(o-tolyl)carbamimidoyl)carbamimidoyl) naphthalene-1-sulfonamide (DanTolB)

This ligand was obtained following the method described above using 354 mg of 1-(o-tolyl)biguanide and 300 mg of dansyl chloride. Yield = 251 mg (53%). ^{1}H NMR (400 MHz, MeOD-d_4): δ_H 2.05 (s, 3H), 2.86 (s, 6H), 7.11-7.16 (m, 2H), 7.20-7.26 (m, 3H), 7.33 (t, *J* = 7.9 Hz, 1H), 7.54 (t, *J* = 8.3 Hz, 1H), 8.23 (d, *J* = 6.6 Hz, 1H), 8.41 (d, *J* = 8.7 Hz, 1H), 8.49 (d, *J* = 8.5 Hz, 1H). ESI-MS: Calc for $[C_{21}H_{24}N_6O_2S + H]^+$ 425.1 *m/z*, found: 425.0 *m/z*.

2.3 Instruments and Assays

2.3.1 Nuclear Magnetic Resonance Spectroscopy (NMR)

NMR spectra were acquired in 5 mm NMR tubes at 298 K on either Bruker HD-300, HD-400 or AV III 600 spectrometers. Data processing was carried out using Topspin-NMR version 2.1 (Bruker U.K. Ltd.). ^{1}H NMR chemical shifts were internally referenced to TMS via 1, 4-dioxane in D_2O (δ = 3.75 ppm) or residual MeOD-d_4 (δ = 3.31 ppm), $CDCl_3$ (δ = 7.26 ppm),

or DMSO-d_6 (δ = 2.50 ppm). 1D spectrum were recorded using standard pulse sequences. Typically, data were acquired with 16 transients into 32 k data points over a spectral width of 14 ppm; and 32 transients into 32 k data points over a spectral width of 30 ppm using a relaxation delay of 2 s for the kinetic experiment.

2.3.2 UV-vis Spectroscopy

UV-vis spectra were recorded on a Varian Cary 300 UV-vis spectrometry using a 1 cm path-length quartz cuvette with a PTP1 Peltier temperature controller. Spectra were monitored over a width of 200-800 nm, bandwidth of 1.0 nm and a scan rate of 600 nm/min.

2.3.3 Portable pH Meter

A minilab IQ125 pH meter equipped with an ISFET silicon chip pH sensor and referenced in KCl gel was used to measure the pH. The electrode was calibrated with Aldrich buffer solutions of pH 4, 7 and 10. pH^* values (pH meter reading without correction for the effect of deuterium on chip sensor) of NMR samples in D_2O were measured at 298 K. pH^* values were adjusted with KOD or DNO_3 solutions in D_2O. pH values of the reaction mixtures and UV-Vis samples in H_2O were also measured at 298 K. pH values were adjusted with KOH or HNO_3 solutions.

2.3.4 X-ray Crystallography

X-ray diffraction data were collected and the structures solved by Dr Guy Clarkson at the University of Warwick.

Diffraction data were collected on an Oxford Diffraction Gemini four-circle system with a Ruby CCD area detector. All structures were refined by full-matrix least squares against F^2 using SHELXL[8] and were solved by direct methods using SHELXS[9] (TREF) with additional light atoms found by Fourier methods. Anisotropic displacement parameters were used for all

non-H atoms; H-atoms were given an isotropic displacement parameter equal to 1.2 (or 1.5 for methyl and NH H-atoms) times the equivalent isotropic displacement parameter of the atom to which they are attached. The data were processed by the modelling program Mercury 3.8.

To assess whether the bond distances were statistically different (when the difference between was greater than 3σ).

$\sigma = \sqrt{(\sigma_1^2+\sigma_2^2)}$;

where σ_1 and σ_2 are the standard deviations of the bond lengths compared.

2.3.5 Elemental Analysis

Elemental analyses were performed by Warwick Analytical Service using an Exeter Analytical elemental analyzer (CE440).

2.3.6 Electrospray Ionization Mass Spectrometry (ESI-MS)

Low resolution positive ion electrospray mass spectra were obtained on an Agilent 6130B ion mass spectrometer. All samples were prepared in methanol (95 %)/water or methanol (100%). And filtered before testing. Mass spectra were recorded with a scan range of 50 to 1000 m/z.

2.3.7 High Resolution Mass Spectrometry (HR-MS)

All the samples was analysed by Dr. Lijiang Song and Mr Philip Aston.

High resolution positive-ion mass spectra were obtained on a Bruker Maxis Q-TOF. All the samples were analised by positive electrospray ionization mass spectra. All samples were prepared in double deionised water (ddw), methanol/water (95%), or methanol (100%). Injection of 2 μL min^{-1}, nebuliser gas (N_2) 0.4 bar, dry gas (N_2) 4 L min^{-1}, dry temp. 453 K, capillary -3000 V (positive mode) end plate offset -500 V. Capillary exit 166 V, funnel RF 300

vpp, Multiplole RF 300 vpp, quadrupole ion energy 4 eV, Collision cell 1200 eV, ion cooler RF settins, ramp from 50 to 250 V. Mass spectra were recorded with a scan range of 50 to 3000 m/z.

2.3.8 High Performance Liquid Chromatography (HPLC)

HPLC analysis was performed on a HP 1200 Series HPLC System (Agilent) with a 100 μL loop, using an Agilent ZORBAX Eclipse Plus C_{18} (250 × 4.6 mm, 5 μm pore size) column. The mobile phases include A: water (HPLC grade, Sigma-Aldrich) containing 0.1% trifluoroacetic acid, and B: acetonitrile (HPLC grade, Sigma-Aldrich) containing 0.1% trifluoroacetic acid. Gradients of t = 0 min (10% B), t = 30 min (80% B), t = 40 min (80% B), t = 41 min (10% B) and t = 55 min (10% B) over a 55 min period. Flow rate was 1 mL/min. A wavelength was detected at 254 nm with the reference wavelength at either 360 or 510 nm was used. Samples were prepared in doubly deionized water (DDW) or a mixture methanol (5%, HPLC grade)/ddw. Sample injections were half of the loop volume (50 μL).

2.3.9 Liquid Chromatography–Mass Spectrometry (LC-MS)

LC-MS was performed on a HP 1200 Series HPLC System (Agilent) coupled to a Bruker HCT-Ultra ETD II PTR PTM mass spectrometer. The column used was an Agilent ZORBAX Eclipse Plus C-18 (4.6 × 250 mm, 5 μm pore size). The mobile phases were A: water (HPLC grade, Sigma-Aldrich, with 0.1% TFA), and B: acetonitrile (HPLC grade, Sigma-Aldrich, with 0.1% TFA). Specific gradients are described in the corresponding chapter. Samples were prepared in DDW. Sample injections were 50 μL. The mass spectrometer was operated in electrospray positive mode with scan range 50-2000 *m/z*, and related parameters are: Nebuliser gas (N_2) 40 psi, dry gas (N_2) 10 L/min, dry temp. 573 K, HV capillary -4000 V (positive mode) end plate offset -500 V, capillary exit 166 V, and Octapole RF 200 Vpp.

2.3.10 Inductively Coupled Plasma−Optical Emission Spectrometry (ICP-OES)

ICP-OES analyses were carried out on a PerkinElmer Optima 5300 DV series ICP-OES instrument. The DDW was used for ICP-OES analysis from a Millipore Milli-Q water purification system and a USF Elga UHQ water deionizer. Standards for Ru, Os or Ir were purchased from Inorganic Ventures, Fluka or Alfa Asar, respectively. The Ru and Ir Specupure plasma standards were diluted with 3.6% v/v HNO_3, Os standards were diluted with 3.6% v/v HNO_3 containing thiourea and ascorbic acid as stabilizers,[10] to freshly prepare calibrants at concentrations of 50-700 ppb. Calibration standards were adjusted to match the salinity of the samples by standard addition of sodium chloride–(TraceSELECT®) solution.

2.3.11 Inductively Coupled Plasma−Mass Spectrometry (ICP-MS)

ICP-MS analysis were carried out on an Agilent Technologies 7500 series ICP-MS instrument. The water used for ICP-MS analysis was the same for the ICP-OES water source. The Ru and Ir Specpure plasma standards were diluted with 3.6% v/v HNO_3, Os standards were diluted with 3.6% v/v HNO_3 containing thiourea and ascorbic acid as stabilizers,[10] and calibrants were freshly prepared at concentrations of 0.1-500 ppb. The ICP-MS instrument was set to detect ^{101}Ru, ^{189}Os or ^{193}Ir in no gas mode.

2.3.12 Cellular Biological Study *in Vitro*

All the biological experiments were performed by Dr. Isolda Romero-Caneón, Ji-Inn Song and Bindy Heer at the University of Warwick. General antiproliferative assays are outlined below, for the specific protocols will be described in appropriate chapters.

2.3.13 *In Vitro* Growth Inhibition Assays

The antiproliferative activity were determined in A2780 ovarian cancer cells. Briefly, 5,000 cells per well were seeded in 96-well plates. The plates were left to pre-incubate with drug-free medium at 310 K for 48 h before adding different concentrations of the tested complexes. Exact complex concentrations were determined by ICP-OES. A drug exposure period of 24 h was allowed. After this, supernatants were removed by suction and each well was washed with PBS. A further 72 h were allowed for the cells to recover in drug-free medium at 310 K. Cell viability was determined by the sulforhodamine B (SRB) assay. IC_{50} values, as the concentration that causes 50% cell death, were determined as duplicates of triplicates in two independent sets of experiments and their standard deviations were calculated.

2.3.14 Cellular Accumulation

Cellular accumulation studies were performed on A2780 ovarian cancer cells. 1.5×10^6 cells per well were seeded on a six-well plate. After 24 h of pre-incubation in drug-free medium at 310 K, cells were exposed to complexes at equipotent IC_{50} concentrations for 24 h. After this time, drug solutions were removed by suction, and cells were washed with PBS and then treated with trypsin-EDTA. A suspension of single cells was counted, and cell pellets were collected. Each pellet was digested overnight in freshly-distilled concentrated nitric acid (72% v/v) at 353 K; the resulting solutions were diluted with double-distilled water to a final concentration of 3.6% v/v HNO_3 (thiourea and L-ascorbic acid used as stabilizers for solutions containing Os^{10}),

and the amount of Ru in A2780 ovarian cells was determined by ICP-MS. These experiments did not include any cell recovery time in drug-free media; they were carried out in triplicate, and the standard deviations were calculated.

2.3.15 Co-administration of Ru Complexes with Formate

Cell viability assays were carried out in A2780 ovarian cancer cells. These experiments were carried out with the following modifications: a fixed concentration of each Ru complex equal to 1/3 × IC_{50} was used in coadministration with three different concentrations of sodium formate (0.5, 1.0 and 2.0 mM). Drug stock solutions (*ca.* 100 μM) were prepared as described for *in vitro* growth inhibition assays. The stocks were further diluted using media until working concentrations were achieved. Separately, a stock solution of sodium formate was prepared in saline. The complex and formate solutions were added to each well independently, but within 5 min of each other.

2.4 References

(1) a) Betanzos-Lara, S.; Liu, Z.; Habtemariam, A.; Pizarro, A. M.; Qamar, B.; Sadler, P. J. *Angew. Chem. Int. Ed.* **2012**, *51*, 3897-3900; b) Liu, Z.; Habtemariam, A.; Pizarro, A. M.; Fletcher, S. A.; Kisova, A.; Vrana, O.; Salassa, L.; Bruijnincx, P. C. A.; Clarkson, G. J.; Brabec, V.; Sadler, P. J. *J. Med. Chem.* **2011**, *54*, 3011-3026; c) Björgvinsson, M.; Halldorsson, S.; Arnason, I.; Magull, J.; Fenske, D. *J. Organomet. Chem.* **1997**, *544*, 207-215.

(2) a) Zelonka, R. A.; Baird, M. C. *Can. J. Chem.* **1972**, *50*, 3063-3072; b) Habtemariam, A.; Melchart, M.; Fernández, R.; Parsons, S.; Oswald, I. D. H.; Parkin, A.; Fabbiani, F. P. A.; Davidson, J. E.; Dawson, A.; Aird, R. E.; Jodrell, D. I.; Sadler, P. J. *J. Med. Chem.* **2006**, *49*, 6858-6868; c) Harvey, R. G.; Lindow, D. F.; Rabideau, P. W. *J. Am. Chem. Soc.* **1972**, *94*, 5412-5420.

(3) a) Needham, R. J.; Sanchez-Cano, C.; Zhang, X.; Romero-Canelón, I. Habtemariam, A.; Cooper, M. S.; Meszaros, L.; Clarkson, G. J.; Blower, P. J.; Sadler, P. J. *Angew. Chem. Int. Ed.* **2017**, *56*, 1017-1020; b) Fu, Y.; Romero, M. J.; Habtemariam, A.; Snowden, M. E.; Song, L.; Clarkson, G. J.; Qamar, B.; Pizarro, A. M.; Unwin, P. R.; Sadler, P. J. *Chem. Sci.* **2012**, *3*, 2485-2494.

(4) Tönnemann, J.; Risse, J.; Grote, Z.; Scopelliti, R.; Severin, K. *Eur. J. Inorg. Chem.* **2013**, *2013*, 4558-4562.

(5) a) Wu, X.; Liu, J.; Li, X.; Zanotti-Gerosa, A.; Hancock, F.; Vinci, D.; Ruan, J.; Xiao, J. *Angew. Chem. Int. Ed.* **2006**, *45*, 6718-6722; b) Li, X.; Li, L.; Tang, Y.; Zhong, L.; Cun, L.; Zhu, J.; Liao, J.; Deng, J. *J. Org. Chem.* **2010**, *75*, 2981-2988; c) Soldevila-Barreda, J. J.; Bruijnincx, P. C. A.; Habtemariam, A.; Clarkson, G. J.; Deeth, R. J.; Sadler, P. J. *Organometallics* **2012**, *31*, 5958-5967.

(6) Martins, J. E. D.; Clarkson, G. J.; Wills, M. *Org. Lett.* **2009**, *11*, 847-850.

(7) Gabano, E.; Cassino, C.; Bonetti, S.; Prandi, C.; Colangelo, D.; Ghiglia, A.; Osella, D. *Org. Biomol. Chem.* **2005**, *3*, 3531-3539.

(8) Sheldrick, G. M. SHELXL-97, University of Gottingen: Gottingen.

(9) Sheldrick, G. M. *Acta Crystallogr* **2007**, *A64*, 112-122.

(10) Venzago, C.; Popp, M.; Kovac, J.; Kunkel, A. *J. Anal. At. Spectrom.* **2013**, *28*, 1125–1129.

Chapter 3

Ru^{II} Arene Anticancer Catalysts for Transfer Hydrogenation of Coenzyme NAD^+ by Formate

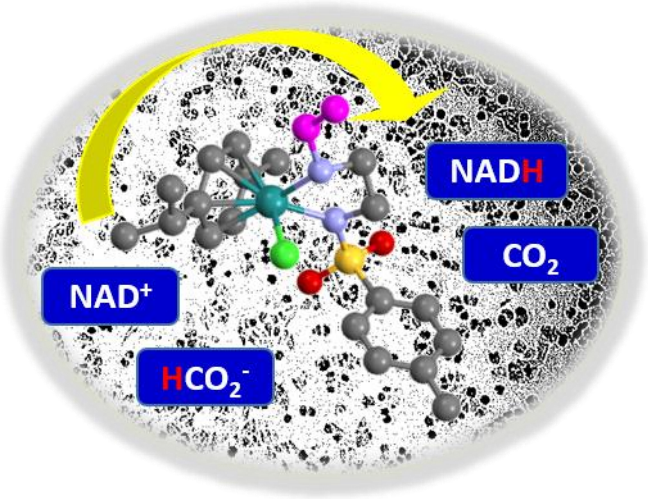

3.1 Introduction

Nicotinamide adenine dinucleotide (NAD^+) and its reduced form (NADH), as well as their phosphorylated derivatives, $NADP^+$ and NADPH, are important coenzymes,[1] involving in over 400 enzymatic redox reactions.[2] The reduction of pyridine salts (*e.g.* NAD^+) to dihydropyridine compounds (*e.g.* NADH) is of the critical importance for energy storage and release in cell metabolism.[2b,2c] Over the last three decades, organometallic complexes-mediated catalytic reduction of NAD^+ to NADH using hydrogen,[3] 2-propanol,[4] glycerol[5] and sodium formate as hydride donors has been intensively studied.[6] Compared to reduction with H_2 (hydrogenation), transfer hydrogenation (TH) reactions possess the advantage of being simpler, without any high external pressure, readily available and safer-to-handle.[7] Also, TH reduction of $NAD(P)^+$ artificially has attracted wide interest as an *in vitro* mimic for enzymatic reactions performed under biologically relevant conditions.[8]

The pathways of hydride transfer between pyridine salts and dihydropyridine compounds are also of interest. The first mechanistic study of the TH reduction of BNA^+ (1-benzylnicotinamide, a model for NAD^+) was reported by Steckhan and Fish *et al.* using [(η^5-Cp*)Rh(bipy)Cl] as catalyst and sodium formate as hydride source.[6b,6d,9] A catalytic cycle involving a Cp* ring-slipped intermediate with Rh coordinated to the amide of the pyridine ring was proposed.[10] Knör *et al.* revealed a Rh coordinated poly(arylene-ethynylene)-*alt*-poly(arylene-vinylene) polymer as photocatalyst for the reduction of NAD^+; involving a possible photoexcited polymer chain being quenched and transferring an electron to the Rh^{III} active center.[11] More recently, a mechanism involving hydride transfer to Cp* and formation of Rh^I intermediate [(η^4-Cp*-H)Rh(($CH_2OH)_2$-bipy)]$^+$ followed by hydride transfer from the endo orientation of the C-H bond to maintain the 1,4-regioselectivity of NADH was discovered Yoon and coworkers.[12]

The half-sandwich ruthenium complex [(η^6-*p*-cym)Ru(TsDPEN)Cl] (TsDPEN: N-((1S,2S)-2-amino-1,2-diphenylethyl)-4-methylbenzenesulfonamide) was reported by Noyori and coworkers in 1995.[13] Potent catalytic activity was shown in asymmetric TH reduction of aromatic ketones. However, the hydrophobic nature of the two phenyl groups on the ethylene backbone limits its application as a possible catalyst for TH reduction of NAD^+ under biologically relevant conditions. Complexes with chelating diamine ligands such as **RM175** in **Figure 3.1**, display good aqueous solubility but poor catalytic activity in TH reduction of NAD^+.[14] But complexes with functional sulfonyl substituents such as [(η^6-*p*-cym)Ru(TsEn)Cl] (*e.g.* **JS2** in **Figure 3.1**),[15] exhibit good solubility in water and improved catalytic activity for TH reduction of NAD^+ in aqueous media. Moreover, coadministration of [(η^6-*p*-cym)Ru (TsEn)Cl] with low non-cytotoxic dose of sodium formate led to an enhancement of the antiproliferative activity against A2780 human ovarian cancer cells by up to 50×.[8, 16]

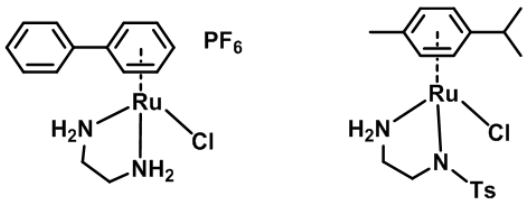

RM175 **JS2**

Figure 3.1 Organometallic Ru^{II} complexes [(η^6-biph)Ru(en)Cl]PF_6 (**RM175**) and [(η^6-*p*-cym) Ru(TsEn)Cl] (**JS2**).

In this chapter, the effect on catalysis of formate reduction of NAD^+ of substituents on the amino group of the *N*,*N*-chelating TsEn ligand in Ru^{II} complexes [(η^6-*p*-cym)Ru(*N*,*N'*)Cl] where *N*,*N'* is N-(2-(methylamino)ethyl)-4-toluenesulfonamide (TsEnMe, **1**), N-(2-(dimethyl amino)ethyl)-4-toluenesulfonamide ($TsEnMe_2$, **2**), N-(2-(ethylamino)ethyl)-4-toluenesulfon amide (TsEnEt, **3**), N-(2-(benzylamino)ethyl)-4-toluenesulfonamide (TsEnBz, **4**), N-(2-((4-fluorobenzyl)amino) ethyl)-4-toluenesulfonamide (4-F-BzTsEn, **5**) and N-(2-((naphthalen-2-

ylmethyl)amino)ethyl)-4-toluenesulfonamide (TsEnNaphth, **6**) (**Chart 3.1**) have been investigated. In addition, the catalytic mechanism was investigated both experimentally and by density functional theory (DFT) calculations, and the effect of formate on the antiproliferative activity of these complexes against A2780 human ovarian cancer cells.

Chart 3.1 Ru^{II} complexes studied in this chapter

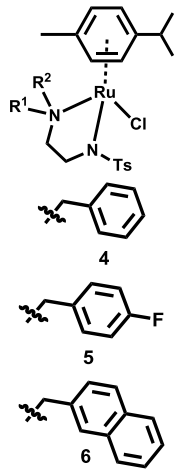

Complex	R^1	R^2
1	H	Me
2	Me	Me
3	H	Et
4	H	Bz
5	H	4-F-Bz
6	H	Naphth (NA)

3.2 Experimental Section

3.2.1 Materials and Methods

Toluenesulfonyl chloride, sodium formate and *β*-nicotinamide adenine dinucleotide hydrate (NAD^+) were obtained from Sigma-Aldrich. Magnesium sulfate, potassium hydroxide, sodium chloride, and hydrochloric acid were obtained from Fisher Scientific. *α*-Phellandrene was purchased from SAFC. The Ru^{II}-arene precursor dimers $[(p\text{-cym})RuCl_2]_2$,[17] as were the ligands 4-methyl-N-(2-(methylamino)ethyl)benzenesulphon- amide (TsEnMe),[18] N-(2-(dimethyl amino)ethyl)-4-methylbenzenesulfonamide ($TsEnMe_2$).[19] The solvents used for NMR spectroscopy were purchased from Sigma-Aldrich and Cambridge Isotope Laboratories Inc. Non-dried solvents used in syntheses were obtained from Fisher Scientific.

3.2.2 Synthesis of the Ru^{II} Complexes

$[(\eta^6\text{-}p\text{-cym})Ru(TsEnMe)Cl]$ (1). All Ru^{II} complexes were prepared according to related reported methods:[12] $[(p\text{-cym})RuCl_2]_2$ (100 mg, 0.163 mmol) and TsEnMe (80 mg, 0.35 mmol) were placed in a round-bottom flask to which 2-propanol (100 mL) and triethylamine (91 μL, 0.653 mmol) were added. The solution was heated (365 K) in a nitrogen atmosphere for 12 h with stirring. After this the solvent was removed on a rotary evaporator to give a dark red solid. The crude product was re-dissolved in dichloromethane and was washed with brine after which the organic solvent was dried over $MgSO_4$ and filtered. A dark red solid was obtained after removal of DCM and recrystallized from methanol and diethyl ether (1:4). Yield = 72 mg (44.3%). **^{1}H NMR** (400 MHz, $CDCl_3$): δ_H 1.26 (d, J = 6.9 Hz, 3H), 1.32 (d, J = 6.9 Hz, 3H), 2.20 (s, 3H), 2.16-2.27 (m, 1H), 2.33 (s, 3H), 2.52-2.55 (m, 1H), 2.89-2.96 (m, 1H), 3.06 (d, J = 6.1 Hz, 3H), 3.09 (s, 1H), 3.54 (s, 1H), 5.33 (t, J = 4.5 Hz, 2H), 5.56 (s, 1H), 5.85 (s, 1H), 7.14 (d, J = 7.9 Hz, 2H), 7.71 (d, J = 7.9 Hz, 2H). **^{13}C NMR** (125.8 MHz, $CDCl_3$): δ_C 19.0,

21.4, 22.0, 23.0, 30.7, 44.5, 48.3, 58.8, 127.6, 128.5, 140.1, 140.4. HR-MS: *Calcd* for $[C_{20}H_{29}N_2O_2SRu]^+$ 463.0993 *m/z*, found: 463.0992 *m/z*. Elemental analysis: *Calcd* for $[C_{20}H_{29}ClN_2O_2SRu]$: C, 48.23%; H, 5.87%; N, 5.62%. Found: C, 48.11%, H 5.81%; N, 5.50%.

[(η^6-*p*-cym)Ru(TsEnMe$_2$)Cl] (2). Complex **2** was obtained following the method described in literature using the ligand TsEnMe$_2$ (84.7 mg, 0.35 mmol).[20] Recrystallization from methanol and diethyl ether resulted in bright wine red solid. Yield = 75 mg (45%). **^{1}H NMR** (400 MHz, MeOD-d$_4$): δ_H 1.62 (d, *J* = 6.9 Hz, 6H), 1.53 (dd, *J* = 2.7 Hz, 11.1 Hz, 1H), 2.32 (d, *J* = 5.0 Hz, 6H), 2.49 (dd, *J* = 5.4 Hz, 12.5 Hz, 1H), 2.76-2.84 (m, 1H), 2.90 (s, 3H), 2.98-3.05 (m, 1H), 3.06 (s, 3H), 3.19-3.29 (m, 1H), 5.14 (d, *J* = 5.8 Hz, 1H), 5.25 (d, *J* = 5.8 Hz, 1H), 5.76 (d, *J* = 5.0 Hz, 1H), 5.84 (d, *J* = 5.7 Hz, 1H), 7.14 (d, *J* = 8 Hz, 2H), 7.93 (d, *J* = 8.1 Hz, 2H). **^{13}C NMR** (125.8 MHz, CDCl$_3$): δ_C 18.8, 21.4, 22.2, 22.6, 30.7, 47.0, 54.8, 55.9, 63.7, 128.3, 128.7, 139.9, 140.5. HR-MS: *Calcd* for $[C_{21}H_{31}N_2O_2SRu]^+$ 477.1150 *m/z*, found: 477.1153 *m/z*. Elemental analysis: *Calcd* for $[C_{21}H_{31}ClN_2O_2SRu]$: C, 49.26%; H, 6.10%; N, 5.47%. Found: C, 48.85%; H, 6.32%; N, 5.35%.

[(η^6-*p*-cym)Ru(TsEnEt)Cl] (3). Complex **3** was obtained following the method described above for complex **1** using the ligand TsEnEt (97 mg, 0.40 mmol). Recrystallization from methanol and diethyl ether resulted in bright wine red solid. Yield = 108 mg (65%). **^{1}H NMR** (400 MHz, CDCl$_3$): δ_H 1.27 (d, *J* = 6.8 Hz, 3H), 1.27-1.35 (m, 6H), 2.15 (d, *J* = 7.8 Hz, 2H), 2.20 (s, 3H), 2.33 (s, 3H), 2.73 (d, *J* = 4.0 Hz, 1H), 2.87-2.94 (m, 1H), 3.12 (d, *J* = 6.9 Hz, 1H), 3.15-3.24 (m, 2H), 3.59-3.63 (m, 1H), 5.32-5.36 (m, 2H), 5.51 (s, 1H), 5.90 (s, 1H), 7.14 (d, *J* = 7.9 Hz, 2H), 7.21 (d, *J* = 7.9 Hz, 2H). **^{13}C NMR** (125.8 MHz, CDCl$_3$): δ_C 14.9, 19.0, 21.4, 22.0, 23.0, 30.8, 48.3, 51.8, 54.9, 127.6, 128.5, 140.0, 140.4. HR-MS: *Calcd* for $[C_{21}H_{31}N_2O_2SRu]^+$ 477.1150 *m/z*, found: 477.1153 *m/z*. Elemental analysis: *Calcd* for $[C_{21}H_{31}ClN_2O_2SRu]$: C, 49.26%; H, 6.10%; N, 5.47%. Found: C, 48.24%; H, 6.06%; N, 5.36%.

[(η^6-*p*-cym)Ru(TsEnBz)Cl] (4). Complex **4** was obtained following the method described above for complex **1** using the ligand TsEnBz (106.4 mg, 0.35 mmol). Crude product was Purified by silica column chromatography (ethyl acetate/hexane 2:1 (v/v)) and then recrystallized from ethyl acetate and hexane at ambient temperature, giving a bright red solid. Yield = 99.2 mg (53%). **^{1}H NMR** (400 MHz, $CDCl_3$): δ_H 1.20 (d, *J* = 6.8 Hz, 3H), 1.26 (d, *J* = 6.8 Hz, 3H), 1.91-1.97 (m, 1H), 2.02-2.08 (m, 1H), 2.13 (s, 3H), 2.22 (s, 3H), 2.13 (d, *J* = 10.1 Hz 1H), 2.83-2.88 (m, 1H), 2.94 (d, *J* = 10.9 Hz, 1H), 3.70 (t, *J* = 9.5 Hz, 1H), 4.03 (t, *J* = 10.8 Hz, 1H), 4.64 (d, *J* = 13.1 Hz, 1H), 5.41 (s, 1H), 5.74 (s, 1H), 7.03 (d, *J* = 7.8 Hz, 2H), 7.17-7.20 (m, 3H), 7.26 (s, 3H), 7.59 (d, *J* = 7.9 Hz, 2H). **^{13}C NMR** (125.8 MHz, $CDCl_3$): δ_C 19.1, 21.4, 21.9, 23.1, 30.9, 48.2, 54.7, 61.5, 127.6, 128.4, 128.5, 128.7, 129.2, 135.8, 139.9, 140.4. HR-MS: *Calcd* for $[C_{26}H_{33}N_2O_2SRu]^+$ 539.1306 *m/z*, found: 539.1307 *m/z*. Elemental analysis: *Calcd* for $[C_{26}H_{33}ClN_2O_2SRu]$: C, 54.39%; H, 5.79%; N, 4.88%. Found: C, 54.37%; H, 5.82%; N, 4.82%.

[(η^6-*p*-cym)Ru(TsEn(4-F-Bz)Cl] (5). Complex **5** was obtained following the method described above for complex **1** using the ligand TsEn(4-F-benzyl) (200 mg, 0.621 mmol) and $[(p\text{-cym})RuCl_2]_2$ (184 mg, 0.3 mmol). A bright red solid was obtained by following the purification method for complex **5**. Yield = 124 mg (34%). **^{1}H NMR** (300 MHz, $CDCl_3$): δ_H 1.30 (d, *J* = 6.8 Hz, 3H), 1.36 (d, *J* = 6.9 Hz, 3H), 2.00-2.16 (m, 2H), 2.02-2.08 (m, 1H), 2.23 (s, 3H), 2.32 (s, 3H), 2.38-2.41 (m, 1H), 2.91-3.00 (m, 1H), 3.05 (d, *J* = 12.0 Hz, 1H), 3.76 (t, *J* = 9.6 Hz, 1H), 4.10 (t, *J* = 12.0 Hz, 1H), 4.72 (d, *J* = 14.2 Hz, 1H), 5.40-5.42 (m, 2H), 5.51 (s, 1H), 5.84 (s, 1H), 7.06 (t, *J* = 8.3 Hz, 2H), 7.13 (d, *J* = 7.5 Hz, 3H), 7.26-7.30 (m ,2H), 7.69 (d, *J* = 7.3 Hz, 2H). **^{13}C NMR** (125.8 MHz, $CDCl_3$): δ_C 19.1, 21.4, 21.9, 23.1, 31.0, 48.2, 54.5, 60.6, 116.1, 116.3, 127.6, 128.5, 130.3, 130.3, 131.6, 131.7, 139.8, 140.4, 161.7, 163.7. **^{19}F NMR** (376.4 MHz, $CDCl_3$, referenced to CF_3COOH, at -76.55 ppm): -112.3. HR-MS: *Calcd* for $[C_{26}H_{32}FN_2O_2SRu]^+$ 557.1212 *m/z*, found: 557.1213 *m/z*. Elemental analysis: *Calcd* for

[$C_{26}H_{32}ClFN_2O_2SRu$]: C, 52.74%; H, 5.45%; N, 4.73%. Found: C, 52.20%; H, 5.34%; N, 4.67%.

[(η^6-*p*-cym)Ru(TsEnNA)Cl] (6). Complex **6** was obtained following the method described above for complex **1** using the ligand TsEn-naphthalene (272 mg, 0.77 mmol) and [(*p*-cym)$RuCl_2$]$_2$ (235.2 mg, 0.38 mmol). A dark red solid was obtained by following the purification method for complex **5**. Yield = 156 mg (33%). **^{1}H NMR** (300 MHz, $CDCl_3$): δ_H 1.32 (d, *J* = 7.1 Hz, 3H), 1.37 (d, *J* = 9.0 Hz, 3H), 2.02-2.10 (m, 1H), 2.16-2.28 (m, 3H), 2.32 (s, 3H), 2.42-2.45 (m, 1H), 2.94-3.10 (m, 2H), 3.94-4.11 (m, 1H), 4.23-4.34 (m, 1H), 4.90 (d, *J* = 14.2 Hz, 1H), 5.42 (s, 2H), 5.50-5.59 (m, 1H), 5.84-5.87 (m, 1H), 7.13 (d, *J* = 8.1 Hz, 2H), 7.37 (d, *J* = 8.5 Hz, 2H), 7.51-7.53 (m, 2H), 7.69-7.71 (m, 2H), 7.81-7.86 (m, 2H). **^{13}C NMR** (125.8 MHz, $CDCl_3$): δ_C 19.1, 21.4, 21.9, 23.2, 31.0, 48.2, 54.8, 61.6, 125.5, 126.8, 126.9, 127.6, 127.7, 127.8, 127.8, 127.9, 128.5, 129.3, 129.3, 133.1, 133.2, 139.9, 140.4. HR-MS: *Calcd* for [$C_{30}H_{35}N_2O_2SRu$]$^+$ 589.1463 *m/z*, found: 589.1463 *m/z*. Elemental analysis: *Calcd* for [$C_{30}H_{35}ClN_2O_2SRu$]: C, 57.73%; H, 5.65%; N, 4.49%. Found: C, 56.10%; H, 5.44%; N, 4.32%.

3.2.3 TOFs Determined by UV-vis Spectroscopy

Complexes **1-6** were dissolved in MeOH/H_2O (1:9 v/v) (84 μM) in a glass vial. Solutions of sodium formate (102 mM) and NAD^+ in H_2O (510 μM) were also prepared. In a typical experiment, an aliquot of 330 μL from each solution was added to a 1 mL cuvette bringing the total volume to 1 mL (final concentrations were Ru complex 28 μM; NAD^+ 170 μM; $NaHCO_2$ 34 mM; molar ratio 1:6:1200), and the pH was adjusted to 7.2 before the sample was introduced into the UV-vis instrument. UV spectra are recorded every 5 min until completion of the reaction. The spectrum was monitored by following an absorbance in the band at 340 nm, which corresponds to the absorption of NADH.

3.2.4 TOFs Determined by NMR Spectroscopy

Solutions of complexes in MeOD-d_4/D_2O (1:4 v/v) (1.4 mM), sodium formate (35 mM) and NAD^+ in D_2O (5.6 mM) were prepared in separate vials. An aliquot of 200 μL from each solution was added into a 5 mm NMR tube, getting the final volume to 0.64 mL (Ru complex 0.44 mM; NAD^+ 1.75 mM; $NaHCO_2$ 10.94 mM; molar ratio 1:4:25). The pH^* was adjusted to 7.2 ± 0.1. The ^1H NMR spectrum were recorded at 310 K every 162 s until the completion of the reaction. Molar ratios of NAD^+ and NADH were determined by integrating the ^1H NMR peaks corresponding to NAD^+ (9.33 ppm) and of 1, 4-NADH (6.96 ppm). The turnover number (TON) for the reaction was calculated as follows:

$$\mathrm{TON} = \frac{I_{6.96}}{I_{6.96} + I_{9.93}} \frac{[\mathrm{NAD^+}]}{\mathrm{catalyst}}$$

where I_n is the integral of the signal at n ppm and [NAD^+] is the concentration of NAD^+ at the start of the reaction. Catalyst is the concentration of Ru^{II} complex. TOFs (h^{-1}) were determined as the slope of the linear plot of TONs versus time (h).

Another series of experiments were performed where complex **4** (3.29 mg, 0.0057 mmol) was dissolved in MeOD-d_4 (60%)/D_2O (40%) (1.4 mM) in a vial. Following the procedure used above, the kinetics of the reaction using different concentrations of sodium formate (complex **4**, NAD^+ and sodium formate in the ratio 1: 4: X, where X = 10, 25, 50, and 100 mol equiv) and different concentrations of NAD^+ (complex **4**, NAD^+ and sodium formate in ratio of 1: Y: 25, where Y = 2, 4, 6 and 10) were studied. A second series of experiments using different pH* values of the reaction solutions (5, 6, 7, 8 and 9) were also performed.

3.2.5 Interaction with DNA Nucleobases

The reaction of complex **4** (*ca.* 2 mM) with nucleobases (9-ethylguanine and adenosine 5'-monophosphate) were studied typically by addition of an aqueous solution of DNA nucleobases (1 mM each, 0.5 mol equiv) in MeOD-d_4/D_2O (1:9). The pH^* values were adjusted to 7.2 ± 0.1 with chip pH sensor, all the reactions were monitored by ^1H NMR at 310 K.

The following DNA related experiments (in **Sections 3.2.6-3.2.8**) were performed by Professor Viktor Brabec and Dr. Jana Kasparkova (Institute of Biophysics, Academy of Sciences of the Czech Republic).

3.2.6 Binding to Calf Thymus DNA

Solutions of double-helical calf thymus DNA (ct-DNA) at a concentration of 32 μg/mL were incubated with the complex **4** at a r_i value of 0.1 in $NaClO_4$ (10 mM) at 310 K (r_i is defined as the molar ratio of free Ru complex to nucleotide phosphates at the onset of incubation with DNA). The reaction was stopped after 24 h incubation, and samples were dialyzed exhaustively against water to remove unbound ruthenium (or, alternatively, free Ru complex was removed by gel filtration through a Sephadex G25 coarse column). The concentration of ruthenium associated with DNA in these samples was determined by flameless atomic absorption spectrometry (FAAS). The concentrations of DNA were determined by absorption spectrophotometry.

3.2.7 Binding to Bacterial Circular Plasmid DNA

Reaction mixtures containing plasmid DNA pBR322 (28 μg/mL) and complex **4** in various molar ratios (r_i = 0.05-1) were incubated in 0.01 M $NaClO_4$ at 310 K in the dark for 24 h. The samples were then mixed with the loading buffer and loaded onto a 1% agarose gel running at 298 K in the dark with Tris-acetate-EDTA (TAE) buffer and the voltage set at 25 V. No

separation step was included before loading the samples into the gel to catch potential noncovalent binding (if any). The gels were then stained with EtBr, followed by photography with a transilluminator.

3.2.8 Binding to Short Single- or Double-stranded Oligonucleotides

50-mer oligonucleotides (single or double stranded) were incubated with complex **4** (r_i = 1 – concentration of oligonucleotide related to phosphates) in 0.05 M $NaClO_4$ at 310 K in the dark. After 24 h, the reaction was stopped, and samples were exhaustively dialyzed against water. The ruthenium content in these samples was determined by FAAS and the concentrations of oligonucletides were determined by absorption spectrophotometry.

3.2.9 Relative Hydrophobicity

Measurements were performed utilizing the Agilent 1200 system with a VWD and 50 µL loop. The column was an Agilent Zorbax 300SB C_{18}, 150 × 4.6 mm with a 5 µm pore size. The mobile phase was H_2O (50mM NaCl)/H_2O/CH_3CN 1:1 (50 mM NaCl), with a flow of 1 mL min^{-1}. The detection wavelength was set at 254 nm with the reference wavelength at 360 nm. All compounds were dissolved in 10% MeOH/90% H_2O (v/v) in 50 mM NaCl to ensure that hydrolysis was prevented. Sample injections were the loop volume (50 µL) with needle washes of MeOH and H_2O between injections. Reported retention times (t_R) and standard deviations (SD) are from triplicate measurements. The gradient used is shown in **Figure 3.2**.

Time (min)	% B
0	20
15	100
40	100
41	20
55	20

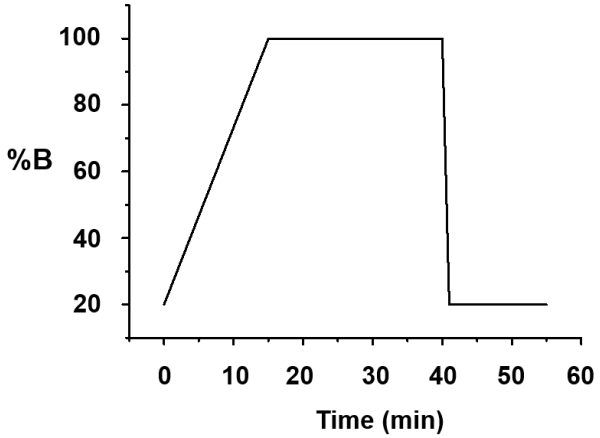

Figure 3.2 Relative hydrophobicity measurements by HPLC using H_2O 50 mM NaCl (Solvent A) and H_2O/CH_3CN 1:1 50 mM NaCl (solvent B).

3.2.10 Cellular Accumulation

The mode of action studies in **Section 3.2.10-3.2.12** were carried out by Dr. Isolda Romero-Canelon.

The accumulation studies for Ru complexes **1-6** were carried out towards A2780 ovarian cancer cells. 1.5×10^6 cells were seeded on a six-well plate. After 24 h of incubation in medium (drug-free) at 310 K, cells were exposed to complexes at equipotent IC_{50} concentrations for 24 h, without any cell recovery time in drug-free media. Drug solutions were subsequently removed by suction, cells were then washed with PBS and treated with trypsin-EDTA. A suspension of single cells was counted, and cell pellets were collected. Each pellet was digested overnight in freshly-distilled concentrated nitric acid (72%, v/v) at 353 K; the resulting solutions were diluted with doubly deionized water (DDW) to a final concentration of 3.6% v/v HNO_3, and the amount of Ru in A2780 ovarian cells was determined by ICP-MS. These experiments were carried out in triplicate, and the standard deviations were calculated.

3.2.11 Co-administration of Ru Complexes with Formate

Cell viability assays were carried out with complexes **1–6** in A2780 ovarian cancer cells with the following modifications: a fixed concentration of each Ru complex equal to $1/3 \times IC_{50}$ was co-administered with three different concentrations of sodium formate (0.5, 1.0 and 2.0 mM). Drug stock solutions (*ca.* 100 μM) were prepared as describes for *in vitro* growth inhibition assays. The stocks were further diluted using media until working concentrations were achieved. Separately, a stock solution of sodium formate was prepared in saline. The complex and formate solutions were added to each well independently, within 5 min of each.

3.2.12 ROS Determination

Flow cytometry analysis of ROS/superoxide generation in A2780 cells caused by exposure to complexes **1** and **4** was carried out using the Total ROS/Superoxide detection kit (Enzo-Life Sciences) according to the supplier's instructions. Generally, 1.5×10^6 A2780 cells per well were seeded in a six-well plate. Cells were preincubated in drug-free media at 310 K for 24 h in a 5% CO_2 humidified atmosphere, and then drugs were added in triplicates at equipotent IC_{50} concentrations. After 1 h of drug exposure, supernatants were removed by suction and cells were washed and harvested. The cell pellets were re-suspended in the orange/green fluorescent reagents buffer for staining. The fluorescence was analyzed in a Becton Dickinson FACScan flow cytometer using FL1 channel Ex/Em: 490/525 nm for the oxidative stress and FL2 channel Ex/Em: 550/620 nm for superoxide detection. Data were processed using Flowjo software. At all times, samples were kept under dark conditions to avoid light-induced ROS production.

3.2.13 DFT Computational Details

The DFT calculations were performed by Dr. Juliusz A. Wolny and Professor Volker Schünemann (Department of Physics, University of Kaiserslautern, Germany).

DFT calculations of free energy levels for species in the catalytic cycle were performed and based on the crystal structure of complex **3**. The calculations used functional CAM-B3LYP[21] with basis set CEP-31G,[22] using Gaussian 09 software.[23] Ultrafine grid of integration was used in each case. The starting geometry was taken from X-ray data for **3**, with an appropriate change of substituents for other systems. NAD^+ and NADH were modeled with N-protonated analogues of corresponding nicotinamide species. All given energy values are the result of the full geometry optimisation with the subsequent frequency calculations. The free energy level of each complex is shown in **Scheme 3.4**.

3.3 Results

3.3.1 Synthesis and Characterization

Ru^{II} complexes **1-6** were synthesized by following a reported procedure (**Scheme 3.1**).[15] Typically, trimethylamine (4 mol equiv) and ligands (*ca.* 2 mol equiv) were added to the a solution of $[(p\text{-cym})RuCl_2]_2$ in degassed isopropanol, the reactions was stirred under a N_2 atmosphere at 365 K for 12 h. All synthesized complexes were characterized by ^1H and ^{13}C NMR spectroscopy, mass spectrometry (ESI-MS) and elemental analysis (CHN). A crystal of

complex **3** suitable for X-ray analysis was obtained from diffusion of diethyl ether into methanol.

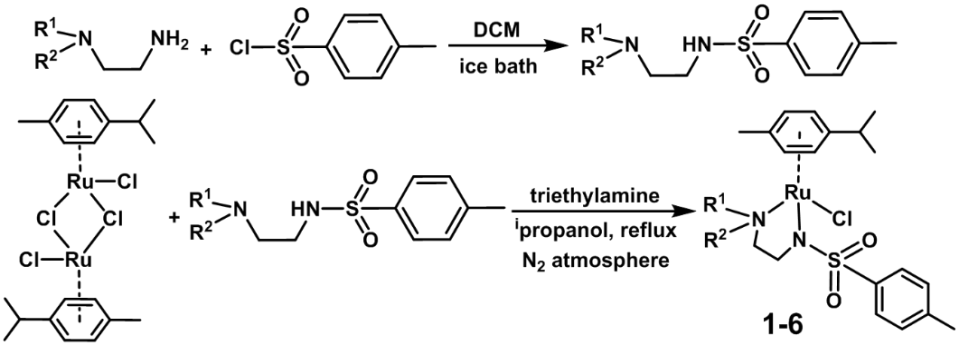

Scheme 3.1 Synthetic routes for diamine ligand and Ru^{II} complexes **1-6**.

3.3.2 X-ray Crystal Structure

Selected bond lengths and angles for complex **3** are listed in **Table 3.1**. Crystallographic data are presented in **Table 3.2**. And the structure of complex **3** is shown in **Figure 3.3**. Complex **3** adopts the *pseudo*-octahedral geometry with the η^6-bonded aromatic ring occupying 3 coordination sites. The chelating ligand is deprotonated and bonded as a monoanionic bidentate ligand. The CH_2CH_2N-Et atoms from N, N' chelated ligand (C10 C11 N12 C13) were modelled as disordered over two positions whose occupancy refined to 86:14.

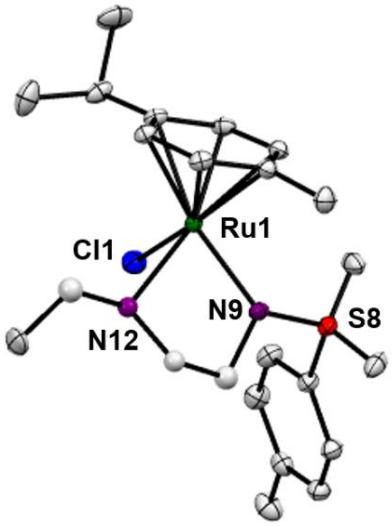

Figure 3.3 ORTEP diagrams for complex **3**. Ellipsoids are shown at the 50% probability level. All hydrogen atoms have been omitted for clarity.

Table 3.1 Selected Bond Lengths (Å) and Angles (deg) for Complex **3**.

Bonds	Length (Å) /Angle(°)
Ru1−N9	2.1256(9)
Ru1−N12	2.1702(11)
Ru1-N12A	2.157(8)
Ru1−Cl1	2.4173(3)
Ru1−arene (centroid)	1.664
N9−Ru1−N12	78.74(4)
N9−Ru1−N12A	76.1(2)
N9−Ru1−Cl1	89.47(3)
N12−Ru1−Cl1	87.55(4)

Table 3.2 Crystallographic Data for Complex **3**.

Crystal character	red block
Empirical formula	$C_{21}H_{31}ClN_2O_2RuS$
Formula weight	512.06
Temp (K)	150(2)
Crystal system	monoclinic
Space group	P21/c
a / Å	13.88136(9)
b / Å	10.43716(8)
c / Å	15.24599(11)
α / °	90
β / °	102.1274(7)
γ / °	90
Volume / Å^3	2159.57(3)
Z	4
D_{calc} (mg/cm^3)	1.575
μ / mm^{-1}	0.966
F (000)	1056.0
Crystal size/mm^3	0.6 × 0.4 × 0.06 orange block
Reflections collected	201186
Indep reflection	11305
R [I>=2σ (I)]	R^1 = 0.0273
Final R [all data]	R^2 = 0.0629

3.3.3 Hydrolysis and pK_a^* Determination

The hydrolysis of complex **4** was studied by dissolving the Ru^{II} complex in MeOD-d_4/D_2O (1.4 mM, 1/9(v/v)). The ^1H NMR spectrum remained unchanged after 24 h and the hydrolysis was assumed to be rapid since the peaks could be assigned to the aqua Ru^{II} species (**4a**) by comparison to those from the aqua species generated in a reaction with silver nitrate in D_2O (1 molar equiv).[15] The pK_a^* (pK_a value determined in deuterated solvent) of complex **4a** was determined by a pH* (meter reading) titration ranging from 2 to 12 by addition of NaOD and DNO_3 solutions. Changes in the chemical shift of the proton of toluene arene ^1H NMR resonance were followed and the data were fitted to the Henderson−Hasselbalch equation, giving a pK_a^* value of 9.73 ± 0.06 (see **Figure 3.4**).

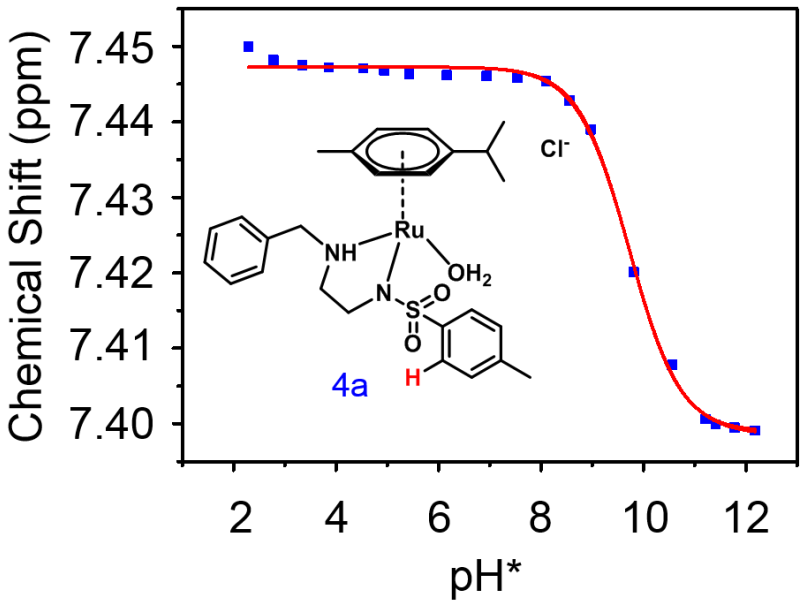

Figure 3.4 Dependence of the ^1H NMR chemical shift of the proton of toluene arene on pH* of aqua complex **4a**.

3.3.4 DNA Nucleobase Binding

The interaction of complex **4** with DNA nucleobase models: 9-ethylguanine (9-EtG) and adenosine 5'-monophosphate (5'-AMP) were studied by ^{1}H NMR spectroscopy (see **Figure 3.5**). The reactions were performed by adding nucleobase solution (3 mM in D_2O) to Ru^{II} complex solution (2 mM in 10% MeOD-d_4/90% D_2O) at 310 K, to give a final 1.5:1 mol ratio. The formation of adducts **4**-9-EtG was confirmed by following the new set of peaks, and up to 90% yield of adduct was obtained when 1.5 mol equiv 9-EtG solution was added. However, no adduct was found when 1.5 mol equiv of 5'-AMP was added to complex **4**, even after 24 h incubation at 310 K.

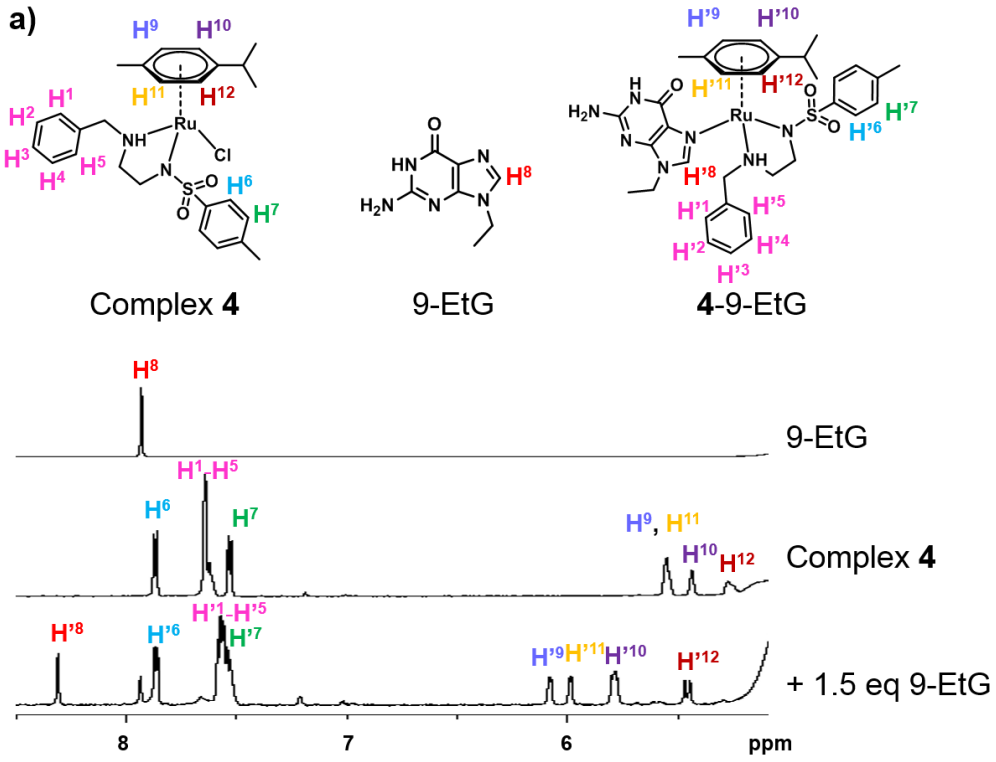

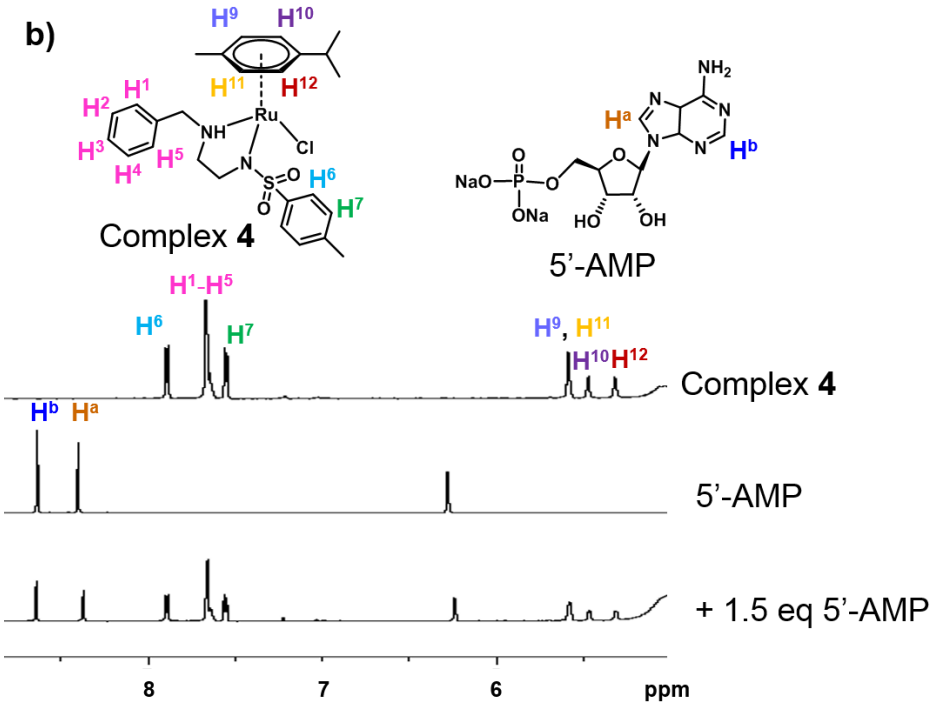

Figure 3.5 Low field protons of complex **4** (2 mM) on reaction with a) 9-ethylguanine (9-EtG) b) adenosine 5'-monophosphate (5'-AMP, 3 mM, 1.5 mol equiv) in 10% MeOD-d_4/90% D_2O, pH at 7.2, 310 K, followed by ^{1}H NMR.

3.3.5 Kinetics of Transfer Hydrogenation Reactions

The reduction of coenzyme nicotinamide adenine dinucleotide (NAD^+) to NADH was investigated in an aqueous medium using complexes **1-6** as catalysts and sodium formate as the hydride source. Initially, the reactions were studied by UV-visible spectroscopy under conditions of pH 7.2 ± 0.1, 310 K and MeOH/H_2O 1:9 (v/v); in all the cases, an increase of intensity of the band at 340 nm was observed, assignable to formation of NADH (see **Figure 3.6**). The kinetics of conversion were monitored by ^{1}H NMR at 310 K and pH* 7.2 ± 0.1. The reactions were performed in a mixed solvent MeOD-d_4/D_2O (1:4 v/v), due to the poor aqueous solubility of complexes **5** and **6**.

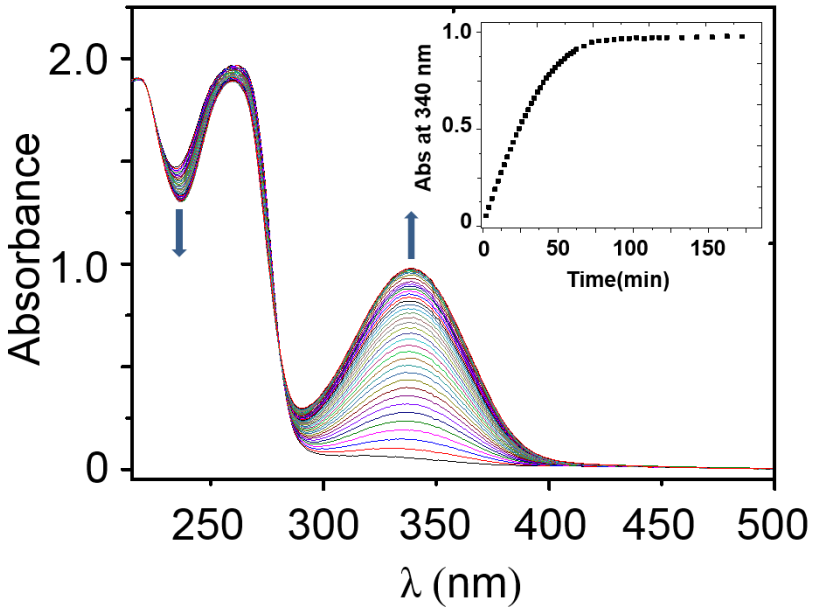

Figure 3.6 Monitoring of kinetics of TH reaction of NAD^+ to NADH catalysed by complex **4** using sodium formate as hydride source by UV-vis spectroscopy (complex **4** 28 µM; NAD^+ 170 µM; $NaHCO_2$ 34 mM; mol ratio 1:6:1200, $MeOH/H_2O$, 1:9 (v/v), pH 7.2, 310 K), and increase in absorbance at 340 nm (inset).

Table 3.3 Turnover Frequencies for Transfer Hydrogenation Reactions Using Ru complexes **1**−**6** as Catalysts.

Complex	R^1	R^2	TOF(h^{-1})[a]	TOF(h^{-1})[b]
1	H	Me	2.97 ± 0.04	4.0 ± 0.3
2	Me	Me	3.9 ± 0.1	4.1 ± 0.1
3	H	Et	4.3 ± 0.1	5.9 ± 0.2
4	H	Bz	7.4 ± 0.1	7.7 ± 0.3
5	H	4-F-Bz	7.1 ± 0.1	6.5 ± 0.4
6	H	Naphth	6.1 ± 0.9	4.9 ± 0.5

[a]By UV-vis spectroscopy.
[b]By NMR spectroscopy.

The dependence of the rate of catalysis for six pH^* values ranging from 5 to 9 was determined for complex **4** at a mol ratio complex **4**: NAD^+: formate of 1: 4: 25, respectively, in the same mixed solvent at 310 K (see **Figure 3.7**). The TOF was relatively insensitive to pH^* over the

range pH^* 6-8 (*ca.* 7.5 h^{-1}), but decreased slightly at lower and higher pH^* (5.6 h^{-1} at pH^* 5, 6.6 h^{-1} at pH^* 9).

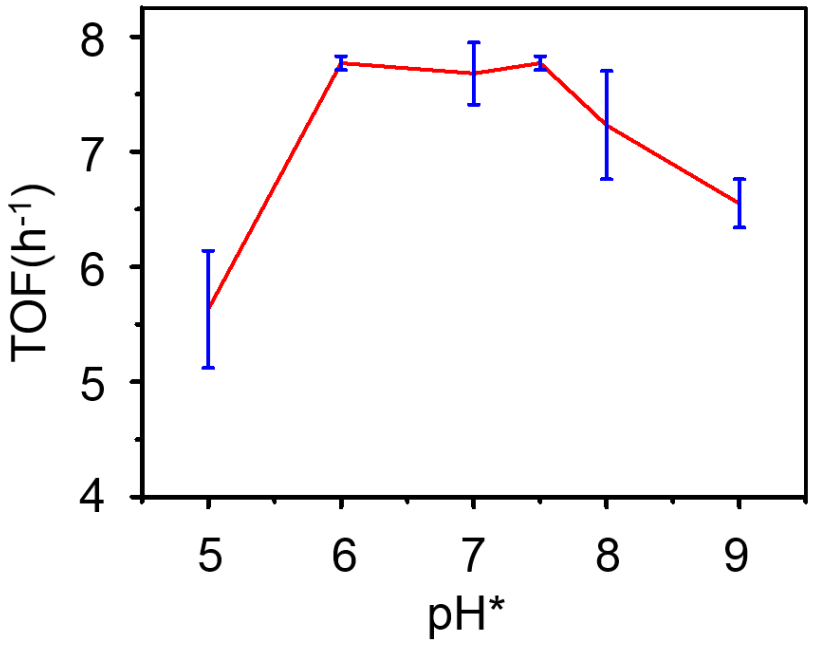

Figure 3.7 Dependence of turnover frequency on pH^* for the reduction of NAD^+ by complex **4** using formate as a hydride source (molar ratio of NAD^+: complex **4**: formate = 4:1:25, 310 K in MeOD-d_4/D_2O (2:8 v/v)).

The dependence of turnover frequency on the concentrations of sodium formate and NAD^+ was investigated for complex **4** in MeOD-d_4/D_2O (1:4) at 310 K. The mol ratio of complex **4**, NAD^+ and sodium formate was 1: 4: X, respectively, where X = 5, 10, 25, 50 and 100 (see **Figure 3.8**). The TOF increased steadily from 2.2 h^{-1} to 18.8 h^{-1} as the excess of formate increased from 7 mM to 140 mM. Next the dependence of TOF on the NAD^+ concentration was studied for mol ratio complex **4**: NAD^+: formate = 1: Y: 25, where Y = 2, 6 and 10. The TOF was found to be independent of NAD^+ concentration (7.7 ± 0.5 h^{-1}).

The Michaelis−Menten kinetic behaviour is apparent from a plot of turnover frequency versus formate concentration. A reciprocal plot of turnover frequency versus sodium formate concentration gave a Michaelis constant of K_M = 0.086 mM (see **Figures 3.8** and **3.9**).

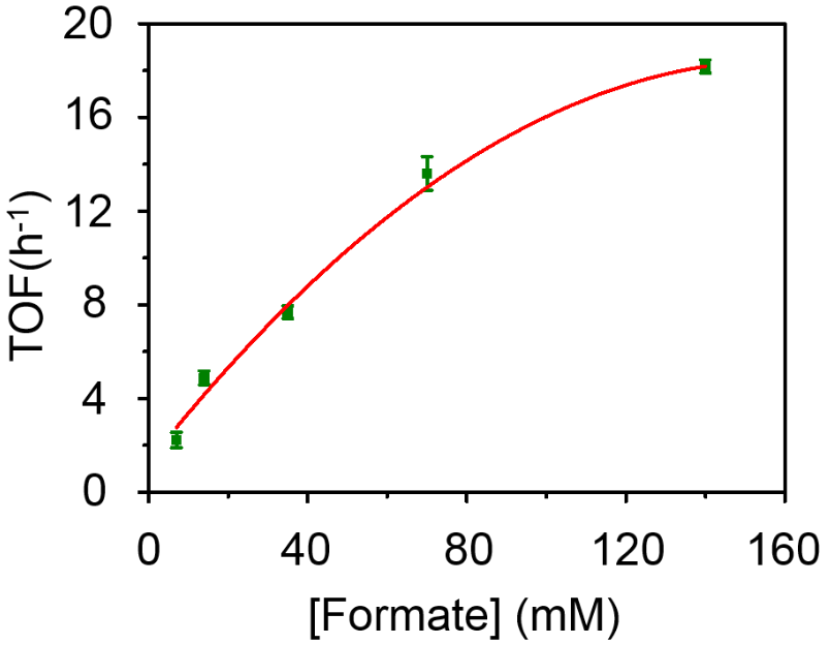

Figure 3.8 Dependence of the reaction rate on the concentration of sodium formate for the transfer reduction of NAD^+ catalysed by complex **4** (molar ratio of NAD^+, complex **4** and sodium formate is 4:1:X, respectively, where X = 5, 10, 25, 50 and 100, at 310 K in MeOD-d_4/D_2O (2:8)).

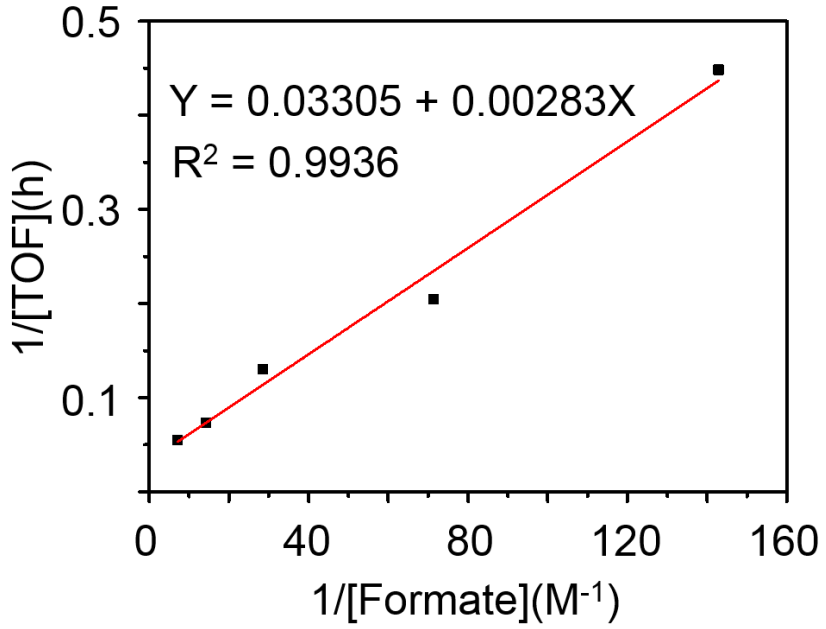

Figure 3.9 Plot of the reciprocal of the TOF against sodium formate concentration for the reduction of NAD^+ in the presence of various mol equiv of formate, catalyzed by complex **4**. For a reaction following Michaelis-type kinetics, TOF = $TOF_{max}[S]/(K_M + [S])$, where TOF_{max}

is the turnover frequency at infinite substrate (formate) concentration, [S] is the substrate concentration, and K_M is the Michaelis constant. Hence, $TOF^{-1} = (K_M/TOF_{max})(1/[S]) + (1/TOF_{max})$, and K_M and TOF_{max} can be obtained from the gradient and y intercept, respectively, of the double-reciprocal plot.

3.3.6 Antiproliferative Activity

The antiproliferative activity of complexes **1**−**6** towards A2780 human ovarian cancer cells was determined in comparison with the clinically approved drug cisplatin, **Figure 3.10**. The IC_{50} values (50% inhibition of cell growth) range from 1 to 6.5 μM for complexes containing aromatic R substituents (**4-6**), whereas those containing aliphatic R substituents are less potent with IC_{50} values of 12-31 μM. The complex [(η^6-*p*-cym)Ru(TsEnBz)Cl] (**4**) (IC_{50}, 1.0 μM) has a potency similar to cisplatin in this cell line (CDDP, 1.20 ± 0.02 μM).

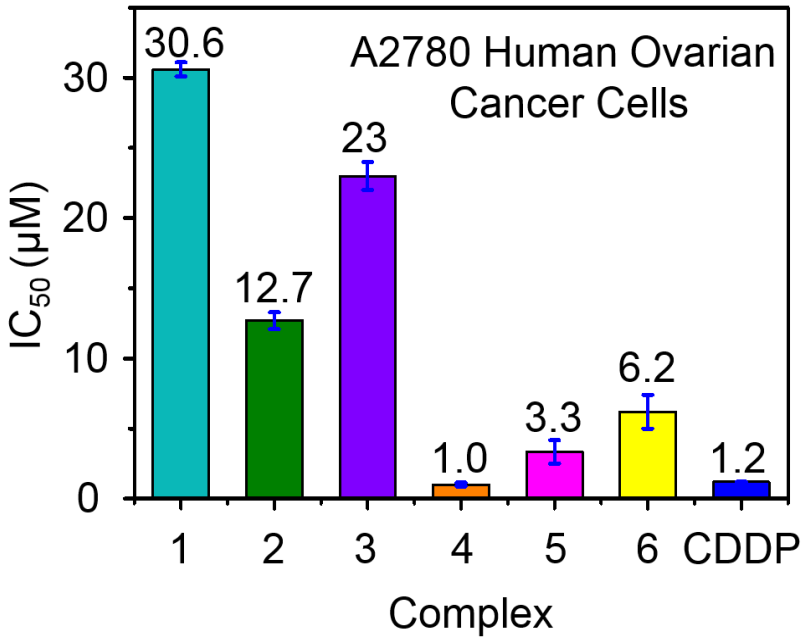

Figure 3.10 Antiproliferative activity of Ru^{II} complexes **1-6** and cisplatin towards A2780 human ovarian cancer cells.

3.3.7 Antiproliferative Activity in the Presence of Sodium Formate

The antiproliferative activity of Ru^{II} complexes in A2780 human ovarian cancer cells in the presence of sodium formate was investigated (see **Figure 3.11**). Firstly, the cytotoxicity of sodium formate alone towards A2780 human ovarian cancer cells was investigated. No significant toxicity was found up to formate concentrations of 2 mM. Then, A2780 human ovarian cancer cells were coincubated with equipotent concentrations of complexes **1-6** (1/3 × IC_{50}) and three different concentrations of sodium formate (0.5, 1 and 2 mM). The antiproliferative activity of complexes **1-6** increased significantly on coincubation with 2 mM formate. The formate-induced decrease in viability of A2780 cells ranged from 20% to 36% in the presence of complex **1-6**. Interestingly for complex **6**, a 28% decrease in cell viability was observed with only 0.5 mM formate present (see **Table 3.4**).

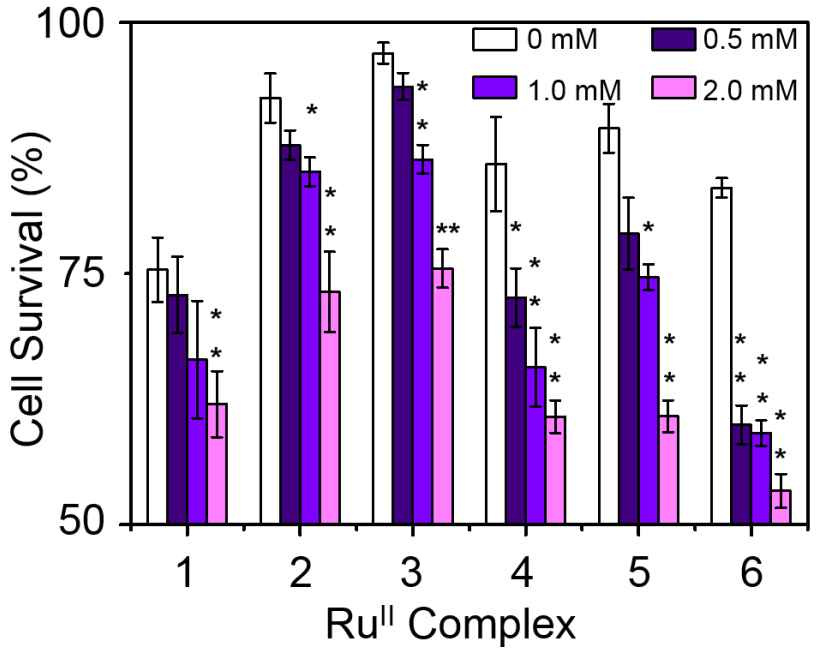

Figure 3.11 Percentage of cell survival when equipotent concentrations of complexes **1–6** (1/3 × IC_{50}) were co-administered with different concentrations of sodium formate, *p*-Values were calculated after a *t*-test against the negative control data (without sodium formate), $*p < 0.05$, $**p < 0.01$.

3.3.8 Cell Accumulation

The cellular accumulation of ruthenium in A2780 human ovarian cancer cells after exposure to complexes **1-6** at its IC_{50} equipotent concentrations was determined by inductively coupled plasma mass spectrometry (ICP-MS) and is shown in **Figure 3.12**.

Complex **4** gave the lowest cellular accumulation (0.52 ± 0.08 ng of Ru per 10^6 cells), while complex **6** with moderate anticancer activity, exhibited the highest extent of cell uptake with 4.5 ± 0.2 ng of Ru per 10^6 cells at IC_{50} concentration, 8.6x higher than complex **4**. Complexes **1-3** and **5**, gave rise to similar cell uptake 2.4 ± 0.3 ng, 1.2 ± 0.2 ng, 3.0 ± 0.2 ng and 1.3 ± 0.2 ng per 10^6 cells, respectively, following the order: **4** < **2**, **5** < **1** < **3** < **6** (see **Table 3.4**).

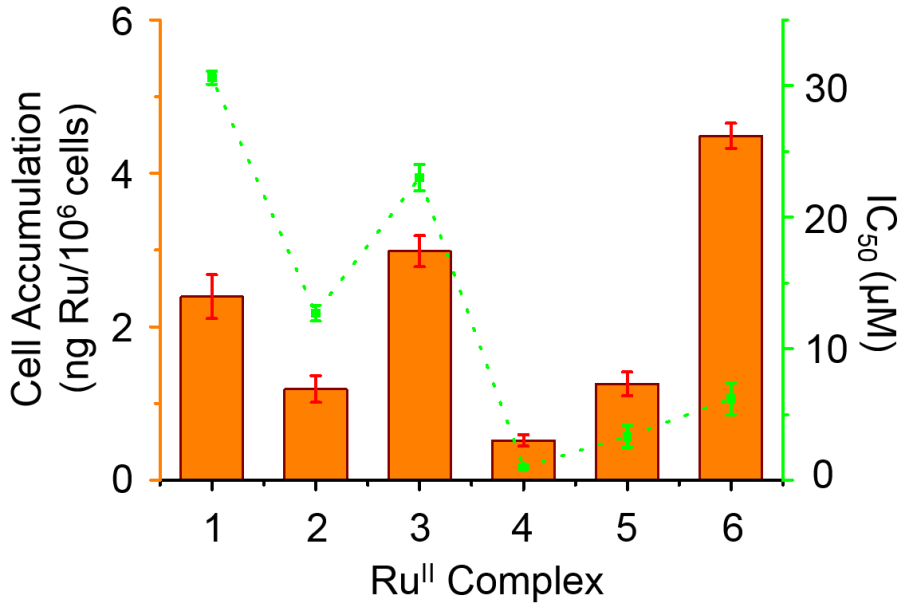

Figure 3.12 IC_{50} values (μM) for complexes **1-6** against A2780 human ovarian cancer cells (in blue) and cellular accumulations in A2780 cancer cells at equipotent IC_{50} concentrations in the absence of sodium formate (in orange).

3.3.9 Relative Hydrophobicity

The relative hydrophobicity of complexes **1-6** was determined by RP-HPLC. The more hydrophobic complexes have longer retention times on a reverse-phase C_{18} column.[24] To ensure solubility of the Ru^{II} complexes, a water/methanol mixture was used (MeOH/H_2O, 1:9 v/v) together with NaCl (50 mM) to suppress hydrolysis of the complexes. The HPLC solvents were also prepared with 50 mM NaCl present. The resulting retention times are shown in **Table 3.4**, and follow the order: **1**, **2**, **3** < **4**, **5** < **6**. Complex **3** shows the shortest retention time (least hydrophobic) of 14.0 min, while complex **6** shows the longest retention time (most hydrophobic), 20.9 min.

Table 3.4 Retention Times (t_R) of Ru^{II} Complexes **1**−**6** by RP-HPLC and Accumulation (at equipotent of IC_{50} concentrations) in A2780 Cells.

Complex	t_R (min)	Cellular-Ru (ng /10^6 cells)
1	15.4 ± 0.9	2.4 ± 0.3
2	14.5 ± 0.3	1.2 ± 0.2
3	14.0 ± 0.3	3.0 ± 0.2
4	17.4 ± 0.2	0.52 ± 0.08
5	17.27± 0.08	1.3 ± 0.2
6	20 ± 1	4.5 ± 0.2

3.3.10 ROS Induction

The levels of reactive oxygen species (ROS) were determined in A2780 human ovarian cancer cells for complexes **1** and **4** at IC_{50} concentrations by flow cytometry fluorescence analysis (see **Figure 3.13**). This included the monitoring of H_2O_2, peroxy and hydroxyl radicals, and

superoxide levels. High concentrations of total ROS and superoxide were observed in A2780 after 1 h exposure to complexes **1** and **4** when compared to negative control. The populations of cells that show high fluorescence in both FL-1 and FL-2 channels (both high total ROS and high superoxide generation) for complexes **1** and **4** are 16.5 ± 1.0 and 31.3 ± 0.3, respectively.

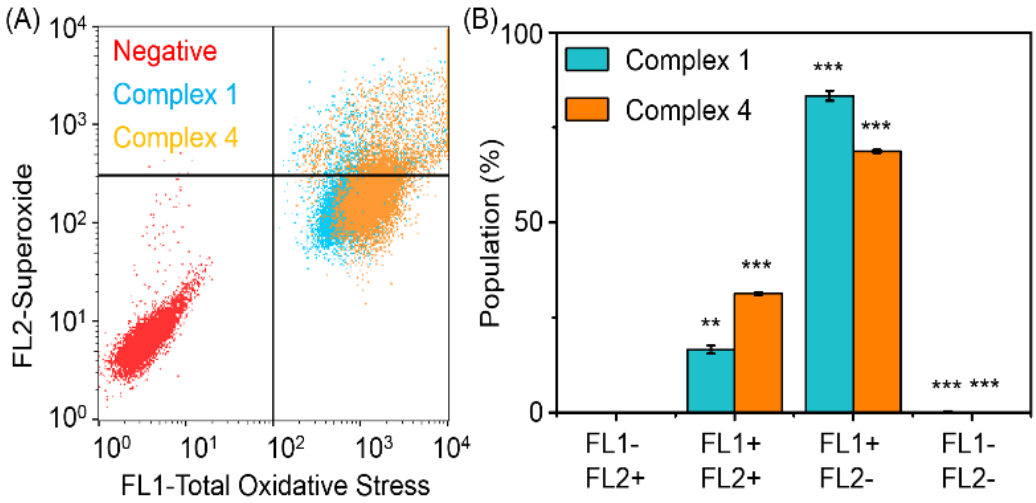

Figure 3.13 ROS in A2780 cells induced by complexes **1** and **4**, FL1 channel detects total oxidative stress, and FL2 channel detects superoxide production. (A) Induction of ROS by complexes **1** and **4**. (B) Four different populations caused by complexes **1** and **4** at equipotent IC_{50} concentrations. *p*-Values were calculated after a *t*-test against the negative control data, $^{**}p < 0.01$, $^{***}p < 0.001$.

3.3.11 Binding to Calf Thymus DNA and Bacterial Circular Plasmid DNA

Reactions of double-helical calf thymus DNA (ct-DNA, 32 µg/mL) and plasmid DNA pBR322 (28 µg/mL) with complex **4** in various molar ratios (r_i = 0.05–1, r_i = the molar ratio of free Ru to nucleotide phosphates at the onset of incubation with DNA) were studied. Very low amounts of ruthenium (5-7% of initial Ru) were found in the samples of DNA treated with complex **4** for 24 h. No significant changes in the mobilities of supercoiled (sc) or open circular (oc) form of plasmid DNA were observed even when incubated with high concentrations of complex **4** (see **Figure 3.14**).

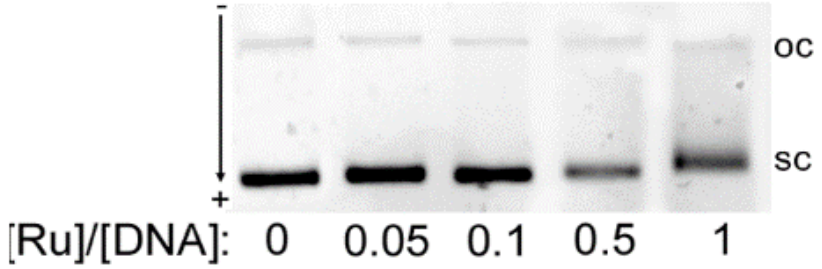

Figure 3.14 Mobilities of supercoiled (sc) and open circular (oc) forms of plasmid DNA in the presence of complex **4**.

In order to test the possibility of non-covalent interaction of complex **4** (in DMSO/H_2O, 1:99, v/v) with ds-DNA (very weak interaction could not survive conditions under exhaustive dialysis, gel filtration or electrophoresis), spectrophotometric titrations of complex **4** with ct-DNA was performed (see **Figure 3.15**). In general, the process of DNA binding situates the molecule of the complex in an environment which is different from that of the free molecule in solution. Consequently, the electron distribution of the molecule is altered and this results in differences between the absorption properties of the free and DNA-bound molecule (usually hypochromism, and in some cases - red/blue shift). However, no significant changes were observed in a spectrum of complex **4** when titrated with ct-DNA (visible region of the spectrum is shown, where DNA does not interfere).

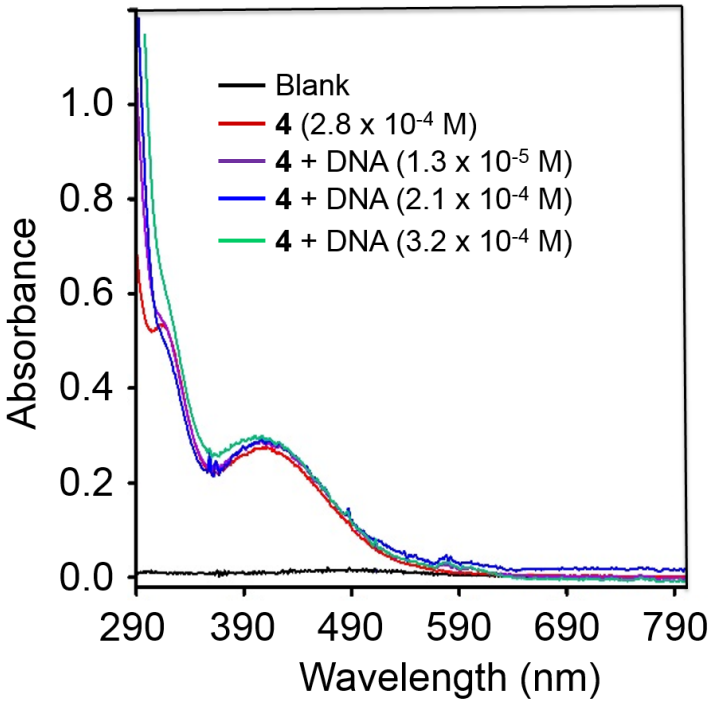

Figure 3.15 Titration of complex **4** (2.8×10^4 M, 1% DMSO in H_2O) with various concentrations of ct-DNA monitored by UV-vis spectroscopy.

As fluorescence is usually more sensitive to the changes in the environment of the fluorophore, possible changes in emission intensity of complex **4** (2×10^{-4} M in 99% H_2O + 1% DMSO) in the presence of ct-DNA were also monitored. Complex **4** provided only a very weak fluorescence signal at 490 nm (λ_{ex} = 420 nm). No significant changes of the intensity of this signal were observed when complex **4** was allowed to interact with ct-DNA (see **Figure 3.16**).

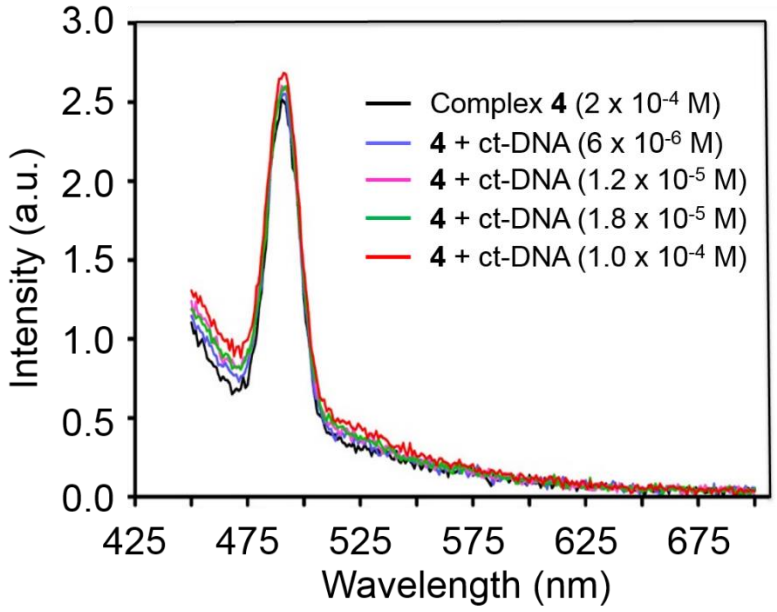

Figure 3.16 Emission intensity of complex **4** (2×10^{-4} M in 99% H_2O + 1% DMSO) in the presence of various concentrations of ct-DNA.

3.3.12 Ethidium Bromide Displacement

The ability of complex **4** to displace ethidium bromide (EtBr) from its intercalation into DNA was also tested. It has been shown that DNA interacting molecules, both intercalators and groove binders are able to displace EtBr from its binding site in DNA and then reduce the fluorescence of EtBr significantly. The efficiency of this competition reaction depends on the affinity of particular DNA binder to DNA and this experiment can be used to estimate binding constant (Kb). In this experiment, DNA-EtBr adduct was titrated with increasing concentration of complex **4**. However, no changes in fluorescence of EtBr were observed even in the concentration of **4** 70-fold higher than EtBr, indicating complex **4** was unable to displace EtBr from its DNA binding sites.

3.3.13 Binding to Short Single- or Double-stranded Oligonucleotides

The interaction of complex **4** with short, single or double-stranded synthetic oligonucleotides was also tested in order to find out the effect of size and structure of DNA. In this experiment, the amount of Ru associated with double- or single-stranded oligonucleotides treated with complex **4** was found to be 4% and 11%, respectively, which indicated a weak binding of complex **4** to the oligonucleotide.

3.3.14 DFT Calculations

DFT calculations of the relative energies of intermediates in a possible catalytic cycle starting with the aqua species of complexes **3**, **4** and **5** were made using structures based on the X-ray crystal structure of complex **3**, in the presence of formate, water, NAD^+ and carbon dioxide (see **Scheme 3.2**). The energy levels of these aqua species were defined as 0 kJ/mol, and a favourable decrease in energy upon binding formate to Ru^{II} of -46, -42 and -42 kJ/mol, respectively, was calculated.[15] The subsequent formation of the Ru-H hydride bond corresponds to a much higher energy transition state including the twist of formate and the elimination of carbon dioxide. The energy levels decreased when hydride was transferred from Ru to NAD^+, giving energy differences of -20, -36 and -29 kJ/mol for **3**, **4** and **5**, respectively (see **Scheme 3.2**). The energy decreased further when NADH was eliminated from the Ru center. The values of the energetic barriers of the transfer hydrogenation cycle of complexes **3**, **4** and **5** are listed in **Table 3.6**.

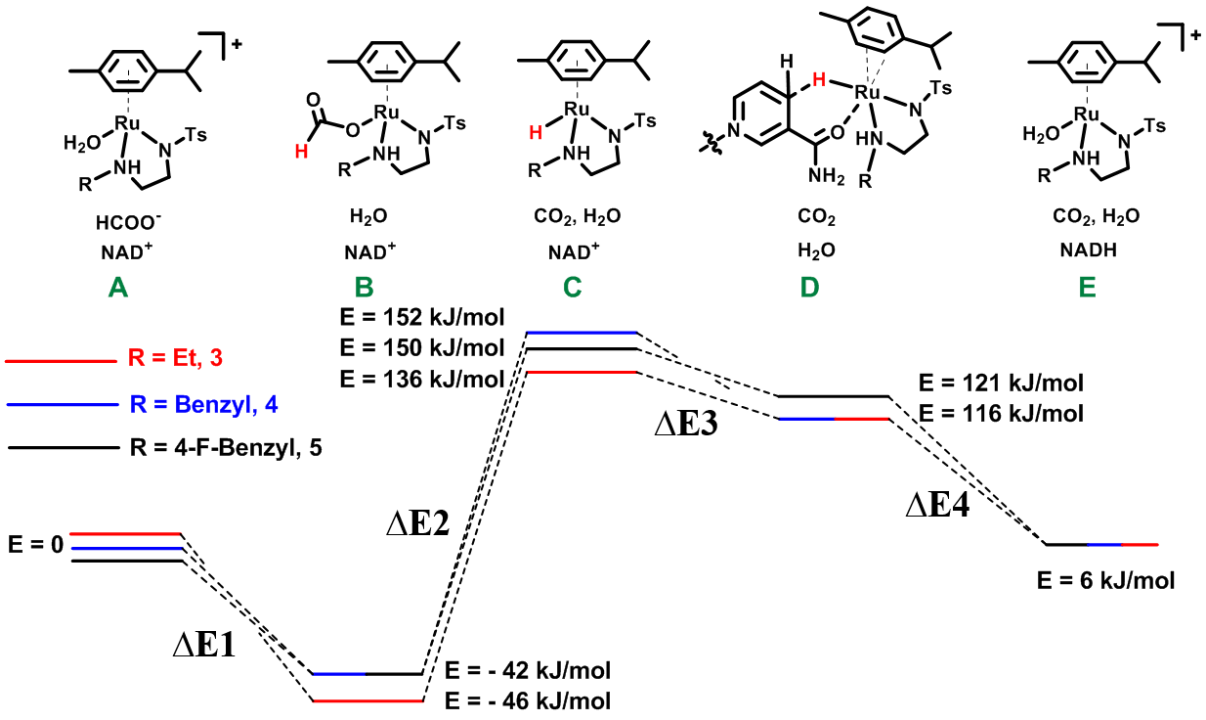

Scheme 3.2 DFT energy profile for the formation of Ru formate species, Ru hydride complex and hydride transfer from metal; red line complex **3**; blue line, complex **4**; black line, complex **5**.

3.4 Discussion

3.4.1 Synthesis and Characterization

The functional groups methyl, ethyl, benzyl, 4-F-benzyl and naphthalene were introduced on the terminal nitrogen of the chelated sulfonyl diamine ligand to study steric and electronic effects on the transfer hydrogenation of NAD^+ to NADH. The X-ray crystal structure of complex **3** [(η^6-*p*-cym)Ru(TsEnEt)Cl] shows it to have a typical 'piano-stool' geometry. Compared to reported ruthenium ethylenediamine complexes,[15, 25] the Ru−N^- bond length (N9, 2.13(9)) is within the expected range of 2.11-2.14 Å,[25] but the Ru−N12 length (2.17(11) Å) is

longer than the analogue [(η^6-biph)Ru(TsEn)Cl] (2.12(3) Å),[15] suggesting that the presence of N-ethyl substituent cause a slight weakening of this Ru-N bond. The remaining bond length and angles show no significant difference.

3.4.2 Kinetics of Transfer Hydrogenation Reactions

The ratio of coenzyme NAD^+/NADH greatly influences the intracellular potential and can drive many reactions *in vivo*.[26]

The turnover frequencies of NAD^+ to NADH catalysed by Ru^{II} complexes **1-6** determined by UV-vis spectroscopy are similar to those from ^{1}H NMR spectroscopy (see **Table 3.3**). In general, the introduction of substituents on the terminal nitrogen improve the catalytic activity. The bulkier the substituents on the terminal nitrogen, the higher the TH reaction rate becomes. The turnover frequency reaches a maximum (*ca.* 7.54 h^{-1}) when the substituent on the terminal N is benzyl (complex **4**), making it as efficient as the Rh^{III} complex [(η^5-Cp*)Rh(bipy)Cl]PF_6.[9a] Interestingly, the TOF decreases when the substituent is 4-F-benzyl (complex **5**) or naphthalene (complex **6**), probably, because these ligands hamper the approach of NAD^+ to the Ru metal center.

Compared to the en complex with unsubstituted nitrogens [(η^6-biph)Ru(en)Cl]PF_6, the turnover frequency of complex **4** is 41× higher,[14] and 2.7× higher compared to [(η^6-*p*-cym)Ru (TsEn)Cl].[12]

The NH proton of chelated diamine ligand appears to be essential for the TH reduction of ketones to alcohols;[27] normally, Ru^{II} catalysts for TH of ketones form 16-e intermediates.[28] It has been reported that an Ru^{II} complex with two N-alkyl groups (*R*,*R*)-[(η^6-benzene) Ru(TsDPEN-Me_2)Cl] exhibited poor catalytic reactivity in TH reaction of ketones.[29] However, complex **2** [(η^6-*p*-cym)Ru(TsEnMe_2)Cl] exhibited good catalytic activity towards the TH reduction of NAD^+ to NADH (TOF = 4.1 h^{-1}, see **Table 3.3**), despite not having a NH proton,

which suggests, as expected, that an N-H is not essential in the transfer reduction of NAD^+ to NADH.

Plots of the TOF versus formate concentration, show a typical Michaelis-Menten behaviour. The maximum turnover frequency TOF_{max} for complex **4** (30.3 h^{-1}) is *ca.* 5× higher than for [(η^6-*p*-cym)Ru(TsEn)Cl] (**JS2** in **Figure 3.1**, TOF_{max} = 6.4 h^{-1})[15] and 20× faster than the complex [(η^6-hmb)Ru(en)Cl]PF_6 (TOF_{max} = 1.46 h^{-1}).[14] The much lower Michaelis-Menten constant (K_M = 0.086 mM) of complex **4** indicates a stronger affinity of the complex for formate compared to [(η^6-*p*-cym)Ru(TsEn)Cl] (K_M = 27.8 mM)[15] and [(η^6-hmb)Ru(en)Cl]PF_6 (K_M = 58 mM).[14]

The maximum turnover frequency was observed at pH^* 6 (TOF_{max} = 7.7 h^{-1}) (see **Figure 3.8**). The TOF for complex **4** gradually decreases when pH was raised above 6 (see **Figure 3.8**). Transfer hydrogenation was halted below pH^* 4 because of the decomposition of the complex.

3.4.3 Antiproliferative Activity

Ruthenium complexes have shown promise for their activity against various type of cancer cells.[30] Here the antiproliferative activity of complexes **1-6** towards A2780 human ovarian cells was determined. It is apparent that the presence of aromatic substituents on the chelated ligands of complexes **4-6** give rise to more potent cytotoxicity than aliphatic substituents in complexes **1-3**, most probably due to their higher lipophilicity.

Combination treatment with formate can greatly increase the antiproliferative of Ru^{II} arene sulfonyl diamine complexes,[8] which offers a potential new strategy for cancer treatment. Previous work has suggested that reduction of NAD^+ by transfer hydrogenation from formate can be catalysed by Ru^{II} sulfonyl diamine complexes in cells.[8]

In this work, the antiproliferative activity against A2780 cancer cells of complexes **1-6** on coadministration with sodium formate was studied. The potency of each of these complexes

increased with increase in formate concentration (see **Figure 3.12**).[8] The largest decrease of cell survival was 31% for complex **6** in the presence of 2 mM sodium formate, followed 29% and 32% for complexes **4** and **5**, respectively, the other two complexes with aromatic substituents, complexes **1-3** with aliphatic functional groups showed increase in potency of 18%, 21% and 22%, respectively (**Table 3.5**).

Table 3.5 Percentage of Cell Viability Decrease Induced by Complexes **1-6** in the Presence of Different Concentrations of Formate.

Complex	Cell Viability Decrease (%)		
	[Formate]		
	0.5 mM	1.0 mM	2.0 mM
1	6.1±3.8	14.4±5.4	20.4±3.1
2	6.3±2.4	8.8±2.4	20.8±3.2
3	2.6±1.7	11.2±1.8	20.3±2.3
4	17.3±3.4	26.2±4.8	32.0±3.6
5	11.7±4.8	16.6±3.1	32.0±3.2
6	28.3±2.6	29.2±1.9	36.1±2.3

3.4.4 Ruthenium Cellular Uptake and Hydrophobicity Determination

The hydrophobicity and cellular accumulation are often important factors that play roles in the potency of organometallic and other anticancer drugs.[24] The cellular uptake of Ru in A2780 human ovarian cancer cells for complexes **1-6** was determined at IC_{50} concentrations to investigate a possible correlation with hydrophobicity determined by reverse-phase (RP) HPLC and antiproliferative activity.

The relative hydrophobicity of a series of complexes can be determined on the basis of their HPLC retention times (t_R) on a RP-HPLC column, which relies on the relative interaction

between the hydrophilic mobile phase and hydrophobic stationary phase.[24] It is evident from **Table 3.4** that the Ru^{II} complexes with aromatic substituents (complexes **4-6**) have exhibited higher hydrophobicity than complexes with aliphatic substituents (complexes **1-3**). The most hydrophobic complex (**6**) shows the highest cell accumulation, although complex **4** has the lowest cell uptake extent, but the most potent antiproliferative activity, suggesting that it is the chemical properties of the intracellular drug that are more important to activity than the total amount of Ru entering cell. In general, a high hydrophobicity can facilitate interaction between the organometallic complex and cell membrane, also correlates well the potency of the complex.[31] For this series of complexes, there is no clear relationship between cell accumulation of Ru, hydrophobicity of the complexes and the anticancer potency.

3.4.5 Binding with Calf Thymus and Bacterial Circular Plasmid DNA

DNA was thought to be a cellular target for the en complex **RM175** (see **Figure 3.1**).[32, 33] However, the introduction of functional sulfonyl substituents on the terminal nitrogen was found to greatly weaken the affinity of complex [(η^6-*p*-cym)Ru(TsEn)Cl] for DNA.[8] In this research, no obvious unwinding of DNA was observed after coincubation of ct-DNA with complex **4**, suggesting that binding is weak, and no changes in the ratio of sc and oc forms of plasmid DNA, suggesting that complex **4** does not cleave DNA.

3.4.6 ROS Determination

Reactive oxygen species (ROS) are metabolic byproducts of aerobic respiration and are responsible for maintaining redox homeostasis in cells.[34] ROS also play a significant role in the mode of action for anticancer agents.[35] Many organometallic complexes, *e.g.* Ir and Os,[36] can generate high ROS levels in cancer cells to induce cell apoptosis. The total ROS level in A2780 cancer cells exposure to complexes **1** and **4** was determined. Both complexes increase

ROS levels at IC_{50} concentrations; the population in FL1 and FL2 channels for complex **4** is 31.3 ± 0.3, about 2 fold higher than for complex **1** (16.5 ± 1.0, in **Table 3.6**) indicating higher total oxidative stress as well as high superoxide levels. These ROS may play a major role in killing the cancer cells.

Table 3.6 The induction of ROS and superoxide detected by flow cytometry experiments in A2780 ovarian cancer cells.

	Populations (%)			
	FL-1-/FL-2-	FL-1+/FL-2-	FL-1-/FL-2+	FL-1+/FL-2+
Complex **1**	0.13±0.1 ***	83.3±1.3 ***	0.02±0.01	16.5±1.0 **
Complex **4**	0 ***	68.7±0.7 ***	0	31.3±0.3 ***
Negative control	99.89 ± 0.04	0.09 ± 0.03	0.04±0.01	0

The monitoring of H_2O_2, peroxy and hydroxyl radicals using a green probe FL-1, and superoxide levels using the orange channel FL-2. All values compared to the untreated controls. In all cases, independent two-sample *t*-tests with unequal variances, Welch's tests, were carried out to establish statistical significance of the variations ($p < 0.001$ for ***, $p < 0.01$ for **, and $p < 0.05$ for *).

3.4.7 DFT Calculations

Calculations were carried out for complexes **3** (N-Et), **4** (N-Bz) and **5** (4-F-Bz). The calculations suggest that the displacement of water from $[(\eta^6\text{-}p\text{-cym})Ru(TsEn)(H_2O)]^+$ by formate is energy favourable by 42-46 kJ mol^{-1}, **Table 3.6**. As expected from previous calculations of related complexes,[15] the next step involving the transfer of hydride and liberation of CO_2 is costly in energy for **4** > **5** > **3**. The interaction with NAD^+ and hydride transfer then produces a lower energy intermediate is more favourable for **4** < **5** < **3**, which is perhaps related to the lower catalytic efficiency of complex **3**. The final release of NADH and reformation of aqua complex lowers the energy by 110-115 kJ mol^{-1}.

Table 3.6 Computed DFT Free Energy Barriers ΔE (kJ/ mol) Leading to Cycle of Hydride Transfer.

Step	ΔE(kJ/mol)		
	3	**4**	**5**
ΔE1	-46	-42	-42
ΔE2	+182	+194	+192
ΔE3	-20	-36	-29
ΔE4	-110	-110	-115

3.5 Conclusions

In this chapter, a series of Ru^{II} complexes of the type [(η^6-*p*-cym)Ru(*N*,*N'*)Cl] where *N*,*N'* are monosulfonamide chelating ligands derived from tosylethylenediamine, with either alkyl (Me (**1**), Me_2 (**2**), Et (**3**)) or aryl (Bz (**4**), 4-F-Bz (**5**), naphthyl (**6**)) substituents on the terminal N have been synthesised. These substituents have a significant effect on the rate of transfer hydrogenation of coenzyme NADH with formate as hydride donor as determined by NMR and UV-vis spectroscopy. In general the bulkier aromatic substituents gave rise to faster hydrogenation rates.

To investigate the possibility of achieving transfer hydrogenation from formate in cells, the effect of formation on antiproliferative activity of these complexes towards human ovarian cancer cells was investigated. In each case a dose-dependent increase in potency of the complexes (20-36%) was observed with increase in formate concentration over a range of non-toxic formate concentration (0-2 mM).The complexes with aromatic substituents were the most potent, complex **4** being as potent as the anticancer drug cisplatin (see **Figure 3.11**). In general, the most hydrophobic complexes are the most biologically active, but the activity does not correlate closely with total Ru uptake by the cell (see **Table 3.4**). Although DNA can be a target for related arene Ru^{II} diamine complexes, it does not appear to be a target for these sulfonyl Ru^{II} catalysts since we observe very weak binding to both calf thymus and plasmid DNA (**Figure 3.16-3.18**).

Complexes **1** and **4** can generate high levels of ROS in A2780 human ovarian cancer cells, especially **4**, the most potent complex. This is consistent with interference in cellular redox pathways and possible attack on NAD^+ if sodium formate present.

The enhancement of anticancer activity by low non-toxic dose of formate might be useful clinically since it introduces a new mechanism of activity which does not involve DNA attack, unlike the clinical drug cisplatin. Such treatment might therefore avoid some unwanted side-

effects. Formate itself is a natural biochemical molecule enriched in some cancer cells.[37] However, more work remains to be done to investigate possible intracellular catalysis, especially since a range of metabolites might readily poison these catalysts in cells.

3.6 References

(1) Eisner, U.; Kuthan, J. *Chem. Rev.* **1972**, *72*, 1−42.

(2) a) Gębicki, J.; Marcinek, A.; Zielonka, J. *Acc. Chem. Res.* **2004**, *37*, 379−386; b) McSkimming, A.; Colbran, S. B. *Chem. Soc. Rev.* **2013**, *42*, 5439−5488; c) Fukuzumi, S.; Suenobu, T. *Dalton. Trans.* **2013**, *42*, 18−28.

(3) Barrett, S. M.; Pitman, C. L.; Walden, A. G.; Miller, A. J. M. *J. Am. Chem. Soc.* **2014**, *136*, 14718−14721.

(4) a) Carrión, M. C.; Sepúlveda, F.; Jalón, F. A.; Manzano, B. R.; Rodríguez, A. M. *Organometallics* **2009**, *28*, 3822−3833; b) Maenaka, Y.; Suenobu, T.; Fukuzumi, S. *J. Am. Chem. Soc.* **2012**, *134*, 9417−9427.

(5) Wolfson, A.; Dlugy, C.; Shotland, Y.; Tavor, D. *Tetrahedron Lett.* **2009**, *50*, 5951−5953.

(6) a) Ruppert, R.; Herrmann, S.; Steckhan, E. *Tetrahedron Lett.* **1987**, *28*, 6583−6586; b) Steckhan, E.; Herrmann, S.; Ruppert, R.; Dietz, E.; Frede, M.; Spika, E. *Organometallics* **1991**, *10*, 1568−1577; c) Steckhan, E.; Herrmann, S.; Ruppert, R.; Thömmes, J.; Wandrey, C. *Angew. Chem. Int. Ed.* **1990**, *29*, 388−390; d) Westerhausen, V. D.; Herrmann, S.; Hummel, W.; Steckhan, E. *Angew. Chem. Int. Ed.* **1992**, *31*, 1529−1531; e) Hembre, R. T., McQueen, S. *J. Am. Chem. Soc.* **1994**, *116*, 2141−2142.

(7) Wang, C.; Villa-Marcos, B.; Xiao, J. *Chem. Commun.* **2011**, *47*, 9773−9785.

(8) Soldevila-Barreda, J. J.; Romero-Canelón, I.; Habtemariam, A.; Sadler, P. J. *Nat. Commun* **2015**, *6*, 6582.

(9) a) Lo, H. C.; Buriez, O.; Kerr, J. B.; Fish, R. H. *Angew. Chem. Int. Ed.* **1999**, *38*, 1429−1432; b) Lo, H. C.; Fish, R. H. *Angew. Chem. Int. Ed.* **2002**, *41*, 478−481; c) Lo, H. C.; Leiva, C.; Buriez, O.; Kerr, J. B.; Olmstead, M. M.; Fish, R. H. *Inorg. Chem.* **2001**, *40*, 6705−6716.

(10) O' Connor, J. M.; Casey, C. P. *Chem. Rev.* **1987**, *87*, 307−318.

(11) Oppelt, K. T.; Gasiorowski, J.; Egbe, D. A. M.; Kollender, J. P.; Himmelsbach, M.; Hassel, A. W.; Sariciftci, N. S.; Knör, G. *J. Am. Chem. Soc.* **2014**, *136*, 12721−12729.

(12) Ganesan, V.; Sivanesan, D.; Yoon, S. *Inorg. Chem.* **2017**, *56*, 1366−1374.

(13) a) Hashiguchi, S.; Fujii, A.; Takehara, J.; Ikariya, T.; Noyori, R. *J. Am. Chem. Soc.* **1995**, *117*, 7562-7563; b) Fujii, A.; Hashiguchi, S.; Uematsu, N.; Ikariya, T. and Noyori, R. *J. Am. Chem. Soc.* **1996**, *118*, 2521−2522.

(14) Yan, Y. K.; Melchart, M.; Habtemariam, A.; Peacock, A. F. A.; Sadler, P. J. *J. Biol. Inorg. Chem.* **2006**, *11*, 483−488.

(15) Soldevila-Barreda, J. J.; Bruijnincx, P. C. A.; Habtemariam, A.; Clarkson, G. J.; Deeth, R. J.; Sadler, P. J. *Organometallics* **2012**, *31*, 5958−5967.

(16) Betanzos-Lara, S.; Liu, Z.; Habtemariam, A.; Pizarro, A. M.; Qamar, B.; Sadler, P. J. *Angew. Chem. Int. Ed.* **2012**, *51*, 3897−3900.

(17) Habtemariam, A.; Melchart, M.; Fernández, R.; Parsons, S.; Oswald, I. D. H.; Parkin, A.; Fabbiani, F. P. A.; Davidson, J. E.; Dawson, A.; Aird, R. E.; Jodrell, D. I.; Sadler, P. J. *J. Med. Chem.* **2006**, *49*, 6858−6868.

(18) Martins, J. E. D.; Clarkson, G. J.; Wills, M. *Org. Lett.* **2009**, *11*, 847−850.

(19) Li, X.; Li, L.; Tang, Y.; Zhong, L.; Cun, L.; Zhu, J.; Liao, J.; Deng, J. *J. Org. Chem.* **2010**, *75*, 2981−2988.

(20) Koike, T.; Ikariya, T. *Organometallics* **2005**, *24*, 724−730.

(21) Yanai, D. T. T. and Handy, N. *Chem. Phys. Lett.* **2004**, *393*, 51−57.

(22) a) Stevens, W. J. B.; Krauss, H. J.; *J. Phys. Chem.* **1984**, *81*, 6026–6033; b) Stevens, W. J. K.; Basch, H.; Jasien, P.G. *Can. J. Chem.* **1992**, *70*, 612-630; c) Cundari, T. R. S. *J. Chem. Phys.* **1993**, *98*, 5555–5565.

(23) Frisch, M. J. T.; Schlegel, H. B.; Scuseria, G. E.; Robb, M. A.; Cheeseman, J. R.; Scalmani, G.; Barone, V.; Mennucci, B.; Petersson G. A. **2013**, Gaussian 09, Revision D.01; Gaussian: Wallingford, CT, USA.

(24) Millett, A. J.; Habtemariam, A.; Romero-Canelón, I.; Clarkson, G. J.; Sadler, P. J. *Organometallics* **2015**, *34*, 2683−2694.

(25) a) Morris, R. E.; Aird, R. E.; Socorro Murdoch, P.; Chen, H.; Cummings, J.; Hughes, N. D.; Parsons, S.; Parkin, A.; Boyd, G.; Jodrell, D. I.; Sadler, P. J. *J. Med. Chem.* **2001**, *44*, 3616−3621; b) Peacock, A. F. A.; Habtemariam, A.; Fernández, R.; Walland, V.; Fabbiani, F. P. A.; Parsons, S.; Aird, R. E.; Jodrell, D. I.; Sadler, P. J. *J. Am. Chem. Soc.* **2006**, *128*, 1739−1748.

(26) Zhang, J.; Pierick, A.; Rossum, H. M.; Seifar, R. M.; Ras, C.; Daran, J.; Heijnen, J. J.; Wahl, S. A. *Sci. Rep.* **2015**, *5*, 12846.

(27) Yamakawa, M.; Ito, H.; Noyori, R. *J. Am. Chem. Soc.* **2000**, *122*, 1466−1478.

(28) a) Soni, R.; Cheung, F. K.; Clarkson, G. C.; Martins, J. E. D.; Graham, M. A.; Wills, M. *Org. Biomol. Chem*. **2011**, *9*, 3290−3294; b) Wu, X.; Li, X.; Hems, W.; King, F.; Xiao, J. *Org. Biomol. Chem*. **2004**, *2*, 1818−1821.

(29) Kövâri, E.; Krämer, R. *J. Am. Chem. Soc.* **1996**, *118*, 12704−12709.

(30) Adhireksan, Z.; Davey, G. E.; Campomanes, P.; Groessl, M.; Clavel, C. M.; Yu, H.; Nazarov, A. A.; Yeo, C. H. F.; Ang, W. H.; Dro¨ge, P.; Rothlisberger, U.; Dyson, P. J.; Davey, C. A. *Nat. Commun* **2014**, *5*, 3462.

(31) a) Mendoza-Ferri, M.-G.; Hartinger, C. G.; Eichinger, R. E.; Stolyarova, N.; Severin, K.; Jakupec, M. A.; Nazarov, A. A.; Keppler, B. K. *Organometallics* **2008**, *27*, 2405−2407; b) Hanif, M.; Nazarov, A. A.; Hartinger, C. G.; Kandioller, W.; Jakupec, M. A.; Arion, V. B.; Dyson, P. J.; Keppler, B. K. *Dalton Trans.* **2010**, *39*, 7345−7352; c) Ruiz, J.; Rodríguez, V.; Cutillas, N.; Espinosa, A.; Hannon, M. *J. Inorg. Chem.* **2011**, *50*, 9164−9171.

(32) Chen, H.; Parkinson, J. A.; Parsons, S.; Coxall, R. A.; Gould, R. O.; Sadler, P. J. *J. Am. Chem. Soc.* **2002**, *124*, 3064−3082.

(33) Gasser, G.; Ott, I.; Metzler-Nolte, N. *J. Med. Chem.* **2010**, *54*, 3−25.

(34) Dharmaraja, A. T. *J. Med. Chem.* **2017**, *60*, 3221−3240.

(35) a) Trachootham, D.; Alexandre, J.; Huang, P. *Nat. Rev. Drug Discovery* **2009**, *8*, 579−591; b) Watson, J. *Open Biol.* **2013**, *3*, 120144.

(36) a) Liu, Z.; Romero-Canelón, I.; Habtemariam, A.; Clarkson, G. J.; Sadler, P. J. *Organometallics* **2014**, *33*, 5324−5333; b) Liu, Z.; Romero-Canelón, I.; Qamar, B.; Hearn, J. M.; Habtemariam, A.; Barry, N. P. E.; Pizarro, A. M.; Clarkson, G. J.; Sadler, P. J. *Angew. Chem. Int. Ed.* **2014**, *53*, 3941 –3946; c) Fu, Y.; Romero, M. J.; Habtemariam, A.; Snowden, M. E.; Song, L.; Clarkson, G. J.; Qamar, B.; Pizarro, A. M.; Unwin, P. R.; Sadler, P. J. *Chem. Sci.* **2012**, *3*, 2485–2494.

(37) Tedeschi, P. M.; Markert, E. K.; Gounder, M.; Lin, H.; Dvorzhinski, D.; Dolfi, S. C.; Chan, L. L. Y.; Qiu, J.; DiPaola, R. S.; Hirshfield, K. M.; Boros, L. G.; Bertino, J. R.; Oltvai, Z. N.; Vazquez, A. *Cell Death Dis* **2013**, *4*, 877.

Chapter 4

Glutathione Activation of Ru^{II} Sulfonyl-ethylenediamine Complexes and Its Role in Anticancer Activity

4.1 Introduction

The antiproliferative activity study of organometallic complexes has been well stimulated due to the success of platinum-series anticancer agents, *e.g.* cisplatin, carboplatin and oxiliplatin.[1] Organometallic complexes often possess some obvious merits, for example variable coordination numbers and chelating ligands with tuneable biological properties.[2,3] Among the various platinum group metals, organo-ruthenium complexes have exhibited relative higher promise due to the great potency against carcinoma cells and low cytotoxicity to normal cells.[4,5] Two outstanding representatives of Ru^{III} complexes, namely, **KP1019** ((indazoleH)[trans-$RuCl_4$-$(indazole)_2$] and **NAMI-A** ((imidazoleH)[trans-$RuCl_4$-(imidazole)(DMSO)], are potent anti-metastatic agents.[6] The plausible '*in vivo* activation by reduction' mechanism makes them selectively potent against human colorectal cancers tumours (especially cisplatin resistant colorectal carcinomas).[5,7] Some other Ru complexes with promising properties have also been intensively studied, *e.g.* **RAPTA** has low toxicity *in vitro*, but great anti-angiogenesis activity against tumour metastasis *in vivo* (**Figure 4.1**);[8] **RM175** shows promising anticancer activity against A2780 human ovarian cancer cells, with IC_{50} values in the nanomolar range (**Figure 4.1**).[9] Che *et al.* recently revealed a new series of macrocyclic Ru^{III} complexes of the type [Ru^{III}-$(N_2O_2)Cl_2$]Cl as anti-angiogenesis and anti-tumour agents (**Figure 4.1**).[10] Such a Ru^{III} complex was found to down-regulate the signalling protein of vascular endothelial growth receptor-2 (VEGFR2). Organo-ruthenium complexes have attracted particular attention probably because they have a range of oxidation states and are believed to mimic iron in cell and bind to some plasma proteins.[4, 11]

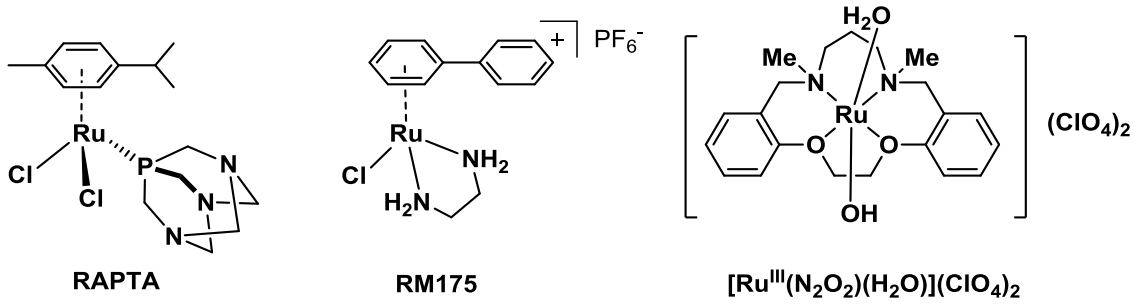

Figure 4.1 Structures of Ru^{II}/Ru^{III} complexes with potent anticancer activity.

In mammalian cells, a basal level of reactive oxygen species (ROS) is important for cell proliferation and survival. As a metabolism side product, excess levels of reactive oxygen species (ROS) often irreversibly damage lipids of cell membrane and guanine or thymine of DNA, which are lethal to cell growth, even though a basal level of ROS is important for signalling (proliferation and survival).[12] To deal with ROS, cancer cells are normally generating higher levels of thiol containing molecules, for instance L-glutathione (GSH) and cysteine.[13] GSH is a non-protein tripeptide and can be oxidized to GSSG in cellular to attenuate damage caused by ROS (**Figure 4.2**),[14] or to scavenge a complex that is toxic to cells since organometallic complexes exhibit high affinity for thiol-containing peptides.[15] Based on thiol-containing organic compounds, Süss-Fink *et al.* have synthesized a series of dithiolato and trithiolato Ru^{II} complexes, these complexes have been shown potent anticancer activity (sub-micromolar range) against both A2780 and A2780 cisplatin-resistant human ovarian cancer cells.[16] Of particular interest, such trithiolato Ru^{II} complexes can change the GSH/GSSH ratio by catalytic oxidation reactions.[17]

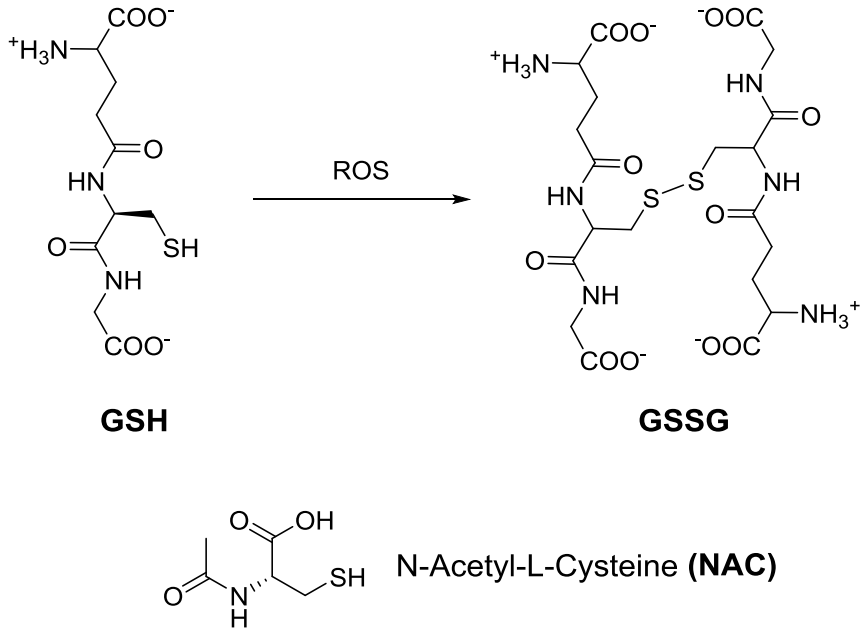

Figure 4.2 Chemical structures of GSH, GSSG (charge shown as at pH 7) and NAC (charge shown as at pH 2).

Ru^{II} sulfonyl ethylenediamine complexes such as [(η^6-*p*-cym)Ru(TsEn)Cl] were reported as efficient catalysts in transfer hydrogenation (TH) reduction of NAD^+ to NADH using formate as hydride donor.[18] In **Chapter 3**, the complexes were modified by introducing a series of (alkyl or aryl) functional groups to the terminal nitrogen of ethylenediamine ligand. The catalytic efficiency and antiproliferative activity were greatly enhanced (see complexes **1-6** in **Chapter 3**). Complex **4** [(η^6-*p*-cym)Ru(TsEnBz)Cl] had the highest catalytic efficiency in NAD^+ TH reduction and antiproliferative activity towards A2780 human ovarian cells (IC_{50}, 1.0 μM).

In this Chapter, given both the promising catalytic and antiproliferative activity of complex **4**, another series of Ru^{II}/Os^{II} complexes **7-15** of the type [(η^6-arene)M(BzEnR)Cl], where arene is benzene, $HO(CH_2)_2O$-phenyl and biphenyl, M is Ru or Os and R is various sulfonyl substituents are synthesized (**Table 4.1**).

Table 4.1 Ru^{II}/Os^{II} Complexes Synthesized and Studied in This Chapter

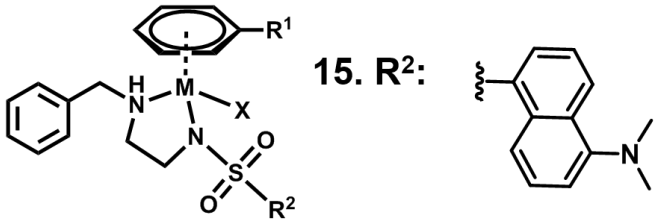

Complex	M	R^1	R^2	X
7	Ru	H	4-Me-Ph	Cl
8	Ru	Ph	4-Me-Ph	Cl
9	Ru	Ph	4-Me-Ph	I
10	Os	Ph	4-Me-Ph	Cl
11	Ru	$-O(CH_2)_2OH$	4-Me-Ph	Cl
12	Ru	Ph	4-Nitro-Ph	Cl
13	Ru	Ph	4-F-Ph	Cl
14	Ru	Ph	Ph	Cl
15	Ru	Ph	Dansyl (Dan)	Cl

Complex **10** is the Os analogue of Ru^{II} complex **8** and was prepared from $[(\eta^6\text{-biph})OsCl_2]_2$ dimers. The catalytic TH reduction of NAD^+ to NADH using sodium formate as hydride source was studied. The interaction of these complexes with thiol-containing low-MW molecules, *e.g.* L-GSH and N-acetyl-L-cysteine (NAC), was studied by NMR and LC-MS. The high thiophilic property of such complexes also allowed investigation of the influence of GSH on the NAD^+ TH reduction. Antiproliferative activity of complexes **7-15** was determined against two cancer cell lines: A2780 human ovarian, A549 human lung cancer cells. In comparison, anticancer activity of complex **8** towards A549 human lung cancer cells in co-administration with thiol-contained molecule GSH/NAC and the redox modulator L-buthionine sulfoximine (L-BSO) was studied. Cell cycle arrest and the effect of complex **8** and **8** with GSH on induction of ROS levels in A2780 human ovarian cancer cells were also investigated.

4.2 Experimental Section

4.2.1 Materials

Dansyl chloride was purchased from Sigma-Aldrich. The Ru^{II}/Os^{II}-η^6-arene precursor dimers were prepared following literature methods, as were the ligands. The solvents used for NMR spectroscopy were purchased from Sigma-Aldrich and Cambridge Isotope Laboratories Inc. Non-dried solvents used in syntheses were obtained from Fisher Scientific. Glutathione and N-acetyl-L-cysteine were purchased from Fisher Scientific.

4.2.2 Synthesis and Characterization

Complexes **12-15** were synthesized and characterized by Neil MacQuarrie.

[(η^6-benzene)Ru(TsEnBz)Cl] (**7**). All the complexes in this Chapter were prepared according to a reported method:[18] [(η^6-benzene)$RuCl_2$]$_2$ (100 mg, 0.2 mmol) and TsEnBz (153 mg, 0.45 mmol) were placed in a round-bottom flask, to which 2-propanol (50 mL) and triethylamine (125 μL, 0.9 mmol) were added. The solution was heated under refluxing in a nitrogen atmosphere (365 K) overnight with stirring. After this the solvent was removed on a rotary evaporator to get a dark red solid. The crude product was purified by silica column chromatography (MeOH/DCM, 1:9 (v/v)), with red solid obtained. Yield = 134.7 mg (65%). **^{1}H NMR** (400 MHz, $CDCl_3$): δ_H 2.09-2.25 (m, 2H), 2.33 (s, 3H), 2.40-2.42 (m, 1H), 3.08 (dd, *J* = 3.1 Hz, 11.2 Hz, 1H), 3.75 (t, *J* = 10.1 Hz, 1H), 4.19 (q, *J* = 10.8 Hz, 13.2 Hz, 1H), 4.85 (dd, *J* = 10.1 Hz, 13.4 Hz, 1H), 5.70 (s, 6H), 7.14 (d, *J* = 8 Hz, 2H), 7.29-7.31 (m, 2H), 7.35-7.38 (m, 3H), 7.71 (d, *J* = 8.1 Hz, 2H); **^{13}C NMR** (125.73 MHz, $CDCl_3$): δ_c 21.4, 48.3, 55.5, 62.2, 83.1, 127.3, 128.4, 128.7, 128.9, 129.3, 135.7, 140.1, 140.7; HR-MS: *Calcd* for $[C_{22}H_{25}N_2O_2SRu]^+$ 483.0680 *m*/*z*, found: 483.0683 *m*/*z*. Elemental analysis: *Calcd* for

$[C_{22}H_{25}N_2O_2SRuCl(H_2O)_{0.1}]$ C, 50.83%; H, 4.89%; N, 5.39%. Found: C, 50.84%; H, 4.81%; N, 5.42%.

[(η^6-biph)Ru(TsEnBz)Cl] (**8**). Complex **8** was obtained following the method described for complex **7**, where $[(\eta^6\text{-biph})RuCl_2]_2$ (100 mg, 0.153 mmol), TsEnBz (110 mg, 0.32 mmol) and triethylamine (89 μL, 0.64 mmol) were added. The crude product was purified by silica column chromatography (MeOH/DCM, 1:9 (v/v)), with orange red solid obtained. Yield = 132.7 mg (73%). **^{1}H NMR** (400 MHz, $CDCl_3$): δ_H 1.89-1.95 (m, 1H), 2.11-2.17 (m, 2H), 2.34 (s, 3H), 3.08 (dd, *J* = 3.6 Hz, 11.2 Hz, 1H), 3.59 (q, *J* = 10.4 Hz, 13.2 Hz, 1H), 3.73 (t, *J* = 11.5 Hz, 1H), 4.38 (dd, *J* = 3.9 Hz, 13.3 Hz, 1H), 5.47 (t, *J* = 7.7 Hz, 1H), 5.98-6.01(m, 2H), 6.06 (t, *J* = 5.6 Hz, 1H), 6.57 (d, *J* = 5.4 Hz, 1H), 7.03-7.05 (m, 2H), 7.15 (d, *J* = 8.0 Hz, 2H), 7.28-7.31 (m, 3H), 7.53-7.56 (m, 3H), 7.69 (d, *J* = 8.1 Hz, 2H), 7.89-7.91 (m, 2H); **^{13}C NMR** (125.73 MHz, $CDCl_3$): δ_c 21.4, 48.3, 53.9, 60.5, 78.7, 78.7, 86.4, 88.1, 89.0, 90.4, 127.4, 128.0, 128.2, 128.7, 129.1, 129.4, 129.6, 134.7, 135.7, 140.0, 140.7; HR-MS: *Calcd* for $[C_{28}H_{29}N_2O_2SRu]^+$ 559.0993 *m*/*z*, found: 559.0990 *m*/*z*. Elemental analysis: *Calcd* for $[C_{28}H_{29}N_2O_2SRuCl(H_2O)_{0.3}]$: C, 56.09%; H, 4.98%; N, 4.67%. Found: C, 56.02%; H, 5.01%; N, 4.73%.

[(η^6-biph)Ru(TsEnBz)I] (**9**). Complex **9** was obtained following the method described for complex **7**, where $[(\eta^6\text{-biph})RuI_2]_2$ (100 mg, 0.098 mmol), TsEnBz (70 mg, 0.204 mmol) and triethylamine (58 μL, 0.408 mmol) were added. The crude product was purified by silica column chromatography (MeOH/DCM, 2:8 (v/v)). Red solid was obtained. Yield = 72.6 (54%). **^{1}H NMR** (400 MHz, $CDCl_3$): δ_H 1.92-1.99 (m, 1H), 2.07-2.15 (m, 2H), 2.35 (s, 3H), 3.14-3.18 (m, 1H), 3.40 (q, *J* = 10.9 Hz, 13.2 Hz, 1H), 3.94 (t, *J* = 11.5 Hz, 1H), 4.32 (dd, *J* = 4.0 Hz, 13.4 Hz, 1H), 5.40 (t, *J* = 5.6 Hz, 1H), 5.88 (d, *J* = 5.8 Hz, 1H), 6.04 (t, *J* = 5.5 Hz, 1H), 6.34 (t, *J* = 5.7 Hz, 1H), 6.85 (d, *J* = 6.1 Hz, 1H), 7.00-7.01 (m, 2H), 7.16 (d, *J* = 8.2 Hz, 1H), 7.29-7.34 (m, 3H), 7.48-7.54 (m, 3H), 7.72 (d, *J* = 8.1 Hz, 2H), 7.81-7.83 (m, 2H); **^{13}C NMR** (125.73 MHz, $CDCl_3$): δ_c 21.4, 49.4, 53.5, 60.5, 78.6, 85.8, 87.4, 90.3, 127.7, 127.8,

128.3, 128.6, 128.8, 129.1, 129.5, 129.7, 134.8, 135.7, 139.3, 140.7; HR-MS: *Calcd* for $[C_{28}H_{29}N_2O_2SRu]^+$ 559.0993 *m*/*z*, found: 559.0994 *m*/*z*. Elemental analysis: *Calcd* for $[C_{28}H_{29}N_2O_2SRuI(H_2O)_{0.2}]$: C, 48.80%; H, 4.30%; N, 4.06%. Found: C, 48.74%; H, 4.17%; N, 3.96%.

[(η^6-biph)Os(TsEnBz)Cl] (**10**). Complex **10** was obtained following the method described for complex **7**, where $[(\eta^6\text{-biph})OsCl_2]_2$ (100 mg, 0.12 mmol), TsEnBz (80 mg, 0.26 mmol) and triethylamine (74 μL, 0.52 mmol) were added. The crude product was purified by silica column chromatography (MeOH/DCM, 1:9 (v/v)). Grey solid was obtained. Yield = 72.2 mg (44%). **^{1}H NMR** (400 MHz, $CDCl_3$): δ_H 1.86-1.96 (m, 1H), 2.18-2.20 (m, 1H), 2.35 (s, 3H), 2.53 (td, *J* = 3.36 Hz, 12.8 Hz, 1H), 3.13 (dd, *J* = 4.3 Hz, 11.84 Hz, 1H), 3.52 (q, *J* = 10.2 Hz, 13.3 Hz, 1H), 4.25 (t, *J* = 10.4 Hz, 1H), 4.33 (dd, *J* = 4 Hz, 13.4 Hz, 1H), 5.70-5.73 (m, 1H), 6.25 (d, *J* = 5.6 Hz, 1H), 6.26-6.28 (m, 2H), 6.86-6.87 (m, 1H), 7.00-7.02 (m, 2H), 7.15 (d, *J* = 8.1 Hz, 2H), 7.31 (t, *J* = 2.8 Hz, 3H), 7.43 (d, *J* = 7.2 Hz, 1H), 7.48 (t, *J* = 6.9 Hz, 2H), 7.69-7.72 (m, 4H); **^{13}C NMR** (125.73 MHz, $CDCl_3$): δ_c 21.4, 49.9, 55.9, 62.0, 67.9, 68.8, 77.4, 79.1, 81.3, 82.1, 127.3, 128.2, 128.3, 128.7, 128.8, 128.97, 129.2, 129.3, 135.7, 136.5, 140.1, 140.9; HR-MS: *Calcd* for $[C_{28}H_{29}N_2O_2SOs]^+$ 649.1565 *m*/*z*, found: 649.1558 *m*/*z*. Elemental analysis: *Calcd* for $[C_{28}H_{29}N_2O_2SOsCl(H_2O)_{0.9}]$: C, 48.08%; H, 4.44%; N, 4.00%. Found: C, 48.07%; H, 4.21%; N, 4.04%.

[(η^6-HOCH$_2$CH$_2$O-Ph)Ru(TsEnBz)Cl] (**11**). Complex **11** was obtained following the method described for complex **7**, where $[(\eta^6\text{-}HOCH_2CH_2O\text{-}Ph)RuCl_2]_2$ (100 mg, 0.161 mmol), TsEnBz (112 mg, 0.33 mmol) and triethylamine (92 μL, 0.66 mmol) were added. The crude product was purified by silica column chromatography (MeOH/DCM, 1:9 (v/v)). Bright red solid was obtained. Yield = 104 mg (56%). **^{1}H NMR** (400 MHz, $CDCl_3$): δ_H 2.12 (td, *J* = 2.8 Hz, 11.6 Hz, 1H), 2.22 (dd, *J* = 4.1 Hz, 11.8 Hz, 1H), 2.34 (s, 3H), 2.48 (d, *J* = 10.1 Hz, 1H), 3.00 (dd, *J* = 3.8 Hz, 11.4 Hz, 1H), 3.24 (s, broad, 1H), 3.76 (t, *J* = 11.3 Hz, 1H), 3.92-3.95 (m, 1H),

4.04-4.08 (m, 1H), 4.17 (q, *J* = 10.3 Hz, 13.3 Hz, 1H), 4.22-4.32 (m, 2H), 4.77 (dd, *J* = 4.1 Hz, 13.4 Hz, 1H), 5.04 (t, *J* = 5.2 Hz, 2H), 5.52 (t, *J* = 5.6 Hz, 1H), 5.56 (dd, *J* = 1.0 Hz, 5.9 Hz, 1H), 6.48 (t, *J* = 5.7 Hz, 1H), 7.15 (d, *J* = 8.0 Hz, 2H), 7.31 (d, *J* = 7.5 Hz, 2H), 7.35-7.40 (m, 3H), 7.75 (d, *J* = 8.2 Hz, 2H); **^{13}C NMR** (125.73 MHz, $CDCl_3$): δ_c 21.4, 47.9, 55.9, 60.8, 61.6, 61.9, 66.5, 68.8, 71.5, 87.1, 90.1, 127.6, 128.4, 128.7, 128.8, 129.3, 134.4, 135.7, 139.9, 140.8; ESI-MS: *Calcd* for $[C_{24}H_{29}N_2O_4SRu]^+$ 543.0891 *m*/*z*, found: 543.0891 *m*/*z*. Elemental analysis: *Calcd* for $[C_{24}H_{29}N_2O_4SRuCl]$: C, 49.87%; H, 5.06%; N, 4.85%. Found: C, 50.60%; H, 5.06%; N, 4.60%.

[(η^6-biph)Ru(4-NO_2-PhSulEnBz)Cl] (**12**). Complex **8** was obtained following the method described for complex **7**, where $[(\eta^6\text{-biph})RuCl_2]_2$ (100 mg, 0.153 mmol), 4-NO_2-PhSulEnBz (105 mg, 0.32 mmol) and triethylamine (90 μL, 0.64 mmol) were added. The crude product was purified by silica column chromatography (MeOH/DCM, 1:9 (v/v)). Dark red solid was obtained. Yield = 90 mg (46%). **^{1}H NMR** (400 MHz, $CDCl_3$): δ_H 1.96-2.02 (m, 1H), 2.09 (td, *J* = 3.2 Hz, 12.8 Hz, 1H), 2.24 (d, *J* = 10.4 Hz, 1H), 3.17 (dd, *J* = 3.6 Hz, 11.0 Hz, 1H), 3.65-3.70 (m, 2H), 4.41 (q, *J* = 9.4 Hz, 18.6 Hz, 1H), 5.48 (t, *J* = 5.7 Hz, 1H), 5.94 (t, *J* = 5.8 Hz, 1H), 6.04-6.07 (m, 2H), 6.51 (d, *J* = 5.7 Hz, 1H), 7.04-7.06 (m, 2H), 7.31-7.33 (m, 3H), 7.53-7.55 (m, 3H), 7.79-7.82 (m, 2H), 7.92 (d, *J* = 8.8 Hz, 2H); **^{13}C NMR** (125.73 MHz, $CDCl_3$): δ_c 48.2, 53.9, 60.7, 78.5, 78.9, 86.7, 88.2, 88.8, 90.9, 123.4, 127.9, 128.2, 128.4, 128.8, 129.2, 129.5, 129.9, 134.3, 135.4, 148.7; HR-MS: *Calcd* for $[C_{27}H_{26}N_3O_4SRu]^+$ 590.0688 *m*/*z*, found: 590.0688 *m*/*z*. Elemental analysis: *Calcd* for $[C_{27}H_{26}N_3O_4SRuCl]$: C, 51.88%; H, 4.19%; N, 6.72%. Found: C, 51.70%; H, 4.22%; N, 6.69%.

[(η^6-biph)Ru((4-F-PhSul)EnBz)Cl] (**13**). Complex **13** was obtained following the method described for complex **7**, where $[(\eta^6\text{-biph})RuCl_2]_2$ (100 mg, 0.153 mmol), (4-F-PhSul)EnBz (98 mg, 0.32 mmol) and triethylamine (89 μL, 0.64 mmol) were added. The crude product was purified by silica column chromatography (MeOH/DCM, 1:9 (v/v)). Dark red solid was

obtained. Yield = 101 mg (54%). **^{1}H NMR** (400 MHz, $CDCl_3$): δ_H 1.88-1.98 (m, 1H), 2.10 (dt, *J* = 3.2 Hz, 12.7 Hz, 1H), 2.17-2.20 (m, 1H), 3.08 (dd, *J* = 4.1 Hz, 11.6 Hz, 1H), 3.62 (dd, *J* = 10.3 Hz, 13.0 Hz, 1H), 3.69-3.76 (m, 1H), 4.39 (dd, *J* = 3.9 Hz, 13.0 Hz, 1H), 5.47 (t, *J* = 5.7 Hz, 1H), 5.97 (t, *J* = 5.7 Hz, 1H), 6.01 (d, *J* = 6.0 Hz, 1H), 6.05 (t, *J* = 5.7 Hz, 1H), 6.55 (d, *J* = 5.6 Hz, 1H), 7.00 (t, *J* = 8.8 Hz, 2H), 7.04-7.06 (m, 2H), 7.30-7.32 (m, 3H), 7.51-7.55 (m, 3H), 7.81-7.84 (m, 4H); **^{13}C NMR** (125.73 MHz, $CDCl_3$): δ_c 48.2, 53.9, 60.6, 78.6, 78.8, 86.5, 88.1, 88.9, 90.6, 114.9, 115.1, 128.0, 128.2, 128.7, 129.2, 129.4, 129.7, 129.7, 129.8, 134.6, 135.6, 163.0, 165.0; **^{19}F NMR** (376.4 MHz, $CDCl_3$, spectrum referenced to trifluoro-acetic acid at -76.55 ppm): δ_F -109.9. HR-MS: *Calcd* for $[C_{27}H_{26}FN_2O_2SRu]^+$ 563.0743 *m*/*z*, found: 563.0742 *m*/*z*. Elemental analysis: *Calcd* for $[C_{27}H_{26}FN_2O_2SRuCl(H_2O)_{1.4}]$: C, 52.03%; H, 4.66%; N, 4.49%. Found: C, 52.02%; H, 4.24%; N, 4.78%.

[(η^6-biph)Ru((PhSul)EnBz)Cl] (**14**). Complex **14** was obtained following the method described for complex **7**, where $[(\eta^6\text{-biph})RuCl_2]_2$ (100 mg, 0.153 mmol), PhSulEnBz (90 mg, 0.32 mmol) and triethylamine (89 μL, 0.64 mmol) were added. The crude product was purified by silica column chromatography (MeOH/DCM, 1:9 (v/v)). Dark red solid was obtained. Yield = 60.3 mg (34%). **^{1}H NMR** (500 MHz, $CDCl_3$): δ_H 1.88-1.95 (m, 1H), 2.11-2.18 (m, 2H), 3.11 (dd, *J* = 5.1 Hz, 9 Hz, 1H), 3.58 (dd, *J* = 10.4 Hz, 13.4 Hz, 1H), 3.71-3.76 (m, 1H), 4.38 (dd, *J* = 4.2 Hz, 13.4 Hz, 1H), 5.46 (t, *J* = 5.7 Hz, 1H), 5.98 (d, *J* = 6.0 Hz, 1H), 6.01 (d, *J* = 5.7 Hz, 1H), 6.05 (t, *J* = 5.7 Hz, 1H), 6.58 (d, *J* = 5.5 Hz, 1H), 7.03-7.05 (m, 2H), 7.29-7.30 (m, 3H), 7.33-7.40 (m, 4H), 7.52 (d, *J* = 7.5 Hz, 2H), 7.83 (t, *J* = 8.5 Hz, 4H); **^{13}C NMR** (125.73 MHz, $CDCl_3$): δ_c 48.3, 53.9, 60.5, 78.7, 78.8, 86.4, 88.1, 88.9, 90.5, 127.3, 128.0, 128.1, 128.2, 128.3, 128.6, 129.1, 129.4, 129.6, 130.5, 134.7, 135.7, 142.9; HR-MS: *Calcd* for $[C_{27}H_{27}N_2O_2SRu]^+$ 545.0837 *m*/*z*, found: 545.0834 *m*/*z*. Elemental analysis: *Calcd* for $[C_{27}H_{27}N_2O_2SRuCl(H_2O)_{0.4}]$: C, 55.22%; H, 4.77%; N, 4.77%. Found: C, 55.14%; H, 4.62%; N, 4.86%.

[(η^6-biph)Ru(DanEnBz)Cl] (**15**). Complex **15** was obtained following the method described for complex **7**, where [(η^6-biph)$RuCl_2$]$_2$ (100 mg, 0.153 mmol), DanEnBz (123 mg, 0.32 mmol) and triethylamine (89 μL, 0.64 mmol) were added. The crude product was purified by silica column chromatography (MeOH/DCM, 1:9 (v/v)). Dark red solid was obtained. Yield = 138 mg (67%). **^{1}H NMR** (400 MHz, $CDCl_3$): δ_H 1.87-1.97 (m, 1H), 2.09-2.12 (m, 1H), 2.35 (dt, *J* = 2.7 Hz, 12.7 Hz, 1H), 2.84 (s, 6H), 3.10 (dd, *J* = 3.9 Hz, 12.7 Hz, 1H), 3.55 (dd, *J* = 10.5 Hz, 13.2 Hz, 1H), 3.92 (s, broad, 1H), 4.38 (dd, *J* = 4.0 Hz, 13.5 Hz, 1H), 5.63 (t, *J* = 5.6 Hz, 1H), 5.99-6.03 (m ,2H), 6.08 (t, *J* = 5.6 Hz, 1H), 6.52 (d, *J* = 5.4 Hz, 1H), 7.04-7.06 (m, 2H), 7.12 (d, *J* = 7.4 Hz, 1H), 7.29-7.32 (m, 3H), 7.39 (t, *J* = 7.8 Hz, 1H), 7.47-7.53 (m, 4H), 7.83-7.84 (m, 2H), 8.38 (dd, *J* = 8.6 Hz, 11.7 Hz, 2H), 8.73 (d, *J* = 8.6 Hz, 1H); **^{13}C NMR** (125.73 MHz, $CDCl_3$): δ_c 45.5, 48.5, 54.36, 60.1, 79.7, 80.2, 85.5, 85.7, 86.5, 92.2, 114.6, 121.5, 123.5, 127.0, 127.1, 127.4, 127.8, 127.9, 128.1, 128.2, 128.3, 128.5, 128.8, 128.9, 129.4, 129.7, 130.0, 130.1, 130.6, 134.7, 135.9, 151.0; HR-MS: *Calcd* for $[C_{33}H_{34}N_3O_2SRu]^+$ 638.1415 *m*/*z*, found: 638.1419 *m*/*z*. Elemental analysis: *Calcd* for $[C_{33}H_{34}N_3O_2SRu\ Cl(H_2O)_{0.9}]$: C, 57.49%; H, 5.23%; N, 6.09%. Found: C, 57.41%; H, 4.97%; N, 6.21%.

4.2.3 X-ray Crystallography

The x-ray crystallographic analysis was carried out by Dr. Guy Clarkson.

Diffraction data for complex **9** were collected on an Oxford Diffraction Gemini four-circle system with an AtlasS2 CCD area detector. The structure of complex **9** was refined by full-matrix least-squares against F2 using Olex2[19] and was solved by with the ShelXT[20] structure solution program using Intrinsic Phasing and refined with the ShelXL[21] refinement package using Least Squares minimisation. The atoms from the sulphonamide nitrogen to the end of the chain (C10 C11 N12 C13) were modelled as disordered over two positions related by a small ruffle in the chain. The occupancy of the two positions was linked to a free variable which

refined to 86:14. The minor component was refined isotopically. The NH of the major component was located in a difference map though both it and the NH of the minor position were placed at calculated positions for the rest of the refinement. The data were processed by the modelling program Mercury 3.8.

4.2.4 *In vitro* Growth Inhibition Assays

The biological testing was carried out by Dr Isolda Romero-Canelón and Ji-Inn Song.

The antiproliferative activity of complexes **7–15** was determined against A2780 human ovarian and A549 human lung cancer cells. Briefly, 5,000 cells per well were seeded in 96-well plates. The plates were left to pre-incubate with drug-free medium at 310 K for 48 h before adding different concentrations of the tested compounds. Exact drug concentrations were determined by ICP-OES. A drug exposure period of 24 h was allowed. After this, supernatants were removed by suction and each well was washed with PBS. A further 72 h were allowed for the cells to recover in drug-free medium at 310 K. The Sulforhodamine B (SRB) assay was used to determine cell viability. IC_{50} values, as the concentration that causes 50% cell death, were determined as duplicates of triplicates in two independent sets of experiments and their standard deviations were calculated.

4.2.5 Cell Cycle Arrest

Approximately 1.5×10^6 per well of A2780 human ovarian cancer cells were cultured in a six-well plate and pre-incubated in drug-free media at 310 K for 24 h, after which complex **8** at equipotent IC_{50} concentration were added. After drug exposure for 24 h, supernatants were removed by suction and cells were washed with PBS. Then A2780 cells were harvested using trypsin-EDTA and fixed with cold 70% ethanol for 2 h. DNA staining was obtained by re-suspension of cell pellets in PBS (containing propidium iodide (PI) and RNase). Cell pellets

were washed and re-suspended in PBS before being analysed in a Becton Dickinson FACScan flow cytometer using excitation of DNA-bound PI at 536 nm, with emission at 617 nm. And data were processed with Flowjo software.

4.2.6 ROS Determination

ROS/superoxide induction in A2780 cells induced by complex **8** was determined using the Total ROS/Superoxide detection kit (Enzo-Life Sciences) according to the instructions. The analysis was performed *via* Flow cytometry. Generally, 1.0×10^6 of A2780 cells per well were seeded in the six-well plate and then pre-incubated in drug-free media at 310 K for 24 h (under 5% CO_2 humidified conditions), and then drugs were added to triplicates wells at equipotent IC_{50} concentration. After 24 h of drug exposure, supernatants were removed by suction and cells were washed with PBS and harvested. Cell pellets were then re-suspended in PBS buffer containing the orange/green fluorescent reagents to achieve cell staining. Cells were analysed in a BD LSR II flow cytometer (488 nm laser) using FITC-A channel: 575/26 nm for the oxidative stress and PE-A channel: 530/30 nm for superoxide detection. Data were gated using positive-stained (pyocyanin positive control), untreated-stained and untreated-unstained control samples, acquired as instrumental triplicates by using Flowjo V10 for Windows software. All samples were kept under dark conditions to avoid light-induced ROS production.

4.3 Results

4.3.1 Synthesis and Characterization

The chelating diamine ligands [BzEnL], where L is phenylsulfonyl, 4-F-phenylsulfonyl, 4-NO_2-phenylsulfonyl and danzyl, were synthesized following a reported protocol (shown in **Chapter 2**) and complexes **7-15** of the type [(η^6-arene)M(BzEnR)Cl], where arene is benzene, $HO(CH_2)_2O$-phenyl and biphenyl, M is Ru or Os, and R is various sulfonyl substituents were synthesized under the same conditions with the reported protocols[18] (**Table 4.1**). The dansyl complex **15** was synthesized specifically for the fluorescence study. Generally, triethylamine (4 mol equiv) and ligand (2-2.1 mol equiv) were added to the a solution of degassed isopropanol with Ru^{II}/Os^{II} dimers [(η^6-arene)Ru/$OsCl_2$]$_2$, the reactions were stirred under a N_2 atmosphere at 365 K for 10 h. All the synthesized complexes were purified by silica chromatography column (MeOH/DCM, 2:8(v/v)) and characterized by NMR spectroscopy (^{1}H, ^{13}C and ^{19}F), high resolution mass spectrometry (HR-MS) and elemental analysis (CHN).

4.3.2 X-ray Crystal Structure

A crystal of complex **9** [(η^6-biph)Ru(BzEnTs)I] suitable for X-ray crystallographic analysis was obtained from a slow diffusion of diethyl ether into saturated methanol solution of complex **9** at ambient temperature. Selected bond lengths and angles for complex **9** are listed in **Table 4.2**, crystallography data in **Table 4.3**, and the X-ray crystal structure is shown in **Figure 4.3**. Complex **9** adopts a *pseudo*-tetrahedral geometry with the η^6-bonded aromatic ring blocking one face of the metal centre occupying 3 coordination sites. The ethylenediamine ligand is deprotonated and bound as a monoanionic bidentate ligand to Ru, together with an iodide completing the coordination sphere of complex.

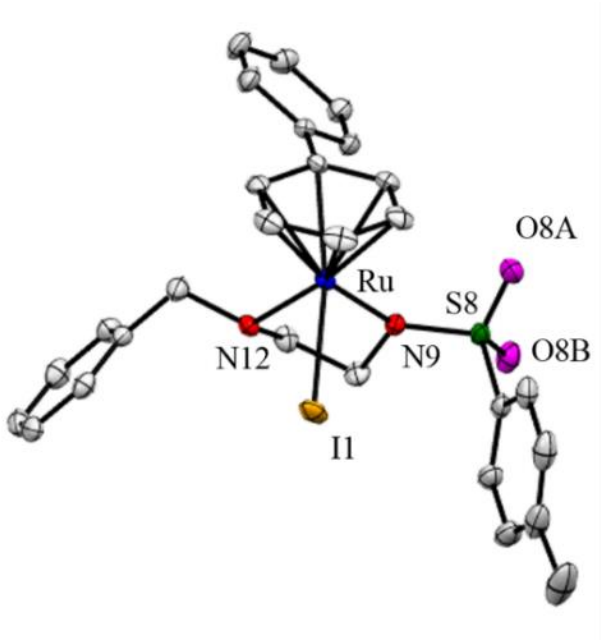

Figure 4.3 ORTEP diagram for complex **9**. Ellipsoids are shown at the 50% probability level. All hydrogen atoms and solvent molecules have been removed for clarity.

Table 4.2 Selected Bond Lengths (Å) and Angles (deg) for Complex **9**

Bonds	Length (Å) /Angle (°)
Ru−N9	2.123(3)
Ru−N12	2.174(3)
Ru−I1	2.7434(3)
Ru−arene (centroid)	1.672
N9−Ru−N12	78.60(11)
N9−Ru−I1	90.65(7)
N12−Ru−I1	83.90(8)

Table 4.3 Crystallographic Data for Complex **9**

Crystal character	red block
Empirical formula	$C_{28}H_{29}IN_2O_2RuS$
Formula weight	685.56
Temp (K)	150(2)
Crystal system	monoclinic
Space group	P_n
a /Å	10.91549(4)
b /Å	9.33603(4)
c /Å	13.28373(5)
α /°	90
β /°	98.2296(3)
γ /°	90
Volume/Å^3	1339.768(9)
Z	2
D_{calc} (mg/cm^3)	1.699
μ/mm^{-1}	14.728
F (000)	680.0
Crystal size/mm^3	0.6 × 0.16 × 0.08 orange block
Reflections collected	38933
Indep reflection	5343
R [I>=2σ (I)]	R^1 = 0.0168
Final R [all data]	R^2 = 0.0426

4.3.3 pK_a^* Determination

The pK_a^* values (pK_a determined in deuterated solvent) of the aqua adducts of complexes **7**, **8** and **10-14** were determined by titration over the pH* range from 2 to 12, and the ^{1}H NMR chemical shifts of protons of the sulfonyl phenyls as a function of pH* were monitored and fitted to the Henderson−Hasselbalch equation (**Figure 4.4**). All the pK_a^* values of aqua complexes are in the range of 9.10-9.75 (**Table 4.5**).

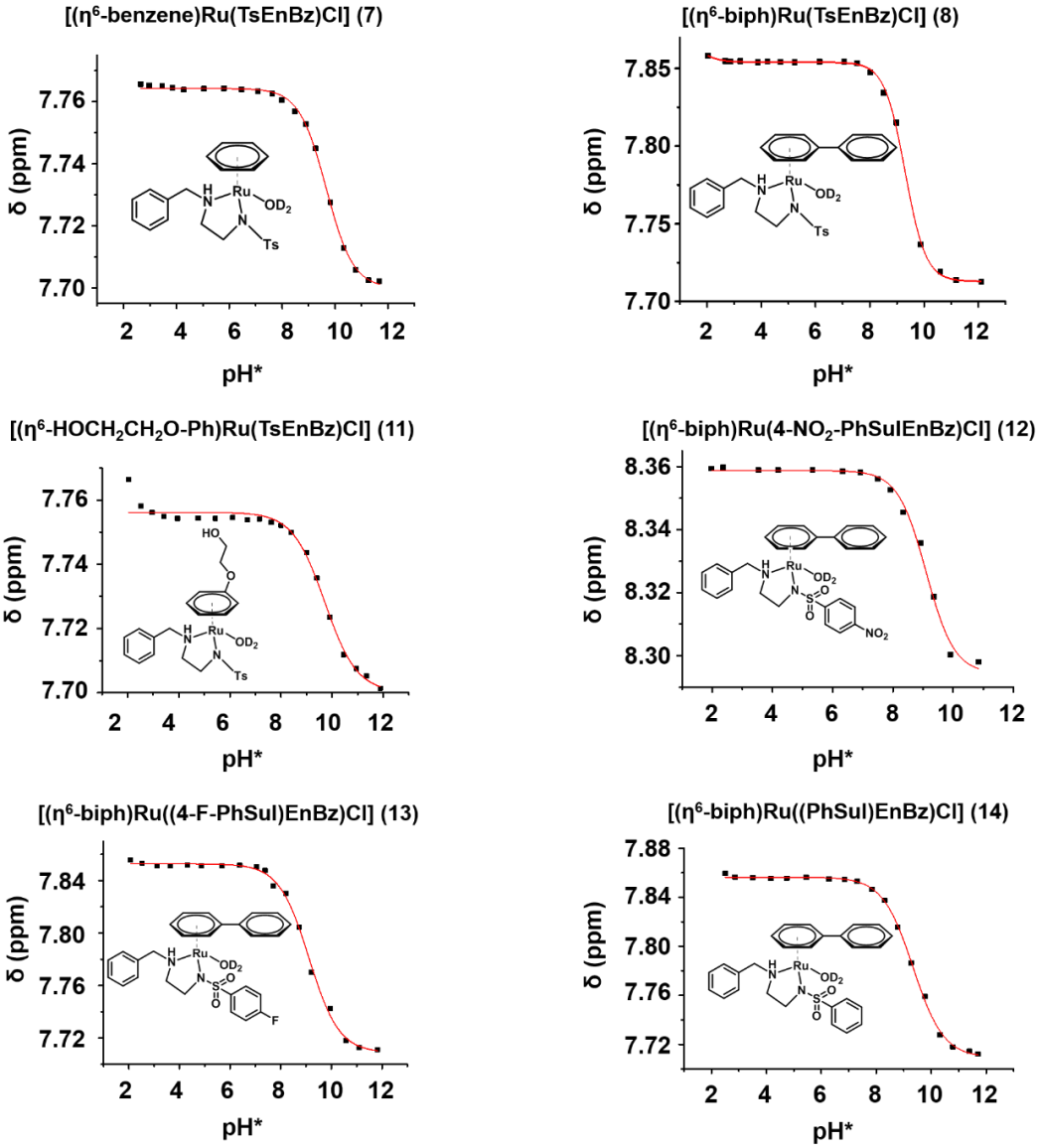

Figure 4.4 Dependence of chemical shift of the sulfonyl-phenyl protons of complexes **7**, **8** and **11-14** on pH*. The lines (red) are the best fits to Henderson-Hasselbalch equation, giving pK_a* values shown in **Table 4.5**.

4.3.4 DNA Nuclear Base Binding

The interaction of complex **8** and **10** with DNA nucleobase model: 9-ethylguanine (9-EtG) was studied by ^{1}H NMR spectroscopy (**Figures 4.5** and **4.6**). The reactions were performed by titrating nucleobase solution (in D_2O) with complexes **8** and **10** (2 mM, 10% MeOD-d_4 in D_2O) at 310 K, in 0.5 mol equiv steps. The binding adducts were confirmed by following a new set of peaks. No peaks for the original complexes peaks were observed when 1.5 mol equiv of 9-EtG was added, indicating completion of the reaction.

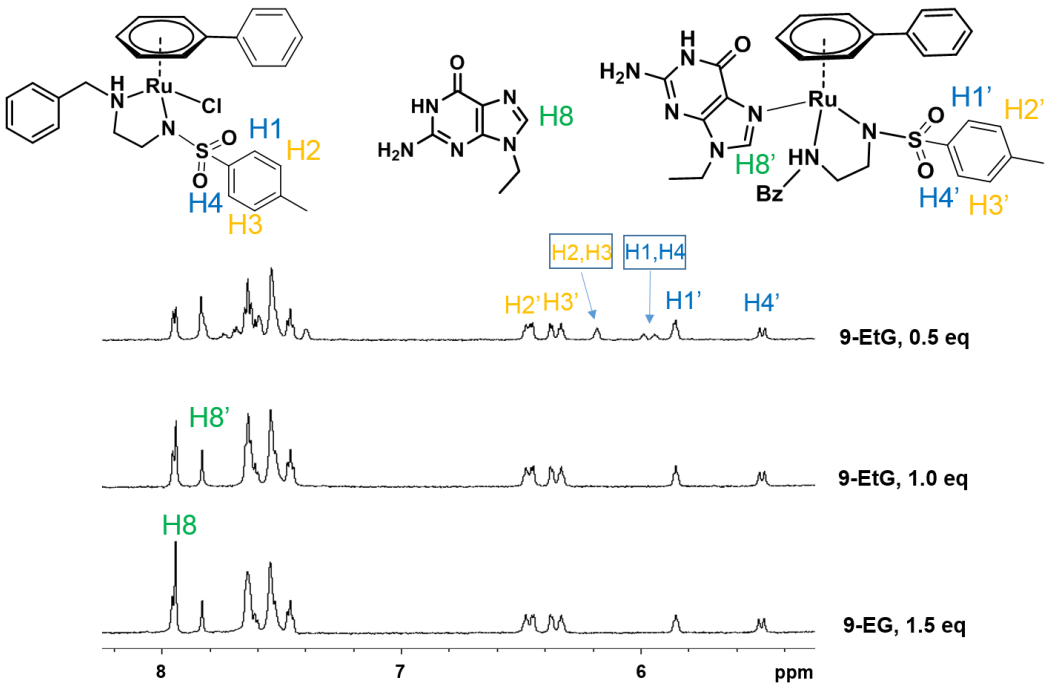

Figure 4.5 Low field ^{1}H NMR spectra for titration of complex **8** (2 mM in MeOD-d_4/D_2O, 2:8 (v/v)) with 9-ethylguanine (9-EtG, 1 mM–3 mM, 0.5–1.5 mol equiv), pH* at 7.2, 310 K. Blue arrows correspond to unreacted Ru complex **8**.

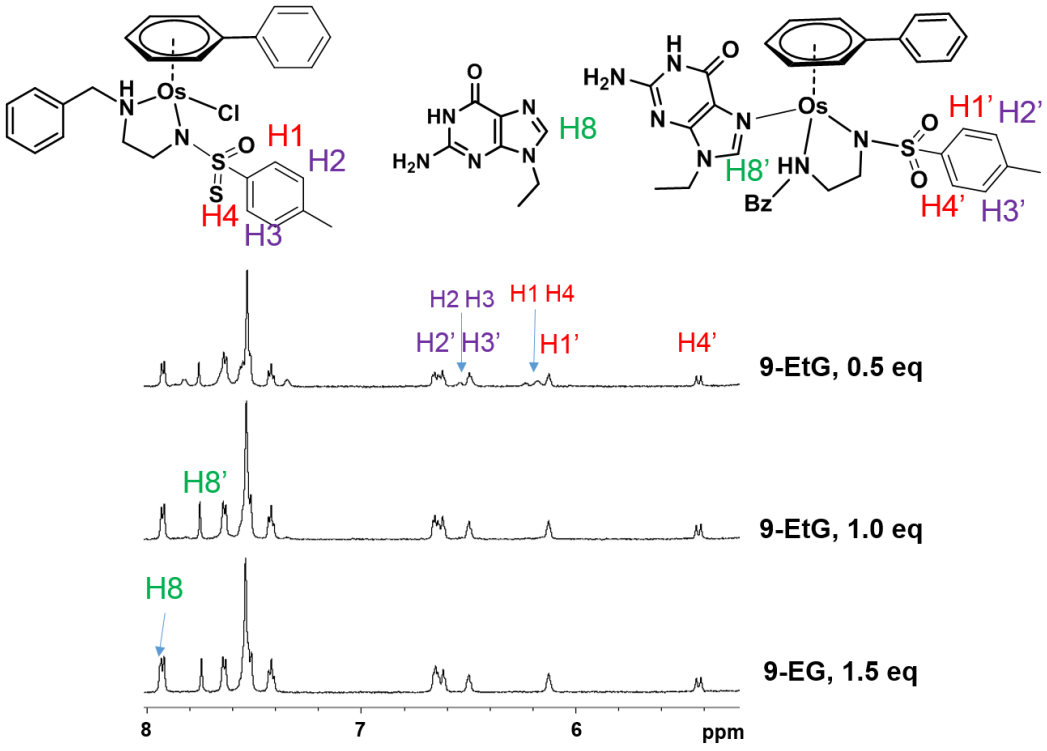

Figure 4.6 Low field ^{1}H NMR spectra for titration of complex **10** (2 mM in MeOD-d_4/D_2O, 2:8 (v/v)) with 9-EtG (in D_2O, 1 mM–3 mM, 0.5–1.5 mol equiv), pH* at 7.2, 310 K. Blue arrows correspond to unreacted Ru complex **10**.

4.3.5 Interaction with Glutathione

The interactions of complex **8** with Glutathione (GSH) was investigated via a series of concentration dependent experiments and monitored by ^{1}H NMR (pH* 7.2, 310 K). Complex **8** (2 mM, MeOD-d_4/D_2O, 2:8 (v/v)) and GSH (in D_2O) were in the ratio of 1: X, where X = 1, 2, 5, 10 mol equiv, respectively. All the reactions were all complete within 10 min. From the spectra, complex **8** reacted rapidly with GSH, and a new set of peaks was found when complex **8** was treated with 1.0 mol equiv of GSH solution (**Figure 4.7**). The arene proton peaks (biphenyl) of complex **8** disappeared (in blue arrow) when excess GSH (2-10 mol equiv) was added, indicating the completion of reaction. However, the adduct species **8**-SG was difficult to identify in the ^{1}H NMR spectrum (**Figure 4.7**).

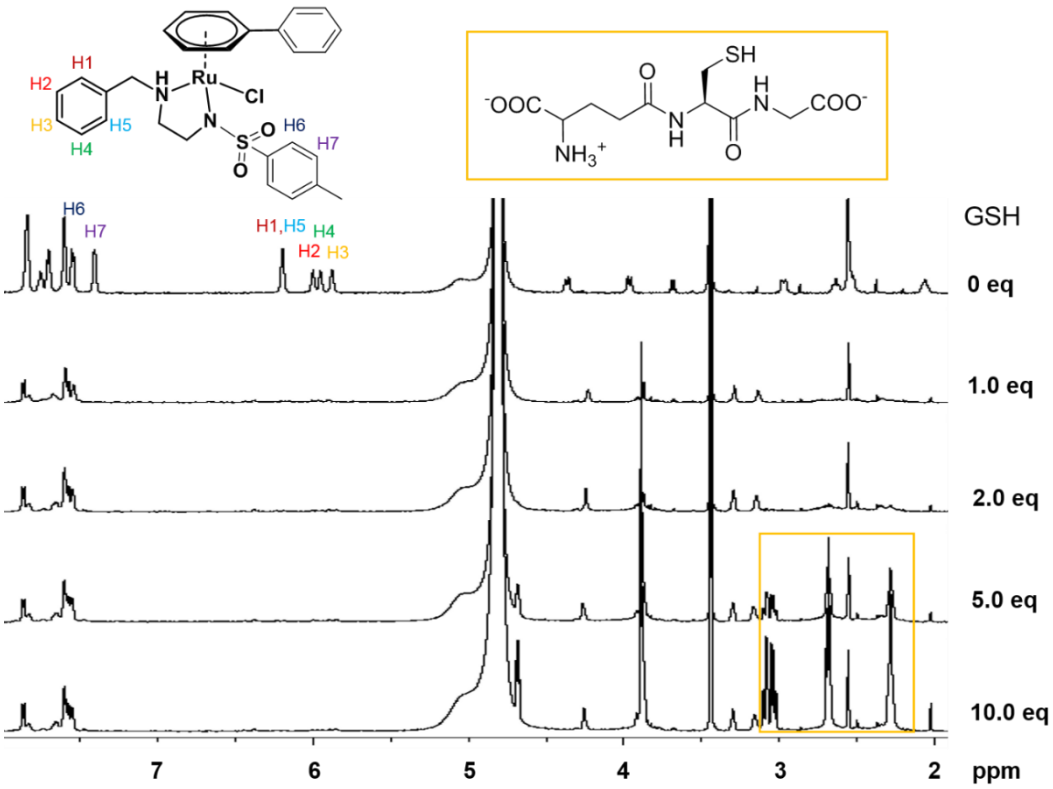

Figure 4.7 Low field region of ^{1}H NMR (600 MHz) spectra of the reactions between complex **8** and various concentrations of GSH (1.0-10 mol equiv) in MeOD-d_4 and D_2O (2:8, v/v). The pH* was adjusted to 7.2 ± 0.1 and all spectra were recorded at 310 K. Peaks for excess GSH are in the orange box.

4.3.6 Identification of GSH/NAC Adducts by LC-MS

In order to identify the binding mode of complex **8** with GSH, a second set of experiments for reaction of complex **8** with GSH was investigated by HPLC and LC-MS (eluent gradients are shown in **Figure 4.8**). Another thiol-containing molecule *N*-acetyl-L-cysteine (NAC) was also studied for comparison.

Time (min)	% B (acetonitrile, 0.1% TFA)
0	2
10	12
15	15
25	25
30	50
50	50
55	2

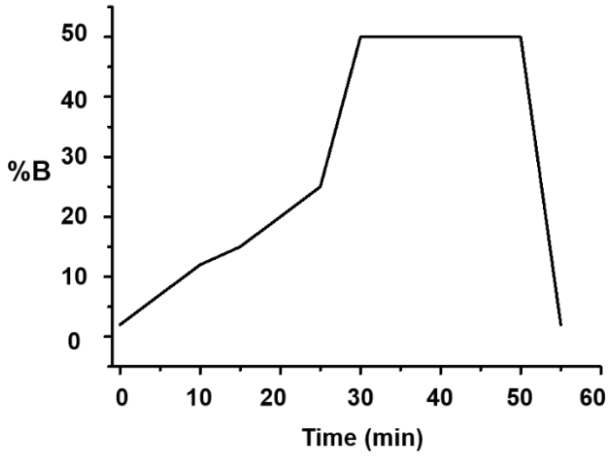

Figure 4.8 HPLC and LC-MS gradients for identification and separation of the Ru-SG and Ru-NAC adducts from the reaction of complex **8** and GSH/NAC, TFA was used to ensure the shape of the peak on HPLC (TFA, trifluoroacetic acid). Column type: ZORBAX Eclipse XDB-C18, 9.4 × 250 mm, 5 µm.

Complex **8** (2 mM in MeOH/H_2O, 1: 9 (v/v)) and GSH or NAC (20 mM in H_2O, 10 mol equiv) were mixed in a vial and pre-incubated at 310 K for 24 h (pH 7.10 ± 0.1). As can be seen from **Figure 4.9**, the reactions proceeded with over 95% and 100% conversions to form the Ru^{II}-SG and Ru^{II}-NAC adducts as determined by HPLC (**Figure 4.9**); peak p4 is assignable to complex **8** and disappeared after 24 h co-incubation at 310 K, with two new peaks p1 and p2 emerging (**Figure 4.9**). Subsequently, reactions were studied by LC-MS using the same conditions, and two dimers $[(\eta^6\text{-biph})_2Ru_2(SG)_3]^{2+}$ **8a** and $[(\eta^6\text{-biph})_2Ru_2(NAC)_3]^{+}$ **8b** which can be assigned to p1 and p2, respectively, were detected. The free chelating TsEnBz ligand was detected as peak p3. The peak assignments are listed in **Table 4.4**.

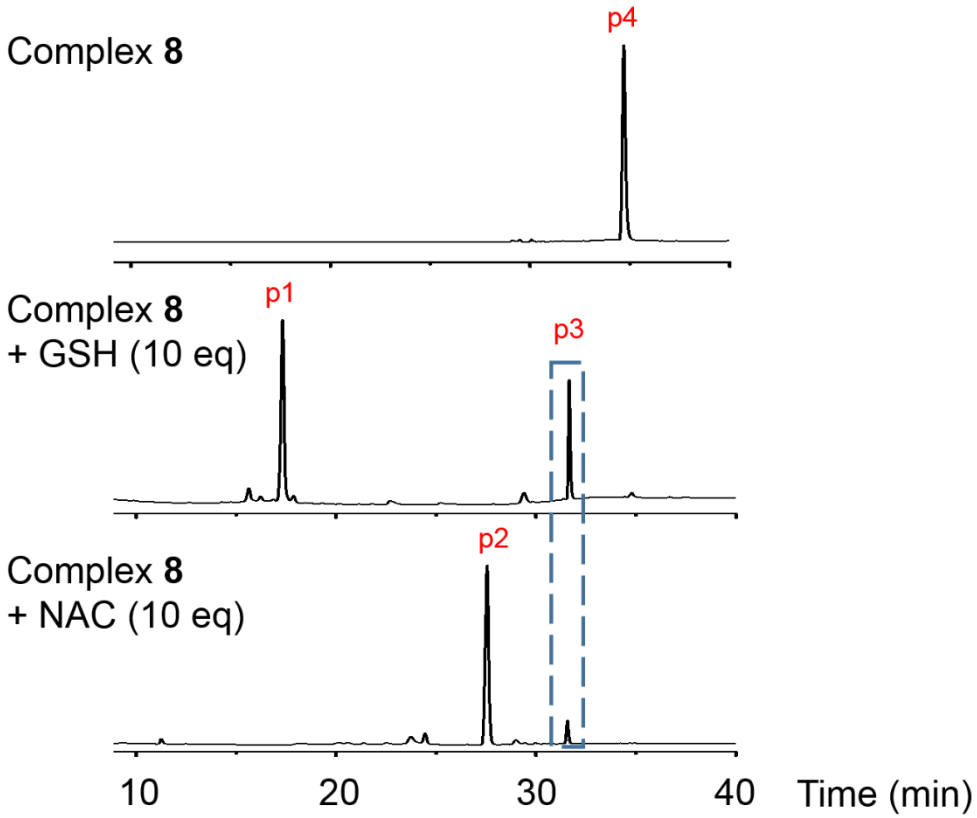

Figure 4.9 HPLC chromatograms for reaction of complex **8** with GSH and NAC monitored at 254 nm. Complex **8** (2 mM, MeOH/H_2O, 1:9 (v/v)) with GSH or NAC (20 mM, H_2O) were pre-incubated for 24 h at 310 K. pH of the solutions was adjusted to 7.2 ± 0.1.

Next, the isolation of the two Ru-S bridged dimers **8a** and **8b** was attempted by using a ZORBAX Eclipse XDB-C18 Semi-preparative HPLC column (9.4 × 250 mm). **8b** was collected and characterized by ^{1}H and ^{13}C NMR (^{1}H NMR spectrum shown in **Figure 4.10**). A high resolution mass peak at 715.6011 m/z was observed, which corresponds to $[(\eta^6\text{-biph})_2Ru_2(SG)_3]^{2+}$ (**8a** in **Figure 4.11**), and the peak at 998.0339 m/z is assigned to $[(\eta^6\text{-biph})_2Ru_2(NAC)_3]^{+}$ (**8b** in **Figure 4.12**).

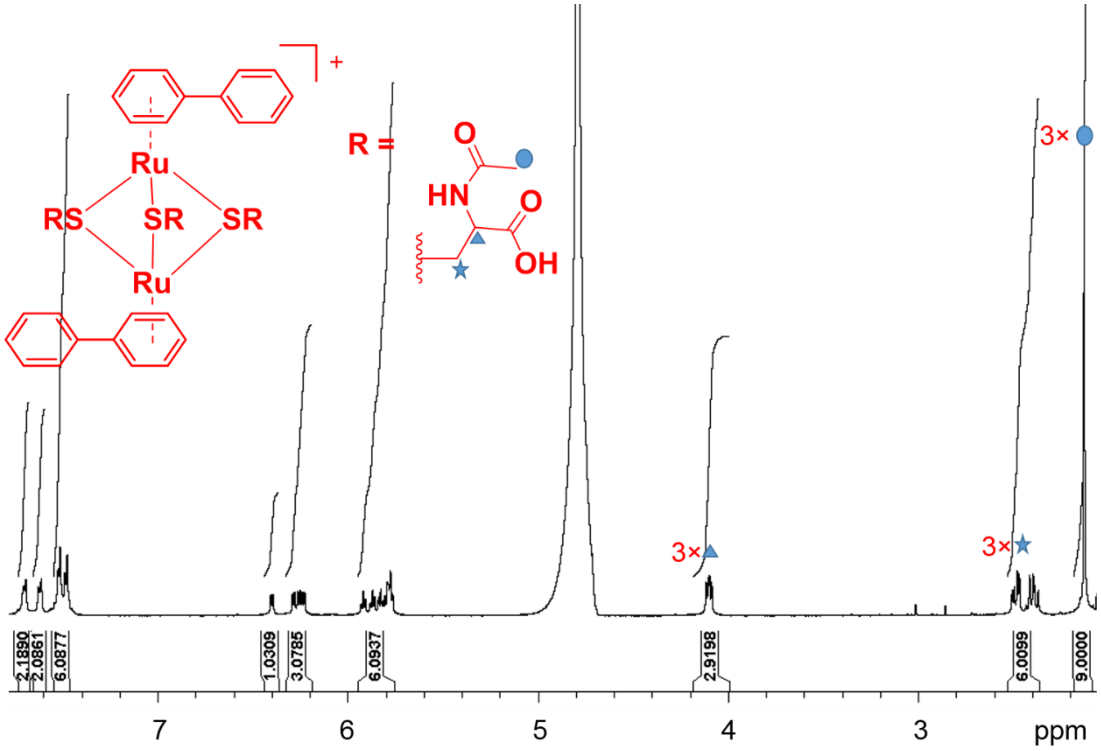

Figure 4.10 ^{1}H NMR spectrum (600 MHz, in D_2O) of $[(biph)_2Ru_2(NAC)_3]^+$ **8b**.

Table 4.4 HPLC Peak Assignments for Reaction of Complex **8** (1 mol equiv) with GSH or NAC (10 mol equiv).

Peak	Retention time (min)	Mass (*m/z*)	Assignment
p1	17.3	715.67	$[(\eta^6\text{-biph})_2Ru_2(GS)_3]^{2+}$
p2	27.6	997.89	$[(\eta^6\text{-biph})_2Ru_2(NAC)_3]^+$
p3	31.6	305.20	ligand [TsEnBz]+H^+
p4	34.7	559.10	complex **8**, $[C_{28}H_{29}N_2O_2RuS]^+$

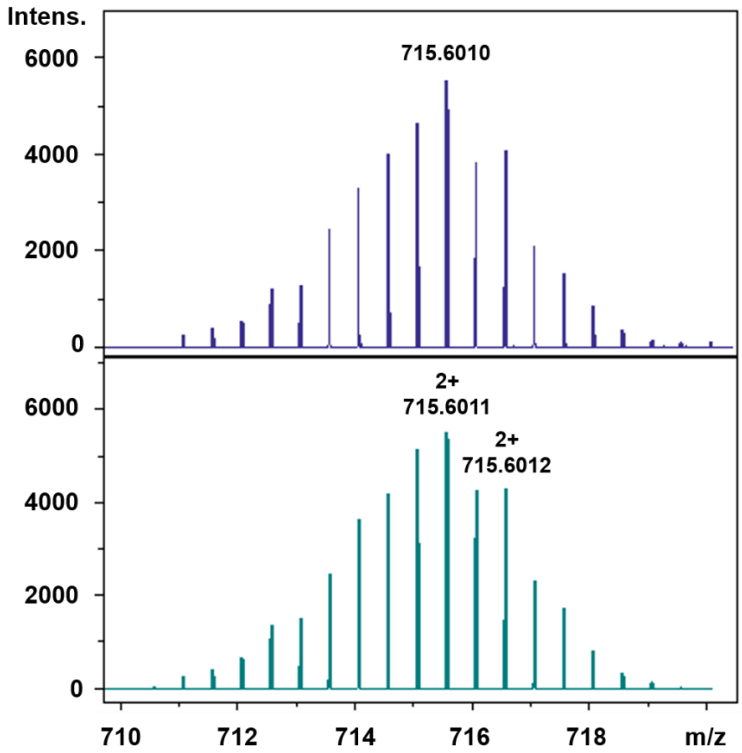

Figure 4.11 High resolution mass spectrum of complex **8a**; the top is the observed spectrum of **8a**; the bottom is the simulated spectrum of **8a**.

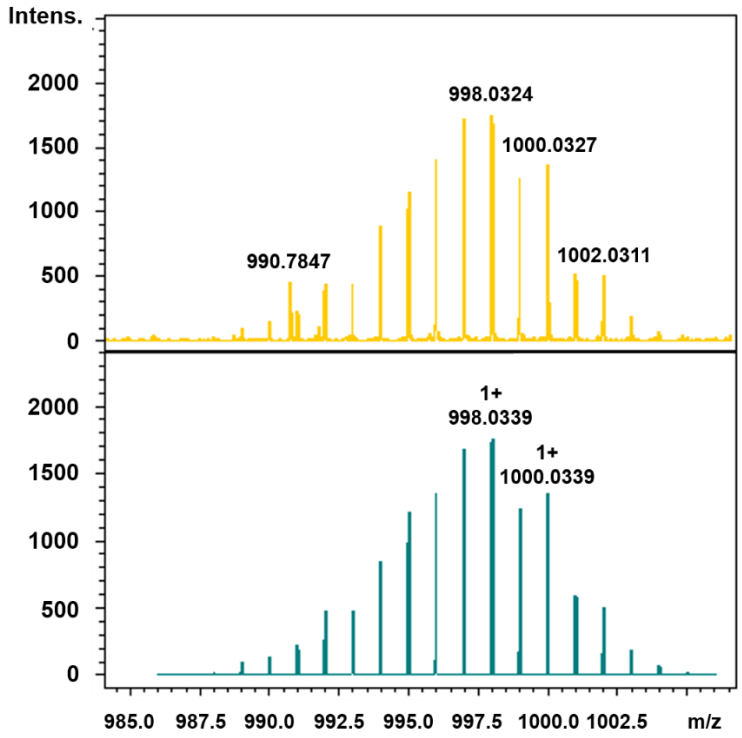

Figure 4.12 High resolution mass spectrum of complex **8b**; the top is the observed spectrum of **8b**; the bottom is the simulated spectrum of **8b**.

4.3.7 Kinetics of Transfer Hydrogenation Reactions

TH reduction of NAD^+ to give NADH was studied in an aqueous media using complexes **7-15** as catalysts and sodium formate as hydride source following a protocol described in **Section 3.2.4** of Chapter 3 (MeOD-d_4/D_2O, 1:9 (v/v), pH^* 7.2 ± 0.1, 310 K). All the kinetic experiments were monitored by ^1H NMR with Ru^{II}, NAD^+ and formate in a ratio of 1: 4: 25. It is evident from **Table 4.5**, that the turnover frequency (TOF) values of complexes **7-15** are in the range 2.5-12.9 h^{-1}, Os^{II} complex **10** has the highest TOF (12.9 ± 0.3 h^{-1}), while complex **11** has the lowest TOF value (2.5 ± 0.1 h^{-1}). Complexes **7** [(η^6-benzene)Ru(TsEnBz)Cl] and **8** [(η^6-biph)Ru(TsEnBz)Cl] bearing TsEnBz ligand have the similar TOF values (7.5 ± 0.3 h^{-1} and 7.9 ± 0.4 h^{-1}, respectively), while complexes **12** and **13** with more electron withdrawing functional groups 4-NO_2-Ph and 4-F-Ph give higher catalytic efficiency than **8**, with TOF values of 9.1 ± 0.5 h^{-1} and 9.7 ± 0.1 h^{-1}, respectively; while complex **14** with weaker electron effect gives slightly lower TOF value (6.74 ± 0.04 h^{-1}).

Table 4.5 Turnover Frequencies for Conversion of NAD^+ to NADH Catalysed by Complexes **7-15** and pK_a^* Values for the Aqua Adducts of Complexes **7-15**

Complex	TOF (h^{-1})	pK_a^*
7	7.5 ± 0.3	9.67 ± 0.03
8	7.9 ± 0.4	9.3 ± 0.1
9	5.7 ± 1.4	n. d.
10	12.9 ± 0.3	n. d.
11	2.5 ± 0.1	9.71 ± 0.05
12	9.1 ± 0.5	9.1 ± 0.2
13	9.7 ± 0.1	9.12 ± 0.04
14	6.74 ± 0.04	9.34 ± 0.07
15	3.7 ± 0.6	n. d.

4.3.8 GSH Mediated TH Reduction of NAD^+

Given the abundance of GSH in mammalian cells, the influence of GSH on NAD^+ TH reaction catalysed by complex **8** was investigated under similar conditions (MeOD-d_4/D_2O, 1:9 (v/v), pH^* 7.2, 310 K). Complex **8** (1.4 mM, MeOD-d_4/D_2O, 2:8 (v/v),), NAD^+, GSH and sodium formate (D_2O) were in the ratio of 1: 4: X: 25, where X = 0.2, 0.5, 1 and 2 mol equiv. The kinetic experiments was recorded every 5 min by ^1H NMR. The catalytic efficiency of complex **8** changed little, with TOF decreasing slightly from 7.9 ± 0.4 h^{-1} to 6.29 ± 0.53 h^{-1} when 0.2 mol equiv GSH was present. However, the TOF dropped dramatically to 0.91 ± 0.43 h^{-1} when 0.5 mol equiv GSH was co-administered. The reaction totally stopped when 1 mol equiv or more GSH was added, probably due to the decomposition of complex **8** when exposed to GSH.

4.3.9 GSH and L-Cysteine Triggered Fluorescence of a Labelled Complex

The fluorescence of DanEnBz was fully quenched when it was present as a chelated ligand in complex **15** (see **Table 4.1** for structure) and no obvious fluorescence was found when complex **15** was dissolved in DMSO and H_2O, **Figure 4.13c**. As found above, GSH can quickly interact with complex **8** to form the $[(\eta^6\text{-biph})_2Ru_2(SG)_3]^{2+}$ dimers, accompanied by release of the sulfonyl ethylenediamine ligand. Such interaction may re-trigger the fluorescence of DanEnBz of complex **15**. As expected, an immediate emission was observed when complex **15** (2mM in DMSO/H_2O, 2:8(v/v)) was treated with GSH or NAC (20 mM in H_2O, **Figure 4.13**). About a 200-fold increase in emission intensity was induced by mixing complex **15** with GSH with excitation at 350 nm (**Figure 4.13a**), NAC induced a stronger increase in fluorescence under the same conditions (*ca.* 1.7-fold stronger than GSH); but when excited solution at 405 nm, the emission intensity was relatively lower, only about 40-fold intensity for GSH and 60-fold for NAC when compared to negative solution (complex **15** only, **Figure 4.13b**). In a further experiment, in order to identify the binding mode (thiol or carboxyl moiety), complex **15** was

reacted with two carboxyl-containing amino acids (thiol-free), L-leucine and L-tryptophan, and one thiol-containing molecule (carboxyl-free), 1-butanethiol. Interestingly, no obvious fluorescence was observed when **15** was mixed with thiol-free amino acids; however, a relatively strong fluorescence emission was found when 1-butanethiol was added, indicating that such a complex has a high thiol affinity.

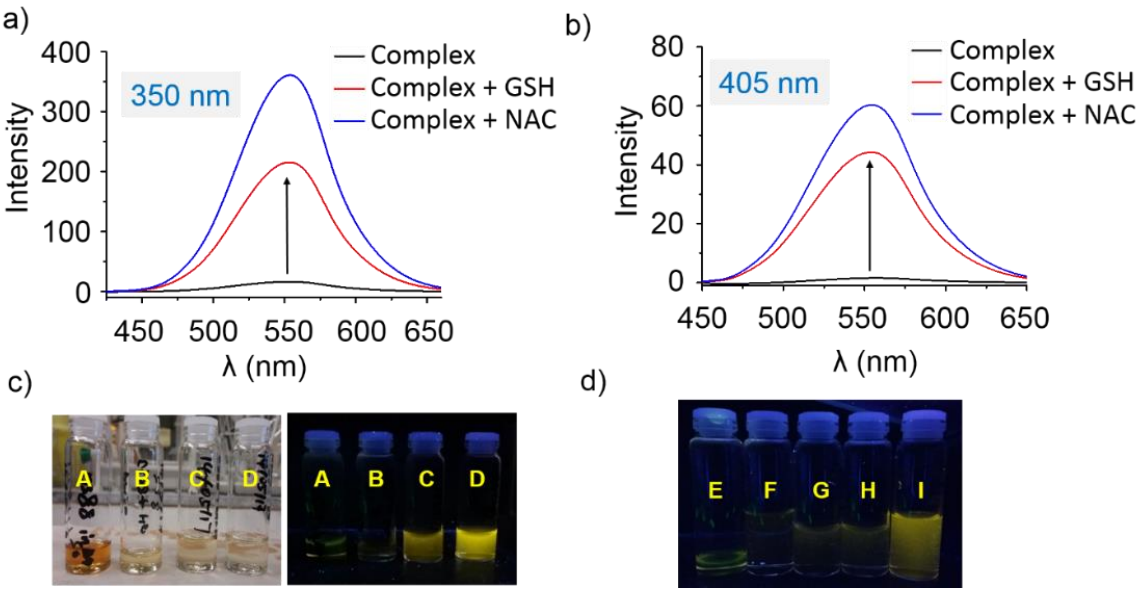

Figure 4.13 GSH- and NAC-triggered fluorescence of complex **15**. a) Solution excited at 350 nm; b) solution excited at 405 nm; c) A: complex **15** in DMSO, B: complex **15** in DMSO/H_2O (1: 9 (v/v)), C: complex **15** (0.1 mM, DMSO/H_2O, 1: 9 (v/v)) with GSH (2 mM in water) and D: complex **15** (0.1 mM, DMSO/H_2O, 1: 9 (v/v)) with NAC (2 mM in water) under UVA; d) induction of fluorescence of complex **15** with L-leucine (G, 10 mol equiv), L-tryptophan (H, 10 mol equiv) and 1-butanethiol (I, 10 mol equiv) under UVA.

4.3.10 Antiproliferative Activity

The antiproliferative activity of complexes **7-15** against A2780 human ovarian, A549 human lung cancer cells was determined (**Table 4.6**). The clinical drug cisplatin (CDDP) was used as a comparison. As can be seen in **Table 4.6**, these complexes gave a broad range of IC_{50} values

ranging from 3.57 - >50 μM and 4.1-38.5 μM against A2780 human ovarian and A549 human lung cancer cells, respectively. Complex **13** has the best anticancer activity against A2780 cancer cells (IC_{50}, 3.57 ± 0.98 μM), while complex **14** [(η^6-biph)Ru(PhEnTs)Cl] is inactive. Complex **14** is potent towards A549 lung cancer cells (IC_{50}, 4.1 ± 1.3 μM), comparable to CDDP (IC_{50}, 3.1 ± 0.1 μM).

Table 4.6 Anticancer Activity of Complexes **7-15** against A2780 Human Ovarian and A549 Human Lung Cancer Cell Lines (IC_{50}, μM)[a]

Complex	IC_{50} (μM)	
	A2780	A549
7	8.32±0.54	28.8±2.6
8	11.25±0.08	13.5±1.4
9	18.4±1.2	32.2±0.7
10	28.18±0.16	n.d.
11	14.25±0.06	16.1±2.4
12	3.57±0.98	29.8±1.1
13	5.6±0.5	13.7±0.1
14	> 50	4.1±1.3
15	39.4±3.4	38.5±1.9
CDDP	1.2±0.02	3.1 ± 0.1

[a] Data are shown in means±standard deviation (STD), cell viability was assessed after 24 h incubation with Ru^{II} complexes and washed with PBS. A2780 human ovarian cancer cells, A549 human lung carcinoma cells.

4.3.11 Effect of L-Buthionine Sulfoximine on Antiproliferative Activity

L-Buthionine sulfoximine (L-BSO) is a specific inhibitor of γ-glutamylcysteine synthetase,[22] an enzyme involved in the biosynthesis of GSH. Treatment with L-BSO can scavenge the intracellular GSH levels up to 40%, which effectively hampers cellular GSH synthesis.[23] Next, the anticancer activity against A549 human lung cancer cells by co-incubation complex **8** with

L-BSO was determined, to investigate the role of GSH in antiproliferative activity. Complex **8** was coadministered with three different concentrations of L-BSO: 1, 5 and 50 μM. Interestingly, after 24 h co-incubation with L-BSO (at concentrations of 1 and 5 μM), the antiproliferative activity (IC_{50}, *ca.* 13 μM) of **8** retained unchanged; but the activity of complex **8** decreased to 8.3 ± 0.5 μM when co-treated with 50 μM L-BSO (decreasing by a factor of 0.64).

4.3.12 Effect of GSH and NAC on Anticancer Activity

GSH often acts as a detoxification agent for metal-based drug in cells, and some drug resistant cancer cells are capable of generating higher levels of GSH to circumvent damage. N-Acetyl-L-cysteine (NAC) is a reactive oxygen species (ROS) scavenger, which can block the cisplatin related caspase-3 activation and cell apoptosis.[24] Since complex **8** can react rapidly with GSH to form the dimers **8a** $[(\eta^6\text{-biph})_2Ru_2(SG)_3]^{2+}$, co-administration of complex **8** with GSH (5, 10 and 50 μM) was studied, to investigate the effect of GSH on antiproliferative activity against A2780 human ovarian carcinoma cells. Cells exposed to three concentrations of GSH (5, 10 and 50 μM) were incubated as controls. The results indicate that only GSH exposure is not toxic towards A2780 cancer cells. After 72 h of recovery time in drug-free medium, cell survival was evaluated using the Sulforhodamine B colorimetric assay. As shown in **Figure 4.14**, the antiproliferative activity decreased gradually with increase of GSH concentrations, giving IC_{50} values of 22.41 ± 1.25, 29.9 ± 2.1 and > 50 μM towards A2780 cells and, 27.33 ± 0.54, 43.93 ± 3.54 and > 50 μM towards A549 cancer cells.

Further co-treatment of complex **8** with NAC displayed a similar trend, in which the anticancer activity reduced with the increase of NAC concentration (same concentrations and protocols as with GSH), IC_{50} values are 25.8 ± 0.9, 39.9 ± 0.9 and 53.8 ± 1.4 μM, for NAC concentration of 5, 10 and 50 μM, respectively.

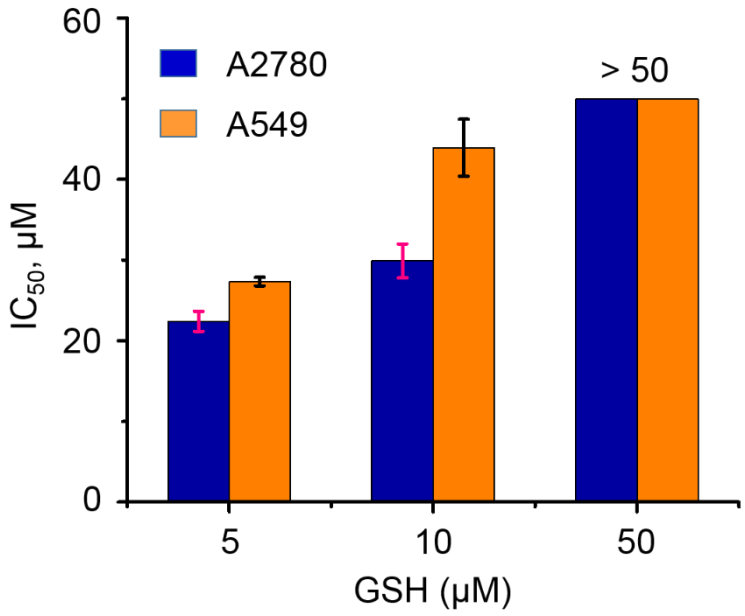

Figure 4.14 Antiproliferative activity of complex **8** against human A2780 ovarian and A549 lung cancer cells induced by co-administration with GSH in three different concentrations 5, 10 and 50 μM (GSH with various concentrations was added to cells firstly, followed by complex **8** following SRB protocols). After 24 h co-incubation with complex **8** and GSH, both cancer cells viability was assessed and washed with PBS. Data are presented in means ± standard deviations (STD).

4.3.13 Cell Cycle Arrest

The cell cycle analysis for complex **8** towards A2780 human ovarian cancer cell was performed by propidium iodide staining and flow cytometry. A2780 cancer cells were incubated with equipotent IC_{50} and 2 × IC_{50} concentrations of complex **8** for 24 h. In comparison to negative control population, complex **8** showed increased cell cycle arrest at G1 phase when the drug concentration increased from equipotent IC_{50} to 2 × IC_{50} (**Figure 4.15**).

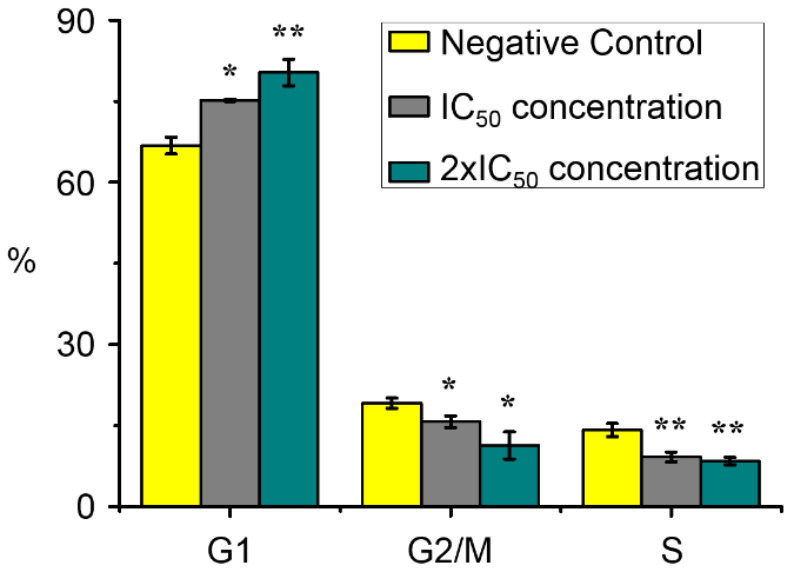

Figure 4.15 Cell cycle arrest analysis of A2780 human ovarian cancer cells after 24 h exposure to complex **8** at 310 K at IC_{50} and 2 × IC_{50} concentrations. Cell staining for flow cytometry was carried out using PI/RNase. Percentage of cell populations in each cell cycle phase for negative control and complex **8** were compared. *p*-Values were calculated after a *t*-test against the negative control data, *$p < 0.05$, **$p < 0.01$.

4.3.14 Reactive Oxygen Species (ROS) Determination

The level of reactive oxygen species (ROS) induced by complex **8** and **8** in combination with GSH in A2780 human ovarian cancer cells was determined at IC_{50} concentrations by flow cytometry fluorescence analysis (**Figure 4.16**). These experiments were carried out following previously described protocols.[25] A2780 cancer cells were treated with a fixed IC_{50} concentration of **8** and GSH (0.5 and 5 μM) without any recovery time. The total level of oxidative stress (including H_2O_2, peroxy and hydroxyl radicals, peroxynitrite, and NO) in FITC-A channel and superoxide production in PE-A channel were monitored. ROS levels were detected in more than 70% of A2780 cancer cells. The population of A2780 cells showed high fluorescence in FITC-A channel (*ca.* 73.1±1.9%) for complex **8** alone and low fluorescence in channel PE-A (*ca.* 26.8±2.0%), indicating a major induction of oxidative stress of complex **8**

in A2780 cancer cells. Interestingly, cell population in FITC-A-/PE-A+ and FITC-A+/PE-A+ channels decreased with increase of GSH concentration, from *ca.* 16.8±0.8% to *ca.* 5.9±0.5%. However, inversely, cell populations in FITC-A+/PE-A- channels increased when 5 μM GSH was co-administered with **8**, from 71.7±1.7% to 86.3±0.5%, suggesting a higher oxidative stress.

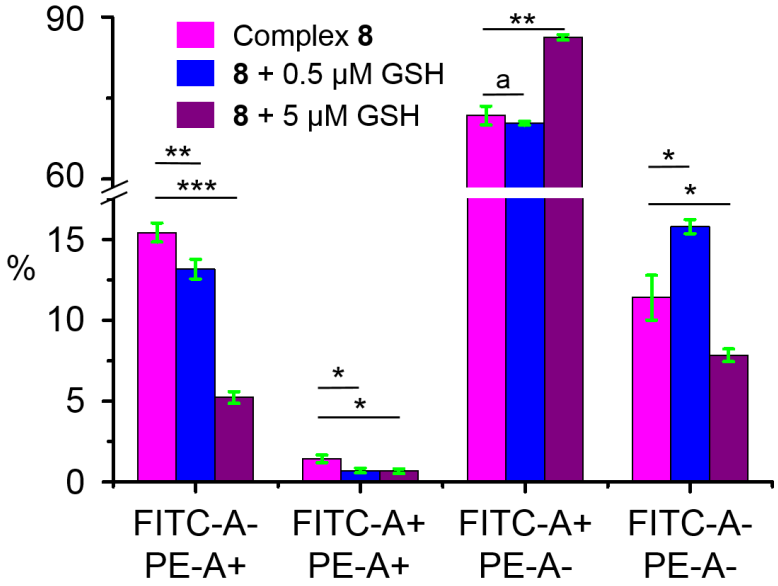

Figure 4.16 ROS induction in A2780 cancer cells exposed to complex **8**, **8** with 0.5 μM GSH and **8** with 5 μM GSH was investigated. FITC-A channel detects total oxidative stress, and PE-A channel detects production of superoxide. *p*-Values were calculated after two-tailed Welch's *t*-tests to determine the significance of variations, $^{a}p > 0.05$, $*p < 0.05$, $**p < 0.01$ and $***p < 0.001$.

4.4 Discussion

The characterized complex **9** [(η^6-biph)Ru(TsEnBz)I] has the 'piano-stool' geometry (**Figure 4.3**), which is structurally similar to the related Ru^{II} complexes.[18,26] The Ru-N bond lengths are 2.123 Å (Ru-$N(^-)$) and 2.174 Å (Ru-N(H)), which are close to those of complexes **3** [(η^6-*p*-cym)Ru(TsEnEt)Cl] (2.126 Å and 2.1702 Å, respectively) in **Chapter 3**, but the Ru-N12 bond

length is 0.067 Å and 0.06 Å longer than the respective complexes [(η^6-biph)Ru(TsEn)Cl] (2.1073 Å) and [(η^6-biph)Ru(en)Cl]$^+$ (2.1104 Å). Interestingly, the Ru-I bond length is much longer than Ru-Cl of complex [(η^6-biph)Ru(TsEn)Cl] (2.7434 Å versus *ca.* 2.4173 Å), and is close to that of Os complex [(η^6-*p*-cym)Os(Impy-OH)I]$^+$ (2.7247 Å).[22] With regard to the bond angle, N12-Ru-I angle is 83.90^o which is smaller than that of [(η^6-*p*-cym)Ru(EtTsEn)Cl] (87.55^o). The rest of the bond lengths and angles showed no significant difference from the other Ru^{II} complexes.

Ru^{II} sulfonyl ethylenediamine complexes have been designed as potent catalysts in the (asymmetric) transfer hydrogenation (TH) reactions of ketones, imines, or importantly cell coenzyme NAD^+.[18,27,28] In Chapter 3, the catalytic efficiency of complex **4** [(η^6-*p*-cym) Ru(TsEnBz)Cl] in the TH reduction of NAD^+ to NADH was determined. In comparison, complexes **7** [(η^6-benzene)Ru(TsEnBz)Cl] and **8** [(η^6-biph)Ru(TsEnBz)Cl] retained the potency (7.4 ± 0.1 h^{-1} versus 7.5 ± 0.3 h^{-1} and 7.9 ± 0.4 h^{-1}), decreased in the order: **8** (biph) > **4** (*p*-cym) > **7** (benzene); which is slightly different from the previous observation that TOFs of complexes variable in arene decreased in the order: benzene > biph > *p*-cym.[18] Complex **11** [(η^6-$HO(CH_2)_2OPh$)Ru(TsEnBz)Cl] with hydrophilic side group $HO(CH_2)_2O$- on the phenyl arene gave lowest TOF (2.5 ± 0.1 h^{-1}), probably because the steric side chain is too bulky to allow close NAD^+ approach to the Ru centre.

L-BSO can limit the cellular synthesis of GSH, and enhance the ROS levels to induce cell apoptosis. Co-treatment of organometallic Ru^{II} or Os^{II} complexes with L-BSO has been developed as a strategy to overcome the GSH mediated detoxification,[29,30] also, L-BSO can restore the CDDP activity against several CDDP-resistant cancer cell lines, due to the inhibition of CDDP bound to GSH. In previous work, Romero-Canelón *et al.* have shown that L-BSO can cause a significant reduction in cellular GSH levels (5 μM L-BSO can induced *ca.* 50% drop in GSH levels) and significant enhancement of anticancer activity towards ovarian cancer

cells upon co-administration of organo-Os complex [Os(η^6-*p*-cym)(*p*-NMe_2-Azpy)I]PF_6 with L-BSO (5 μM dose), with 87% improvement in anticancer activity when equipotent 2 × IC_{50} concentration of complex was drugged.[23,24] However, such restoration of antiproliferative activity by L-BSO only occurs when a complex is already biologically active.[23] In the present work, enhancement of the anticancer activity against A549 cancer cells was observed only at a L-BSO concentration of 50 μM (IC_{50} values remained unchanged at L-BSO concentrations of 1 and 5 μM), with IC_{50} decreased from *ca.* 13 to 8.3 μM; at this L-BSO concentration, levels of GSH can be reduced to *ca*. 63%.[23] High L-BSO concentrations probably severely interfered with the cellular GSH synthesis, with higher ROS accumulated, which caused the cell apoptosis.

Since complex **8** reacted rapidly with 9-ethylguanine, it can potentially react with DNA. However, the cell cycle arrest study of complex **8** in A2780 cancer cells revealed a dose-dependent cell population increase in G1 phase (66.7 ± 1.5% to 75.2 ± 0.2% and 80 ± 2% at IC_{50} and 2 × IC_{50} concentrations), but a cell population depletion in G2/M and S phase, which may mean that the DNA targeting complex **8** is less likely (DNA-targeted compounds normally cause cell accumulation in S phase or G2/M phase, *e.g.* cisplatin[31]). This is in agreement with a previous study that [(η^6-arene)Ru(RTsEn)Cl] complexes are less likely to target DNA.[32]

Reactive Oxygen Species (ROS) display important roles in cell metabolism. As respiratory side-products of mitochondria, over-production from ROS damage proteins or oxidation of DNA nucleobases to induce cell apoptosis, and ROS-mediated apoptotic signalling is usually associated with reduction of cytosol or mitochondrial GSH levels.[33,34] Organo Ir, Os and Ru complexes have been widely reported as potent anticancer agents which can induce cell apoptosis via ROS involving pathways.[24,35-38] Complex **8** can induce significant amounts of superoxide in A2780 cancer cells (up to 16% of cell population, **Table 4.7**) in PE-A channel. Co-administration of complex **8** with GSH reduces both superoxide levels and antiproliferative

activity against A2780 human ovarian cancer cells. Plotting of the superoxide levels versus anticancer activity of complex **8** with or without GSH gives an inverse relationship which indicates that induction of ROS by complex **8** mainly aids in killing cancer cells.

Table 4.7 Induction of ROS and Superoxide Determined by Flow Cytometry Experiments on A2780 Human Ovarian Cancer Cells.

Complex	Population (%)			
	FITC-A-/PE-A+	FITC-A+/PE-A+	FITC-A+/PE-A-	FITC-A-/PE-A-
8	15.4±0.6 ***	1.4±0.2 ***	71.7±1.7 ***	11.4±1.4 ***
8+GSH(0.5)	13.2±0.6 ***	0.7±0.1 **	70.3±0.4 ***	15.8±0.4 ***
8+GSH(5)	5.2±0.4 **	0.67±0.15 **	86.3±0.5 ***	7.8±0.4 ***
Positive	0.66±0.08 **	98.8±0.3 ***	0.77±0.15 ***	0 ***
Negative	2.97 ± 0.15	1.53 ± 0.06	9.3±0.3	86.2±0.5

The FITC-A channel (576/26 nm) detects ROS and PE-A channel (530/30 nm) detects superoxide. All values compared to the untreated controls. In all cases, independent two-sample *t*-tests with unequal variances, two-tailed Welch's *t*-tests, were carried out to establish statistical significance of the variations (***$p < 0.001$, **$p < 0.01$, and *$p < 0.05$).

4.5 Conclusions

In this Chapter, 9 new Ru^{II} sulfonyl-substituted ethylenediamine complexes of the type [(η^6-arene)Ru(REnBz)X] (where the arene *p*-cymene, biphenyl or $HOCH_2CH_2O$-phenyl, R is tosyl, phenylsulfonyl, 4-F-phenylsulfonyl, 4-NO_2-phenylsulfonyl or danzyl, and X is halide) based on the scaffold of complex **4** [(η^6-*p*-cym)Ru(TsEnBz)Cl] in Chapter 3 were synthesized and fully characterized. The half-sandwich structure of complex **9** was confirmed by X-ray crystallography. Initially, to obtain more potent TH catalysts, more electron withdrawing bidentate ligand substituents, *e.g.* 4-F-phenylsulfonyl (**12**), 4-NO_2-phenylsulfonyl (**13**) were used to improve the catalytic activity. As expected, these complexes gave higher potency in TH reduction of coenzyme NAD^+ with formate as hydride donor, when compared with complexes **4**, **7** and **8** (which had similar TOF values). The introduction of the substituted arene $HOCH_2CH_2O$-phenyl in complex **11** improved the water solubility, however, the long side chain dramatically reduced the rate of hydride transfer (probably due to its bulkiness), giving a TOF value *ca.* 3× lower than for complex **4** (**Table 4.5**).

Complex **8** [(η^6-biph)Ru(TsEnBz)Cl] exhibited a high affinity for the free radical scavenger GSH (abundant cellular tripeptide) and N-acetyl-L-cysteine (NAC), to form the Ru-thiol bridged dimers $[(\eta^6\text{-biph})_2Ru_2(GSH)(GS)_2]^{2+}$ and $[(\eta^6\text{-biph})_2Ru_2(NAC)_3]^+$. Co-incubation of complex **8** with GSH can effectively reduce induction of reactive oxygen species, and decrease the antiproliferative activity significantly with the increase of GSH co-treatment concentration. Such decomposition of a Ru^{II} ethylenediamine complex can release the free diamine ligand can hence trigger the fluorescence of complex **15** [(η^6-biph)Ru(DanEnBz)Cl], which may provide a basis for a study the cellular distribution of the complex in the future.

Complex **8** binds to neutral DNA nucleobase 9-ethylguanine to form the **8**-9-EtG adduct (**Figure 4.5**). However, such Ru^{II} complexes only can cause G1 cell cycle arrest on a concentration-dependent mode, are unlikely to target DNA in cells.

The hydrophobicity of the complexes increases with increase of arene size; higher hydrophobicity facilitates uptake into cells, which increase anticancer potency.[39] Complex **7** (benzene) and **8** (biphenyl) with different arene sizes were compared with complex **4** (*p*-cymene); however, the antiproliferative activity of complex **8** (with the largest arene) is lower than complex **4** against A2780 human ovarian cancer cells. No obvious corrections between the anticancer activity of complexes **4**, **7** and **8** and arene size were observed, probably suggesting a difference in metabolic pathway for these complexes in cancer cells. The rapid interaction of complex **8** [(η^6-biph)Ru(TsEnBz)Cl] with cell-abundant GSH suggests a potential metabolic pathway when Ru sulfonyl ethylenediamine complexes enter mammalian cells, and role for GSH in the induction of ROS by Ru sulfonyl ethylenediamine complexes in cancer cells.

4.6 References

(1) a) Rosenberg, B.; Camp, L. v.; Krigas, T. *Nature* **1965**, *205*, 698–699; b) Gossens, C.; Tavernelli, I.; Rothlisberger, U. *J. Chem. Theory Comput.* **2007**, *3*, 1212–1222.

(2) Tripathy, S. K.; Taviti, A. C.; Dehury, N.; Sahoo, A.; Pal, S.; Beuria, T. K.; Patra, S. *Dalton Trans.* **2015**, *44*, 5114–5124.

(3) Dougan, S. J.; Habtemariam, A.; McHale, S. E.; Parsons, S.; Sadler, P. J.; *Proc. Natl. Acad. Sci. U. S. A.* **2008**, *105*, 11628−11633.

(4) a) Aird, R. E.; Cummings, J.; Ritchie, A. A.; Muir, M.; Morris, R. E.; Chen, H.; Sadler, P. J.; Jodrel, D. I. *Br. J. Cancer* **2002**, *86*, 1652–1657.

(5) Reisner, E.; Arion, V. B.; Guedes da Silva, M. F. C.; Lichtenecker, R.; Eichinger, A.; Keppler, B. K.; Kukushkin, V. Y.; Pombeiro, A. J. L. *Inorg. Chem.* **2004**, *43*, 7083–7093.

(6) Alessio, E.; *Eur. J. Inorg. Chem.* **2017**, 1549–1560.

(7) Fung, S. K.; Zou, T.; Cao, B.; Lee, P. Y.; Fung, Y. M. E.; Hu, D.; Lok, C. N.; Che, C. M. *Angew. Chem. Int. Ed.* **2017**, *56*, 3892–3896.

(8) a) Ang, W. H.; Daldini, E.; Scolaro, C.; Scopelliti, R.; Juillerat-Jeannerat, L.; Dyson, P. J. *Inorg. Chem.* **2006**, *45*, 9006–9013; b) Casini, A.; Gabbiani, C.; Sorrentino, F.; Rigobello, M. P.; Bindoli, A.; Geldbach, T. J.; Marrone, A.; Re, N.; Hartinger, C. G.; Dyson, P. J.; Messori, L. *J. Med. Chem.* **2008**, *51*, 6773–6781; c) Pelletier, F.; Comte, V.; Massard, A.; Wenzel, M.; Toulot, S.; Richard, P.; Picquet, M.; Gendre, P. L.; Zava, O.; Edafe, F.; Casini, A.; Dyson, P. J. *J. Med. Chem.* **2010**, *53*, 6923–6933.

(9) a) Chen, H.; Parkinson, J. A.; Parsons, S.; Coxall, R. A.; Gould, R. O.; Sadler, P. J. *J. Am. Chem. Soc.* **2002**, *124*, 3064-3082; b) Wang, F.; Xu, J.; Habtemariam, A.; Bella, J.; Sadler, P. J. *J. Am. Chem. Soc.* **2005**, *127*, 17734–17743.

(10) Kwong, W. L.; Lam, K. Y.; Lok, C. N.; Lai, Y. T.; Lee, P. Y.; Che, C. M. *Angew. Chem. Int. Ed.* **2016**, *55*, 13524–13528.

(11) Allardyce, C. S.; Dyson, P. J. *Platinum Metals Rev.* **2001**, *45*, 62–69.

(12) Dharmaraja, A. T. *J. Med. Chem.* **2017**, *60*, 3221−3240.

(13) Kasherman, Y.; Sturup, S.; Gibson, D. *J. Med. Chem.* **2009**, *52*, 4319–4328.

(14) Garai-Ibabe, G.; Saa, L.; Pavlov, V. *Anal. Chem.* **2013**, *85*, 5542−5546.

(15) a) Kartalou, M.; Essigmann, J. M. *Mutat. Res.* **2001**, *478*, 23–43; b) Zhu, H.; Luo, H.; Zhang, W.; Shen, Z.; Hu, X.; Zhu, X. *Drug Des. Dev. Ther.* **2016**, *10*, 1885–1895.

(16) a) Ibao, A. F.; Gras, M.; Therrien, B.; Süss-Fink, G.; Zava, O.; Dyson, P. J. *Eur. J. Inorg. Chem.* **2012**, 1531–1535; b) Giannini, F.; Paul, L. E. H.; Furrer, J.; Therrien, B.; Süss-Fink, G. *New J. Chem.* **2013**, *37*, 3503—3511; c) Chérioux, F.; Therrien, B.; Süss-Fink, G. *Inorganica Chimica Acta* **2004**, *357*, 834–838.

(17) Giannini, F.; Süss-Fink, G.; Furrer, J. *Inorg. Chem.* **2011**, *50*, 10552–10554.

(18) Soldevila-Barreda, J. J.; Bruijnincx, P. C. A.; Habtemariam, A.; Clarkson, G. J.; Deeth, R. J.; Sadler, P. J. *Organometallics* **2012**, *31*, 5958−5967.

(19) Dolomanov, O.V., Bourhis, L.J., Gildea, R.J, Howard, J. A. K.; Puschmann, H. *J. Appl. Cryst.* **2009**, *42*, 339−341.

(20) Sheldrick, G.M. *Acta Cryst.* **2015**, *A71*, 3−8.

(21) Sheldrick, G.M. *Acta Cryst.* **2015**, *C71*, 3−8.

(22) Fu, Y.; Romero, M. J.; Habtemariam, A.; Snowden, M. E.; Song, L.; Clarkson, G. J.; Qamar, B.; Pizarro, A. M.; Unwin, P. R.; Sadler, P. J. *Chem. Sci.* **2012**, *3*, 2485−2494.

(23) Romero-Canelón, I.; Salassa, L.; Sadler, P. J. *J. Med. Chem.* **2013**, *56*, 1291−1300.

(24) Fu, Y.; Habtemariam, A.; Pizarro, A. M.; van Rijt, S. H.; Healey, D. J.; Cooper, P. A.; Shnyder, S. D.; Clarkson, G. J.; Sadler, P. J. *J. Med. Chem.* **2010**, *53*, 8192−8196.

(25) Romero-Canelón, I.; Mos, M.; Sadler, P. J. *J. Med. Chem.* **2015**, *58*, 7874−7880.

(26) Morris, R. E.; Aird, R. E.; Murdoch, P. S.; Chen, H.; Cummings, J.; Hughes, N. D.; Parsons, S.; Parkin, A.; Boyd, G.; Jodrell, D. I.; Sadler, P. J. *J. Med. Chem.* **2001**, *44*, 3616−3621.

(27) a) Hashiguchi, S.; Fujii, A.; Takehara, J.; Ikariya, T.; Noyori, R. *J. Am. Chem. Soc.* **1995**, *117*, 7562−7563; b) Fujii, A.; Hashiguchi, S.; Uematsu, N.; Ikariya, T.; Noyori, R. *J. Am. Chem. Soc.* **1996**, *118*, 2521-2522; c) Haack, K. J.; Hashiguchi, S.; Fujii, A.; Ikariya, T.; Noyori, R. *Angew. Chem. Int. Ed.* **1997**, *36*, 285−288.

(28) a) Li, X.; Chen, W.; Hems, W.; King, F.; Xiao, J. *Org. Lett.* **2003**, *5*, 4559−4561; b) Li, X.; Wu, X.; Chen, W.; Hancock, F. E.; King, F.; Xiao, J. *Org. Lett.* **2004**, *6*, 3321−3324.

(29) Păunescu, E.; Soudani, M.; Martin, P.; Scopelliti, R.; Bello, M. L.; Dyson, P. J. *Organometallics* **2017**, *36*, 3313−3321.

(30) Romero-Canelón, I.; Sadler, P. J. *Inorg. Chem.* **2013**, *52*, 12276−12291.

(31) Sorenson, C. M.; Barry, M. A.; Eastman, A. *J. Natl. Cancer Inst.* **1990**, *82*, 749-755.

(32) Soldevila-Barreda, J. J.; Romero-Canelon, I.; Habtemariam, A.; Sadler, P. J. *Nat. Commun.* **2015**, *6*, 6582.

(33) Circu, M. L.; Aw, T. Y. *Free Radic. Biol. Med.* **2010**, *48*, 749-762.

(34) Murphy, M. P. *Biochem. J.* **2009**, *417*, 1–13.

(35) Liu, Z.; Romero-Canelon, I.; Qamar, B.; Hearn, J. M.; Habtemariam, A.; Barry, N. P. E.; Pizarro, A. M.; Clarkson, G. J.; Sadler, P. J. *Angew. Chem. Int. Ed.* **2014**, *53*, 3941 –3946.

(36) Liu, Z.; Romero-Canelón, I.; Habtemariam, A.; Clarkson, G. J.; Sadler, P. J. *Organometallics* **2014**, *33*, 5324−5333.

(37) Chow, M. J.; Licona, C.; Wong, D. Y. Q.; Pastorin, G.; Gaiddon, C.; Ang W. H. *J. Med. Chem.* **2014**, *57*, 6043−6059.

(38) Chow, M. J.; Licona, C.; Pastorin, G.; Mellitzer, G.; Ang, W. H.; Gaiddon, C. *Chem. Sci.* **2016**, *7*, 4117–4124.

(39) van Rijt, S. H.; Mukherjee, A.; Pizarro, A. M.; Sadler, P. J. *J. Med. Chem.* **2010**, *53*, 840–849.

Chapter 5

Transfer Hydrogenation and Antiproliferative Activity of Tethered Half-sandwich Organoruthenium Catalysts

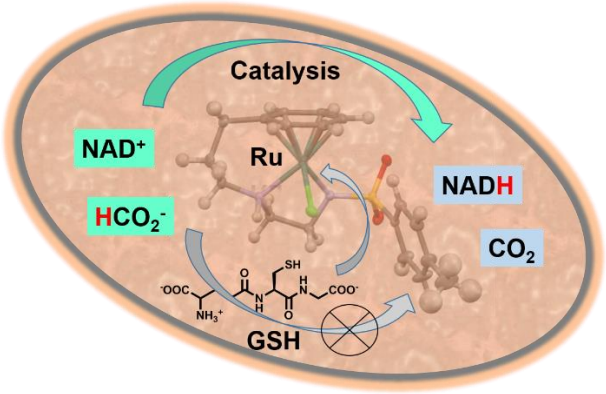

5.1 Introduction

The clinical anticancer drug cisplatin arose from the serendipitous discovery of its biological anticancer activity by Rosenberg *et al.* about fifty years ago.[1] Since then, anticancer complexes based on other platinum-group metals (Ru,[2-4] Rh,[5-8] Os,[9-11] Ir[12-13] and Pd[14-17]) have been well studied. Ruthenium complexes have shown promising potential with relatively low toxicity, and might provide alternatives to platinum drugs. These Ru complexes also have the potential to overcome the severe side effects and drug resistance which is a problem with some platinum-based chemotherapeutics.[18,19] Two Ru^{III} complexes **NAMI-A** and **KP-1019** (**Figure 5.1**), have entered phase II clinical trials, the former as an antimetastatic agent.[20-22] The mode of action of **NAMI-A** and **KP-1019** in cancer cells is not yet understood, but the reduction of Ru^{III} to Ru^{II} is a plausible pathway for their activation.[23,24] The Ru^{II} complex [Ru(η^6-*p*-cym)Cl_2(PTA)](PTA = 1,3,5-triaza-7-phosphatricyclo[3.3.1.1]decane) (**RAPTA** in **Figure 5.1**) also exhibits promising anti-metastatic effects *in vitro* and *in vivo*,[25] and antiangiogenic activity towards chicken chorioallantoic membranes with low dose-dependent antiproliferative activity.[26] [(η^6-biphenyl)Ru(en)Cl]PF_6 (en = ethylenediamine, **RM175** in **Figure 5.1**) is believed to target DNA and can bind to guanine bases accompanied by arene intercalation. It can also induce oxidation of bound glutathione (GSH) which can be displaced by guanine, providing a redox-mediated route to DNA binding.[27,28]

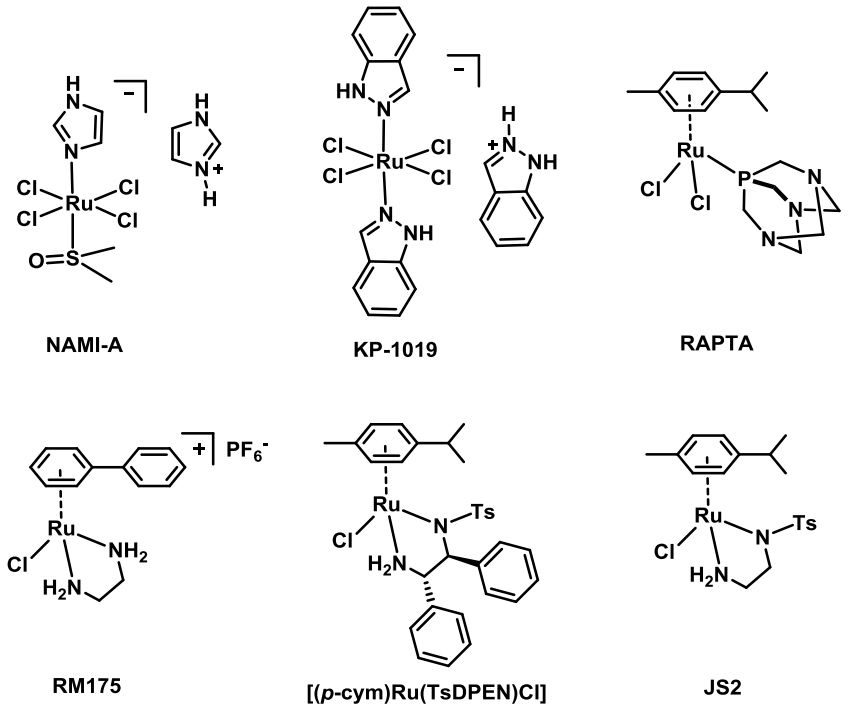

Figure 5.1 Organometallic half-sandwich Ru^{II} complexes as anticancer agents and catalytic transfer hydrogenation catalysts.

Organometallic half-sandwich Ru^{II} complexes also exhibit catalytic activity in transfer hydrogenation (TH) reactions by using a variety of reducing agents as hydride source (*e.g.* H_2, isopropanol, and sodium formate).[29-32] The Noyori-type Ru^{II} complex [(η^6-*p*-cym)Ru (TsDPEN)Cl] (TsDPEN = (*R, R*)-*N*-(*p*-tolylsulfonyl)-1,2-diphenylethylenediamine), is an efficient catalyst for the asymmetric transfer hydrogenation of ketones and amines with high yields and enantiomeric excesses using isopropanol as hydride source (**Figure 5.1**).[33, 34] The sulfonyl Ru^{II} complex [(η^6-arene)Ru(TsEn)Cl] (TsEn: toluenesulfonyl-ethylenediamine) is a more water soluble catalyst and, under biologically relevant conditions, can reduce the coenzyme nicotinamide adenine dinucleotide (NAD^+) *in vitro* and in cells using a non-toxic dose of sodium formate as hydride donor (**JS2** in **Figure 5.1**).[35-37]

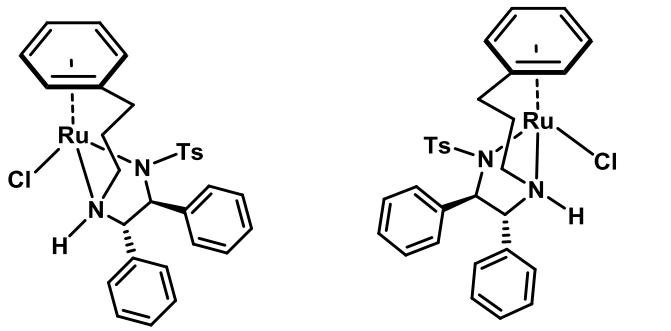

(*S, S*)-Tethered-Ru-TsDPEN (*R, R*)-Tethered-Ru-TsDPEN

Figure 5.2 Structure of enantiomers of chiral tethered Ru TsDPEN complexes.

Tethered Ru^{II} half-sandwich compounds in which the η^6-arene ring and a diamine ligand are connected through a three (or four)-atom chain, have a "locked" arene ring, providing control over the spatial positions of the substituents on the ethylenediamine ligands, and have enhanced stability.[38, 39] Wills *et al.* have reported a series of tethered Ru^{II} η^6-arene complexes and used them as efficient catalysts in the transfer hydrogenation reactions of ketones and amines.[40, 41] However, there have been few investigations on the antiproliferative activity of tethered Ru^{II} complexes. Recently, chiral tethered Ru^{II} complexes (two isomers) were synthesized and found to have potent antiproliferative activity towards the panel of NCI-60 cancer cell lines (IC_{50} against A2780 ovarian cancer cells as low as 1.1 μM, **Figure 5.2**). Interestingly, their potency increased by up to 25% upon incubation of the cancer cells with formate.[42]

In this Chapter, I have synthesized and characterized the water soluble tethered Ru^{II} complexes [Ru(η^6-Ph$(CH_2)_3$- ethylenediamine-*N*-R) Cl], where R = Ms (**16**), Ts (**17**), Tf (**18**) and Nb (**19**) and investigated their catalytic TH reduction of NAD^+ to NADH using sodium formate as a hydride source under biologically relevant conditions. The interaction of complex **17** with the abundant intracellular tripeptide γ-L-Glu-L-Cys-Gly (GSH), and the effect of GSH on catalytic TH reduction of NAD^+ were also studied. I investigated the effect of non-toxic concentrations of formate on the antiproliferative activity of these complexes in several human cancer cell lines, the induction of reactive oxygen species (ROS), and changes in integrity of their membranes.

5.2 Experimental Section

5.2.1 Materials

β-Nicotinamide adenine dinucleotide hydrate (NAD^+) was purchased from Sigma Aldrich. Methylsulfonyl chloride, toluenesulfonyl chloride, 4-trifluoromethylbenzenesulfonyl chloride and 4-nitrobenzenesulfonyl chloride were obtained from Fluka and Sigma Aldrich. L-Glutathione was obtained from Alfa Aesar. The A2780 human ovarian, A549 lung, HEPG 2 hepatocellular and MCF7 breast human adenocarcinoma cell lines as well as MRC 5 human fibroblast cells were purchased from European Collection of Animal Cell Culture (ECACC, Salisbury, UK). Propidium iodide (>94%) and RNase A were obtained from Sigma Aldrich.

5.2.2 Synthesis and Characterization

The ligands and complexes synthesis was performed with help of Dr. Abraha Habtemariam and Dr. Joan J. Soldevila‐Barreda.

[Ru(η^6-Ph(CH_2)$_3$-ethylenediamine-*N*-Ms)Cl] (16). To a stirred solution of dimer (100 mg, 0.1 mmol) in DCM (50 mL) at 273 K was added N, N-diisopropylethylamine (1.4 mL, 0.77 mmol) and the solution was stirred at room temperature for 2 h. The desired ruthenium complex was isolated by recrystallization from methanol and diethyl ether and resulted in a dark red solid. Yield = 47 mg (60%). **^{1}H NMR** (400 MHz, MeOD-d_4): δ_H 1.98-2.04 (m, 1H), 2.29-2.41 (m, 4H), 2.48-2.51 (m, 1H), 2.76 (s, 3H), 2.79-2.82 (m, 2H), 2.87 (d, *J* = 7.7 Hz, 1H), 3.24-3.28 (m, 1H), 5.14-5.20 (m, 2H), 5.71-5.72 (m, 1H), 5.83-5.88 (m, 2H). **^{13}C NMR** (125.7 MHz, DMSO-d_6): δc 33.3, 43.8, 52.7, 56.8, 62.0, 78.5, 82.1, 82.9, 95.3, 98.0, 105.5. HR-MS: *Calcd* for $[C_{13}H_{22}N_2O_2SRu]^+$ 357.0211 *m*/*z*, found: 357.0211 *m*/*z*. Elemental analysis: *calcd* for $[C_{12}H_{19}ClN_2O_2RuS(H_2O)_{0.6}]$: C, 35.79%; H, 5.06%; N, 6.96%. Found: C, 35.83%; H, 4.91%; N, 6.94%.

[Ru(η^6-Ph(CH$_2$)$_3$-ethylenediamine-*N*-Ts)Cl] (17). Complex **17** was obtained following the method described above for complex **16**. Recrystallization from methanol resulted in a bright red solid. Yield = 63 mg (63%). **^{1}H NMR** (400 MHz, $CDCl_3$): δ_H 7.74 (d, *J* = 8.2 Hz, 2H), 7.16 (d, *J* = 8.2 Hz, 2H), 6.39 (t, *J* = 5.6 Hz, 1H), 5.97 (t, 1H, *J* = 5.6 Hz), 5.84 (t, *J* = 5.8 Hz, 1H), 5.01 (d, *J* = 5.6 Hz, 1H), 4.91 (d, *J* = 5.8 Hz, 1H), 3.79 (s, 1H), 3.30–3.23 (m, 1H), 3.03 (dd, *J* = 11.5 Hz, 4.2 Hz, 1H), 2.79–2.71 (m, 1H), 2.66–2.62 (m, 1H), 2.43–2.36 (m, 3H), 2.34 (s, 3H), 2.27–2.19 (m, 2H), 2.08–1.99 (m, 1H). **^{13}C NMR** (125.7 MHz, DMSO-d_6): δc 26.1, 33.2, 33.5, 52.2, 56.7, 62.0, 78.9, 82.1, 83.2, 94.5, 97.6, 104.9, 132.1, 133.6, 144.5, 146.9. HR-MS: *Calcd* for $[C_{18}H_{23}N_2O_2RuS]^+$: 433.0524 *m/z*, found: 433.0522 *m/z*. Elemental analysis: *calcd* for $[C_{18}H_{23}ClN_2O_2RuS(H_2O)_{0.1}]$: C, 46.02%; H, 4.98%; N, 5.96%. Found: C, 46.03%; H, 4.92%; N, 5.93%.

[Ru(η^6-Ph(CH$_2$)$_3$-ethylenediamine-*N*-Tf)Cl] (18). Complex **18** was obtained following the method described above for complex **16**. Recrystallization from methanol resulted in a brownish-red solid. Yield = 38 mg (36%). **^{1}H NMR** (400 MHz, DMSO-d_6): δ_H 1.84-1.86 (m, 1H), 2.10 (t, *J* = 11.2 Hz, 1H), 2.25 (t, *J* = 9.7 Hz, 2H), 2.33-2.46 (m, 2H), 2.64 (d, *J* = 8.9 Hz, 1H), 2.75 (q, *J* = 9.7 Hz, 21.9 Hz, 1H), 2.85 (d, *J* = 8.0 Hz, 1H), 3.14 (s, 1H) (broad single peak), 4.35 (s, 1H) broad single peak, 5.27 (d, *J* = 4.9 Hz, 1H), 5.40 (d, *J* = 5.6 Hz, 1H), 5.83-5.89 (m, 2H), 5.97 (t, *J* = 5.1 Hz, 1H), 7.75 (d, *J* = 8.0 Hz, 2H), 7.93 (d, *J* = 8.0 Hz, 2H). **^{13}C NMR** (125.7 MHz, DMSO-d_6): δc 33.2, 33.4, 52.3, 56.7, 61.9, 79.2, 81.9, 83.6, 94.8, 97.8, 105.3, 130.1, 132.9, 134.8, 135.1, 135.0. **^{19}F NMR** (376.4 MHz, DMSO-d_6): δ_F -61.02. HR-MS: *Calcd* for $[C_{18}H_{20}N_2F_3O_2SRu]^+$ 487.0241 *m/z*, found: 487.0240 *m/z*. Elemental analysis: *calcd* for $[C_{18}H_{20}ClF_3N_2O_2RuS(H_2O)_{0.1}]$: C, 41.28%; H, 3.89%; N, 5.35%. Found: C, 41.20%; H, 3.65%; N, 5.26%.

[Ru(η^6-Ph(CH$_2$)$_3$-ethylenediamine-*N*-Nb)Cl] (19). Complex **19** was obtained following the method described above for complex **16**. Recrystallization from methanol and diethyl ether

resulted in a bright red solid. Yield = 44 mg (43%). **^{1}H NMR** (300 MHz, $CDCl_3$): δ_H 2.00-2.08 (m, 1H), 2.14-2.58 (m, 2H), 2.34-2.50 (m, 3H), 2.69-2.82 (m, 2H), 3.12 (dd, *J* = 5.5 Hz, 14.8 Hz, 1H), 3.23-3.32 (m, 1H), 3.70 (s, 1H) broad single peak, 4.92 (d, *J* = 7.9 Hz, 1H), 5.00 (d, *J* = 7.6 Hz, 1H), 5.86 (t, *J* = 7.6 Hz, 1H), 5.96 (t, *J* = 8.1 Hz, 1H), 6.30 (t, *J* = 7.3 Hz, 1H), 7.96 (d, *J* = 11.6 Hz, 2H), 8.18 (d, *J* = 11.8 Hz, 2H). **^{13}C NMR** (125.7 MHz, DMSO-d_6): δc 33.1, 33.5, 52.4, 56.7, 61.8, 79.3, 81.9, 83.8, 94.8, 97.8, 105.5, 128.4, 133.4, 153.1, 155.0. HR-MS: *Calcd* for $[C_{17}H_{20}N_3O_4SRu]^+$ 464.0218 *m*/*z*, found: 464.0216 *m*/*z*. Elemental analysis: *calcd* for $[C_{17}H_{20}ClN_3O_2RuS(H_2O)_{0.5}]$: C, 40.20%; H, 4.17%; N, 8.27%. Found: C, 40.26%; H, 3.89%; N, 8.04%.

5.2.3 TOFs Determined by UV-vis Spectroscopy

Complexes **16-19** were dissolved in DMSO/H_2O (1:9, v/v) (84 μM) in a glass vial. Solutions of sodium formate (102 mM) and NAD^+ in H_2O (510 μM) were also prepared and then mixed at 310 K. In a typical experiment, an aliquot of 330 μL from each solution was added to a 1 mL cuvette, and the pH adjusted to 7.2 before the sample was introduced into the UV-vis instrument, bringing the total volume to 1 mL (final concentrations were Ru complex 28 μM; NAD^+ 170 μM; $NaHCO_2$ 34 mM; molar ratio 1:6:1200). UV spectra were recorded every 5 min until completion of the reaction. The spectrum was monitored for an increase in the band at 340 nm, which corresponds to the absorption of NADH.

5.2.4 TOFs Determined by NMR

TOF values of complexes **16-19** were determined and calculated following a similar protocol described in **Section 3.2.4** of Chapter 3 with these modifications: complexes **16-19** (1.4 mM) in DMSO-d_6/D_2O (1:4 v/v), sodium formate (35 mM) and NAD^+ (5.6 mM) in D_2O were

prepared. The pH^* adjusted to 7.2 ± 0.1. A ^1H NMR spectrum was recorded at 310 K every 162 s until the completion of the reaction.

A further series of experiments were performed on NMR, where complex **17** (1.4 mM) was dissolved in MeOD-d_4 (20%)/D_2O (80%) (1.4 mM) in a vial; to which NAD^+ (5.6 mM in D_2O), formate (35 mM in D_2O) and different concentrations of GSH (0.5, 1, 2, 5 and 10 mol equiv) were added, following the same procedure used above (at 310 K, pH^* 7.2 ± 0.1).

5.2.5 IC_{50} and *In Vitro* Cytotoxicity Determination

Biological testing was carried out by Dr. Isolda Romero‑Canelón and Ji-Inn Song.

The antiproliferative activity and cytotoxicity of complexes **16–19** were determined in different 5 cancer cell lines and 1 human normal cell line. In general, about 5,000 cells per well were seeded in 96-well plates. The plates were pre-incubated with drug-free medium at 310 K for 48 h before adding the tested compounds (concentrations various). Exact concentrations of complexes were determined by ICP-OES. After 24 h drug exposure, supernatants were removed by suction and each well was washed with PBS. A further cells recovery for 72 h was allowed in drug-free medium at 310 K. The sulforhodamine B (SRB) assay was used to determine cell viability. IC_{50} values, as the concentration that causes 50% cell death, were determined as duplicates of triplicates in two independent sets of experiments and their standard deviation were calculated.

5.2.6 Coincubation of Tethered Ru Complexes with Formate

Cell viability assays of complexes **16-19** were carried out with in A2780 ovarian cancer cells with sodium formate. These experiments were performed with the following modifications: a fixed concentration of each Ru complex equal to 1/3 × IC_{50} was used in co-administration with three different concentrations of sodium formate (0.5, 1.0 and 2.0 mM). Drug stock solutions

(*ca*. 100 μM) were prepared as described for *in vitro* growth inhibition assays. The stocks were further diluted using media until working concentrations were achieved. Separately, a stock solution of sodium formate was prepared in saline. The complex and formate solutions were added to each well independently, but within 5 min of each other.

5.2.7 Cell Cycle Analysis

A2780 cells at 1.5×10^6 per well were seeded in a six-well plate. Cells were pre-incubated in drug-free media at 310 K for 24 h, after which drugs were added at equipotent concentration equal to IC_{50} value. After 24 h of drug exposure, supernatants were removed by suction and cells were washed with PBS. Finally, cells were harvested using trypsin-EDTA and fixed for 2 h using cold 70% ethanol. DNA staining was achieved by re-suspending the cell pellets in PBS containing propidium iodide (PI) and RNase. Cell pellets were washed and re-suspended in PBS before being analysed in a Becton Dickinson FACScan flow cytometer using excitation of DNA-bound PI at 536 nm, with emission at 617 nm. Data were processed with Flowjo software.

5.2.8 ROS Determination

Flow cytometry analysis of ROS/superoxide generation in A2780 cells caused by exposure to complex **17** was carried out using the Total ROS/Superoxide detection kit (Enzo-Life Sciences) according to the instructions. 1.5×10^6 A2780 cells per well were seeded in a six-well plate. Cells were pre-incubated in drug-free media at 310 K for 24 h in a 5% CO_2 humidified atmosphere, and then drugs were added to triplicates at IC_{50} concentration. After 1 h of drug exposure, supernatants were removed by suction and cells were washed and harvested. Staining was achieved by re-suspending the cell pellets in buffer containing the orange/green fluorescent reagents. Cells were analyzed in a Becton Dickinson FACScan flow cytometer using FL1

channel Ex/Em: 490/525 nm for the oxidative stress and FL2 channel Ex/Em: 550/620 nm for superoxide detection. Data were processed using Flowjo software. At all times, samples were kept under dark conditions to avoid light-induced ROS production.

5.2.9 Cell Membrane Integrity Determination

Flow cytometry analysis of cellular membrane integrity of A2780 cells caused by exposure to complex **17** was carried out using flow cytometry and propidium iodide staining. Briefly, A2780 cells were seeded in 6-well plates (1.5×10^6 cells per well), pre-incubated for 24 h in drug-free media at 310 K, after which they were exposed to complex **17** at IC_{50} concentration. Cells were harvested using trypsin and stained in the dark using a mixture of propidium iodide and RNAse without previous fixation of the cells. After staining, cell pellets were analyzed in a Becton Dickinson FACScan Flow Cytometer and the histograms were analysed using Flowjo software.

5.2.10 Calf Thymus DNA and Bacterial Plasmid DNA

DNA experiments in sections **5.2.10** and **5.2.11** were conducted by in collaboration with Professor Viktor Brabec and Dr. Jana Kasparkova of the Institute of Biophysics, Academy of Sciences of the Czech Republic.

The interaction of complex **17** with double-helical calf thymus DNA (ct-DNA) and bacterial plasmid DNA was studied and compared to non-tethered [(η^6-*p*-cym)Ru(TsEn)Cl] (**JS2** in **Figure 5.1**).[37] Double-helical ct-DNA at a concentration of 32 μg/mL was incubated with **JS2** or complex **17** at r_i values of 0.1 or 0.5 in 10 mM $NaClO_4$ at 310 K (r_i = the molar ratio of free ruthenium complex to nucleotide phosphates at the onset of incubation with DNA). The reaction was terminated after 24 h incubation and samples were exhaustively dialyzed against

water. The ruthenium content in these samples was determined by flameless atomic absorption spectrometry (FAAS), and concentration of DNA by absorption spectrophotometry.

In further experiments, solutions containing plasmid DNA pBR322 (28 µg/mL) and complex **JS2** or complex **17** in various molar ratios (r_i = 0.05–1) were incubated in 0.01 M $NaClO_4$ at 310 K for 24 h in the dark. Subsequently the samples were directly mixed with the loading buffer and loaded onto a 1% agarose gel running at 298 K in the dark with Tris-acetate-EDTA (TAE) buffer and the voltage set at 25 V. There was no separation step before loading the samples onto the gel to remove weakly-bound complex, if any. The gels were then stained with EtBr, followed by photography with a transilluminator.

5.2.11 Binding to Short Single- or Double-stranded Oligonucleotides

Binding of complex **17** to short, single or double stranded synthetic oligonucleotides was investigated by co-incubation complex **17** (r_i = 0.5, concentration of oligonucleotide related to phosphates) in 0.05 M $NaClO_4$ with a 50-mer oligonucleotide (single or double stranded having a random nucleotide sequence) at 310 K in the dark, complex **JS2** was used as a comparison. After 24 h, the reaction was stopped, and samples were exhaustively dialyzed against water. The ruthenium content in these samples was determined by FAAS and the concentrations of DNA were determined by absorption spectroscopy.

5.3 Results

5.3.1 Synthesis and Characterization

Four neutral tethered Ru^{II} complexes [Ru(η^6-Ph$(CH_2)_3$-ethylenediamine-*N*-R) Cl] where R = methanesulfonamide (Ms, **16**), or toluenesulfonyl (Ts, **17**), or 4-(trifluoromethyl)benzene sulfonamide (Tf, **18**), or 4-nitrobenzenesulfonamide (Nb, **19**) were synthesized following a literature method for related complexes (**Scheme 5.1**).[43] They were characterized by elemental analysis (CHN), high resolution mass spectrometry, and NMR (^{1}H, ^{13}C and ^{19}F) spectroscopy.

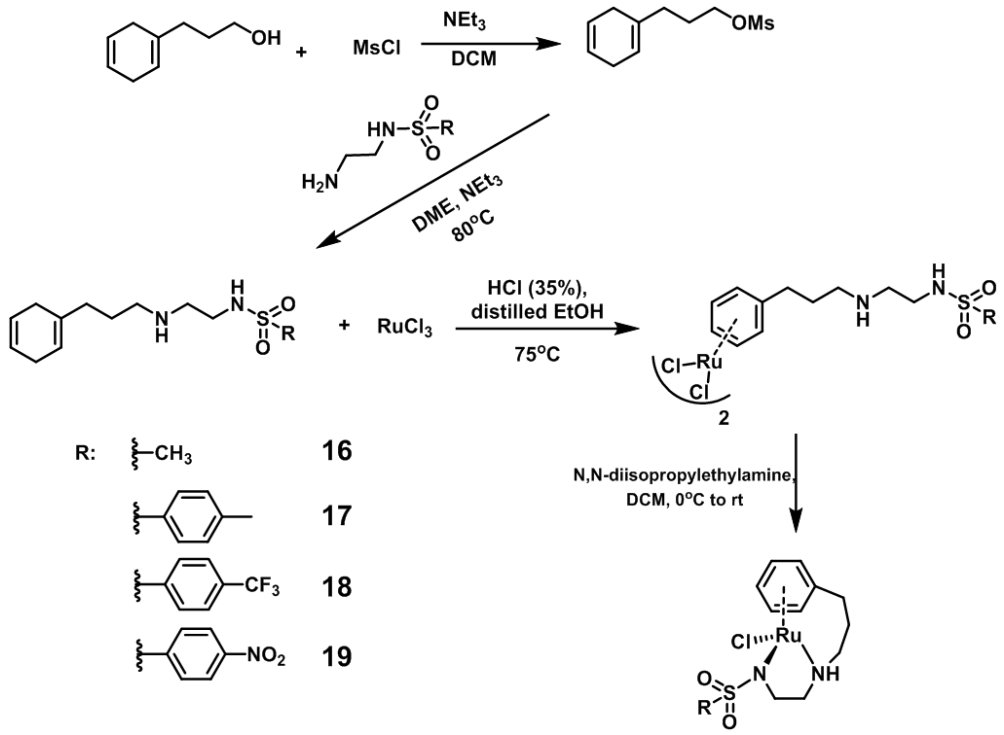

Scheme 5.1 Synthesis Route for Complexes **16-19**; DME: 1, 2-Dimethoxyethane.

Crystals of complexes **16-19** suitable for X-ray diffraction were obtained from a slow diffusion of diethyl ether into MeOH at ambient temperature. The complexes adopt the expected *pseudo*-tetrahedral geometry with η^6-phenyl ring occupying 3 Ru coordination sites, together with nitrogen atoms of the diamine ligand (bond lengths 2.11-2.15 Å), and a monodentate chloride; ethylenediamine ligands are deprotonated and bound as monoanionic bidentate ligands.

Generally, the bond distance Ru-N(H) (range 2.140-2.149 Å) is slightly longer than that of Ru-N(-) (2.112-2.121 Å). The η^6-phenyl ring and ethylenediamine are linked by a three-carbon tether chain. The structures are shown in **Figure 5.3**. Selected bond lengths (Å) and bond angles (deg) are listed in **Table 5.1**, and X-ray crystallographic data in **Table 5.2**.

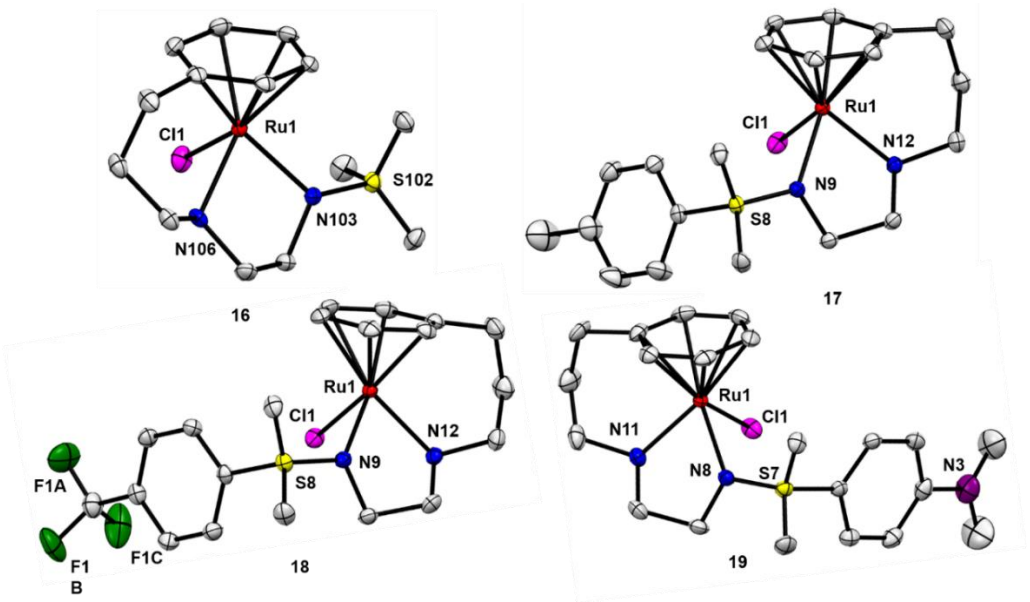

Figure 5.3 ORTEP diagrams for complexes **16**, **17**, **18** and **19**. Ellipsoids are shown at the 50% probability level. All hydrogen atoms have been omitted for clarity.

Table 5.1 Selected Bond Lengths (Å) and Angles (deg) for Complexes **16-19.**

	16	**17**	**18**	**19**
Ru1-N(-)	2.121 (2)	2.1181 (14)	2.1202 (16)	2.1124 (18)
Ru1-N(H)	2.146 (2)	2.1490 (14)	2.1485 (16)	2.140 (2)
Ru1-Cl1	2.4174 (6)	2.4234 (4)	2.4243 (4)	2.4142 (6)
Ru1-arene (centroid)	1.654	1.657	1.658	1.653
N(-)-Ru1-N(H)	78.77 (8)	78.87 (5)	78.87 (6)	78.54 (7)
N(-)-Ru1-Cl1	88.17 (6)	88.29 (4)	87.33 (4)	87.24 (5)
N(H)-Ru1-Cl1	83.20 (6)	83.02 (4)	83.56 (5)	83.43 (6)
N(-) corresponds to N103(16), N9(17, 18), N8(19). N(H) corresponds to N106 (16), N12 (17, 18), N11(19)				

Table 5.2 Crystallographic Data for Complexes **16-19.**

	16	**17**	**17**	**19**
Crystal character	orange block	orange block	red block	red block
Formula	$C_{12}H_{19}ClN_2O_2RuS$	$C_{18}H_{23}ClN_2O_2RuS$	$C_{18}H_{20}ClF_3N_2O_2RuS$	$C_{17}H_{20}ClN_3O_4RuS$
FW	391.99	467.96	521.94	498.94
Temp (K)	150(2)	150(2)	150(2)	150(2)
Crystal system	triclinic	triclinic	monoclinic	Monoclinic
Space group	P-1	P-1	$P2_{1/c}$	$P2_{1/c}$
a (Å)	8.0399(2)	9.9127(3)	10.4998(2)	10.5869(5)
b (Å)	11.6970(3)	10.3545(2)	16.9214(3)	16.4168(6)
c (Å)	16.8127(3)	10.6046(4)	11.6956(3)	11.4551(5)
α (°)	98.2250(17)	108.425(2)	90	90
β (°)	101.4472(18)	106.778(3)	111.867(3)	110.695(5)
γ (°)	106.688(2)	100.997(2)	90	90
Volume ($Å^3$)	1450.30(6)	939.87(5)	1928.47(7)	1862.48(15)
Z	2	2	4	4
Dcalc(mg/cm^3)	1.836	1.654	1.798	1.779
μ(mm^{-1})	1.412	1.101	1.105	1.127
F(000)	812.0	476.0	1048.0	1008.0
Crystal size (mm^3)	0.28 × 0.2 × 0.12	0.2 × 0.2 × 0.1	0.22 × 0.14 × 0.08	0.4 × 0.24 × 0.1
Reflections measured	44720	25185	32356	30846
Indep reflection	9700	6290	6963	6596
*R*1 [$I>2\sigma(I)$]	0.0318	0.0283	0.0255	0.0304
wR2 (all data)	0.1019	0.0611	0.1013	0.1167
CCDC no.	1823319	1823318	1823317	1823316

5.3.2 pK_a^* Determination and Interaction with Guanine

The pK_a^* of the aqua adduct of complex **17** (aqua complex **17a**) in MeOD-d_4/D_2O (1:9, v/v) was determined by ^{1}H NMR at 310 K (**Figure 5.4A**) by titration over the pH* (meter reading) range from 2 to 12 and plots of the chemical shift of a tosyl proton as a function pH* fitted to the Henderson−Hasselbalch equation. The pK_a^* value of aqua complex **17a** was found to be 9.52 ± 0.03; a second pK_a^* value of < 2, assignable to the coordinated N of **17a**, was too low to be determined.

The interaction of complex **17** with the DNA nucleobase model: 9-ethylguanine (9-EtG, **Figure 5.4B**) was studied by ^{1}H NMR spectroscopy. Complex **17** (2 mM in 10% MeOD-d_4/90% D_2O) reacted rapidly with 9-EtG (1 mM) at 310 K. The adduct **17**-9-EtG gave rise to a new set of η^6-arene peaks in low field (**Figure 5.4B**), with up to 90% yield of the **17**-9-EtG when 1.5 mol equiv 9-EtG solution was added.

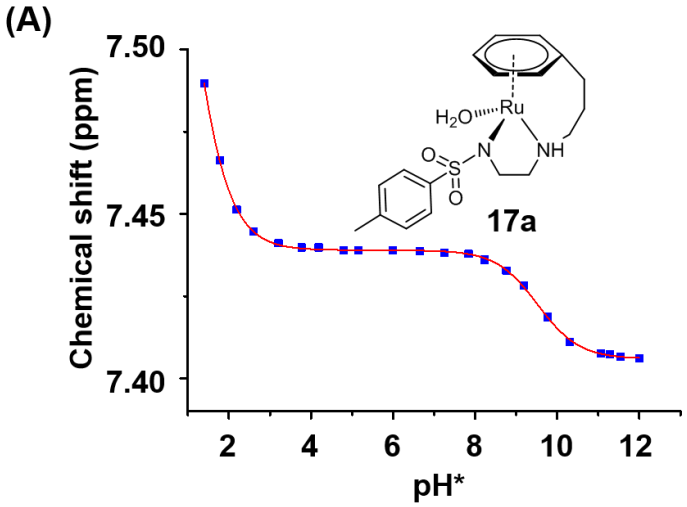

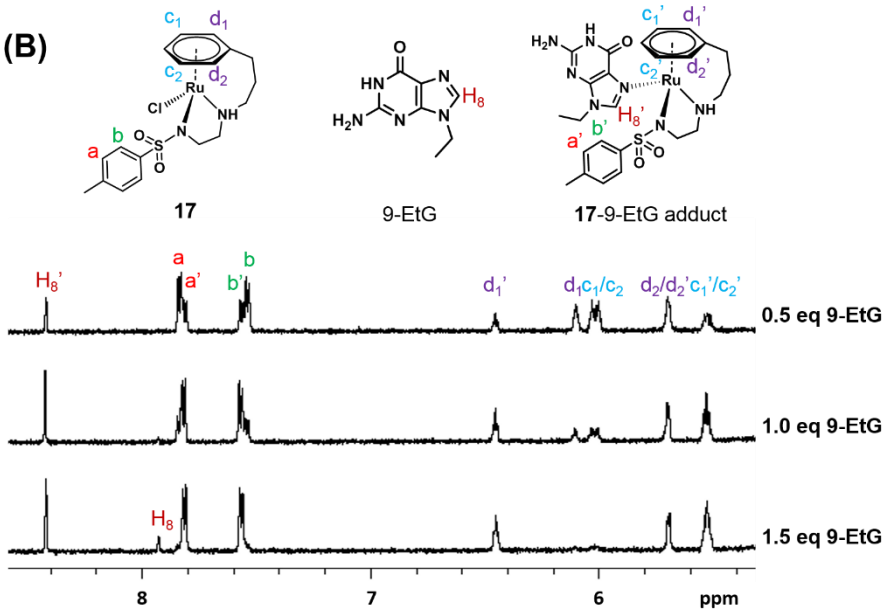

Figure 5.4 (**A**) Dependence of low field ^{1}H NMR chemical resonance shift of the aqua species **17a**, giving the pK_a^* value of 9.52 for the coordinated water; (**B**) Titration reaction of tethered Ru^{II} complex **17** (2 mM) with 9-ethylguanine (1 mM–3 mM, 0.5–1.5 molar equiv) in 10% MeOD-d_4/90% D_2O, pH at 7.2, 310 K, followed by ^{1}H NMR spectroscopy.

5.3.3 Transfer Hydrogenation Reaction Kinetics

Catalytic transfer hydrogenation reactions of complexes **16-19** and sodium formate as hydride donor for conversion of nicotinamide adenine dinucleotide (NAD^+) to NADH were studied in aqueous media by UV-visible spectroscopy (10% DMSO/90% H_2O, pH 7.2 ± 0.1, 310 K) by following the absorbance at 340 nm for NADH, and by ^{1}H NMR spectroscopy (using 20% DMSO-d_6 in D_2O to ensure solubility, pH 7.2 ± 0.1, 310 K), monitoring peaks corresponding to 1, 4-NADH.

All the tethered Ru^{II} complexes exhibited potent catalytic activity, with TOFs by UV-vis and NMR spectroscopy in the range 3.7-8.9 h^{-1} and 5.8-9.9 h^{-1}, respectively (**Table 5.3**), following the order: **16** < 17 < **18** < **19**, suggesting that stronger electron withdrawing groups on the ethylenediamine ligand facilitate hydride transfer between formate and NAD^+.

Table 5.3 TOFs (h^{-1}) for Transfer Hydrogenation Reactions of NAD^+ to NADH using Complexes **1−4** as Catalysts and Sodium Formate as Hydride Donor.

Complex	R	TOF (NMR)	TOF (UV-vis)
16	Ms	3.79 ± 0.05	5.8 ± 0.2
17	Ts	4.7 ± 0.1	8.3 ± 0.1
18	Tf	8.9 ± 0.3	8.69 ± 0.07
19	Nb	8.5 ± 0.2	9.9 ± 0.2

5.3.4 Interaction with Glutathione (GSH)

The reaction of complex **17** [Ru(η^6-Ph$(CH_2)_3$-ethylenediamine-*N*-Ts)Cl] with glutathione (GSH) was investigated in a series of concentration-dependent experiments. Reactions of complex **17** (2 mM, MeOD-d_4/D_2O, 2:8(v/v)) and GSH (in D_2O) in the mol ratio of 1: X, where X = 0.2, 0.5, 1, 2, 5 and 10 were studied by ^{1}H NMR spectroscopy under conditions of MeOD-d_4/D_2O (1:9, v/v), pH* 7.2, 310 K. Each reaction was complete within 10 min. The low-field η^6-phenyl peaks of complex **17** decreased gradually, and a new set of triplets (H1' and H2') emerged when 0.2 and 0.5 mol equiv of GSH were added (**Figure 5.5**). The low field resonances of the tosyl proton of complex **17** (H1 and H2) disappeared and a new set of peaks (H1'-H7') appeared when 1 mol equiv or more GSH was added (**Figure 5.5**). The reaction was confirmed by LC-MS, which revealed that the **17**-SG adduct was formed rapidly when **17** was mixed with GSH (**Figure 5.6**). The eluents are shown in **Figure 5.7**.

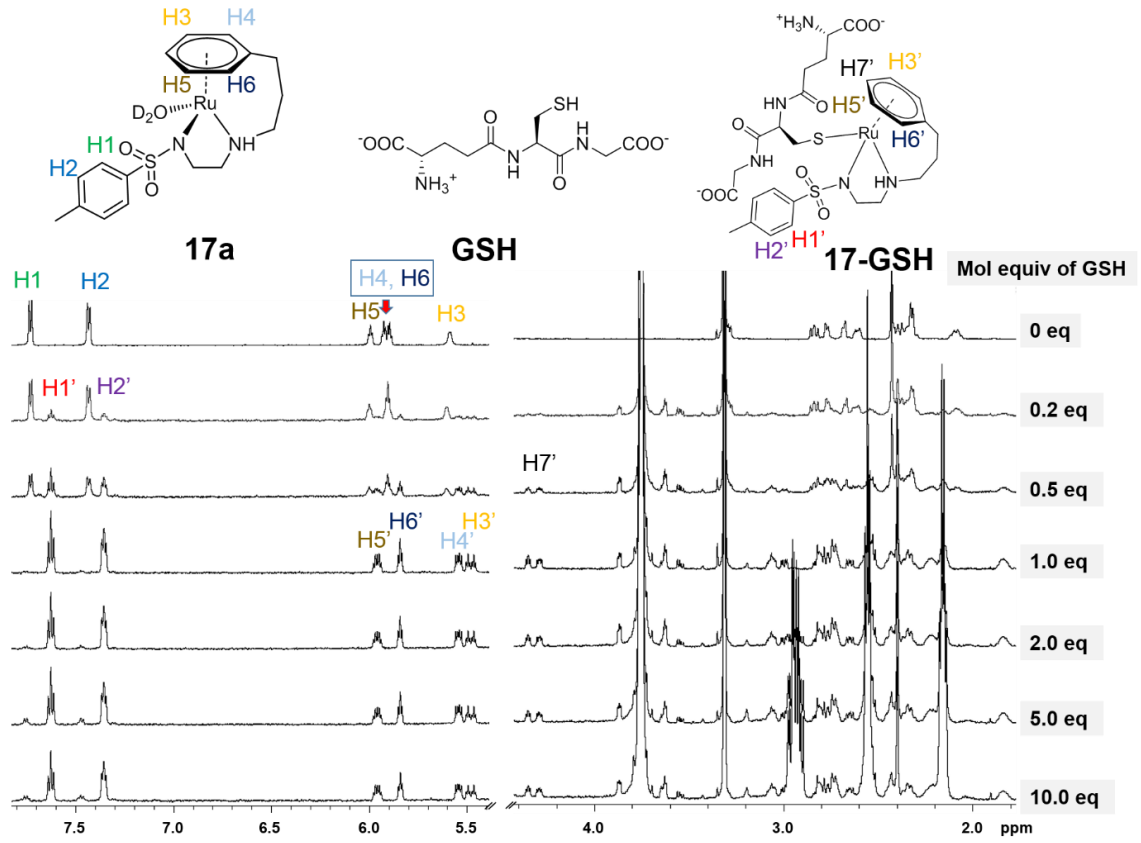

Figure 5.5 ^{1}H NMR (600 MHz) spectra monitoring of the reactions between complex **17** (2 mM in MeOD-d_4/H_2O, 1:9 v/v) and various concentrations of GSH in a mixture of MeOD-d_4 and D_2O (2:8, v/v). The pH* was adjusted to 7.2 ± 0.1 and all spectra were recorded at 310 K.

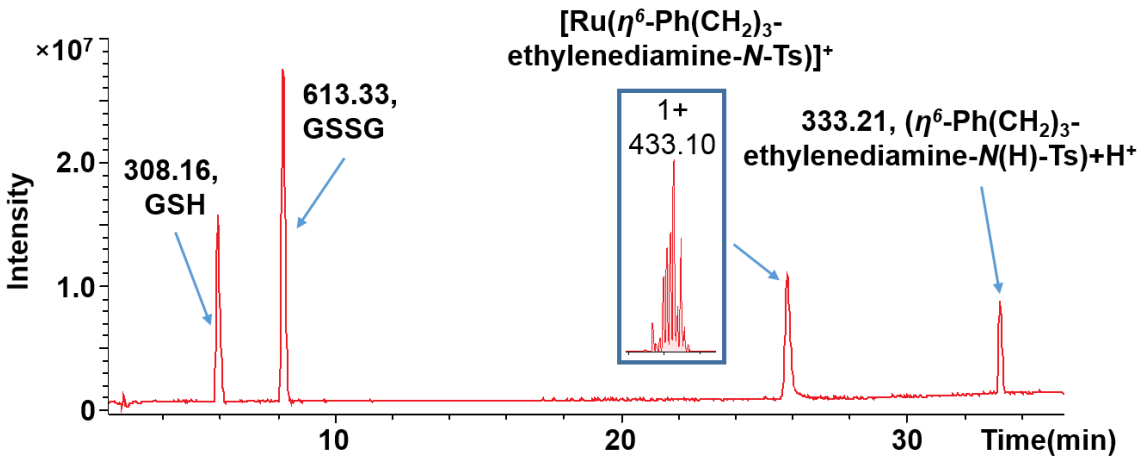

Figure 5.6 Reaction of complex **17** with GSH (10 mol equiv) in MeOH/H_2O (1:9, v/v) after incubation at pH 7.2, 310 K for 24 h monitored by LC-MS. Eluents are shown in **Figure 5.6**.

Time (min)	% B (acetonitrile, 0.1% TFA)
0	2
10	12
15	15
25	25
30	50
50	50
55	2

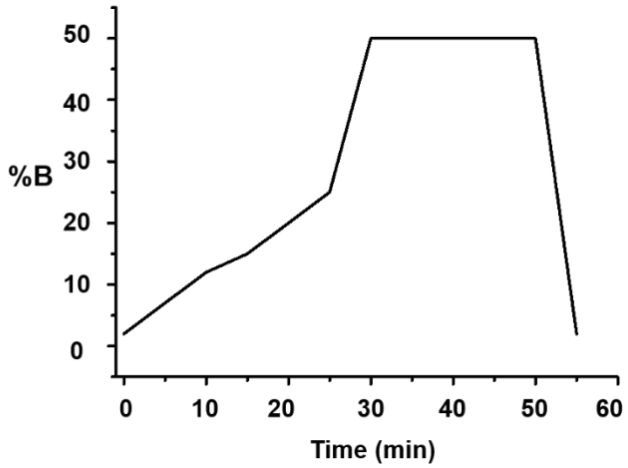

Figure 5.7 LC-MS gradients for identification of **17**-SG adducts from the reaction of complex **17** and GSH using H_2O with 0.1% TFA (v/v) (Solvent A) and CH_3CN with 0.1% TFA (v/v) (solvent B) as eluents (TFA, trifluoroacetic acid). Column type: ZORBAX Eclipse XDB-C18, 9.4 × 250 mm, 5 µm.

Next, the time-dependence of reactions of complex **17** with GSH was studied under similar conditions: 2 mM **17** in MeOD-d_4/D_2O, 2:8(v/v), 20 mM GSH, monitored by ^{1}H NMR spectroscopy from 5 min to 24 h, **Figure 5.8**. As in the above experiments, a new set of low field resonances appeared immediately (H1'-H6') in the presence of excess GSH (10 mol equiv), but with time, the low field resonances H1'-H6' decreased gradually, and disappeared after 24 h (**Figure 5.8**); meanwhile another two new sets of peaks slowly appeared. The 2D NMR COSY spectrum suggested that the **17**-SG adduct degraded with time to release the neutral free ligand η^6-Ph$(CH_2)_3$-ethylenediamine-*N*(H)-Ts (assigned to one of the two sets of low field peaks, **Figure 5.9**) with up to 70% of decomposition observed within 5 h incubation at 310 K, as shown in **Figure 5.10**. Such liberation of free ligand was also detected by LC-MS at 333.21 m/z (calculated $[Ligand+H]^+$ at 333.16 m/z, **Figure 5.6**).

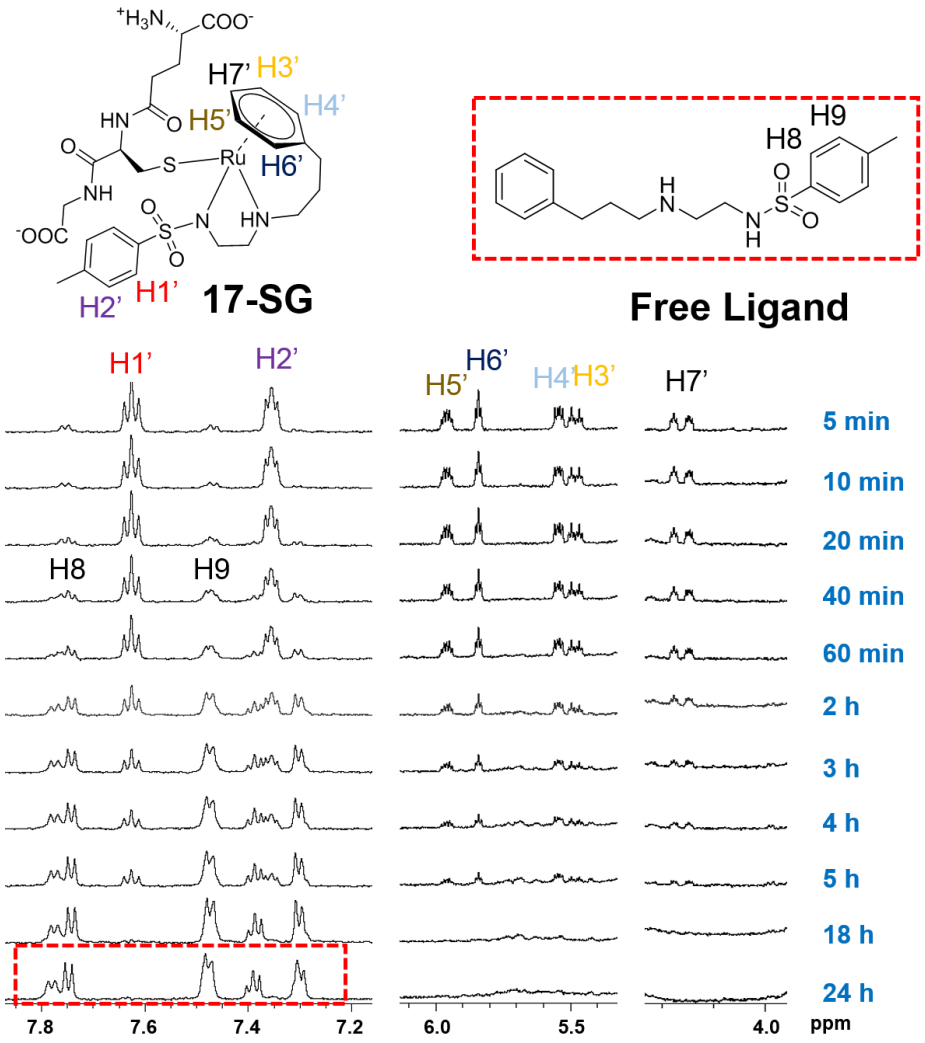

Figure 5.8 Dependence on time of the ^{1}H NMR (600 MHz) spectra for the reaction of complex **17** (2 mM in MeOD-d_4/H_2O, 2:8, v/v) with GSH (20 mM, in D_2O). The pH* was adjusted to 7.2 ± 0.1, and all spectra were recorded at 310 K. Free ligand resonances at low field are shown in the dashed box.

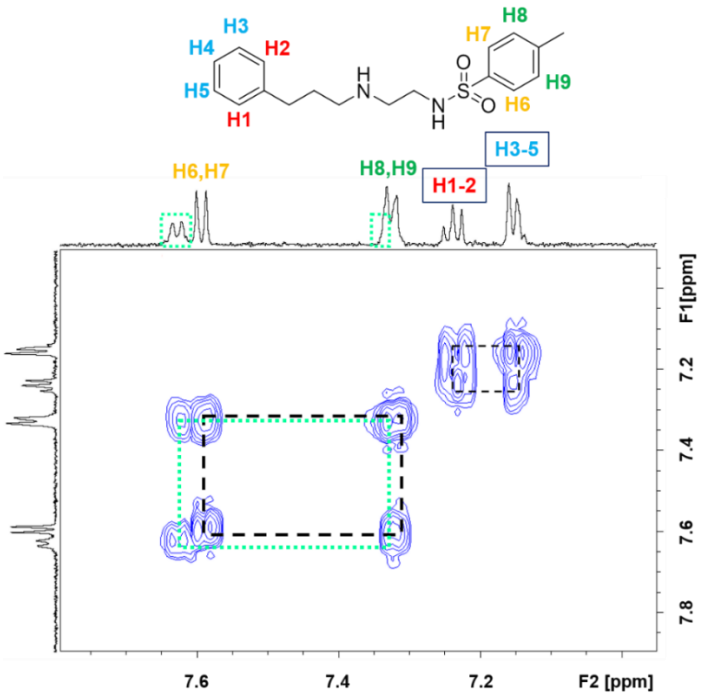

Figure 5.9 Low field 2D NMR resonance peaks of reaction of complex **17** (2 mM in MeOD-d_4/H_2O, 2:8, v/v) with GSH (20 mM, in D_2O) after 24 h incubation at 310 K. pH^* was adjusted to 7.1. Another set of unassigned peaks is marked in the green dashed box.

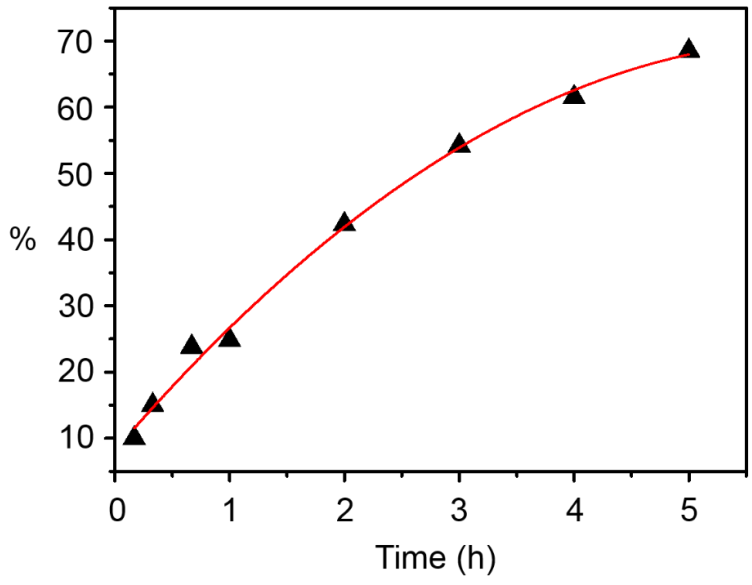

Figure 5.10 Percentage of decomposition of **17**-SG adduct by liberation of free ligand within 5 h for reaction of complex **17** (2 mM in MeOD-d_4/D_2O, 2:8, v/v) with GSH (20 mM, in D_2O) at pH^* 7.1, 310 K, monitored by ^1H NMR. Peak integration is from **Figure 5.8**.

5.3.5 Reduction of NAD^+ by TH in the Presence of GSH

The influence of GSH on conversion of NAD^+ to NADH by TH from complex **17** with sodium formate as hydride source was investigated. ^1H NMR spectra (MeOD-d_4/D_2O, 2:8(v/v), pH* 7.2, 310 K), with complex **17**, NAD^+, GSH and sodium formate in the mol ratio of 1: 4: X: 25, respectively, where X = 0.5, 1, 2) were recorded every 5 min. The turnover frequency of NAD^+ to NADH decreased slightly in the presence of 0.5 mol equiv of GSH (TOF = 4.27 ± 0.05 h^{-1}), however, the TOF decreased dramatically to 1.35 h^{-1} when 1.0 mol equiv of GSH was used. The hydride transfer reaction was completely blocked when excess GSH was added (2 or 5 mol equiv).

5.3.6 Antiproliferative Activity

The antiproliferative activity of tethered Ru^{II} complexes **16-19** against human ovarian (A2780), cisplatin-resistant ovarian (A2780Cis), lung (A549), liver (HEPG2), breast (MCF7) cancer cell lines and human normal lung fibroblast cells (MRC5) was determined, **Table 5.4**, and compared to the clinical drug cisplatin (CDDP). Complexes **16-19** exhibited good to moderate anticancer activity against all these cancer cell lines, with IC_{50} values in the range of 7.3-66.8 μM.

Complex **17** displayed good anticancer activity against A2780 and cisplatin resistant A2780 cancer cells, with IC_{50} values of 7.3 μM and 15 μM, respectively. Remarkably, this complex exhibits a resistance index (RI) of only 2 compared to 11 for cisplatin. The RI is the ratio of the activity (IC_{50}) towards the resistant cell line compared to the parental line. Furthermore, complex **19** exhibited similar anticancer activity against MCF 7 cancer cells to cisplatin, with an IC_{50} value of 9.9 μM (**Table 5.4**).

Table 5.4 *In Vitro* Anticancer Activity of Complexes **16-19** Against Various Cell Lines.

Complex	Cell line [a] IC_{50} (μM)						RI[b]
	A2780	A2780Cis	A549	HEPG2	MCF 7	MRC 5	
16	23±1	>50	33±1	27.8±0.1	28.9±0.9	31±1	>2
17	7.3±0.4	15±1	37.6±0.6	26±4	33±2	38±1	2
18	>50	>50	31±2	>50	24±3	28±3	n.d.
19	16.0±0.3	>50	30±1	23±4	9.9±0.5	26±1	>3
CDDP	1.20±0.02	13.4±0.3	3.1±0.1	5.7±0.9	7.3±0.2	12.8±0.3	11

[a] Data are shown as means ± standard deviations (STD), from duplicates of triplicates, cell viability was assessed after 24 h drug exposure and 72 h recovery in the drug-free medium. Cancer cell lines: A2780 human ovarian cancer cells; A2780Cis cisplatin resistance human ovarian cancer cells; A549 human lung cancer cells; HEPG2 human hepatocellular cancer cells; MCF7 human breast cancer cells; MRC5 human lung fibroblast cells; [b] RI is resistance index defined as ratio of the activity (IC50) towards the resistant cell line compared to the parental cell line; n.d. = not determined.

5.3.7 Effect of Formate on Antiproliferative Activity

The antiproliferative activity of tethered complexes **16-19** against A2780 human ovarian cancer cells in the presence of sodium formate was determined (**Figure 5.11**). Experiments included three sets of controls, the first, negative controls, consisted of untreated cells (only plate exposure), a second set was exposed to three concentrations of sodium formate (0.5, 1 and 2 mM), and a third set exposed to cisplatin as positive controls. The results indicate that formate alone is not toxic towards A2780 ovarian cancer cells under the conditions used (**Table 5.5**). A2780 cancer cells were incubated with equipotent concentrations of complexes **16**–**19** (1/3 × IC_{50}) and three concentrations of sodium formate (0.5, 1 and 2 mM) for 24 h. Following 72 h of recovery time in drug-free medium, cell survival was evaluated using the Sulforhodamine B colorimetric assay. Decrease of cell viability was observed, and importantly this was greater

with increasing concentration of sodium formate. Complex **19** showed the least effect on cell viability decreasing from 95% to 81%, while complex **16** exhibited the highest changes varying from 96% to 74% when 2 mM formate was co-administered. Overall, the percentage of cell viability reduction which accompanies formate co-administration follows the order: **16** > **17** > **18** > **19** (Percentages of cell survival are listed in **Table 5.5**).

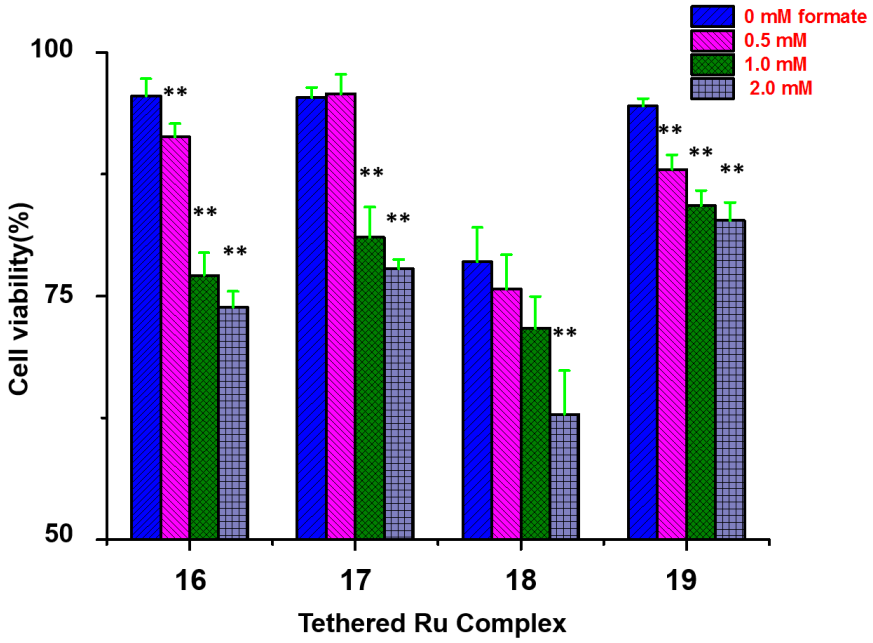

Figure 5.11 Cell viability of A2780 ovarian cancer cells when exposed for 24 h to complexes **16-19** (at equipotent 1/3 × IC_{50} concentrations) and sodium formate at the concentrations of 0, 0.5, 1.0 and 2.0 mM.

Table 5.5 Percentage of Cell Viability (%) of A2780 Cells Exposed to Different Concentrations of Formate and a Fixed Concentration of Complexes **16-19**.

Complex	[Formate]			
	0 mM	0.5 mM	1.0 mM	2.0 mM
16	96 ± 2	91 ± 2	78 ± 3	74 ± 2
17	95 ± 2	96 ± 3	81 ± 4	78 ± 1
18	79 ± 2	75 ± 2	72 ± 3	63 ± 2
19	95 ± 1	88 ± 2	85 ± 2	81 ± 3

5.3.8 Cellular Ru Uptake

Cellular Ru accumulation from administration of complexes **17** and **19** in A2780 human ovarian cancer cells and A2780Cis cells was determined. Stock solutions of both complexes were prepared in a mixture of DMSO/cell culture medium and their accurate Ru concentrations were determined by ICP-OES. Working solutions were then obtained by dilution in cell culture medium. Both cancer cell lines were exposed to complexes **17** and **19** for 24 h, at equipotent IC_{50} concentrations. The experiment did not involve recovery time in drug-free medium. Complex **19** showed a higher cellular Ru accumulation than complex **17** in both A2780 and A2780Cis (**Figure 5.12**). The cellular Ru content for complex **19** was 150 ± 38 ng per 10^6 A2780 cells and 241 ± 10 ng per 10^6 A2780Cis cells, while the cellular Ru content from complex **17** was much lower, 8.8 ± 0.9 ng and 7 ± 1 ng per 10^6 cells, respectively.

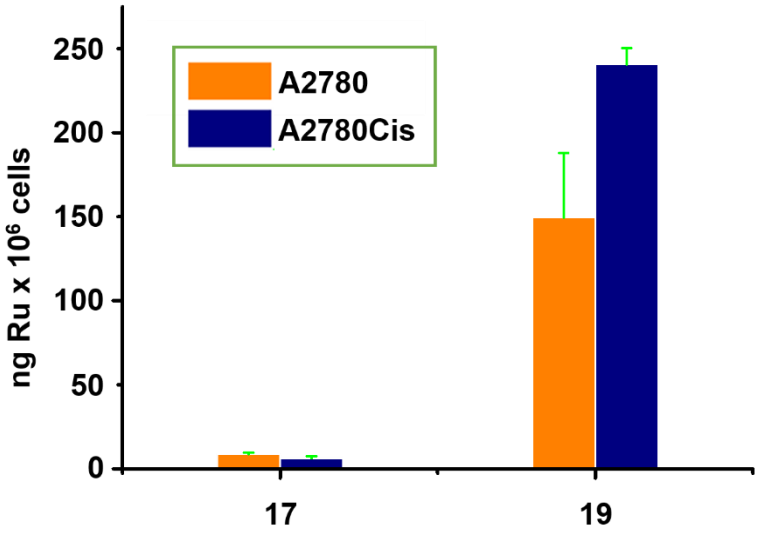

Figure 5.12 Cellular Ru uptake of complex **17** and **19** towards A2780 and A2780 cisplatin-resistance human ovarian cancer cells at IC_{50} equipotent concentrations.

5.3.9 Cell Cycle Arrest

Since complex **17** [Ru(η^6-Ph$(CH_2)_3$-ethylenediamine-*N*-Ts)Cl] binds to the nucleobase guanine (9-EtG), it was possible that DNA might be a target for anticancer activity. In order to investigate this, the effects on the cell cycle of A2780 cells exposed to complex **17** at IC_{50} and 2 × IC_{50} concentrations for 24 h were studied, using propidium iodide staining and flow cytometry (**Figure 5.13**). In comparison to negative control populations, a statistically significant increase of the cell population in the G_1 phase was observed, with percentages increasing to 75 ± 1% at IC_{50} concentration and 85 ± 3% population at 2 × IC_{50} concentration. This evidence of G_1 arrest would, in principle, discard the possibility of DNA targeting which should be evidenced by an accumulation of cells in the S phase. Studies of the interaction of complex **17** with DNA were carried out to investigate this further (*vide infra*).

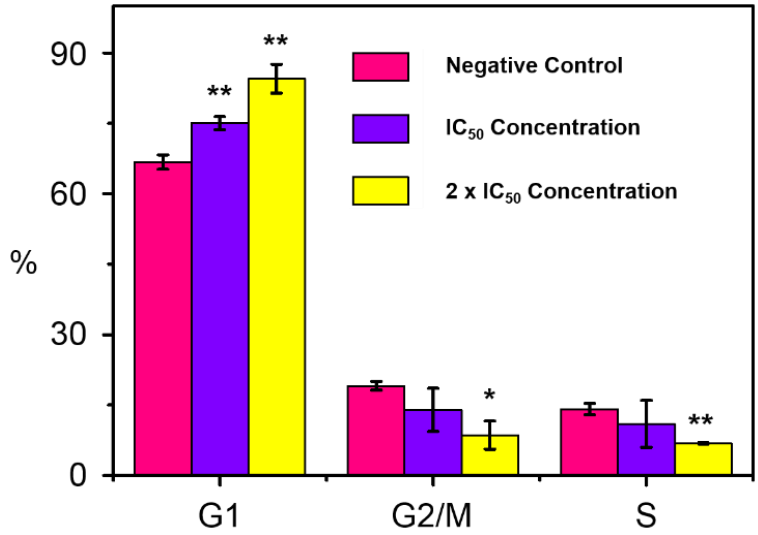

Figure 5.13 Cell cycle arrest analysis of A2780 human ovarian cancer cells after 72 h of exposure to complexes **17** at 310 K at IC_{50} and 2 × IC_{50} concentrations. Cell staining for flow cytometry was carried out using PI/RNase. Cell populations in each cell cycle phase for negative control and complex **17** were present. *p*-Values were calculated after a *t*-test against the negative control data, *$p < 0.05$, **$p < 0.01$..

5.3.10 ROS Determination

The level of reactive oxygen species (ROS) in A2780 human ovarian cancer cells induced by exposure to complex **17** was determined at IC_{50} concentration by flow cytometry fluorescence analysis (**Figure 5.14**). The total level of oxidative stress, including H_2O_2, peroxy and hydroxyl radicals, peroxynitrite, NO and superoxide production, was monitored using the green channel FL1 and orange channel FL2, respectively. Increased ROS levels were detected in the majority of the population of A2780 cells with up to 82% of cells exhibiting high fluorescence in the FL1-green channel. There is only a minimal increase in the levels of cellular superoxide (**Table 5.6**).

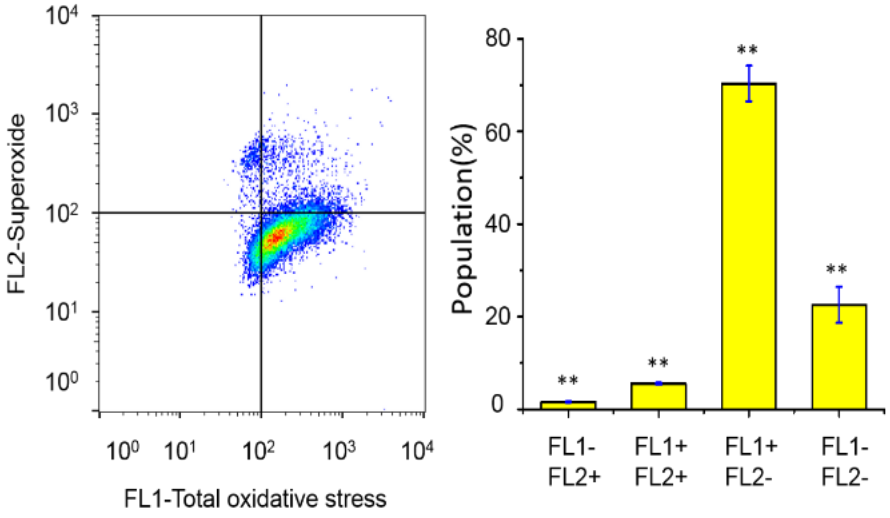

Figure 5.14 ROS induction in A2780 cancer cells exposed to complexes **17**. FL1 channel detects total oxidative stress, and FL2 channel detects superoxide production. *p*-Values were calculated after a *t*-test against the negative control data, *$p < 0.05$, **$p < 0.01$.

Table 5.6 Induction of ROS and Superoxide by Flow Cytometry Analysis of A2780 Ovarian Cancer Cells Exposed to Complex **17** and Negative Control. The Experiment Reads Superoxide in the FL2 Channel and Total ROS in the FL1 Channel.

	Cell Populations (%)			
	FL-1-/FL-2-	FL-1+/FL-2-	FL-1-/FL-2+	FL-1+/FL-2+
17	9 ± 1 **	82 ± 1 **	7.3 ± 0.2**	0.66 ± 0.09 **
Negative control	99.88 ± 0.04	0.10 ± 0.03	0	0.011 ± 0.002

In all cases, independent two-sample *t*-tests with unequal variances, Welch's *t*-tests, were carried out to establish statistical significance of the variations ($p < 0.01$ for **, and $p < 0.05$ for *).

5.3.11 Cell Membrane Integrity

The effect of complex **17** on the cellular membrane integrity of A2780 ovarian cancer cells was investigated using flow cytometry analysis of cells exposed for 24 h to the ruthenium complex and stained in the dark with propidium iodide. This experiment did not include fixation of the cells prior to staining. Results show that there are no induced changes in the membrane integrity of cancer cells as there are no statistical differences between the drug-exposed and negative control cells (**Table 5.7**).

Table 5.7 Cell Membrane Integrity by Flow Cytometry Analysis of A2780 Ovarian Cancer Cells Exposed to Complex **17** and Negative Control.

Complex	Cell Population (%)	
	FL-1-	FL-1+
17	96.0 ± 0.2	3.6 ± 0.2
Negative control	98.6 ± 0.4	1.35 ± 0.05

5.3.12 Calf Thymus DNA and Bacterial Plasmid DNA

The interaction of complex **17** [Ru(η^6-Ph$(CH_2)_3$-ethylenediamine-*N*-Ts)Cl] and **JS2** (in **Figure 5.1**, used as comparison) with double-helical calf thymus DNA (ct-DNA) and bacterial plasmid DNA were determined by absorption spectrophotometry. After 24 h incubation, no detectable amount of ruthenium was found in samples of DNA treated with **JS2**, nor complex **17**, even at very high r_i. Therefore these compounds do not bind strongly to high molecular mass DNA under the experimental condition used.

As shown in **Figure 5.15**, no significant changes in the mobilities of supercoiled (SC) or open circle form (OC) were observed even at very high concentrations of Ru compounds (r_i = 1), indicating that these complexes do not unwind DNA and do not form DNA adducts. No changes in intensities of SC and OC forms also indicated that the Ru complexes do not cleave DNA in dark.

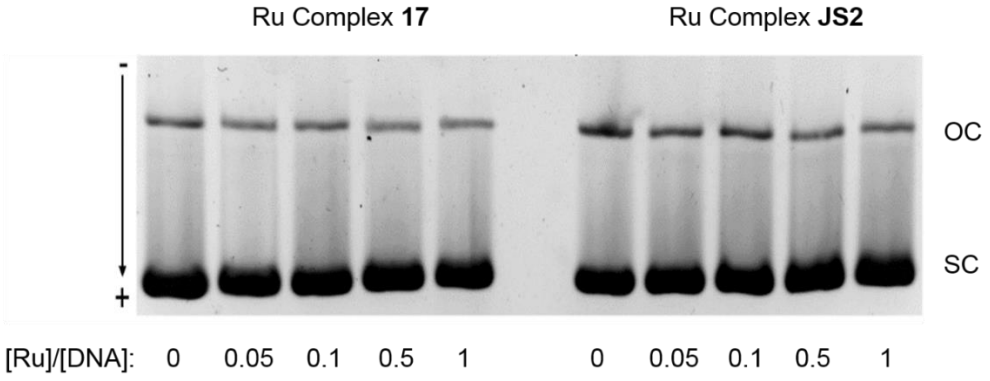

Figure 5.15 Interaction of complex **17** and complex **JS2** with bacterial plasmid DNA at various concentrations (r_i = 0–1). DNA samples were run on agarose gel followed by ethidium bromide staining. SC: supercoiled; OC: open circle. No significant changes of SC or OC were observed.

5.3.13 Binding to Short Single- or Double-stranded Oligonucleotides

Binding of complex **17** to short, single and double stranded synthetic oligonucleotides was also determined by flameless atomic absorption spectrometry (FAAS) and the concentrations of DNA were determined by absorption spectrophotometry. However, after 24 h reaction, no Ru associated with single- or double-stranded oligonucleotides treated with complex **JS2** was found in this experiment, whereas 3-4% of Ru was bound to single-stranded oligonucleotide when incubated with complex **17**, but no detectable amount of Ru was bound to double-stranded oligonucleotide.

5.4 Discussion

The X-ray crystal structures of complexes **16-19** show that they adopt the well-known 'piano-stool' geometry, with nitrogens of the diamine and a chloride bound to the metal center forming the three-legs and a phenyl ring forming the seat, being linked to the ethylenediamine by a three-carbon tether.[44, 45] Complexes **16-19** all have similar tethered structures. The length of the bond between Ru and the deprotonated N (Ru-N^-) lies within the range 2.112-2.121 Å, shorter than in the chiral tethered complexes (*R*, *R*)-[Ru(η^6-Ph$(CH_2)_3$-TsDPEN-NH)Cl] (2.144(3) Å) and [(η^6-*p*-cym)Ru(TsDPEN)Cl] (2.139(6) Å), while the Ru-N(H) bond length is within the range 2.14-2.149 Å longer than these two complexes (2.134(3) Å and 2.105(6) Å, respectively).[38, 40, 46] Complexes **16-19** have very similar Ru-N($^-$) and Ru-N(H) bond lengths to the complex [(η^6-hmb)Ru(TsEn)Cl] (hmb: hexamethylbenzene, 2.129(3) Å and 2.141(3) Å, respectively).[36] The N-Ru-N angles are in the range 78.54-78.87º, close to the chiral tethered

Ru complex (*R*, *R*)-[Ru(η^6-Ph$(CH_2)_3$-TsDPEN-NH)Cl].[38] The remaining bond lengths and angles show no significant difference to either tethered or non-tethered Ru sulfonyl ethylenediamine compared.

Complex **17** reacted rapidly with guanine (9-EtG) as studied by NMR at millimolar concentrations.[28] However, at lower concentration (micromolar), little binding to DNA was observed when calf thymus and bacterial plasma DNA was exposed to complex **17**, consistent with results reported previously for the non-tethered Ru^{II} complex [(η^6-*p*-cym)Ru(TsEn)Cl] (**JS2**), implying that DNA is not likely a target for Ru sulfonamide complexes.[37]

Hydride transfer between coenzyme NAD^+ and NADH plays a pivotal role in cell metabolism,[47] this pair of coenzymes is believed to be involved in over 400 cellular reactions.[48] Studies of TH reactions for the conversion of NAD^+ to NADH catalysed by transition metal complexes were initiated by Fish and Steckhan.[49-51] The use of Ru^{II} catalysts to mimic the cellular reaction and achieve TH reduction of NAD^+ under biologically relevant conditions has now been well studied.[52, 53] The en complex **RM175** showed strong DNA affinity, but low catalytic efficiency towards TH reduction of NAD^+ (TOF, 0.18 h^{-1});[35] whereas the introduction of a sulfonyl functional group raised the TOF up to 2.88 h^{-1} (**JS2** in **Figure 5.1**).[35] In this chapter, complexes **16-19** displayed more potent catalytic activity towards TH of NAD^+ to NADH. The reaction rate for tosylated complex **17** is ca. 25.8× and 1.6× faster than that for Ru-en and Ru-TsEn complexes, and comparable to Rh^{III} complex [(η^5-Cp^*)Rh(bipy)Cl]PF_6.[54, 55] This probably arises because the longer Ru-N(H) bond length and shorter Ru-N($^-$) bond distance (discussed above) make the tethered complex more approachable to NAD^+ when involved in the TH catalytic cycle, and the water-solubility allows tethered complexes to hydrolyse more readily which facilitates the hydride transfer. Generally, TOF values determined by UV-vis were found to be higher than TOFs determined by NMR spectroscopy (**Table 5.3**), probably due to the lower NAD^+ concentration and higher excess of formate used

in the TH reaction, since TOF depends strongly on molar ratio of formate used, with higher formate concentrations giving a higher TH reaction rate.[36] It appears that the presence of electron withdrawing sulfonamide on the chelating ligand gives rise to higher catalytic activity, consistent with the previous reported TH reduction of aldehydes and quinoxalines.[36, 56, 57]

Cellular accumulation is an important factor in drug cytotoxicity.[58] Cellular accumulation of Ru from complexes **17** and **19**, in A2780 and A2780Cis cancer cells does not correlate with their cytotoxicity (IC_{50}). However, the plot of Ru accumulation of complexes **17** and **19** in A2780 cells with decrease of cell viability (in the presence of 2 mM formate) indicates a reverse relationship: the higher cellular Ru uptake (complex **19**) induces lower cell proliferation decrease. TOFs of complexes **16**–**19** determined by UV-vis spectroscopy also exhibit an inverse correlation with the reduction of cell viability induced by 2 mM sodium formate, following the order: **19 < 18 < 17 < 16**. In UV-vis experiments, over a one thousand mol excess of formate was used, similar to ratio used in the *in vitro* A2780 cell viability determinations. Complex **19** displayed highest cell accumulation and catalytic reaction rate, while gave the lowest induction of cell viability decrease. Such behavior implies that complex **19** with stronger electron-withdrawing functional group ($-NO_2$) might be more labile in cells and interact more readily with cellular components, *e.g.* GSH, to become inactive. The catalytic rate for conversion of NAD^+ to NADH as observed in an aqueous medium appears not to be directly related to the crucial steps in the cellular mechanism of antiproliferative activity.

As a major peptide in cells, GSH plays a significant role in cell metabolism, e.g. in maintenance of cellular redox state and signal transduction.[59] It functions as an important reducing agent (GSH/GSSG couple) and has a high affinity for transition metal complexes.[60] Acquired drug resistance in cancer cells is often associated with over-expression of GSH which can act as a detoxification agent.[61] Complex **17** (2 mM, MeOD-d_4/H_2O, 1:4(v/v)) reacted rapidly with GSH (0.5-10 mol equiv, pH^* 7.1, 310 K, **Figure 5.5**) to form the adduct **17**-SG, but this decomposed

slowly after 24 h at 310 K in aqueous solution. This high thiol affinity of complex **17** may mean that the Ru complex rapidly binds to GSH on entering cells, and the decomposition of the adduct may lead to metabolites which is toxic to cells.[60] This may partially explain why the TH reduction of NAD^+ was hampered in the presence of GSH and limited increase in potency is observed in A2780 cancer cells exposed to complex **17** and sodium formate, compared to the Ru complex [(η^6-*p*-cym)Ru(TsEn)Cl], even though the TH reduction of NAD^+ was believed to be taking place in the cancer cells.[37]

Cisplatin is frequently used clinically in combination chemotherapy, especially for the ovarian and testicular cancers.[62] However, poor 5-year survival rates in ovarian cancer patients are partly attributable to the development of drug resistance.[63] Complex **17** showed much lower cross-resistance with cisplatin (resistance index of ca. 2 versus 11 for cisplatin) despite the low cell uptake in resistant human ovarian A2780Cis cancer cells. Furthermore, the higher selectivity index between MRC5 normal cells and A2780Cis cancer cells (2.6 for complex **17** versus 0.95 for cisplatin), indicates that complex **17** might be able to overcome cisplatin resistance with fewer side-effects.

In contrast to the negative control (A2780 cells not drugged, **Figure 5.13**), complex **17** can induce concentration-dependent G_1 cell cycle arrest, which inhibits cell division. Previously, Ru^{II} complexes have been reported to induce G1 arrest, *e.g.* Ru-Norharman complex [$Ru(bipy)_2$(*9H*-pyrido-[3,4-b]indole)$_2$]$^{2+}$ and [Ru(η^6-*p*-cym)(*p*-Impy−NMe_2)Cl].[64,65] Clinical anticancer drugs can also induce G_1 cell cycle arrest, for instance Clotrimazole and Paclitaxel.[66, 67] Paclitaxel can inhibit cell proliferation by activation of the p53 tumour suppressor gene.[67] Microtubules are also potential targets. They are important cycloskeletal polymers, which can form a constantly reorganized solid backbone that serves as a polarity information source, for separating chromosomes through cell division.[68] Recently reported Ru^{II} complexes [Ru(η^6-Ph$(CH_2)_3$-TsDPEN-NH)Cl] (*R*,*R* or *S*,*S*) distribute mainly in the

cycloskeleton and can effectively target and inhibit microtubule polymerization.[42] In view its structural similarity, complex **17** might also potentially target microtubules and subsequently trigger G1 cell arrest.

ROS are important factors in cell signalling, and can control cell survival, cell proliferation and the maintenance of cell redox homeostasis.[69] A moderate level of intracellular ROS would encourage the growth of cancer cells, however, at higher levels will cause damage and even induce apoptosis of cancer cells.[70] Complex **17** significantly increased the ROS level in A2780 cancer cells at IC_{50} concentrations, giving over 80% of cancer cells under total oxidative stress, which may contribute to cell death.

5.5 Conclusions

Four tethered Ru^{II} catalysts **16**–**19** were synthesized, and their structures determined by X-ray crystallography. Tethered Ru^{II} complexes usually display higher stability compared to non-tethered Ru^{II} complexes, since the arene is 'locked' with a bidentate ligand. Tethered complexes especially the chiral ones have been widely studied and used as potent catalysts in asymmetric transfer hydrogenation reaction of aromatic ketones using alcohol, *i.e.* ^{i}propanol as hydride sources.[40] The non-chiral tethered complex **17** was reported to have a high reaction rate in ketone TH reduction,[43] however, its catalytic TH reduction in conversion of NAD^+ to NADH and biological activity had not been previously studied. In this Chapter, detailed studies have been made of such tethered Ru^{II} complexes, including their crystal structures, TH catalytic activity, biological activity (with or without formate) and their mode of anticancer action.

All the complexes exhibit potent reductive catalytic activity *via* transfer hydrogenation as shown by the conversion of coenzyme NAD^+ to NADH, and follow a general reactivity trend: **16** < **17** < **18** < **19**. Coincubation of complexes **16**–**19** with A2780 cancer cells in the presence of nontoxic levels of formate resulted in the reduction of cell viability, and the correlation between TOFs and cell viability (**Figure 5.16**) suggest that electron withdrawing substituents on catalysts can increase the catalytic efficiency, however this reduces the anticancer activity when excess formate used. Such a combination of catalyst and non-toxic co-catalyst may provide a promising strategy for the design of catalysts which are effective in cancer treatment. These complexes exhibit moderate to good anticancer activity towards A2780, A2780Cis, A549, MCF7 and HEPG2 cancer cell lines, but relatively low toxicity against normal MRC5 cells. Some of the complexes displayed comparable cytotoxicity to the clinically used drug cisplatin. Complex **17** [Ru(η^6-Ph$(CH_2)_3$-ethylenediamine-*N*-Ts)Cl] gives better selectivity than in A2780 human ovarian cancer cells and MRC 5 normal cells, and likely to have a low cross-resistant with cisplatin. However, such antiproliferative behaviour appears not to involve a DNA-targeting mechanism of action.

Complex **17** reacts rapidly with GSH to form a **17**-SG adduct, which can effectively block the TH reduction of NAD^+. At NMR concentrations, the chelated tethered ligand is displaced by excess GSH. However such displacement is expected to be >200× slower (second order reaction). Concentration dependent G_1 cell cycle arrest was observed on exposure of A2780 cells to complex **17**. In addition complex **17** can induce high level of intracellular ROS, which may provide a basis for killing cancer cells.

5.6 References

(1) Rosenberg, B., Camp, L. V., Krigas, T. *Nature* **1965**, *205*, 698-699.

(2) Bugarcic, T.; Habtemariam, A.; Deeth, R. J.; Fabbiani, F. P. A.; Parsons, S.; Sadler, P. J. *Inorg. Chem.* **2009**, *48*, 9444–9453.

(3) Castonguay, A.; Doucet, C.; Juhas, M.; Maysinger, D. *J. Med. Chem*. **2012**, *55*, 8799−8806.

(4) Aman, F.; Hanif, M.; Siddiqui, W. A.; Ashraf, A.; Filak, L. K.; Reynisson, J.; Söhnel, T.; Jamieson, S. M. F.; Hartinger, C. G. *Organometallics* **2014**, *33*, 5546−5553.

(5) Barry, N. P. E.; Sadler, P. J. *Chem. Soc. Rev.* **2012**, *41*, 3264–3279.

(6) Mukhopadhyay, S.; Gupta, R. K.; Paitandi, R. P.; Rana, N. K.; Sharma, G.; Koch, B.; Rana, L. K., Hundal, M. S.; Pandey, D. S. *Organometallics* **2015**, *34*, 4491−4506.

(7) Han, S. H.; Kim, S.; De, U.; Mishra, N. K.; Park, J.; Sharma, S.; Kwak, J. H.; Han, S.; Kim, H. S.; Kim, I. S. *J. Org. Chem*. **2016**, *81*, 12416−12425

(8) Gras, M.; Therrien, B.; Süss-Fink, G.; Casini, A.; Edafe, F.; Dyson, P. J. *J. Organomet. Chem.* **2010**, *695*, 1119–1125.

(9) Fu, Y.; Romero, M. J.; Habtemariam, A.; Snowden, M. E.; Song, L.; Clarkson, G. J.; Qamar, B.; Pizarro, A. M.; Unwin, P. R.; Sadler, P. J. *Chem. Sci.* **2012**, *3*, 2485–2494.

(10) Suntharalingam, K.; Johnstone, T. C.; Bruno, P. M.; Lin, W.; Hemann, M. T.; Lippard, S. J. *J. Am. Chem. Soc.* **2013**, *135*, 14060–14063.

(11) Fu, Y.; Habtemariam, A.; Pizarro, A. M.; van Rijt, S. H.; Healey, D. J.; Cooper, P. A.; Shnyder, S. D.; Clarkson, G. J.; Sadler, P. J. *J. Med. Chem.* **2010**, *53*, 8192–8196.

(12) Almodares, Z.; Lucas, S. J.; Crossley, B. D.; Basri, A. M.; Pask, C. M.; Hebden, A. J.; Phillips, R. M.; McGowan, P. C. *Inorg. Chem.* **2014**, *53*, 727−736.

(13) Liu, Z.; Romero-Canelon, I.; Qamar, B.; Hearn, J. M.; Habtemariam, A.; Barry, N. P. E.; Pizarro, A. M.; Clarkson, G. J.; Sadler, P. J. *Angew. Chem. Int. Ed.* **2014**, *53*, 3941 –3946.

(14) Divsalar, A.; Bagheri, M. J.; Saboury, A. A.; Mansoori-Torshizi, H.; Amani, M. *J. Phys. Chem.* **2009**, *113*, 14035–14042.

(15) Lease, N.; Vasilevski, V.; Carreira, M.; de Almeida, A.; Sanaú, M.; Hirva, P.; Casini, A.; Contel, M. *J. Med. Chem.* **2013**, *56*, 5806−5818.

(16) Reddy, E. R.; Trivedi, R.; Sarma, A. V. S.; Sridhar, B.; Anantaraju, H. S.; Sriram, D.; Yogeeswarid, P.; Nagesh, N. *Dalton Trans.* **2015**, *44*, 17600–17616.

(17) Spencer, J.; Rathnam, R. P.; Motukuri, M.; Kotha, A. K.; Richardson, S. C. W.; Hazrati, A.; Hartley, J. A.; Malec, L.; Hursthouse, M. B. *Dalton Trans.* **2009**, *22*, 4299–4303.

(18) Aird, R. E.; Cummings, J.; Ritchie, A. A.; Muir, M.; Morris, R. E.; Chen, H.; Sadler, P. J.; Jodrell, D. I. *Br. J. Cancer* **2002**, *86*, 1652–1657.

(19) Xue, S. S.; Tan, C. P.; Chen, M. H.; Cao, J. J.; Zhang, D. Y.; Ye, R. R.; Ji, L. N.; Mao, Z. W. *Chem. Commun.* **2017**, *53*, 842–845.

(20) Gianferrara, T.; Bergamo, A.; Bratsos, I.; Milani, B.; Spagnul, C.; Sava, G.; Alessio, E. *J. Med. Chem.* **2010**, *53*, 4678–4690.

(21) Bergamo, A.; Gava, B.; Alessio, E.; Mestroni, G.; Serli, B.; Cocchietto, M.; Zorzet, S.; Sava, G. *Int. J. Oncol.* **2002**, *21*, 1331–1338.

(22) Kapitza, S.; Pongratz, M.; Jakupec, M. A.; Heffeter, P.; Berger, W.; Lackinger, L.; Keppler, B. K.; Marian, B. J. *Cancer Res. Clin. Oncol.* **2005**, *131*, 101–110.

(23) Ang, W. H.; Daldini, E.; Scolaro, C.; Scopelliti, R.; Juillerat-Jeannerat, L.; Dyson, P. J. *Inorg. Chem.* **2006**, *45*, 9006–9013.

(24) Reisner, E.; Arion, V. B.; Eichinger, A.; Kandler, N.; Giester, G.; Pombeiro, A. J. L.; Keppler, B. K. *Inorg. Chem.* **2005**, *44*, 6704–6716.

(25) Pelletier, F.; Comte, V.; Massard, A.; Wenzel, M.; Toulot, S.; Richard, P.; Pquet, M.; Gendre, P. L.; Zava, O.; Edafe, F.; Casini, A.; Dyson, P. J. *J. Med. Chem.* **2010**, *53*, 6923–6933.

(26) Nowak-Sliwinska, P.; Beijnum, J. R.; Casini, A.; Nazarov, A. A.; Wagnieres, G.; van den Bergh, H.; Dyson, P. J.; Griffioen, A. W. *J. Med. Chem.* **2011**, *54*, 3895–3902.

(27) Chen, H.; Parkinson, J. A.; Parsons, S.; Coxall, R. A.; Gould, R. O.; Sadler, P. J. *J. Am. Chem. Soc.* **2002**, *124*, 3064–3082.

(28) Wang, F.; Xu, J.; Habtemariam, A.; Bella, J.; Sadler, P. J. *J. Am. Chem. Soc.* **2005**, *127*, 17734–17743.

(29) Barrett, S. M.; Pitman, C. L.; Walden, A. G.; Miller, A. J. M. *J. Am. Chem. Soc.* **2014**, *136*, 14718–14721.

(30) Carrión, M. C.; Sepúlveda, F.; Jalón, F. A.; Manzano, B. R.; Rodríguez, A. M. *Organometallics* **2009**, *28*, 3822–3833.

(31) Maenaka, Y.; Suenobu, T.; Fukuzumi, S. *J. Am. Chem. Soc.* **2012**, *134*, 9417–9427.

(32) Wolfson, A.; Dlugy, C.; Shotland, Y.; Tavor, D. *Tetrahedron Lett.* **2009**, *50*, 5951–5953.

(33) Fujii, A.; Hashiguchi, S.; Uematsu, N.; Ikariya, T.; Noyori, R. *J. Am. Chem. Soc.* **1996**, *118*, 2521–2522.

(34) Hashiguchi, S.; Fujii, A.; Takehara, J.; Ikariya, T.; Noyori, R. *J. Am. Chem. Soc.* **1995**, *117*, 7562–7563.

(35) Yan, Y.; Melchart, M.; Habtemariam, A.; Peacock, A. F. A.; Sadler, P. J. *J. Biol. Inorg. Chem.* **2006**, *11*, 483–488.

(36) Soldevila-Barreda, J. J.; Bruijnincx, P. C. A.; Habtemariam, A.; Clarkson, G. J.; Deeth, R. J.; Sadler, P. J. *Organometallics* **2012**, *31*, 5958−5967.

(37) Soldevila-Barreda, J. J.; Romero-Canelon, I.; Habtemariam, A.; Sadler, P. J. *Nat. Commun.* **2015**, *6*, 6582.

(38) Hayes, A. M.; Morris, D. J.; Clarkson, G. J.; Wills, M. *J. Am. Chem. Soc.* **2005**, *127*, 7318–7319.

(39) Martins, J. E. D.; Clarkson, G. J.; Wills, M. *Org. Lett.* **2009**, *11*, 847–850.

(40) Hannedouche, J.; Clarkson, G. J.; Wills, M. *J. Am. Chem. Soc.* **2004**, *126*, 986–987.

(41) Soni, R.; Cheung, F. K.; Clarkson, G. C.; Martins, J. E. D.; Graham, M. A.; Wills, M. *Org. Biomol. Chem.* **2011**, *9*, 3290–3294.

(42) Fu, Y.; Sanchez-Cano, C.; Soni, R.; Romero-Canelon, I.; Hearn, J. M.; Liu, Z.; Wills, M.; Sadler, P. J. *Dalton Trans.* **2016**, *45*, 8367–8378.

(43) Jolley, K. E.; Zanotti-Gerosa, A.; Hancock, F.; Dyke, A.; Grainger, D. M.; Medlock, J. A.; Nedden, H. G.; LePaih, J. J. M.; Roseblade, S. J.; Seger, A.; Sivakumar, V.; Prokes, I.; Morris, D. J.; Wills, M. *Adv. Synth. & Catal.* **2012**, *354*, 2545–2555.

(44) Habtemariam, A.; Melchart, M.; Fernández, R.; Parsons, S.; Oswald, I. D. H.; Parkin, A.; Fabbiani, F. P. A.; Davidson, J. E.; Dawson, A.; Aird, R. E.; Jodrell, D. I.; Sadler, P. J. *J. Med. Chem.* **2006**, *49*, 6858–6868.

(45) Morris, R. E.; Aird, R. E.; Murdoch, P. S.; Chen, H.; Cummings, J.; Hughes, N. D.; Parsons, S.; Parkin, A.; Boyd, G.; Jodrell, D. I.; Sadler, P. J. *J. Med. Chem.* **2001**, *44*, 3616–3621.

(46) Cheung, F. K.; Clarke, A. J.; Clarkson, G. J.; Fox, D. J.; Graham, M. A.; Lin, C.; Crivill´ea. A. L.; Wills, M. *Dalton Trans.* **2010**, *39*, 1395–1402.

(47) Ying, W. *Antioxid. Redox Signaling* **2008**, *10*, 179−206.

(48) McSkimming, A.; Colbran, S. B. *Chem. Soc. Rev.* **2013**, *42*, 5439.

(49) Steckhan, E.; Herrmann, S.; Ruppert, R.; Dietz, E.; Frede, M.; Spika, E. *Organometallics* **1991**, *10*, 1568–1577.

(50) Westerhausen, V. D.; Herrmann, S.; Hummel, W.; Steckhan, E. *Angew. Chem. Int. Ed.* **1992**, *31*, 1529–1531.

(51) Lo, H. C.; Leiva, C.; Buriez, O.; Kerr, J. B.; Olmstead, M. M.; Fish, R. H. *Inorg. Chem.* **2001**, *40*, 6705–6716.

(52) Zhou, H.; Li, Z.; Wang, Z.; Wang, T.; Xu, L.; He, Y.; Fan, Q.; Pan, J.; Gu, L.; Chan, A. S. C. *Angew. Chem. Int. Ed.* **2008**, *47*, 8464–8467.

(53) Wang, C.; Li, C.; Wu, X.; Pettman, A.; Xiao, J. *Angew. Chem. Int. Ed.* **2009**, *48*, 6524–6528.

(54) Lo, H. C.; Buriez, O.; Kerr, J. B.; Fish, R. H. *Angew. Chem. Int. Ed.* **1999**, *38*, 1429–1432.

(55) Lo, H. C.; Fish, R. H. *Angew. Chem. Int. Ed.* **2002**, *41*, 478–481.

(56) Wu, X.; Liu, J.; Li, X.; Zanotti-Gerosa, A.; Hancock, F.; Vinci, D.; Ruan, J.; Xiao, J. *Angew. Chem. Int. Ed.* **2006**, *45*, 6718−6722.

(57) Tan, J.; Tang, W.; Sun, Y.; Jiang, Z.; Chen, F.; Xu, L.; Fan, Q.; Xiao, J. *Tetrahedron* **2011**, *67*, 6206−6213.

(58) Bugarcic, T.; Nováková, O.; Halámiková, A.; Zerzánková, L.; Vrána, O.; Kašpárková, J.; Habtemariam, A.; Parsons, S.; Sadler, P. J.; Brabec, V. *J. Med. Chem.* **2008**, *51*, 5310–5319.

(59) Garai-Ibabe, G.; Saa, L.; Pavlov, V. *Anal. Chem.* **2013**, *85*, 5542−5546.

(60) Mu, C.; Chang, S. W.; Prosser, K. E.; Leung, A. W. Y.; Santacruz, S.; Jang, T.; Thompson, J. R.; Yapp, D. T. T.; Warren, J. J.; Bally, M. B.; Beischlag, T. V.; Walsby, C. J. *Inorg. Chem.* **2016**, *55*, 177−190.

(61) Kartalou, M.; Essigmann, J. M. *Mutat. Res.* **2001**, *478*, 23–43.

(62) Belani, C. P. *Semin. Oncol.* **2004**, *31*, 25–33.

(63) Coley, H. M.; Sarju, J.; Wagner, G. *J. Med. Chem.* **2008**, *51*, 135–141.

(64) Tan, C.; Wu, S.; Lai, S.; Wang, M.; Chen, Y.; Zhou, L.; Zhu, Y.; Lian, W.; Peng, W.; Ji, L.. Xu, A. *Dalton Trans.* **2011**, *40*, 8611−8621.

(65) Romero-Canelón, I.; Salassa, L.; Sadler, P. J. *J. Med. Chem.* **2013**, *56*, 1291−1300.

(66) Liu, H.; Li, Y. *Anticancer Drugs* **2010**, *21*, 841−849.

(67) Demidenko, Z. N.; Kalurupalle, S.; Hanko, C.; Lim, C.; Broude, E.; Blagosklonny, M. V.; *Oncogene* **2008**, *27*, 4402−4410.

(68) Karsenti, E.; Vernos, I. *Science* **2001**, *294*, 543–547.

(69) D'Autreaux, B.; Toledano, M. B. *Nat. Rev. Mol. Cell Biol.* **2007**, *8*, 813−824.

(70) Dharmaraja, A. T. *J. Med. Chem.* **2017**, *60*, 3221–3240.

Chapter 6

Synthesis, Antimicrobial Activity and Biocompatibility of Novel Organometallic Biguanide Complexes

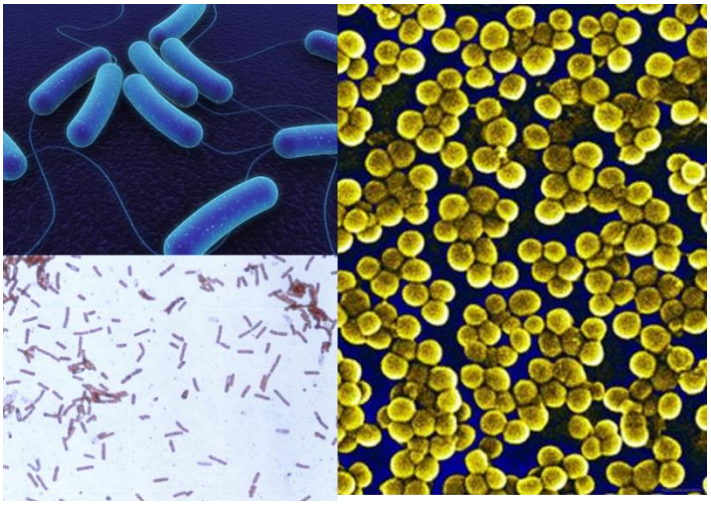

6.1 Introduction

Microscopic organisms ('microbes') are living organisms too small to be visible for human eyes.[1] Microbes cover broad definitions, mainly including bacteria, fungi, archaea, viruses, protists and microscopic animals.[2] Bacterial infections are a major health threat to human beings; conflicts between human and bacteria have lasted for centuries.[3] Bacteria mainly consist of two types: Gram-positive and Gram-negative bacteria (identified from Gram-staining); both of which have cell envelopes to guard against changes in osmotic pressure, chemical and enzymatic lysis, to survive under extreme conditions.[4] The envelopes of bacteria contain thick peptidoglycans layers (Gram-positive bacteria) and the additional outer membrane is populated with lipopolysaccharides (LPS, Gram-negative bacteria), such envelopes can protect bacteria from antibiotics (**Figure 6.1**).[5,6] Cell envelopes of fungii contain various layers of the polysaccharides chitin, β-glucan and mannan proteins.[7] Fungal infections are also a human health threat,[8] and their clinical treatment presents profound challenges.[9]

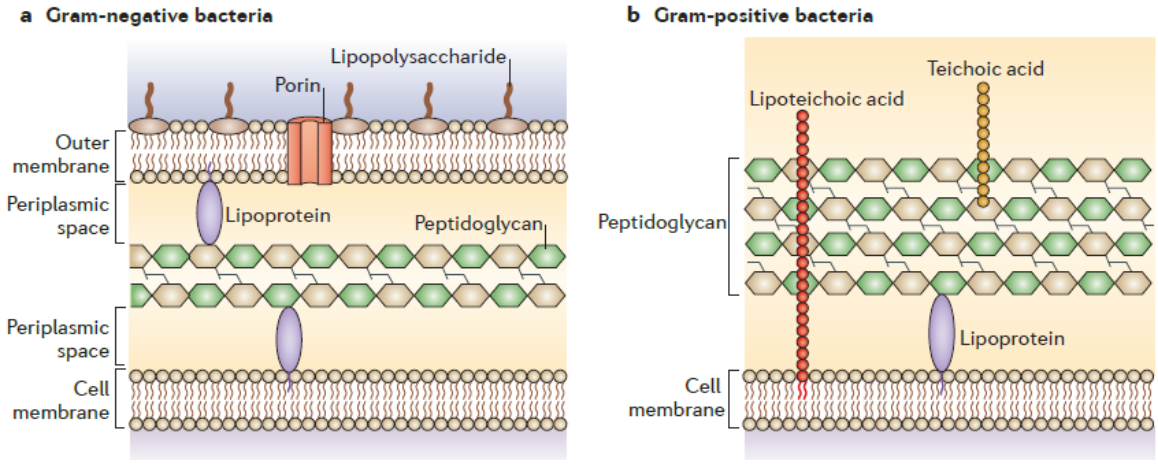

Figure 6.1 The envelopes of Gram-negative (a) and Gram-positive (b) bacteria.[6b]

Infectious diseases caused by drug resistance are currently the second main cause of death worldwide and the third leading cause of death in developed countries.[10] The use of antibiotics has saved millions of lives from microbial infections.[11] However, the inappropriate use of

antibiotics has severely led to the multidrug resistance, *e.g.* sulfonamide-resistant *Streptoccoccus pyogenes* emerged in the 1930s and *Staphylococcus aureus* showed resistance shortly after penicillin was introduced in the 1940s.[12] Multidrug resistant bacteria, including the notorious *Enterococcus faecium*, *Staphylococcus aureus*, *Klebsiella pneumoniae*, *Acetinobacter baumanii*, *Pseudomonas aeruginosa*, and *Enterobacteriaceae* species, abbreviated as 'ESKAPE' (underlined initial letters these bacteria), are a major threat to human health and cause of bacterial infections with high mortality.[13,14] Therefore, novel, effective, and safe antibiotics are urgently needed.[11]

Organometallic half-sandwich complexes can provide large families of compounds for drug design.[15] The antiproliferative and antimicrobial activities of organometallic complexes have been intensively studied due to the fine-tuneable choice of the π-bonded arene or cyclopentadienyl ligands, the metals themselves and their variable oxidation states, or the other monodentate or chelating ligands.[16] The third-row transition metal ions with low-spin $5d^6$ outer shell electronic configurations possess several potential advantages; *i.e.* they are relatively inert and likely to reach drug target sites with at least some of their initial ligands still bound.[17] To date, there are relatively few reports on the antimicrobial properties of organometallic complexes.[17,18]

Biguanide compounds are an important class of biological active molecules that have wide pharmaceutical applications. One of the best known biguanide derivatives is metformin (Metf), which has been widely as a drug to treat type II diabetes for over 60 years. Other derivatives such as phenformin (Phen), buformin, 1-phenylbiguanide (PB) and chlorophenylbiguanide are reported to exhibit antimicrobial and antiviral activity (**Figure 6.2**).[19] Jiang *et al.* have reported the synergistic effect of gold nanoparticles and metformin, generating broad-spectrum antibacterial and bactericidal activity against 'ESKAPE', with low cytotoxicity towards human mammalian cells. Such nanoparticles decorated with biguanide ligands can penetrate cell

membranes readily and also have significant biofilm disruption ability.[14a] Clardy *et al.* have synthesized a series of norspermidine-mimicking guanide and biguanide compounds with activity in disrupting biofilms in the pathogenic model of *B. subtilis* and *S. aureus*.[20] Over the last two decades, a library of biguanide chelated transition metal complexes has been synthesized, including $[Mn^{IV}(biguanide)_3]^{4+}$, $[Au^{III}(biguanide)]^{+}$, $[Cu(biguanide)_2]^{2+}$, $[Zn(biguanide)Cl_2]$, $[Pt(biguanide)Cl_2]$ and $[M(biguanide)]^{2+}$ (M: Mn, Co, Cu and Zn).[21-25] Some of those complexes show promising antimicrobial activity, but their mode of action (MoA) has yet to be elucidated.

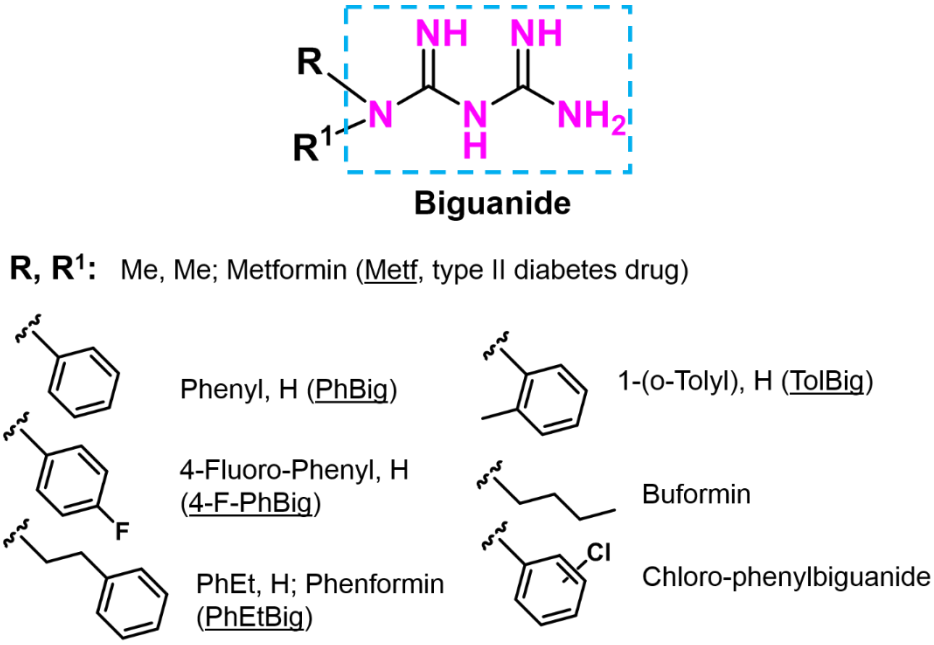

Figure 6.2 Neutral biguanide molecules with antidiabetic and antimicrobial activity.

In this Chapter, a series of novel organometallic biguanide complexes **20-37** containing either *p*-cymene, biphenyl, Cp*, Cp^{xph} or Cp^{xbiph}, a chelated metformin or an *N*-substituted biguanide, together with a monodentate halido ligand, Cl, Br or I (**Chart 6.1**) is synthesized and characterized. Broad range of antimicrobial screening against fungii, Gram–negative and Gram–positive bacteria was undertaken. The introduction of a sulfonyl functional groups on the biguanide ligand (complexes **33-37**) allowed the role of the terminal NH_2 in activity to be studied. The bio-compatibility of selected complexes were studied towards human mammalian

cells, stability of the Ir^{III} biguanide complexes in culture medium, and the mutation rate of *S. aureus* treated with complexes **26**, **27** and **30** were also investigated. The synergistic effect of complexes **27**, **30** and **33** on co-administration with vancomycin against vancomycin-resistant Enterococci (VRE), was studied, as well as the anti-biofilm activity of complexes **27-32** in the biofilm model of *S. aureus*. Confocal microscopy and TEM cell, permeability and morphology changes in *S. aureus* induced by complex **30** were also investigated by to gain insight into the mechanism of action.

Chart 6.1 Structures of Complexes 20-37 Studied in This Chapter

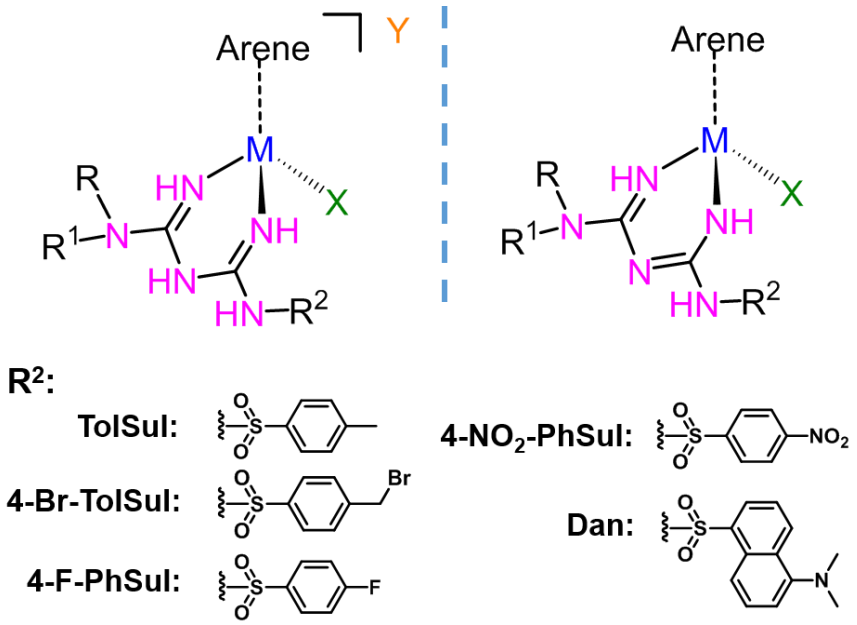

Complex	Arene/Cp^X	R	R^1	R^2	M	X	Y
20	*p*-cymene	Me	Me	H	Ru	Cl	Cl
21	biphenyl	Me	Me	H	Ru	Cl	Cl
22	*p*-cymene	Me	Me	H	Os	Cl	Cl
23	biphenyl	Me	Me	H	Os	Cl	Cl
24	Cp*	Me	Me	H	Ir	Cl	Cl
25	Cp^{XPh}	Me	Me	H	Ir	Cl	Cl
26	Cp^{Xbiph}	Me	Me	H	Ir	Cl	Cl
27	Cp^{Xbiph}	Phenyl	H	H	Ir	-	Cl
28	Cp^{Xbiph}	4-F-phenyl	H	H	Ir	-	Cl
29	Cp^{Xbiph}	PhEt	H	H	Ir	Cl	Cl
30	Cp^{Xbiph}	*o*-Tolyl	H	H	Ir	Cl	Cl
31	Cp^{Xbiph}	*o*-Tolyl	H	H	Ir	Br	Br
32	Cp^{Xbiph}	*o*-Tolyl	H	H	Ir	I	I
33	Cp^{Xbiph}	*o*-Tolyl	H	TolSul	Ir	Cl	-
34	Cp^{Xbiph}	*o*-Tolyl	H	4-Br-TolSul	Ir	Cl	-
35	Cp^{Xbiph}	*o*-Tolyl	H	4-F-PhSul	Ir	Cl	-
36	Cp^{Xbiph}	*o*-Tolyl	H	4-NO_2-PhSul	Ir	Cl	-
37	Cp^{Xbiph}	*o*-Tolyl	H	danzyl	Ir	Cl	-

6.2 Experimental Section

6.2.1 Materials

Iridium trichloride, ruthenium trichloride and osmium trichloride were purchased from Precious Metals Online (PMO Pty Ltd.) and used as received. Biguanide ligands (metformin, 1-phenylbiguanide hydrochloride, 1-(4-Fluorophenyl) biguanide hydrochloride, 1-(*o*-Tolyl)biguanide and phenformin) were purchased from Sigma-Aldrich and used as received. All the sulfonyl chloride compounds used in this research were obtained from Sigma-Aldrich. High concentration rat tail collagen was obtained from Scientific Laboratory Supplies. Collagenase was obtained from VWR. Fetal bovine serum was purchased from Fisher Scientific, and peptone water and anaerobic atmosphere generation bag were from Sigma-Aldrich. The NMR spectroscopy solvent, *e.g.* MeOD-d_4 and DMSO-d_6, were purchased from Cambridge Isotope Laboratories Inc, and D_2O and $CDCl_3$ from Sigma-Aldrich. The bacterial strains, *B. subtilis* DSM 10, *S. pyogenes* ATCC 151112, *E. faecalis* ATCC 29212, *S. aureus* ATCC 29213 and *S. epidermidis* ATCC 12228 were provided by Mr John Moat from the Department of Life Sciences, University of Warwick. The *HaCaT* keratinocyte cells were provided by Miss Jessica P. Furner-Pardoe and Dr. Freya Harrison. The rest of the antimicrobial and cytotoxicity screen were carried out by the 'Community for Open Antimicrobial Drug Discovery' (CO-ADD) from University of Queensland, Australia.

6.2.2 Synthesis and Characterization

[(η^6-*p*-cym)Ru(Metf)Cl]Cl (**20**). [(η^6-*p*-cym)$RuCl_2$]$_2$ (86 mg, 0.14 mmol) and metformin hydrochloride (50 mg, 0.3 mmol) were placed in a round-bottom flask to which anhydrous methanol (50 mL) and triethylamine (40 µL, 0.3 mmol) were added. The solution was heated under refluxed in a nitrogen atmosphere (323 K) overnight. After which the solvent was

removed on a rotary evaporator to get a red solid. The crude product was purified by recrystallization from mixed solvent of MeOH and diethyl ether (4/6, v/v), to obtain bright a red solid. Yield = 72 mg (55%). **^{1}H NMR** (400 MHz, MeOD-d_4): δ_H 1.25 (d, *J* = 6.9 Hz, 6H), 2.15 (s, 3H), 2.71-2.74 (m, 1H), 3.03 (s, 6H), 3.35 (s, 3H), 5.35 (d, *J* = 4.6 Hz, 2H), 5.62 (d, *J* = 5.8 Hz, 2H), 6.87 (s, 0.5H broad single), 7.37 (s, 0.3H broad single); **^{13}C NMR** (125.73 MHz, MeOD-d_4) δ_C 18.6, 22.6, 31.9, 39.0, 82.6, 84.7. HR-MS: *Calcd* for $[C_{14}H_{24}N_5Ru]^+$ 364.1075 m/z, found: 364.1075 m/z.

[(η^6-biph)Ru(Metf)Cl]Cl (**21**). Complex **21** was synthesized following the method similar to complex **20**, where $[(\eta^6\text{-biph})RuCl_2]_2$ (100 mg, 0.153 mmol), metformin hydrochloride (57 mg, 0.31 mmol) and triethylamine (42 µL, 0.31 mmol) were used. The crude product was purified by recrystallization from mixed solvent of MeOH and diethyl ether (4/6, v/v), to obtain a green solid. Yield = 73 mg (52%). **^{1}H NMR** (400 MHz, MeOD-d_4): δ_H 2.94 (s, 6H), 5.82-5.91 (m, 3H), 6.04 (d, *J* = 5.2 Hz, 2H), 7.50-7.61 (m, 3H), 7.63-7.78 (m, 2H); **^{13}C NMR** (125.73 MHz, D_2O) δ_c 38.0, 78.7, 81.8, 85.7, 128.1, 129.4, 130.4. HR-MS: *Calcd* for $[C_{16}H_{20}N_5Ru]^+$ 384.0762 *m*/*z*, found: 384.0758 *m*/*z*.

[(η^6-*p*-cym)Os(Metf)Cl]Cl (**22**). Complex **22** was synthesized following the method similar to complex **20**, where $[(\eta^6\text{-}p\text{-cym})OsCl_2]_2$ (55.3 mg, 0.07 mmol), metformin hydrochloride (25 mg, 0.15 mmol) and triethylamine (21 µL, 0.15 mmol) were used. The crude product was purified by recrystallization from mixed solvent of MeOH and diethyl ether (4/6, v/v), to obtain a dark grey solid. Yield = 39 mg (51%). **^{1}H NMR** (500 MHz, D_2O): δ_H 1.23 (d, *J* = 6.9 Hz, 6H), 2.21 (s, 3H), 2.52-2.57 (m, 1H), 3.04 (s, 6H), 5.74 (d, *J* = 5.4 Hz, 2H), 5.99 (d, *J* = 5.6 Hz, 2H); **^{13}C NMR** (125.73 MHz, D_2O) δ_c 8.2, 17.5, 21.8, 30.6, 38.2, 46.6, 71.0, 74.2; HR-MS: *Calcd* for $[C_{14}H_{24}N_5Os]^+$ 454.1646 *m*/*z*, found: 454.1641 *m*/*z*.

[(η^6-biph)Os(Metf)Cl]Cl (**23**). Complex **23** was synthesized following the method similar to complex **20**, where $[(\eta^6\text{-biph})OsCl_2]_2$ (100 mg, 0.12 mmol), metformin hydrochloride (42 mg,

0.25 mmol) and triethylamine (35 µL, 0.25 mmol) were used. The crude product was purified by recrystallization from mixed solvent of MeOH and diethyl ether (4/6, v/v), to obtain a yellow solid. Yield = 78 mg (60%). **^{1}H NMR** (400 MHz, MeOD-d_4): δ_H 2.97 (s, 6H), 5.93 (s, broad 3H), 6.21 (s, broad, 2H), 7.43-7.53 (m, 3H), 7.64 (d, *J* = 7.2 Hz, 2H). **^{13}C NMR** (125.73 MHz, D_2O) δ_c 38.1, 70.4, 72.9, 75.3, 87.1, 128.4, 129.4, 129.8; HR-MS: *Calcd* for $[C_{16}H_{20}N_5Os]^+$ 474.1333 *m*/*z*, found: 474.1312 *m*/*z*.

[(η^5-Cp*)Ir(Metf)Cl]Cl (**24**). Complex **24** was synthesized following the method similar to complex **20**, where $[(\eta^5\text{-Cp}^*)IrCl_2]_2$ (56 mg, 0.07 mmol), metformin hydrochloride (25 mg, 0.15 mmol) and triethylamine (21 µL, 0.15 mmol) were used. The crude product was purified by recrystallization from mixed solvent of MeOH and diethyl ether (4/6, v/v), to obtain an orange solid. Yield = 49 mg (66%). **^{1}H NMR** (400 MHz, MeOD-d_4): δ_H 1.68 (s, 15H), 3.07 (s, 6H); **^{13}C NMR** (125.73 MHz, D_2O): δ_c 8.2, 38.2, 88.5; HR-MS: *Calc* for $[C_{14}H_{26}N_5(Ir\text{-}HCl_2)]^+$ 456.1739 *m*/*z*, found: 456.1734 *m*/*z*. Elemental analysis: *Calcd* for $C_{14}H_{26}\ Cl_2N_5Ir(H_2O)_{0.5}$: C, 31.34%; H, 5.07%; N, 13.05%. Found: C, 31.29%; H, 4.78%; N, 12.87%.

[(η^5-Cp^{Xph})Ir(Metf)Cl]Cl (**25**). Complex **25** was synthesized following the method similar to complex **20**, where $[(\eta^5\text{-Cp}^{Xph})IrCl_2]_2$ (150 mg, 0.163 mmol), metformin hydrochloride (55 mg, 0.33 mmol) and triethylamine (92 µL, 0.66 mmol) were used. The crude product was purified by recrystallization from mixed solvent of MeOH and diethyl ether (4/6, v/v), to obtain a yellow solid. Yield = 104 mg (54%). **^{1}H NMR** (300 MHz, D_2O): δ_H. 1.71 (s, 6H), 1.84 (s, 6H), 3.09 (s, 6H), 7.52 (s, 5H); **^{13}C NMR** (125.73 MHz, D_2O): δc 8.3, 8.9, 38.2, 88.3, 92.0, 129.0, 129.06, 129.5, 130.2; HR-MS: *Calcd* for $[C_{19}H_{27}N_5(Ir\text{-}HCl_2)]^+$ 518.1896 m/z, found: 518.1893 m/z. Elemental analysis: *Calcd* for $C_{19}H_{28}Cl_2IrN_5$: C, 38.71%; H, 4.79%; N, 11.88%. Found: C, 38.60%; H, 4.79%; N, 11.50%.

[(η^5-Cp^{Xbiph})Ir(Metf)Cl]Cl (**26**). Complex **26** was synthesized following the method similar to complex **20**, where $[(\eta^5\text{-Cp}^{Xbiph})IrCl_2]_2$ (100 mg, 0.0933 mmol), metformin hydrochloride

(32 mg, 0.188 mmol) and triethylamine (53 µL, 0.376 mmol) were used. The crude product was purified by chromatography column (DCM/MeOH (10:1, v/v)), to obtain a red solid. Yield = 72 mg (58%). **^{1}H NMR** (300 MHz, MeOD-d_4): δ_H 1.94 (s, 6H), 2.05 (s, 6H), 3.16 (s, 6H), 7.38-7.43 (m, 1H), 7.49 (t, *J* = 8.1 Hz, 2H), 7.67 (q, *J* = 7.7 Hz, 15.0 Hz, 4H), 7.78 (d, *J* = 7.4 Hz, 2H); **^{13}C NMR** (125.73 MHz, D_2O): δ_c 8.8, 9.3, 37.2, 90.0, 91.1, 126.8, 127.33, 128.2, 129.2, 130.9, 139.4, 141.2; HR-MS: *Calcd* for $[C_{25}H_{31}N_5(Ir\text{-}HCl_2)]^+$ 594.2209 *m*/*z*, found: 594.2204 *m*/*z*. Elemental analysis: *Calcd* for $C_{25}H_{31}ClIrN_5(H_2O)_{0.5}$: C, 47.05%; H, 5.05%; N, 10.97%. Found: C, 46.88%; H, 4.86%; N, 10.63%.

[(η^5-Cp^{Xbiph})Ir(PhBig)]Cl (**27**). Complex **27** was synthesized following the method similar to complex **20**, where $[(\eta^5\text{-}Cp^{Xbiph})IrCl_2]_2$ (100 mg, 0.0933 mmol), 1-Phenylbiguanide hydrochloride (41 mg, 0.188 mmol) and triethylamine (53 µL, 0.376 mmol) were used. The crude product was purified by chromatography column (DCM/MeOH (10:1, v/v)), to obtain a dark red solid. Yield = 57 mg (45%). **^{1}H NMR** (400 MHz, DMSO-d_6): δ_H 1.90 (s, 6H), 1.98 (s, 6H), 6.44 (s, 2H), 6.94 (t, *J* = 7.1 Hz, 1H), 7.24 (t, *J* = 7.8 Hz, 2H), 7.41 (t, *J* = 7.0 Hz, 1H), 7.50 (t, *J* = 7.6 Hz, 2H), 7.56 (d, *J* = 8.1 Hz, 2H), 7.63 (d, *J* = 8.2 Hz, 2H), 7.72 (d, *J* = 7.6 Hz, 2H), 7.77 (d, *J* = 8.1 Hz, 2H), 9.18 (s, 2H), 9.24 (s, 1H); **^{13}C NMR** (125.73 MHz, $CDCl_3$): δ_c 127.0, 127.9, 128.0, 129.0, 129.6, 130.5; HR-MS: *Calcd* for $[C_{29}H_{31}N_5(Ir\text{-}Cl)]^+$ 642.2209 *m*/*z*, found: 642.2209 *m*/*z*. Elemental analysis: *Calcd* for $C_{25}H_{31}ClIrN_5(H_2O)_{0.5}$: C, 50.75%; H, 4.70%; N, 10.21%. Found: C, 50.78%; H, 4.54%; N, 10.10%.

[(η^5-Cp^{Xbiph})Ir(4-F-PhBig)]Cl (**28**). Complex **28** was synthesized following the method similar to complex **20**, where $[(\eta^5\text{-}Cp^{Xbiph})IrCl_2]_2$ (200 mg, 0.187 mmol), 1-(4-Fluoro phenyl)biguanide hydrochloride (93 mg, 0.4 mmol) and triethylamine (112 µL, 0.8 mmol) were added. The crude product was purified by chromatography column (DCM/MeOH (10:1, v/v)), to obtain a dark red solid. Yield = 118 mg (43%). **^{1}H NMR** (400 MHz, MeOD-d_4): δ_H 1.96 (s, 6H), 2.06 (s, 6H), 7.05 (t, *J* = 8.6 Hz, 2H), 7.41 (t, *J* = 7.2 Hz, 1H), 7.47-7.51 (m, 4H),

7.64 (d, *J* = 8.2 Hz, 2H), 7. 96 (d, *J* = 7.4 Hz, 2H), 7.77 (d, *J* = 8.2 Hz, 2H); **^{13}C NMR** (125.73 MHz, $CDCl_3$): δ_c 127.0, 127.9, 128.0, 129.1, 130.6; **^{19}F NMR** (376.4 MHz, D_2O): δ_F -121.8; HR-MS: *Calcd* for $[C_{29}H_{30}FN_5(Ir\text{-}HCl_2)]^+$ 660.2114 *m*/*z*, found: 660.2105 *m*/*z*. Elemental analysis: *Calcd* for $C_{29}H_{30}ClFIrN_5(H_2O)$: C, 48.83%; H, 4.52%; N, 9.82%. Found: C, 48.97%; H, 4.19%; N, 9.77%.

[(η^5-Cp^{Xbiph})Ir(Phen)Cl]Cl (**29**). Complex **29** was synthesized following the method similar to complex **20**, where $[(\eta^5\text{-}Cp^{Xbiph})IrCl_2]_2$ (200 mg, 0.187 mmol), phenformin hydrochloride (92 mg, 0.38 mmol) and triethylamine (110 μL, 0.76 mmol) were added. The crude product was purified by chromatography column (DCM/MeOH (10:1, v/v)), giving a dark red solid. Yield = 183 mg (66%). **^{1}H NMR** (300 MHz, MeOD-d_4): δ_H 1.93 (s, 6H), 2.02 (s, 6H), 2.82 (t, *J* = 7.1 Hz, 2H), 3.38-3.40 (m, 2H), 7.20-7.29 (m, 5H), 7.42 (d, *J* = 6.5 Hz, 1H), 7.47-7.52 (m, 2H), 7.61 (d, *J* = 7.7 Hz, 2H), 7.68 (d, *J* = 7.6 Hz, 2H), 7.75 (d, *J* = 7.5 Hz, 2H); **^{13}C NMR** (125.73 MHz, MeOD-d_4): δ_c 42.4, 126.6, 127.3, 127.6, 128.1, 128.5, 128.7, 130.9; HR-MS: *Calcd* for $[C_{31}H_{34}N_5(Ir\text{-}HCl_2)]^+$ 670.2522 *m*/*z*, found: 670.2519 *m*/*z*. Elemental analysis: *Calcd* for $C_{31}H_{36}Cl_2IrN_5$: C, 50.20%; H, 4.89%; N, 9.44%. Found: C, 50.74%; H, 4.88%; N, 9.38%.

[(η^5-Cp^{Xbiph})Ir(TolBig)Cl]Cl (**30**). Complex **30** was synthesized following the method similar to complex **20**, where $[(\eta^5\text{-}Cp^{Xbiph})IrCl_2]_2$ (200 mg, 0.187 mmol), 1-(o-Tolyl)biguanide (73 mg, 0.38 mmol) and triethylamine (110 μL, 0.76 mmol) were added. The crude product was purified by chromatography column (DCM/MeOH (10:1, v/v)), giving a dark red solid. Yield = 125 mg (46%). **^{1}H NMR** (300 MHz, MeOD-d_4): δ_H 1.92 (s, 6H), 2.04 (s, 6H), 2.26 (s, 3H), 7.11-7.16 (m, 1H), 7.21 (d, *J* = 7.7 MHz, 1H), 7.28 (d, *J* = 7.7 Hz, 1H), 7.38-7.44 (m, 2H), 7.48-7.53 (m, 2H), 7.57 (d, *J* = 7.5 Hz, 2H), 7.71 (t, *J* = 8.6 Hz, 4H); **^{13}C NMR** (125.73 MHz, $CDCl_3$): δ_c 126.8, 127.0, 127.3, 127.4, 127.9, 128.0, 129.1, 130.2, 131.7. HR-MS: *Calcd* for $[C_{30}H_{33}N_5(Ir\text{-}HCl_2)]^+$ 656.2365 *m*/*z*, found: 656.2362 *m*/*z*. Elemental analysis: *Calcd* for $C_{30}H_{34}Cl_2IrN_5$: C, 49.51%; H, 4.71%; N, 9.62%. Found: C, 49.49%; H, 4.46%; N, 9.69%.

[(η^5-Cp^{Xbiph})Ir(TolBig)Br]Br (**31**). [(η^5-Cp^{Xbiph})IrCl$_2$]$_2$ (100 mg, 0.093 mmol) in methanol (30 mL) and sodium bromide (1.92 g, 18.7 mmol) in deionised water (10 mL) were mixed in a round bottom flask. The solution was heated to 343 K for 1 h. Then, a solution of 1-(o-Tolyl)biguanide (36.6 mg, 0.191 mmol) and triethylamine (54 µL, 0.383 mmol) were added, the reaction was heated at 343 K under nitrogen atmosphere for 12 h. After which the solvent was removed on a rotary evaporator giving a dark red solid. The solid was re-dissolved in chloroform and washed with brine (3 × 50 mL), and dried over $MgSO_4$. The crude product was further purified by chromatography column (DCM/MeOH (20:1, v/v)). Yield = 100 mg (65%). **^{1}H NMR** (400 MHz, MeOD-d$_4$): δ_H 1.69 (s, 6H), 1.82 (s, 6H), 2.14 (s, 3H), 7.31 (t, *J* = 7.6 Hz, 1H), 7.10 (t, *J* = 6.8 Hz, 1H), 7.17 (d, *J* = 7.3 Hz, 2H), 7.30 (t, *J* = 7.4 Hz, 1H), 7.39 (t, *J* = 7.2 Hz, 4H), 7.56 (t, *J* = 7.4 Hz, 4H); **^{13}C NMR** (125.73 MHz, $CDCl_3$): δ_c 16.6, 65.5, 126.6, 127.3, 127.5, 128.7, 130.5, 140.0. HR-MS: *Calcd* for [$C_{30}H_{33}N_5$(Ir-HBr_2)]$^+$ 656.2365 *m*/*z*, found: 656.2376 *m*/*z*. Elemental analysis: *Calcd* for $C_{30}H_{34}Br_2IrN_5(Et_2O)_{0.6}$: C, 45.19%; H, 4.68%; N, 8.13%. Found: C, 45.24%; H, 4.32%; N, 8.33%.

[(η^5-Cp^{Xbiph})Ir(TolBig)I]I (**32**). [(η^5-Cp^{Xbiph})IrCl$_2$]$_2$ (100 mg, 0.093 mmol) in methanol (30 mL) and potassium iodide (3.1 g, 18.7 mmol) in deionised water (10 mL) were mixed in a round bottom flask. The solution was heated to 343 K for 1 h. Then, a solution of 1-(o-Tolyl)biguanide (36.6 mg, 0.191 mmol) and triethylamine (54 µL, 0.383 mmol) were added, the reaction was heated at 343 K under nitrogen atmosphere for 12 h and a scarlet precipitate was observed. After which the solvent was removed on a rotary evaporator giving a dark red solid. The solid was re-dissolved in chloroform and washed with brine (3 × 50 mL), and dried over $MgSO_4$. The crude product was further purified by chromatography column (DCM/MeOH (20:1, v/v)), to get an orange solid. Yield = 102 mg (59%). **^{1}H NMR** (400 MHz, MeOD-d$_4$): δ_H 1.76 (s, 6H), 1.90 (s, 6H), 2.23 (s, 3H), 7.11-7.18 (m, 3H), 7.26 (d, *J* = 7.4 Hz, 1H), 7.41 (d, *J* = 8.0 Hz, 3H), 7.50 (t, *J* = 7.4 Hz, 2H), 7.59 (d, *J* = 8.2 Hz, 2H), 7.66 (d, *J* = 7.2 Hz, 2H); **^{13}C**

NMR (125.73 MHz, $CDCl_3$): δ_c 8.3, 9.0, 16.7, 126.6, 127.2, 127.5, 128.7, 130.4, 131.3, 140.0, 141.2; HR-MS: *Calcd* for $[C_{30}H_{34}IN_5(Ir\text{-}I)]^+$ 784.1488 *m*/*z*, found: 784.1488 *m*/*z*. Elemental analysis: *Calcd* for $C_{30}H_{34}I_2IrN_5$: C, 39.57%; H, 3.76%; N, 7.69%. Found: C, 39.96%; H, 3.77%; N, 7.60%.

[(η^5-Cp^{Xbiph})Ir(TsTolBig)Cl] (**33**). Complex **33** was synthesized following the method similar to complex **20**, where $[(\eta^5\text{-}Cp^{Xbiph})IrCl_2]_2$ (130 mg, 0.121 mmol), 4-methyl-N-(N-(N-(o-tolyl)carbamimidoyl)carbamimidoyl)benzenesulfonamide (93 mg, 0.269 mmol) and triethylamine (110 µL, 0.76 mmol) were added. The crude product was purified by chromatography column (DCM/MeOH (25:1, v/v)), giving a yellow solid. Yield = 139 mg (68%). **^{1}H NMR** (400 MHz, MeOD-d_4): δ_H 1.53 (s, 6H), 1.72 (s, 6H), 2.17 (s, 3H), 2.30 (s, 3H), 7.17-7.22 (m, 5H), 7.27 (d, *J* = 6.9 Hz, 1H), 7.36 (d, *J* = 8.2 Hz, 2H), 7.40 (d, *J* = 7.4 Hz, 1H), 7.49 (t, *J* = 7.4 Hz, 2H), 7.57 (d, *J* = 8.2 Hz, 2H), 7.65-7.67 (m, 4); **^{13}C NMR** (125.73 MHz, MeOD-d_4): δ_c 8.7, 18.0, 21.4, 126.1, 127.0, 127.6, 127.6, 128.9, 129.2, 130.4, 131.5, 133.8, 140.3, 140.8, 141.3, 141.4, 151.7, 152.9; HR-MS: *Calcd* for $[C_{37}H_{39}N_5O_2S(Ir\text{-}Cl)]^+$ 810.2454 *m*/*z*, found: 810.2449 *m*/*z*. Elemental analysis: *Calcd* for $C_{37}H_{39}ClIrN_5O_2S(H_2O)_{0.4}$: C, 52.12%; H, 4.70%; N, 8.21%. Found: C, 52.16%, H, 4.62%, N, 8.07%.

[(η^5-Cp^{Xbiph})Ir(4-BrTolSulTolBig)Cl] (**34**). Complex **34** was synthesized following the method similar to complex **20**, where $[(\eta^5\text{-}Cp^{Xbiph})IrCl_2]_2$ (200 mg, 0.187 mmol), 4-(bromomethyl)-N-(N-(N-(o-tolyl)carbamimidoyl)carbamimidoyl)benzenesulfonamide (173.6 mg, 0.410 mmol) and triethylamine (116 µL, 0.83 mmol) were added. The crude product was purified by chromatography column (DCM/MeOH (25:1, v/v)), giving a yellow solid. Yield = 131 mg (38%). **^{1}H NMR** (300 MHz, MeOD-d_4): δ_H 1.56 (s, 6H), 1.75 (s, 6H), 2.18 (s, 3H), 2.32 (s, 1H), 4.60 (s, 1H), 7.19-7.22 (m, 3H), 7.27 (d, *J* = 8.8 Hz, 1H), 7.37-7.52 (m, 5H), 7.57-7.59 (m, 2H), 7.67 (d, *J* = 9.2 Hz, 3H), 7.79 (d, *J* = 10.4 Hz, 1H); **^{13}C NMR** (125.73 MHz, MeOD-d_4): δ_c 7.6, 8.4, 16.5, 44.4, 91.2, 126.2, 126.6, 127.2, 127.2, 127.3, 127.5, 128.6, 128.7,

128.9, 129.1, 130.4, 131.3, 140.1. HR-MS: *Calcd* for $[C_{37}H_{38}N_5O_2SBr(Ir\text{-}Cl)]^+$ 888.1559 *m*/*z*, found: 888.1551 *m*/*z*. Elemental analysis: *Calcd* for $C_{37}H_{38}ClBrIrN_5O_2S$: C, 48.08%; H, 4.14%; N, 7.58%. Found: C, 48.09%; H, 4.14%; N, 7.45%.

[(η^5-Cp^{Xbiph})Ir(4-F-PhSulTolBig)Cl] (**35**). Complex **35** was synthesized following the method similar to complex **20**, where $[(\eta^5\text{-}Cp^{Xbiph})IrCl_2]_2$ (111 mg, 0.103 mmol), 4-(bromomethyl)-N-(N-(N-(o-tolyl)carbamimidoyl)carbamimidoyl)benzenesulfonamide (86 mg, 0.228 mmol) and triethylamine (64 µL, 0.455 mmol) were used. The crude product was purified by chromatography column (DCM/MeOH (25:1, v/v)), giving a yellow solid. Yield = 84 mg (48%). **^{1}H NMR** (400 MHz, MeOD-d_4): δ_H 1.58 (s, 6H), 1.75 (s, 6H), 2.18 (s, 3H), 7.18-7.21 (m, 3H), 7.27 (d, *J* = 6.9 Hz, 1H), 7.37-7.41 (m, 3H), 7.49 (t, *J* = 7.4 Hz, 2H), 7.58 (d, *J* = 8.0 Hz, 2H), 7.65 (d, *J* = 7.7 Hz, 2H), 8.02 (d, *J* = 8.6 Hz, 2H), 8.25 (d, *J* = 8.3 Hz, 2H); **^{13}C NMR** (125.73 MHz, MeOD-d_4): δ_c 7.5, 8.3, 16.4, 123.5, 126.6, 127.1, 127.2, 127.5, 128.7, 130.4, 131.2, 140.0; HR-MS: *Calc* for $[C_{36}H_{36}N_6O_4S(Ir\text{-}Cl)]^+$ 841.2148 *m*/*z*, found: 841.2143 *m*/*z*. Elemental analysis: *Calcd* for $C_{36}H_{36}ClFIrN_5O_2S$: C, 50.90%; H, 4.27%; N: 8.24%. Found: C, 50.56%; H, 4.26%; N, 8.20%.

[(η^5-Cp^{Xbiph})Ir(4-NO$_2$-PhSulTolBig)Cl] (**36**). Complex **36** was synthesized following the method similar to complex **20**, where $[(\eta^5\text{-}Cp^{Xbiph})IrCl_2]_2$ (150 mg, 0.140 mmol), 4-fluoro-N-(N-(N-(o-tolyl) carbamimidoyl)carbamimidoyl)benzenesulfonamide (103 mg, 0.294 mmol) and triethylamine (82 µL, 0.588 mmol) were added. The crude product was purified by chromatography column (DCM/MeOH (25:1, v/v)), and a yellow solid was obtained. Yield = 162 mg (66%). **^{1}H NMR** (400 MHz, MeOD-d_4): δ_H 1.58 (s, 6H), 1.75 (s, 6H), 2.18 (s, 3H), 7.12-7.22 (m, 5H), 7.28 (d, *J* = 6.9 Hz, 1H), 7.38-7.41 (m, 3H), 7.49 (t, *J* = 7.4 Hz, 2H), 7.60 (d, *J* = 8.1 Hz, 2H), 7.67 (d, *J* = 7.44 Hz, 2H), 7.82 (t, *J* = 7.5 Hz, 2H); **^{13}C NMR** (125.73 MHz, MeOD-d_4): δ_c 7.4, 8.3, 16.4, 91.4, 115.2, 115.4, 126.6, 127.2, 127.2, 127.5, 127.8, 128.7, 130.4, 131.3, 140.0, 141.4; **^{19}F NMR** (376.38 MHz, MeOD-d_4): δ_F -109.97; HR-MS: *Calcd* for

$[C_{36}H_{36}N_5O_2SF(Ir\text{-}Cl)]^+$ 814.2203 *m*/*z*, found: 814.2200 *m*/*z*. Elemental analysis: *Calcd* for $C_{36}H_{36}IrN_6O_4S$: C, 49.33%; H, 4.14%; N, 9.59%. Found: C, 49.14%; H, 4.06%; N, 9.49%.

[(η^5-Cp^{Xbiph})Ir(DsTolBig)Cl] (**37**). Complex **37** was synthesized following the method similar to complex **20**, where $[(\eta^5\text{-}Cp^{Xbiph})IrCl_2]_2$ (120 mg, 0.112 mmol), 5-(dimethylamino)-N-(N-(N-(o-tolyl)carbamimidoyl)carbamimidoyl)naphthalene-1-sulfonamide (100 mg, 0.236 mmol) and triethylamine (66 µL, 0.472 mmol) were added. The crude product was purified by chromatography column (DCM/MeOH (25:1, v/v)), giving a yellow solid. Yield = 91.2 mg (44%). **^{1}H NMR** (400 MHz, MeOD-d_4): δ_H 1.45 (s, 6H), 1.68 (s, 6H), 2.06 (s, 3H), 2.76 (s, 6H), 7.11 (s, 1H), 7.17-7.24 (m, 6H), 7.36-7.41 (m, 4H), 7.47-7.54 (m, 3H), 7.60 (d, *J* = 7.4 Hz, 2H), 8.06 (d, *J* = 6.8 Hz, 1H), 8.40 (d, *J* = 8.5 Hz, 1H), 8.56 (d, *J* = 8.6 Hz, 1H); **^{13}C NMR** (125.73 MHz, MeOD-d_4): δ_c 7.4, 8.2, 16.3, 44.3, 91.9, 114.7, 122.9, 126.6, 127.0, 127.1, 127.1, 127.2, 127.5, 128.7, 129.9, 130.3, 131.3, 140.0, 151.4; HR-MS: *Calcd* for $[C_{42}H_{44}N_6O_2S\ (Ir\text{-}Cl)]^+$ 889.2876 *m*/*z*, found: 889.2883 *m*/*z*. Elemental analysis: *Calcd* for $C_{42}H_{44}ClIrN_6O_2S$: C, 54.56%; H, 4.80%; N, 9.09%. Found: C, 54.23%; H, 4.77%; N, 8.75%.

6.2.3 Preparation of Samples and Antibiotic Standards

Antimicrobial screening against Gram-negative bacteria, fungi, and MRSA as well as the cytotoxicity determination against HEK-293 human kidney cells and blood cells was carried out by Community for Open Antimicrobial Drug Discovery (CO-ADD) of the University of Queensland, Australia.

Colistin and vancomycin were used as positive bacterial inhibitor standards for Gram-negative and Gram-positive bacteria, respectively. Fluconazole was used as a positive fungal inhibitor standard for *C. albicans* and *C. neoformans*. The antibiotics were provided in 4 concentrations, with 2 above and 2 below its MIC value, and plated into the first 8 wells of column 23 of the 384-well NBS plates. The quality control (QC) of the assays was determined by the

antimicrobial controls and the Z'-factor (using positive and negative controls). Each plate was deemed to fulfil the quality criteria (pass QC), if the Z'-factor was above 0.4, and the antimicrobial standards showed full range of activity, with full growth inhibition at their highest concentration, and no growth inhibition at their lowest concentration.

6.2.4 Antibacterial Assay

All bacteria were cultured in Cation-adjusted Mueller Hinton Broth (CAMHB) at 310 K overnight. A sample of each culture was then diluted 40-fold in fresh broth and incubated at 310 K for 1.5-3 h. The resultant mid-log phase cultures were diluted (CFU/mL measured by OD_{600}), then added to each well of the compound containing plates, giving a cell density of 5 × 10^5 CFU/mL and a total volume of 50 μL. All the plates were covered and incubated at 310 K for 18 h without shaking. Inhibition of bacterial growth was determined measuring absorbance at 600 nm (OD_{600}), using a Tecan M1000 Pro monochromator plate reader. The percentage of growth inhibition was calculated for each well, using the negative control (media only) and positive control (bacteria without inhibitors) on the same plate as references. The significance of the inhibition values was determined by modified Z-scores, calculated using the median and MAD of the samples (no controls) on the same plate. Samples with inhibition value above 80% and Z-Score above 2.5 for either replicate (n = 2 on different plates) were classed as actives. Samples with inhibition values between 50-80% and Z-Score above 2.5 for either replicate (n = 2 on different plates) were classed as partial actives.

6.2.5 Antifungal Assay

Fungi strains were cultured for 3 days on Yeast Extract-Peptone Dextrose (YPD) agar at 303 K. A yeast suspension of 1 × 10^6 to 5 × 10^6 CFU/mL (as determined by OD_{530}) was prepared from five colonies. The suspension was subsequently diluted and added to each well of the

compound-containing plates giving a final cell density of fungi suspension of 2.5×10^3 CFU/mL and a total volume of 50 µL. All plates were covered and incubated at 308 K for 24 h without shaking. Growth inhibition of *C. albicans* was determined by measuring absorbance at 530 nm (OD_{530}), while the growth inhibition of *C. neoformans* was determined measuring the difference in absorbance between 600 and 570 nm ($OD_{600-570}$), after the addition of resazurin (0.001% final concentration) and incubation at 308 K for additional 2 h. The absorbance was measured using a Biotek Synergy HTX plate reader. The percentage of growth inhibition was calculated for each well, using the negative control (media only) and positive control (fungi without inhibitors) on the same plate. The significance of the inhibition values was determined by modified Z-scores, calculated using the median and MAD of the samples (no controls) on the same plate. Samples with inhibition value above 80% and Z-Score above 2.5 for either replicate (n = 2 on different plates) were classed as actives. Samples with inhibition values between 50-80% and Z-Score above 2.5 for either replicate (n = 2 on different plates) were classed as partial actives.

6.2.6 Cytotoxicity Determination

Growth inhibitions of *HEK-293* and *RBC* cells were determined measuring fluorescence at ex: 530/10 nm and em: 590/10 nm (F560/590), after the addition of resazurin (25 µg/mL final concentration) and incubation at 310 K and 5% CO_2, for additional 3 h. The fluorescence was measured using a Tecan M1000 Pro monochromator plate reader. The percentage of growth inhibition was calculated for each well, using the negative control (media only) and positive control (cell culture without inhibitors) on the same plate.

CC_{50} values (concentration giving 50% cytotoxicity against *HEK-293*) were calculated by curve fitting the inhibition values vs. log (concentration) using a sigmoidal dose-response function, with variable values for bottom, top and slope. The curve fitting is implemented using

Pipeline Pilot's dose-response component (giving similar results to similar tools such as GraphPad's Prism and IDBS's XlFit). Any value with > indicates a sample with no activity (low DMax value) or samples with CC_{50} values above the maximum tested concentration (higher DMax value).

HC_{10} (concentration producing 10% haemolytic activity, human red blood cells) were calculated by curve fitting the inhibition values vs. log (concentration) using Sigmoidal dose-response function, with variable values for bottom, top and slope. The curve fitting is implemented using Pipeline Pilot's dose-response component (giving similar results to similar tools such as GraphPad's Prism and IDBS's XlFit). The curve fitting resulted in HC_{50} (50%) values, which are converted into HC_{10} by $HC_{10} = HC_{50}*(10/90)^{(1/Slope)}$; Any value with > indicates a sample with no activity (low DMax value) or samples with HC10 values above the maximum.

Cytopathic Effect. *HaCaT* keratinocyte cells were cultured in freshly prepared growth media (including 10 mL 10 × Minimal Essential Medium (MEM), 3 mL 7.5% sodium bicarbonate and 10 mL foetal bovine serum). 1×10^4 cells per well of *HaCaT* cells were incubated in 96-well plates with concentration range of 0-256 μg mL^{-1} for complexes **27**-**30**, **34**, **35** and **37** in 200 μL of growth medium at 310 K with 5% CO_2. The cytopathic effect was checked every hour under microscopy.

6.2.7 Antibacterial Assay for Gram-positive Bacteria

Antibacterial screening against Gram-positive bacteria was carried out under the supervision of Mr. John Moat; and anti-biofilm study in Section **6.2.11** was performed with the help of Dr. Freya Harrison in School of Life Sciences at Warwick.

The minimum inhibitory concentrations (MICs) against a variety of Gram-positive bacteria were determined by following the broth microdilution method in the CLSI guidelines.[26] The

bacterial strains were cultured in Cation-adjusted Mueller Hinton Broth (CAMHB) and was diluted to give the concentration of 5×10^5 CFU/mL. The Ir^{III} complexes in broth were serially diluted in the sterile 96-well plate to give the volume of 100 μL. The media solutions with bacteria were then dispensed to each well cell to make the final volume of 200 μL and the final concentration of Ir^{III} complexes ranged from 0.125-256 μg/mL; all the plates were covered and incubated at 310 K for 18 h without shaking. Inhibition of bacterial growth was determined measuring absorbance at 600 nm (OD_{600}), using a Tecan SPARK 10M plate reader. The negative control (media only) and positive control (bacteria without inhibitors) on the same plate were used as references to determine the growth inhibition of bacteria. Samples with inhibition value above 90% were classified as active agents. The minimum bactericidal concentrations (MBCs) were determined by treating the agar plate with 5 μL sample solutions from each well with no visible growth observed. The agar plates were placed in a 310 K oven for 18 h without shaking (*S. pyogenes* were incubated under a 5% CO_2 atmosphere at 310 K). The ones with no colony formed at minimum concentrations were taken as MBCs.

6.2.8 Generation of Resistance

The standard bacterial strain *S. aureus* (ATCC 29213) was cultured in HB medium (1 mL) in the presence of 0.25 μg/mL (1/4 of MICs) of complexes **27**, **28** and **30**, and overnight incubation at 310 K was considered as the first passage. At the second day, 40 μL of bacterial medium was added to the prepared complex stockings (1 mL), and such a treatment was repeated for 24 times (count as 24 passages). The antibacterial activity of complexes **27**, **28** and **30** against the treated *S. aureus* was determined by culturing the microbe on agar plate containing Ir^{III} complexes **27**, **28** and **30** (at MIC concentrations) every 4 days.

6.2.9 Kinetics of Growth Inhibition

Bacterial strain *S. aureus* (Bacterial strain: ATCC 29213) was cultured in CAMHB overnight at 310 K. Three bacterial suspensions of 1×10^5, 1×10^7 and 1×10^8 CFU/mL were prepared by culture dilution. Complex in broth was diluted to give the concentration 0.125× MIC to 8× MIC. The negative control (media only) and positive control (culture bacteria with DMSO (1%-10%)) were used as comparisons. The measurement of absorbance at OD_{600} was determined on a Tecan SPARK 10 M plate reader with shaking for 18 h at 310 K, the absorbance was detected every 5 min for the first one hour and every 30 min for the rest of 17 h. No growth was observed for the negative control.

6.2.10 Relative Hydrophobicity

Relative hydrophobicity measurements were performed utilizing an Agilent 1200 HPLC system with a VWD and 50 µL loop. The column used was an Agilent Zorbax 300SB C18, 150 × 4.6 mm with a 5 µm pore size. The mobile phase was H_2O (50mM NaCl)/H_2O/CH_3CN 1:1 (50 mM NaCl), with a flow of 1 mL min^{-1}. The detection wavelength was set at 254 nm with the reference wavelength at 360 nm. All compounds were dissolved in 10% MeOH/90% H_2O (v/v) in 50 mM NaCl to ensure that hydrolysis was prevented. Sample injections were the loop volume (50 µL) with needle washes of H_2O and MeOH between injections. Reported retention times (tR) and standard deviations (SD) are from duplicates of triplicate measurements. The gradient used is shown in **Figure 6.3**.

Time (min)	% B
0	20
15	100
40	100
41	20
55	20

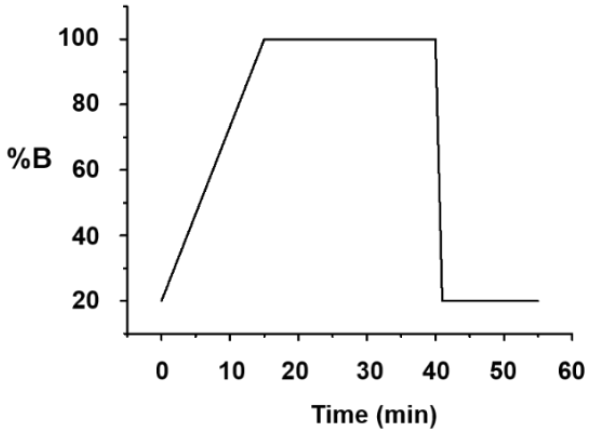

Figure 6.3 Relative hydrophobicity measurements on HPLC using H_2O 50 mM NaCl (Solvent A) and H_2O/CH_3CN 1:1 50 mM NaCl (solvent B).

6.2.11 Biofilm Cultivation and Antibiotic Treatment

Biofilm was prepared according to a reported literature with modifications.[27] Generally, bacterial strain: *S. aureus* (ATCC 29213) were cultured in synthetic wound fluid (SWF, consisting of 50% fetal bovine serum and 50% autoclaved peptone water, v/v) at 310 K on an orbital shaker. To a sterile falcon tube, polymerized rat tail collagen matrix was prepared and kept on ice bath, containing (for example 10 mL collagen matrix) 2 mL collagen stock solution (10 mg/mL), 6 mL SWF solution, 1 mL acetic acid (0.1%, v/v) and 1 mL NaOH solution (0.1 M in deionized water). After mixing, 400 μL of the collagen solution was added to separate well of 24-wells polystyrene microtiter plate without introducing bubbles and placed at 310 K for 1 h. Then 100 μL of diluted bacteria culture (OD_{600} at approximately 0.1 in SWF) was added to each collagen matrix, at least on well was left empty as negative control and collagen matrix with SWF as positive control (check for contamination). The plate was incubated at 310 K without shaking for 24 h.

On the second day, 200 μL of the tested complexes (complexes **27-32**, in DMSO/H_2O, 5:95(v/v)) was added to the collagen matrix and placed at 310 K for further 24 h. Then 600 μL

of collagenase (0.5 mg/mL in PBS) was added to each wound, and incubated at 310 K for 1 h. Serial dilution of each wound was made in PBS using a sterile 96-well plate, and 10 μL of each dilution were dropped onto a LB agar plate for triplicate. The potency against biofilm of each complex was calculated based on the bacteria colonies on the LB plate. The Welch's *t*-tests were carried out to determine the variations of the data.

6.2.12 Live/Dead Cell Assessment by PI Staining

1×10^8 CFU/mL of *S. aureus* cells were seeded in 50-mL Falcon tubes and exposed to two concentrations of complex **30** (equipotent MIC and 2 MIC) for 2 h without shaking. *S. aureus* cells without any antibiotics were used as negative comparison. After the indicated incubation time, cell suspensions were collected by centrifugation at 8000 rpm for 10 min and washed with PBS (0.01 M) 3 times. The cell pellets were then re-suspended in water in 2 mL Eppendorf tubes and treated with 3 μM PI for 30 min in the dark at room temperature. Excessive PI was removed by washing cells with PBS 3 times, and 20 μL of samples were placed on a glass slide with a glass coverslip. The fluorescence of each glass slide was detected on a confocal microscope (LSM 880, AxioObserver) at excitation and emission wavelengths of 514/642 nm.

6.2.13 Transmission Electron Microscopy

5×10^8 CFU/mL of *S, aureus* cells were cultured in 50-mL Falcon tubes and exposed to two concentrations of complex **30** (10 MBC and 50 MBC) at 310 K for 2 h without shaking. After incubation, the cell suspensions were harvested by centrifugation at 8000 rpm for 3 min and washed with PBS (0.01 M) 2 times at 277 K. The cells were fixed by 2.5% glutaraldehyde in PBS at 277 K for 1 h, washed with PBS (2 times)/water (1 time) and centrifuged. Then the bacterial pellet was re-suspended in 10% ethanol, and dehydrated with 20%-100% ethanol with 20 min of each. Cells were left in 100% fresh ethanol for over 24 h. Then the cell pellets were

left in propylene oxide for 2 h, propylene/LV resin (1:1, v/v) for 5 h and 100% LV resin overnight. After which, cells were polymerised at 338 K for 24 h and cut on Ultracut E Microtome to 100 nm and stained with 4% uranyl acetate. Finally, TEM monitoring was carried out on a JEOL 2011 LaB6 instrument with Gatan Ultrascan 1000 camera.

6.3 Results and Discussion

6.3.1 Synthesis and Characterization

Generally, Ru^{II}, Os^{II} or Ir^{III} dimers and biguanide ligands were dissolved in anhydrous methanol, to which trimethylamine was added, and the solution was allowed to heated at 318 K under nitrogen for 18 h.[28] Dark red solid was obtained after removal of solvent on a rotary evaporator, which was further purified by recrystallization (MeOH and diethyl ether) or by column chromatography (MeOH and DCM). Particularly, complexes **31** (Ir-Br) and **32** (Ir-I) were synthesized by adding a 100-fold excess of sodium bromide and potassium iodide for the halogen exchange (**Scheme 6.1**).

Crystals of complexes **22** [(η^6-*p*-cym)Os(Metf)Cl]Cl, **23** [(η^6-biph)Os(Metf)Cl]Cl, **24** [(η^5-Cp*)Ir(Metf)Cl]Cl and **27** [(η^5-Cp^{Xbiph})Ir(Metf)]Cl suitable for x-ray diffraction were obtained by slow diffusion of diethyl ether into the saturated complex methanol solution at ambient temperature (**Figure 6.4**). The crystallographic data and selected bond lengths and angles are given in **Table 6.1** and **Table 6.2**. The +1 charged complexes **22**, **23** and **24** adopt *pseudo*-octahedral structures with metal bound to the arene, neutral metformin and chloride to form a typical 'piano-stool' geometry, and chloride as counter anion to make the complex an 18 e species. Ir in complex **27** is coordinated to η^5-Cp^{Xbiph} ring and deprotonated *N*,*N*-bound phenylbiguanide forming a non-typical 16 e^- species, with a chloride counter anion. The

asymmetric unit of complex **27** contains two crystallographically independent but chemically identical complexes, two chloride counter ions and a small amount of electron density modelled as a partially occupied methanol (40% occupancy). The M-N2 (M: Os or Ir) lengths of complexes **22**, **23** and **24** are around 2.07-2.08 Å, slightly longer than for complex **27** (1.97(3) Å). The N-M-N angles for complexes **22**, **23** and **24** (range 82.33°-83.21°) are smaller than that of complex **27** (85.25°). The compositions of complexes **22**, **23**, **24** and **27** suggest that these novel complexes can be fine-tuned by the chelated ligands to be 16-e or 18-e species.

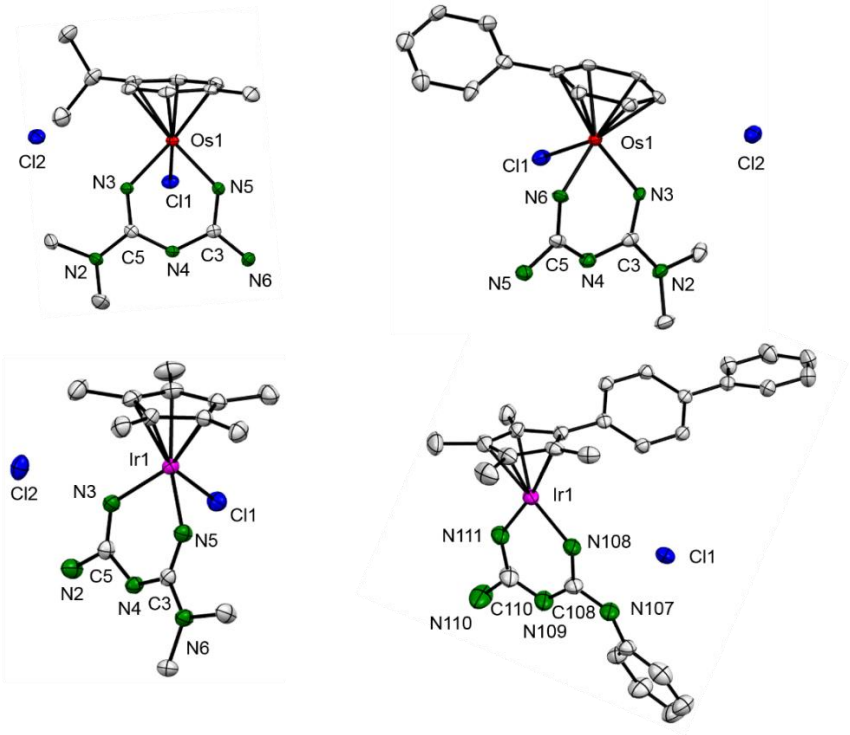

Figure 6.4 Structures of complexes **22**, **23**, **24** and **27**, and with atom labelling. Thermal ellipsoids are drawn at 50% probability level. All hydrogen atoms and solvent molecule have been omitted for clarity.

Table 6.1 Selected Bond Length (Å) and Angles (˚) for Complexes **22**, **23**, **24** and **27**.

Bonds	Bond Length (Å)/Angle (°)			
	22	**23**	**25**	**27**
M–N^a	2.076(3)	2.080(4)	2.087(2)	1.975(3)
M–N^b	2.075(3)	2.070(4)	2.074(2)	1.973(3)
M–arene (centroid)	1.663	1.647	1.777	1.775
C^a–N^a	1.299(4)	1.299(7)	1.301(4)	1.334 (5)
C^a–N^c	1.376(4)	1.378(7)	1.369(3)	1.331(5)
C^b–N^b	1.293(4)	1.298(7)	1.287(4)	1.348(4)
C^b–N^c	1.377(4)	1.374(7)	1.390(4)	1.321(5)
N^a–M–N^b	82.33(11)	83.09(17)	81.97(9)	85.38(13)
C^1–N^c–C^2	127.0(3)	125.5(4)	124.3(2)	122.2(3)

N^a corresponds to N3, N3, N5, N111; N^b: N5, N6, N3, N108. N^c: N4, N4, N4, N109

C^a corresponds to C5, C3, C3, C110; C^b: C3, C5, C5, C108

Table 6.2 Crystallographic Data for Complexes **22**, **23**, **24** and **27**.

	22	**23**	**24**	**27**
Formula	$C_{15}H_{29}Cl_2N_5OOs$	$C_{17}H_{25}Cl_2N_5OOs$	$C_{14}H_{26}Cl_2IrN_5$	$C_{29}H_{32}ClIrN_5$
FW	556.53	576.52	527.50	683.64
Temp (K)	150(2)	150(2)	150(2)	150(2)
Crystal system	monoclinic	monoclinic	monoclinic	triclinic
Space group	$P2_{1/c}$	$P2_{1/n}$	$P2_{1/c}$	P-1
a (Å)	10.22801(15)	7.22327(18)	13.09904(18)	9.80400(17)
b (Å)	11.96146(14)	31.0708(6)	7.96973(11)	15.8991(2)
c (Å)	16.9490(3)	9.2514(2)	17.6195(2)	18.4457(3)
α (º)	90	90	90	82.7271(13)
β (º)	106.7580(16)	109.557(3)	92.2718(14)	86.7456(14)
γ (º)	90	90	90	72.2390(14)
Volume ($Å^3$)	1985.51(5)	1956.54(8)	1837.95(4)	2715.64(8)
Z	4	4	4	4
Dcalc(mg/cm^3)	1.862	1.957	1.906	1.672
$\mu(mm^{-1})$	6.704	14.964	7.559	5.043
F(000)	1088.0	1120.0	1024.0	1350.0
Crystal size (mm^3)	0.24 × 0.18 × 0.08 yellow/olive block	0.2 × 0.08 × 0.01 yellow block	0.35 × 0.35 × 0.08 orange block	0.5 × 0.13 × 0.038 brown block
Reflections measured	31218	7696	29267	83915
Indep reflection	6647	4051	6136	18356
R1 [I>2σ(I)]	0.0238	0.0426	0.0258	0.0330
wR2 (all data)	0.0810	0.1208	0.0903	0.0751

6.3.2 Relative Hydrophobicity

The relative hydrophobicities of complexes **24-37** were determined by RP-HPLC using a reverse-phase C_{18} column. To ensure solubility of the Ir^{III} complexes, MeOH/H_2O, 1:9 v/v was used with NaCl (50 mM) present to suppress the hydrolysis. The HPLC eluents were also prepared with 50 mM NaCl (The measurements were listed in **Figure 6.2**). The resulting retention times are shown in **Table 6.5**. Complex **24** [(η^5-Cp*)Ir(Metf)Cl]Cl shows the shortest retention time (least hydrophobic) at 13.0 min. It is evident that complexes with more phenyl groups on the η^5-Cp^X (complexes **25-26**), have higher retention times, indicating higher hydrophobicity. Complexes **27-32** with more hydrophobic functional phenyls on the chelating biguanide ligands have retention times range within 20.9-25.3 min, and the introduction of sulfonyl groups with aromatic substituents on the chelated biguanide ligands significantly enhances the hydrophobicity with retention time various of 32-37 min with the exception of complex **33** (toluene sulfonyl, 21.44 min) which was much less hydrophobic.

6.3.3 Antimicrobial Activity

The minimum inhibitory concentrations (MIC) of complexes **20-37** were determined against Gram-negative bacterial strains: FDA-controlled *Escherichia coli*, multi-drug resistant *Klebsiella pneumoniae*, *Pseudomonas aeruginosa*, *Acinetobacter baumannii*, and Gram-positive bacteria strains: *Bacillus subtilis*, *Streptococcus pyogenes*, *Enterococcus faecalis*, *Staphylococcus epidermidis* and *Staphylococcus aureus* (including methicillin resistant strain type MRSA). Antifungal activity against *Candida albicans* and *Cryptococcus neoformans* was also studied.

First, the antimicrobial activity of the biguanide chelating ligands alone was determined against Gram-positive, Gram-negative bacteria and fungii. None of these ligands showed any antimicrobial activity or cytotoxicity, with MICs > 32 μg/mL, **Table 6.3**.

Table 6.3 Antimicrobial Activity and Cytotoxicity Determination of Biguanide Ligands Screened by CO-ADD (μg/mL).

Ligand	MRSA	*E. c*	*K. p*	*A. b*	*C. a*	*C. n*	*HEK-293*	RBC
Met	>32	>32	>32	>32	>32	>32	>32	>32
PB	>32	>32	>32	>32	>32	>32	>32	>32
4-F-PB	>32	>32	>32	>32	>32	>32	>32	>32
Phen	>32	>32	>32	>32	>32	>32	>32	>32
TolB	>32	>32	>32	>32	>32	>32	>32	>32
TsTolB	>32	>32	>32	>32	>32	>32	>32	>32
DsTolB	>32	>32	>32	>32	>32	>32	>32	>32

Initially, the antibacterial activity against *S. aureus* and *B. subtilis* of metformin Ru^{II} and Os^{II} complexes **20**-**23** was determined in comparison with metformin Ir^{III} complexes **24**-**26**. Complexes **20**-**23** are probably more hydrophilic and have shown low antimicrobial activity with MIC values > 128 μg/mL. By contrast, complex **24** with the lowest hydrophobicity gives a similar MIC value, however, antibacterial activity of complexes **24-26** increased with increase in hydrophobicity (longer HPLC retention times, **Table 6.4**), probably due to the increased uptake of the complexes within the membranes of the bacteria.[29] This trend is also apparent from the antibacterial activity of complexes **24-27** against MRSA (**Figure 6.5**).

Table 6.4 Antibacterial Activity of Metformin Complexes **20-26** against *S. aureus* and *B. subtilis* (μg/mL, in brackets μM)[a].

Complex	M	Arene/Cp*	*S. a*	*B. s*
20	Ru	*p*-cymene	>128 (>294)	>128 (>294)
21	Ru	biphenyl	128 (281)	128 (281)
22	Os	*p*-cymene	>128 (244)	>128 (244)
23	Os	biphenyl	128 (235)	64 (117)
24	Ir	Cp*	>128 (>243)	>128 (>243)
25	Ir	Cp^{XPh}	64 (109)	64 (109)
26	Ir	Cp^{Xbiph}	8 (12)	4 (6)

[a] Bacterial strains: *S. aureus* R 34, *B. subtilis* DSM 10.

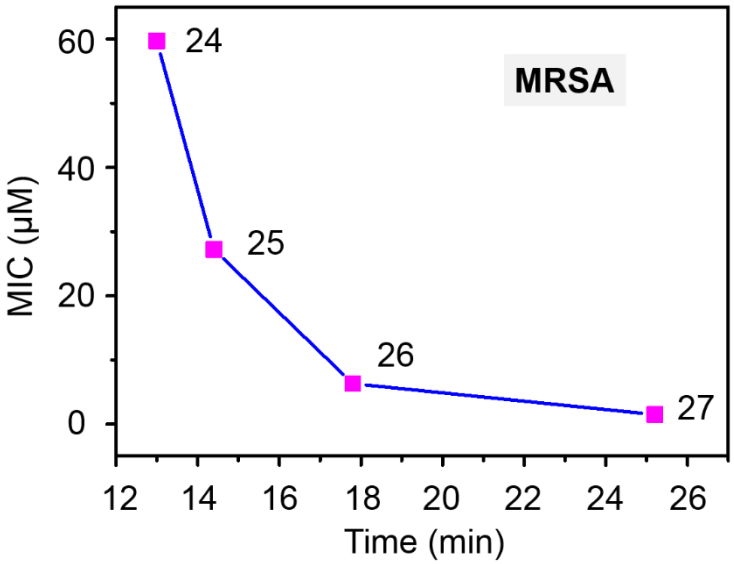

Figure 6.5 Correlation of MIC (μM) values for complexes **24-27** against MRSA with HPLC retention times (hydrophobicity).

Next antimicrobial activity of complexes **24-37** against a broader spectrum of nosocomial pathogens was screened by CO-ADD.

Complexes **27-30** exhibit the highest potency (MICs, 4 μg/mL (5.4-5.8 μM)) against *A. baumannii*, an important nosocomial Gram-negative non-motile aerobic bacterial pathogen;[30] and show potent activity (MICs 4-8 μg/mL (5.4-11.2 μM)) towards *E. coli* (FDA controlled). However, all Ir^{III} biguanide complexes had little activity towards *P. aeruginosa*, probably due to the poor membrane permeability, only about 8% of that of *E. coli*; also, *P. aeruginosa* has very effective efflux system, which has made this type of strain intrinsically antibiotic resistant.[31] Complexes **27-30** have moderate potency of (MICs 16-32 μg/mL (21.6-44 μM)) towards *K. pneumoniae*, a Gram-negative nosocomial bacterium that is known to cause a range of infections, *e. g.* urinary tract, pneumoniae, and intra-abdominal infections.[32]

In order to study the effect of the halide ligand on the antimicrobial activity, the Cl in complex **30** was substituted by Br and I to obtain complexes **31** [(η^5-Cp^{Xbiph})Ir(TolBig)Br]Br and **32** [(η^5-Cp^{Xbiph})Ir(TolBig)I]I, respectively. To increase the hydrophobicity and potentially enhance uptake of the complexes, a sulfonyl group with an aromatic substituent was introduced onto the terminal nitrogen of the 1-(*o*-tolyl)biguanide ligand, complexes **33-37** (**Scheme 6.1**). Interestingly, complexes bromido **31** and iodido **32** showed higher antibacterial activity against *K. pneumoniae* compared to chloride complex **30**, but were less potent towards *E. coli* and *A. baumannii*. By introducing the sulfonyl substituents, the potency of complexes **33-37** decreased dramatically, with MICs all above 32 μg/mL. This suggests that the terminal NH_2 on biguanide ligands may play an important role in activity (**Table 6.5**).

The antifungal activity of complexes **24-37** was screened towards, *C. albicans*, a very common fungus in humans which can cause superficial mycoses, invasive mucosal infections, and disseminated systemic disease,[33] and *C. neoformans*, an opportunistic yeast that can cause meningitis).[34] The clinical antifungal agent Fluconazole was used as a reference compound

(**Table 6.5**). Interestingly, complexes **27-32** exhibited excellent antifungal activity against these fungii (MICs = 0.25-1 μg/mL (0.34-1.45 μM)), *ca.* 76-fold more active than Fluconazole (8 μg/mL (26.1 μM)). The monodentate halido ligand had little effect on the antifungal activity. The introduction of sulfonyl functional groups lowered the activity slightly (MICs of complexes **33-37** of 1-2 μg/mL (1.1-2.4 μM)).

Complexes **27-37** showed higher antibacterial activity against Gram-positive bacteria MRSA, compared to Gram-negative bacteria, with MICs of 1 μg/mL (1.1-1.4 μM), as good as the benchmark compound Vancomycin, a broad-spectrum clinical drug against Gram-positive pathogens.

Table 6.5 Antimicrobial Activity of Ir^{III} Complexes **24-37** (MICs, μg/mL (μM))[a], compared with colistin, vancomycin and fluconazole.

Complex	MRSA[b]	*E. c*	*K. p*	*P. a*	*A. b*	*C. a*	*C. n*	R-T (min)[d]
24	32 (59.7)	>32 (>59.7)	>32 (>59.7)	>32 (>59.7)	>32 (>59.7)	>32 (>59.7)	>32 (>59.7)	13.0±1.4
25	16 (27.2)	>32 (>54.3)	>32 (>54.3)	>32 (>54.3)	>32 (>54.3)	>32 (>54.3)	>32 (>54.3)	14.4±0.6
26	4 (6.3)	16 (25)	>32 (>50)	>32 (>50)	32 (>50)	4 (6.3)	4 (6.3)	17.8±0.3
27	1 (1.5)	4 (5.8)	32 (46.6)	32 (46.6)	4 (5.8)	1 (1.5)	0.25 (0.36)	25.2±1.1
28	1 (1.4)	8 (11.2)	>32 (>44.8)	>32 (>44.8)	4 (5.6)	1 (1.4)	0.25 (0.35)	23.4±0.3
29	1 (1.3)	4 (5.4)	16 (21.6)	32 (43.2)	4 (5.4)	1 (1.3)	0.25 (0.34)	22.6±0.3
30	1 (1.4)	4 (5.5)	32 (44)	>32 (>44)	4 (5.5)	1 (1.4)	0.5 (0.7)	22.5±0.3
31	1 (1.2)	8 (9.3)	8 (9.3)	>32 (>37.2)	4 (4.7)	1 (1.2)	0.5 (0.6)	20.93±0.02
32	1 (1.1)	8 (8.8)	16 (17.6)	>32 (>35)	16 (17.6)	1 (1.1)	0.5 (0.55)	20.95±0.02
33	1 (1.2)	>32 (>38)	>32 (>38)	>32 (>38)	>32 (>38)	2 (2.4)	1 (1.2)	21.44±0.07
34	1 (1.1)	>32 (>35)	>32 (>35)	>32 (>35)	>32 (>35)	2 (2.2)	2 (2.2)	32.2±0.1
35	1 (1.2)	>32 (>38)	>32 (>38)	>32 (>38)	>32 (>38)	2 (2.4)	2 (2.4)	36.93±0.08
36	1 (1.2)	>32 (>38)	>32 (>38)	>32 (>38)	>32 (>38)	2 (2.4)	1 (1.2)	34.89±0.02
37	1 (1.1)	>32 (>35)	>32 (>35)	>32 (>35)	>32 (>35)	2 (2.2)	1 (1.1)	32.42±0.01
Colis.[c]	>32 (>27.7)	0.125 (0.11)	0.125 (0.11)	0.25 (0.22)	0.25 (0.22)	>32 (>27.7)	32 (27.7)	n. d.
Vanc.	1 (0.7)	>32 (>22)	>32 (>22)	>32 (>22)	>32 (>22)	>32 (>22)	>32 (>22)	n. d.
Flucon.	>32 (>104)	>32 (>104)	>32 (>104)	>32 (>104)	>32 (>104)	0.125 (0.41)	8 (26)	n. d.

[a]MIC: the minimal concentration at which no visible bacterial growth is found (μg/mL). [b]Bacterial strains: MRSA: Methicillin-resistant *S. aureus*, ATCC 43300; *E. c*: *E. coli* (FDA control), ATCC 25922; *K. p*: MDR *K. pneumoniae*, ATCC 700603; *P. a*: *P. aeruginosa*, ATCC 27853; *A. b*: *A. baumannii*, ATCC 19606. Fungus strains: *C. a*: *C. albicans*, ATCC 90028; *C. n*: *C. neoformans*, ATCC 208821. [c]Model antibiotics: Colistin (Colis.) and Vancomycin (Vanc.) as antibacterial agents; Fluconazole (Flucon.) as antifungal agent; [d]R-T: retention time on RP-HPLC.

The minimum bactericidal concentrations (MBCs) of complexes **27-37** were also determined. Generally, as can be seen from **Table 6.6**, complexes **27-37** show higher antibacterial activity against Gram-positive bacteria strains when compared to the benchmark compound Vancomycin, with MICs within the range 0.125-32 μg/mL (0.17-38 μM). In particular, complexes **27-37** exhibit excellent inhibitory and bactericidal activity towards *S. pyogenes* and *S. epidermidis*. *S. pyogenes* is a pathogenic strain also known as Group A Streptococcus (GAS), among the top 10 pathogens, and responsible for ca. 517000 deaths annually.[35] *S. pyogenes* can cause invasive diseases, *e. g.* necrotizing fasciitis, rheumatic fever and rheumatic heart disease.[36] *S. epidermidis* is an opportunistic microorganism which exists in human skin and mucosa.[37] Nosocomial genotypes of *S. epidermidis* are the main cause of catheter-related bloodstream infections and frequently cause joint and biomedical device-related infections.[38]

Complexes **27-32** show potent antibacterial activity against *E. faecalis* (MICs, 0.5-1 μg/mL (0.58-1.45 μM)), about 4× more potent than vancomycin (2.8 μM). The MBCs of complexes **27-32** range from 4-32 μg/mL (5.5-43 μM), are also lower than that of Vancomycin (> 64 μg/mL (> 44 μM)). *E. faecalis* is part of the intestinal flora, causes about 90% of enterococcal infections by inhibiting alimentary canals of man which can induce lethal diseases, *E. faecalis* can survive in nosocomial (hospital infection) environments due to intrinsic resistance to several antibiotics.[39]

Complexes **33-37** exhibited significant inhibitory activity against *S. aureus*, *B. subtilis*, *S. pyogenes* and *S. epidermidis*, with MICs all below 1 μg/mL (0.3-1.2 μM). However, bactericidal activity against these pathogens decreased dramatically, with MBCs against *S. aureus* and *S. epidermidis* of >32 μg/mL (>38 μM). Hence it is again apparent that introduction of sulfonyl functional groups which block the NH_2 of the biguanide ligand diminishes the antibacterial activity against Gram-positive bacteria as well as Gram-negative bacteria and fungii, suggesting an important role of this NH_2 in target recognition.

Table 6.6 Antibacterial Activity (MIC/MBC[a]), Cytotoxicity and Haemolytic Activity of Complexes **27-37** (μg/mL (μM)).

Complex	*S. a*	*B. s*	*S. p*	*S. e*	*E. f*	*HEK-293*	*RBC*	*HaCaT*
	Gram-positive bacteria[b]					Mammalian[c]		
27	2/2 (2.9)	0.5/0.5 (0.7)	0.25/1 (0.4/2.9)	0.25/0.5 (0.4/0.7)	1/8 (2.9/11.7)	>32 (>47)	1.40 (2.0)	64 (94)
28	2/2 (2.8)	0.5/0.5 (0.7)	0.25/0.25 (0.4)	0.5/0.5 (0.7)	1/8 (1.4/11.2)	>32 (>45)	1.26 (1.8)	128 (179)
29	2/2 (2.7)	1/2 (1.3/2.7)	0.125/0.5 (0.17/0.7)	0.25/0.25 (0.3)	1/32 (1.3/43.1)	17.2 (23.2)	0.89 (1.2)	128 (173)
30	1/2 (1.4/2.8)	0.25/0.5 (0.3/0.7)	0.125/0.125 (0.17)	0.5/0.5 (0.7)	1/4 (1.4/5.6)	>32 (>44)	2.40 (3.3)	128 (176)
31	0.5/1 (0.6/1.2)	0.5/1 (0.6/1.2)	0.25/0.25 (0.3)	0.5/1 (0.6/1.2)	0.5/32 (0.6/37)	23.72 (27.6)	1.03 (1.2)	n. d.
32	0.5/4 (0.5/4.4)	0.25/1 (0.3/1.1)	0.25/0.25 (0.3)	0.5/0.5 (0.5)	1/16 (1.1/17.6)	16.99 (18.6)	1.29 (1.4)	n. d.
33	0.5/>32 (0.6/>38)	0.5/16 (0.6/19)	0.25/0.25 (0.3)	0.25/>32 (0.3/>38)	>32/>32 (>38)	>32 (>38)	14.6 (17)	n. d.
34	0.5/>32 (0.5/>35)	0.5/16 (0.5/17)	1/2 (1.1/2.2)	0.5/>32 (0.5/>35)	>32/>32 (>35)	>32 (>35)	>32 (>35)	128 (139)
35	0.5/>32 (0.6/>38)	1/32 (1.2/38)	1/8 (1.2/9.4)	0.25/>32 (0.3/>38)	>32/>32 (>38)	>32 (>38)	>32 (>38)	128 (151)
36	0.5/>32 (0.6/>38)	0.5/16 (0.6/19)	0.5/8 (0.6/9.5)	0.25/>32 (0.3/>38)	>32/>32 (>38)	>32 (>38)	8.53 (10.1)	n. d.
37	0.5/>32 (0.5>35)	0.5/32 (0.5/35)	1/4 (1.1/4.4)	0.25/>32 (0.3/>35)	>32/>32 (>35)	>32 (>35)	>32 (>35)	32 (35)
Vanc.	2/>64 (1.4/>44)	0.25/0.25 (0.2)	1/1 (0.7)	4/4 (2.8)	4/>64 (2.8/>44)	n. d.	n. d.	n. d.

[a]MBC: the minimum bactericidal concentration (μg/mL). [b]Bacterial strains: *S. a*: *S. aureus*, ATCC 29213; *B. s*: *B. subtilis*, DSM 10; *S. p*: *S. pyogenes*, ATCC 151112; *S. e*: *S. epidermidis*, ATCC 12228; *E. f*: *E. faecalis*, ATCC 29212. [c]Mammalian cells: *HEK-293* human embryonic kidney cells ATCC CRL-1573, *RBC* human red blood cells, *HaCaT* human keratinocytes.

Superoxide dismutase (SOD) is an important enzyme in mammalian cells and microorganisms which quenches high levels of superoxide.[40] Next, the minimum inhibitory concentrations of complexes **27-33** under anaerobic conditions were determined against bacterial strains: *S.*

aureus (ATCC 29213, SOD sufficient) and *S. pyogenes* (ATCC 151112, SOD deficient). The anaerobic atmosphere was generated with Oxoid AnaeroGen 2.5L Sachets (from Thermo Scientific) in a plastic container. As can be seen from **Table 6.7**, no significant change of MICs of complexes **27-33** was discerned against those organisms when compared to MICs under aerobic conditions, which indicates that these complexes are less likely to induce ROS in bacteria, and may have a new mechanism of action.

Table 6.7 Antibacterial Activity (MICs, μg/mL) of Complexes **27-33** against *S. aureus* and *S. pyogenes* under Anaerobic Conditions.

Complex	MIC (μg/mL)	
	S. aureus	*S. pyogenes*
27	2	0.5
28	2	0.5
29	2	0.5
30	2	0.5
31	2	1
32	2	1
33	2	1

6.3.4 Cytotoxicity (CC_{50}), Haemolytic Activity (HC_{10}) and Cytopathic Effects

To investigate the selectivity of the complexes for microorganisms versus mammalian cells, the concentrations giving 50% cytotoxicity towards human embryonic kidney cells (*HEK-293*) and 10% haemolytic activity towards human red blood cells for active Ir^{III} complexes **27-37** were determined (**Table 6.6**). As shown in **Table 6.6**, Ir^{III} complexes with high potency against Gram-positive bacteria, exhibited high CC_{50} values (>32 μg/mL, except complexes **29**, **31** and **32**), indicating a high tolerance towards human mammalian cells.

Complexes **27-32** show high haemolytic activity, with HC_{10} values within the range of 0.89-2.40 μg/mL (1.2-3.3 μM). However, complexes **33-35** and **37** have relatively high HC_{50} values (*i.e.* a low level of haemolysis of human red blood cells), and *ca.* 20× higher than the respective antibacterial MIC values.

Subtle changes on the organometallic complex structures often have a significant effect on the biological properties.[41] Complexes **31** and **32**, with monodentate Br and I, respectively, as halido ligand show higher cytotoxicity towards *HEK-293* cells, decreasing in the order: **30** > **31** > **32**, and haemolytic activity in blood cells. This is probably because complexes **31** and **32** are more inert and less likely to hydrolysis in aqua media, and may have different targets.[42]

The cytopathic effect of a representative set of Ir complexes **27-30**, **34**, **35** and **37** on *HaCaT* keratinocyte cells (a immortalized, non-tumorigenic cell line) was also determined.[43] A 4 h-exposure of keratinocyte cells to these selected antimicrobial agents induced morphological changes in keratinocytes cells at concentrations of 128 μg/mL (139-179 μM) for **28-30** and **34-35**, and of 64 μg/mL (94 μM) and 32 μg/mL (35 μM) for complexes **27** and **37**, respectively. These concentrations are *ca.* 64× higher than the corresponding MIC values against Gram-positive bacteria, suggesting sensitivity of human keratinocyte to these Ir^{III} complexes against human keratinocyte cells and excellent selectivity between pathogens and human mammalian cells.

6.3.5 Long-term Antibacterial Activity

The stability of complexes **27-33** by using *S. aureus* as model bacterium was investigated by determining their MICs after various time intervals (1-21 days). The complexes were dissolved in Cation-adjusted Mueller Hinton Broth at the concentration of 128 μg/mL and stored at three different temperatures: 255 K, 291 K and 315 K. Antibacterial testing was performed on days 1, 4, 8 and 21 (**Table 6.8**). Little change in MICs of complexes **27-30** was observed after 21

days at 315 K (in the range of 2-4 μg/mL), indicative of high stability. However, MICs of complexes **31-33** increased gradually from day 8 to day 21 at 315 K, with MICs rising from 1 μg/mL to 16, 8 and 32 μg/mL, respectively, indicative of some degradation of these complexes at this temperature (315 K).

Table 6.8 Stability Testing of Active Complexes **27-33** as Indicated by MICs (μg/mL).

Complex	Day 1			Day 4			Day 8	Day 21
	255 K	291 K	315 K	255 K	291 K	315 K	315 K	315 K
27	2	2	2	2	1	2	2	4
28	2	2	2	2	1	4	1	4
29	2	2	2	2	1	4	8	4
30	2	2	1	2	2	2	2	4
31	4	2	1	1	4	2	4	16
32	2	2	1	2	1	1	2	8
33	2	1	1	2	2	4	8	32

6.3.6 Resistance Generation

To investigate the rate of generation of bacterial resistance towards these novel Ir^{III} biguanide complexes, the mutation rate of standard strain *S. aureus* exposed to complexes **27** [(η^5-Cp^{Xbiph})Ir(PhBig)]Cl, **28** [(η^5-Cp^{Xbiph})Ir(4-F-PhBig)]Cl and **30** [(η^5-Cp^{Xbiph})Ir(TolBig)Cl]Cl at concentrations of 0.25× MIC, for sustained passages was determined. MICs were determined after every 4 passages. After a total of 24 passages, MIC values for complexes **27**, **28** and **30** against *S. aureus* remained unchanged, suggesting that Gram-positive bacteria are unlikely to become resistant to these Ir^{III} biguanide complexes.

6.3.7 Kinetics of Growth Inhibition

The kinetics of growth inhibition by complex **30** [(η^5-Cp^{Xbiph})Ir(TolBig)Cl]Cl was studied in three different *S. aureus* cultures of density 10^5, 10^7 and 10^8 CFU/mL (**Figure 6.6a-c**), and the effect of DMSO concentration (1%, 5% and 10% DMSO in medium, v/v) in the broth medium on the cell growth (at bacterial intensity of 10^5 CFU/mL, **Figure 6.6d**). It is evident that high DMSO concentrations can greatly inhibit the bacterial growth (slower growth in 10% DMSO/90% medium). Concentrations of complex **30** in three ranges in bacterial culture medium were studied: 0.125 MIC to 2 MIC (cell density of 1×10^5 CFU/mL), 0.25× MIC to 4× MIC (1×10^7 CFU/mL) and 0.5× MIC to 8× MIC (1×10^8 CFU/mL). As can be seen in the **Figure 6.6**, bacterial growth was well inhibited at MIC concentration when the cell culture density was 1×10^5 CFU/mL; at higher cell culture densities (1×10^7 and 1×10^8 CFU/mL), the total bacterial growth inhibition concentration of complex **30** increased to 2× MIC, but the complex inhibited the growth of *S. aureus* for *ca.* 500 min at MIC concentration when the cell culture density was 1×10^7 CFU/mL. Complex **30** exhibits a density-dependent antibacterial activity against *S. aureus*, consistent with MIC values. The growth of *S. aureus* was effectively hindered at sub-MIC and MIC concentrations of complex **30** at different culture cell densities, which indicates that these Ir^{III} complexes may be sequestered inside bacteria and exhibit a constant bactericidal activity towards Gram-positive bacteria such as *S. aureus*.

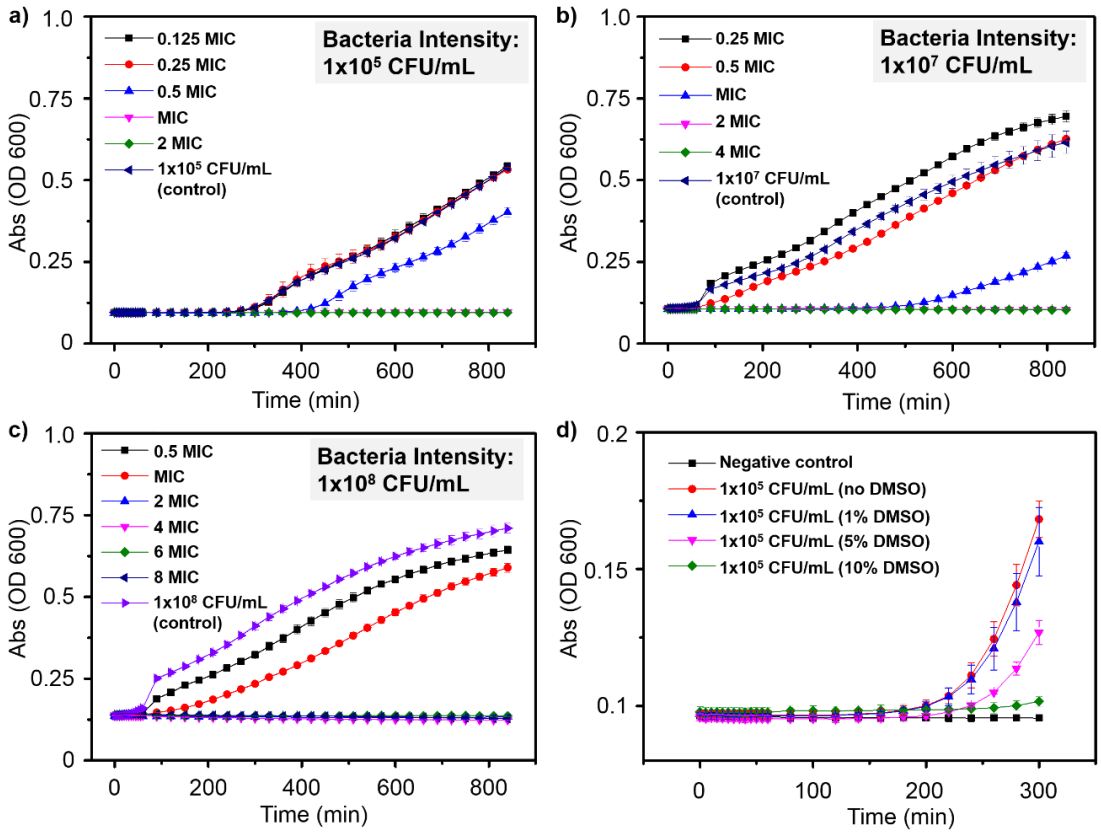

Figure 6.6 Kinetics of growth inhibition study for complex **30** against *S. aureus*, a) bacterial suspension of 1 × 10^5 CFU/mL with complex concentrations range with 0.125× MIC to 2× MIC; b) bacterial suspension of 1 × 10^7 CFU/mL with complex concentrations range with 0.25× MIC to 4× MIC; c) bacterial suspension of 1 × 10^8 CFU/mL with complex concentrations range with 0.5× MIC to 8× MIC; d) DMSO effect on the growth of bacteria.

6.3.8 Synergistic Effects

The emergence in pathogens of intrinsic and acquired resistance towards antibiotics has become a major problem.[44] Some newer antibiotics have little effect on highly resistant microorganisms, and the problem of antibiotic resistance has diminished the odds of new antimicrobial drugs being approved.[45] Co-administration of new antibiotics with different mechanisms of action with existing clinical drugs (to which pathogens have developed resistance) may re-activate their antimicrobial activity. Here the synergistic activity of organo-

iridium complexes **27**[(η^5-Cp^{Xbiph})Ir(PhBig)]Cl, **30** [(η^5-Cp^{Xbiph})Ir(TolBig)Cl]Cl, and **33** [(η^5-Cp^{Xbiph})Ir(TsTolBig)Cl]Cl and the clinical drugs Cefoxitin and Vancomycin towards two highly resistant nosocomial pathogens: Vancomycin-resistant *Enterococci* (VRE), Methicillin-resistant *Staphylococcus aureus* (MRSA), has been investigated.

Table 6.9 Antibacterial Activity of Ir^{III} Complexes **27**, **30** and **33** and Clinical Drugs against MRSA and VRE (μg/mL).

Strains	Compound				
	27	**30**	**33**	vancomycin	cefoxitin
MRSA	2	0.5	0.5	n. d.	32
VRE	4	2	4	64	n. d.

Initially MICs of Ir^{III} complexes and clinical drugs towards VRE and MRSA according to CLSI guidelines were examined with concentrations within the range 0.007-512 μg/mL (MIC values listed in **Table 6.9**). The Ir^{III} complexes themselves exhibit high antibacterial activity against VRE and MRSA with MICs of 0.5-4 μg/mL. MICs of Cefoxitin against MRSA and Vancomycin against VRE are 32 μg/mL and 64 μg/mL, respectively. As can be seen from **Table 6.10**, no synergistic effect of Cefoxitin against MRSA was observed when co-administered with Ir^{III} complexes **27**, **30** and **33** (at equipotent of 0.5× MIC concentrations over the range 0.007-256 μg/mL). Interestingly, the combination of complexes **27**, **30** and **33** with vancomycin towards VRE showed very high synergy, significantly decreasing the MIC values to 0.25, 4 and 2 μg/mL, respectively.

Table 6.10 Synergy Study of Complexes **27**, **30** and **33** with cefoxitin and vancomycin.

Strain	**27**		**30**		**33**	
	27+Cef.	**27**+Vanc.	**30**+Cef.	**30**+Vanc.	**33**+Cef.	**33**+Vanc.
MRSA	32	n. d.	32	n. d.	32	n. d.
VRE	n. d.	0.25	n. d.	4	n. d.	2

In further experiments, the reverse synergistic effect by co-incubation of vancomycin (at the MIC concentrations of 0.25, 4 and 2 μg/mL) with complexes **27**, **30** and **33** (in the concentration scope of 8-0.007 μg/mL) against VRE was examined. However, no growth inhibitory towards VRE below 0.5 MIC complex concentrations was observed after 24 h, at 310 K.

6.3.9 Anti-biofilm Action

Biofilms are integrations of microorganism communities with extracellular polymeric substances which consist mainly of a variety of bio-polymers.[46] The slow growth rate or low metabolism of organisms in biofilms makes the bacteria difficult to eradicate, and thus generates antibiotic resistance.[46,47] Biguanide derivatives, both polymers[48] and low weight molecules[14a] are reported as biofilm disruptors. The efficacy of complexes **27-32** (at 100, 50, 30, 20, 10, 5 and 2 μg/mL) in biofilm disruption in a *S. aureus* model was studied. The logarithm of the numbers of bacterial colonies is listed in **Table 6.11**.

Table 6.11 Disruption Biofilms of *S. aureus* (log) by Various Concentration of Complexes **27-32** (2-100 μg/mL).

Complex	Logarithm of Number of *S. aureus*							
	Complex Concentration (μg/mL)							Negative Control
	100	50	30	20	10	5	2	
27	3.33±0.35	3.73±0.05	7.40±0.02	8.10±0.19	8.84±0.06	8.92±0.08	9.07±0.11	9.13±0.11
28	3.40±0.17	3.97±0.07	7.35±0.04	7.99±0.08	8.59±0.11	8.81±0.29	8.86±0.09	
29	3.91±0.12	4.09±0.09	7.44±0.03	8.16±0.11	8.89±0.11	8.88±0.03	8.96±0.10	
30	3.61±0.39	4.05±0.02	7.12±0.07	8.03±0.12	8.78±0.15	8.77±0.21	8.80±0.04	
31	3.89±0.21	4.98±0.09	7.42±0.11	8.14±0.14	8.76±0.15	9.17±0.11	8.93±0.08	
32	3.85±0.14	6.11±0.07	7.86±0.09	8.22±0.09	8.74±0.24	8.99±0.09	8.90±0.05	

It is evident from **Figure 6.7**, that after treatment of mature biofilms with Ir^{III} biguanide complexes, at the concentrations of 100 and 50 μg/mL, at least a 3-log difference from the negative control is observed, suggesting that at such complex concentrations, over 99.9% of *S. aureus* are killed. Anti-biofilm efficacy at complex concentrations of 30 and 20 μg/mL decreased significantly, but there was still a reduction of 1.5 and 1 log, respectively, compared to the negative control, which indicates that Ir^{III} biguanide complexes can eradicate over 90% biofilm cells at equipotent 10× to 15× MIC concentrations. No significant decrease of cell viability was observed at lower complex concentrations (10, 5 and 2 μg/mL).

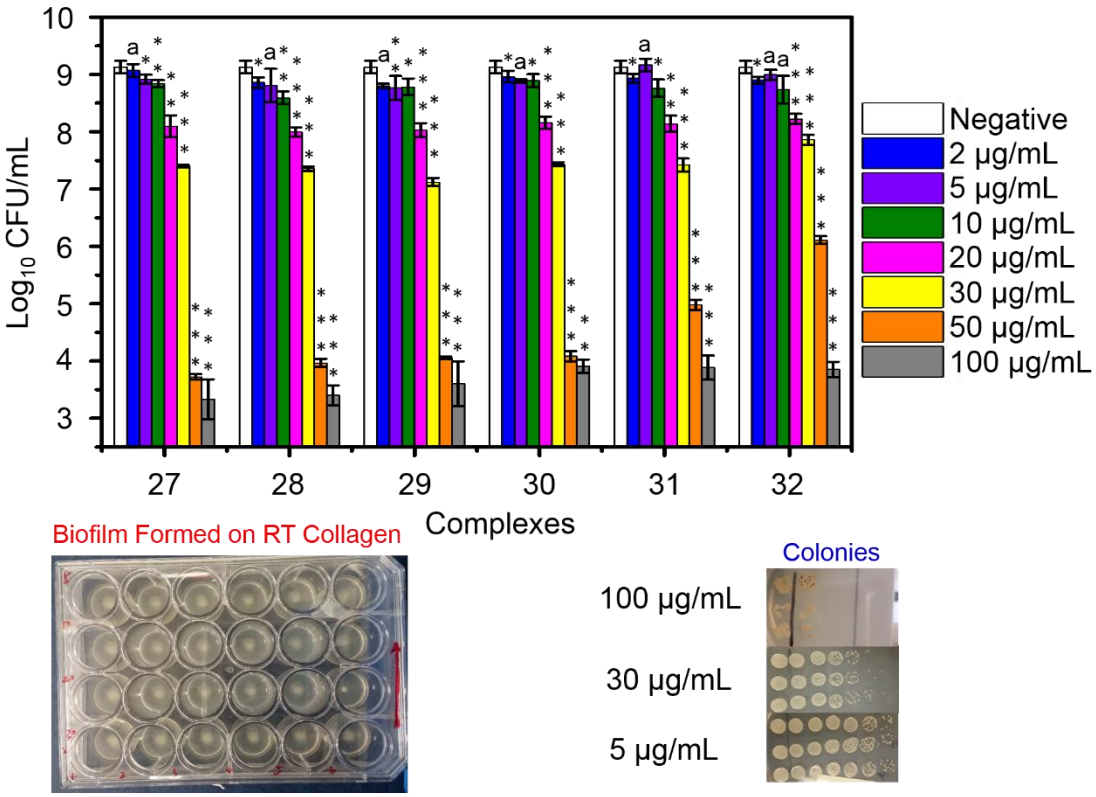

Figure 6.7 Effect of complexes **27-32** on disruption of *S. aureus* biofilms at a variety of complex concentrations, determined as the logarithm transformation from bacteria density; *t*-tests with unequal variances, Welch's tests, were calculated, comparing to negative control (bacteria culture without treating any antibiotics), $p < 0.001$ for ***, $p < 0.01$ for **, $p < 0.05$ for * and $p > 0.05$ for a.

6.3.10 Induced Permeability Change in Bacterial Cell Walls

In order to provide insight into the mode of action for the potent bactericidal activity of Ir^{III} biguanide complexes against Gram-positive bacteria, the permeability change of bacterial cells were measured based on a fluorescence DEAD/LIVE assay by exposure of *S. aureus* to complex **30** [(η^5-Cp^{Xbiph})Ir(TolBig)Cl]Cl at equipotent 4× MBC and 8× MBC concentrations, without adding any antibiotic as negative control. The bacterial viability was checked before staining. Propidium iodide (PI) is an effective dye which can bind uniquely to DNA or RNA nucleobase. PI itself cannot cross the membranes of viable cells, while dead cells with broken cell membranes are readily recognized by PI for intracellular staining.[49,50] It is evident from the images in **Figure 6.8a-c**, that little PI fluorescence was observed in the negative control, the percentage of PI stained cells is *ca.* 7% when treated with complex **30** at equipotent 4× MBC concentration. Interestingly, the percentage increased significantly up to *ca.* 28% at 8× MBC concentration of **30**. However, either at 4× MBC or 8× MBC concentration of complex **7**, no obvious diffused fluorescence clusters were found, which implies that the bacterial cell membranes are intact with no leakage of nucleobases.

Next, the change of cell wall morphology was examined by transmission electron microscopy (TEM). It is apparent from **Figure 6.8d**, that complex **30** did not break the cell wall at equipotent concentrations of 10× MBC and 50× MBC. This is highly consistent with the confocal microscopy observations, which indicates that these biguanide Ir complexes are not likely to target bacterial cell walls.

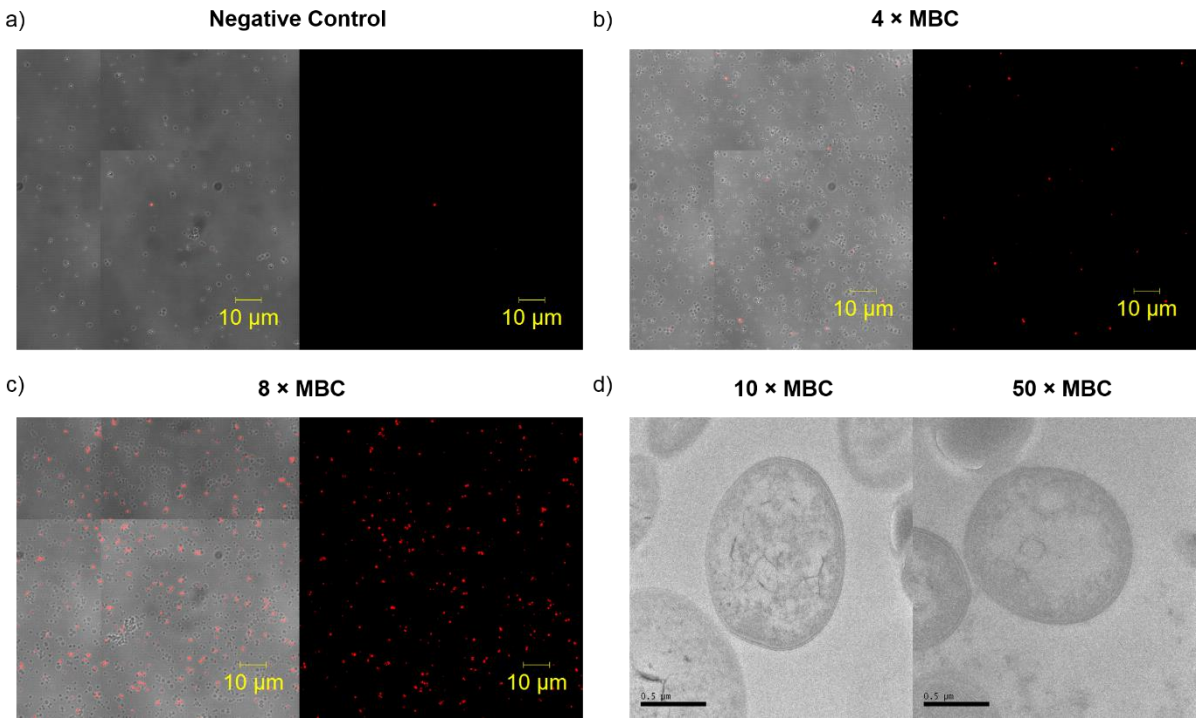

Figure 6.8 Monitoring of complex **30** induced permeability change of cell membranes of *S. aureus* (ATCC 29213) via PI staining by confocal microscopy and morphological change by TEM; a-c) complex **30** at concentrations of 0, 4× MBC and 8× MBC, respectively; the left images show the contrast mode of both stained and unstained cells and the right images the PI fluorescent cells; d) TEM image, complex **30** at concentrations of 10× MBC (left) and 50× MBC (right).

6.4 Conclusions

In summary, a library of novel Ru^{II}, Os^{II} and Ir^{III} biguanide complexes [(arene)M(Big)Z]Z (where arene = η^5-Cp*, η^5-Cp^{XPh}, η^5-Cp^{XBiph}, η^6-*p*-cymene or η^6-biphenyl, M = Ru, Os or Ir, Big = biguanide ligands and functional sulfonyl substituted biguanide ligands, Z = Cl, Br or I) has been synthesized. The X-ray crystal structures of complexes **22** [(η^6-*p*-cym)Os(Metf)Cl]Cl, **23** [(η^6-biph)Os(Metf)Cl]Cl, **24** [(η^5-Cp*)Ir(Metf)Cl]Cl and **27** [(η^5-Cp^{Xbiph})Ir(PhBig)]Cl show that they can form both 16-e and 18-e species. Most of the Ir^{III} biguanide complexes displayed high antimicrobial potency against Gram-positive bacteria and fungii, with MICs as low as 0.125 and 0.25 μg/mL, respectively; and moderate-to-good antibacterial activity towards Gram-negative bacteria. The potency of these complexes towards microbes and human mammalian cells can be tuned effectively by modifying the chelated biguanide ligands or the monodentate halides; the more hydrophilic Metformin complexes (either Ru, Os or Ir) show less potency against microorganisms, Ir (Cp^{Xbiph}) complexes with more hydrophobic ligands (as indicated by reverse phase HPLC retention times), *e.g.* Phenylbiguanide (PhBig), 4-F-PhBig and Phenformin, display excellent antimicrobial activity; and the unsubstituted NH_2 of biguanide ligands is very important for both inhibition and bactericidal activity. Probably the more cationic terminal NH_2 can mimic peptides which is be identified by negatively charged cell membranes,[51] and the higher hydrophobicity facilitates cellular uptake and lead to protein binding on entering bacteria.

The stability and mutation study against *S. aureus* suggest that these novel complexes are highly stable in broth medium and less likely to generate mutations. These complexes also have a significant synergy with vancomycin against VRE, with MIC of Vancomycin dramatically decreasing from 64 μg/mL to 0.25 μg/mL when complex **27** was used. Reactivation of vancomycin makes these Ir^{III} biguanide complexes promising potentiators and may provide an alternative strategy to treat multidrug resistance. Such Ir^{III} complexes also display anti-biofilm

activity in the biofilm model of *S. aureus*. However, biguanide Ir^{III} complexes do not appear to target cell walls of Gram-positive bacteria, and may have a different mode of action in killing bacteria. The excellent properties make those novel biguanide complexes promising antimicrobial drug candidates and may provide an alternative strategy for treating multidrug resistance.

6.5 References

(1) Clark, D. P.; Pazdernik, N. J. *Molecular Biology* 2nd Ed.; Elsevier, 2013.

(2) Buée, M.; De Boer, W.; Martin, F.; van Overbeek, L.; Jurkevitch, E. *Plant Soil* **2009**, *321*, 189–212.

(3) Jenkinson, H. F.; Lamont, R. J. *Trends in Microbiology* **2005**, 13, 589–595.

(4) Li, F.; Collins, J. G.; Keene, F. R. *Chem. Soc. Rev.* **2015**, *44*, 2529–2542.

(5) Feng, Z. V.; Gunsolus, I. L.; Qiu, T. A.; Hurley, K. R.; Nyberg, L. H.; Frew, H.; Johnson, K. P.; Vartanian, A. M.; Jacob, L. M.; Lohse, S. E.; Torelli, M. D.; Hamers, R. J.; Murphy, C. J.; Haynes, C. L. *Chem. Sci.* **2015**, *6*, 5186–5196.

(6) a) Papo, N.; Shai, Y. *J. Biol. Chem.* **2005**, *280*, 10378–10387; b) Brown, L.; Wolf, J. M.; Prados-Rosales, R.; Casadevall, A. *Nat. Rev. Microbiol.* **2015**, *13*, 620–630.

(7) Bowman, S. M.; Free, S. J. *Bioessays* **2006**, *28*, 799–808.

(8) Liu, R.; Chen, X.; Falk, S. P.; Mowery, B. P.; Karlsson, A. J.; Weisblum, B.; Palecek, S. P.; Masters, K. S.; Gellman, S. H. *J. Am. Chem. Soc.* **2014**, *136*, 4333−4342.

(9) Karlsson, A. J.; Pomerantz, W. C.; Weisblum, B.; Gellman, S. H.; Palecek, S. P. *J. Am. Chem. Soc.* **2006**, *128*, 12630–12631.

(10) Nathan, C. *Nature* **2004**, *431*, 899–902.

(11) von Nussbaum, F.; Brands, M.; Hinzen, B.; Weigand, S.; Häbich, D. *Angew. Chem. Int. Ed.* **2006**, *45*, 5072–5129

(12) Levy, S. B.; Marshall, B. *Nat. Med.* **2004**, *10*, 122–129.

(13) Ng, N. S.; Leverett, P.; Hibbs, D. E.; Yang, Q.; Bulanadi, J. C.; Wu, M.; Aldrich-Wright, J. R. *Dalton Trans.* **2013**, *42*, 3196–3209.

(14) a) Zhao, Y.; Chen, Z.; Chen, Y.; Xu, J.; Li, J.; Jiang, X. *J. Am. Chem. Soc.* **2013**, *135*, 12940−12943; b) Bouley, R.; Ding, D.; Peng, Z.; Bastian, M.; Lastochkin, E.; Song, W.;

Suckow, M. A.; Schroeder, V. A.; Wolter, W. R.; Mobashery, S.; Chang, M. *J. Med. Chem.* **2016**, *59*, 5011−5021.

(15) Noffke, A. L.; Habtemariam, A.; Pizarro, A. M.; Sadler, P. J. *Chem. Commun.* **2012**, *48*, 5219–5246.

(16) Tripathy, S. K.; Taviti, A. C.; Dehury, N.; Sahoo, A.; Pal, S.; Beuria, T. K.; Patra, S. *Dalton Trans.* **2015**, *44*, 5114–5124.

(17) Liu, Z.; Sadler, P. J. *Acc. Chem. Res.* **2014**, *47*, 1174−1185.

(18) a) Simpson, P. V.; Schmidt, C.; Ott, I.; Bruhn, H.; Schatzschneider, U. *Eur. J. Inorg. Chem.* **2013**, *2013*, 5547–5554. b) Pandrala, M.; Li, F.; Feterl, M.; Mulyana, Y.; Warner, J. M.; Wallace, L.; Keene, F. R.; Collins, J. G. *Dalton Trans.* **2013**, *42*, 4686–4694. c) Jain, N.; Alam, P.; Laskar, I. R.; Panwar, J. *RSC Adv.* **2015**, *5*, 61983–61988.

(19) a) Thomas, L.; Russell, A. D.; Maillard, J. Y. *J. Appl. Microbiol.* **2005**, *98*, 533–543; b) Denys, A.; Machlanski, T.; Bialek, J.; Mrozicki, S. *Praeventivmedizin* **1977**, *164*, 85–89; c) Bharatam, P. V.; Patel, D. S.; Iqbal, P. *J. Med. Chem.* **2005**, *48*, 7615–7622; d) Samart, N.; Beuning, C. N.; Haller, K. J.; Rithner, C. D.; Crans, D. C. *Langmuir* **2014**, *30*, 8697−8706.

(20) Böttcher, T.; Kolodkin-Gal, I.; Kolter, R.; Losick, R.; Clardy, J. *J. Am. Chem. Soc.* **2013**, *135*, 2927−2930.

(21) Das, G.; Bharadwaj, P. K.; Ghosh, D.; Chaudhuri, B.; Banerjee, R. *Chem. Commun.* **2001**, *0*, 323–324.

(22) Zhang, J.; Sun, R. W.; Che, C. M. *Chem. Commun.* **2012**, *48*, 3388–3390.

(23) Quan, X.; Uddin, R.; Heiskanen, A.; Parmvi, M.; Nilson, K.; Donolato, M.; Hansen, M. F.; Renac, G.; Boisen, A. *Chem. Commun.* **2015**, *51*, 17313–17316.

(24) Olar, R.; Badea, M.; Cristurean, E.; Lazar, V.; Cernat, R.; Balotescu, C. *J. Therm. Anal. Cal.* **2005**, *80*, 451–455.

(25) Olar, R.; Badea, M.; Marinescu, D.; Chifiriuc, M.; Bleotu, C.; Grecu, M. N.; Iorgulescu, E.; Lazar, V. *Eur. J. Med. Chem.* **2010**, *45*, 3027–3034.

(26) P. A. Wayne and Clinical and Laboratory Standards Institute, *Performance Standards for Antimicrobial Susceptibility Testing: Nineteenth Informational Supplement M100–S19*, C.L.S.I., USA, **2009**.

(27) Werthen, M.; Henriksson, L.; Jensen, P. O.; Sternberg, C.; Givskov, M.; Bjarnsholt, T. *APMIS* **2010**, *118*, 156–164.

(28) Soldevila-Barreda, J. J.; Bruijnincx, P. C. A.; Habtemariam, A.; Clarkson, G. J.; Deeth, R. J.; Sadler, P. J. *Organometallics* **2012**, 31, 5958–5967.

(29) Millett, A. J.; Habtemariam, A.; Romero-Canelón, I.; Clarkson, G. J.; Sadler, P. J. *Organometallics* **2015**, *34*, 2683−2694.

(30) Yun, S.; Choi, C.; Kwon, S.; Park, G. W.; Cho, K.; Kwon, K.; Kim, J. Y.; Yoo, J. S.; Lee, J. C.; Choi, J.; Kim, S. *J. Proteome Res.* **2011**, *10*, 459–469.

(31) Hancock, R. E. W.; Brinkman, F. S. L. *Annu. Rev. Microbiol*. **2002**, *56*, 17–38.

(32) Worthington, R. J.; Bunders, C. A.; Reed, C. S.; Melander, C. *ACS Med. Chem. Lett.* **2012**, *3*, 357−361.

(33) a) Xu, Y.; Wang, Y.; Yan, L.; Liang, R.; Dai, B.; Tang, R.; Gao, P.; Jiang, Y. *J. Proteome Res.* **2009**, *8*, 5296–5304; b) Yan, L.; Zhang, J.; Cao, Y.; Gao, P.; Jiang, Y. *J. Proteome Res.* **2007**, *6*, 2248–2256.

(34) Zerpa, R.; Huicho, L.; Guillen, A. *J. Clin. Microbiol.* **1996**, *34*, 2290–2291.

(35) Zaman, M.; Abdel-Aal, A. B. M.; Fujita, Y.; Ziora, Z. M.; Batzloff, M. R.; Good, M. F.; Toth, I. *J. Med. Chem.* **2012**, *55*, 8515−8523.

(36) Ferretti, J. J.; Stevens, D. L.; Bryant, A. E. *Streptococcus pyogenes*: Basic biology to clinical manifestations. Oklahoma City (OK): University of Oklahoma Health Sciences Center, **2016**.

(37) Otto, M. *Nat Rev Microbiol.* **2009**, *7*, 555–567.

(38) a) Widerström, M. *J. Clin. Microbiol.* **2016**, *54*, 1679-1681; b) Pavlovsky, L.; Sturtevant, R. A.; Younger, J. G.; Solomon, M. J. *Langmuir* **2015**, *31*, 2036−2042; c) O'Gara, J. P.; Humphreys, H. *J. Med. Microbiol.* **2001**, *50*, 582–587.

(39) Jeong, K. W.; Lee, J. Y.; Kang, D.; Lee, J. U.; Shin, S. Y.; Kim, Y. *J. Nat. Prod.* **2009**, *72*, 719–724.

(40) Dharmaraja, A. T. *J. Med. Chem.* **2017**, *60*, 3221−3240.

(41) Romero-Canelón, I.; Salassa, L.; Sadler, P. J. *J. Med. Chem.* **2013**, *56*, 1291−1300.

(42) Dougan, S. J.; Habtemariam, A.; McHale, S. E.; Parsons, S.; Sadler, P. J.; *Proc. Natl. Acad. Sci. U. S. A.* **2008**, *105*, 11628−11633.

(43) a) Boukamp, P.; Petrussevska, R. T.; Breitkreutz, D.; Hornung, J.; Markham, A.; Fusenig, N. E. *J. Cell Biol.* **1988**, *106*, 761–71. b) Amigo, M.; Terencio, M. C.; Mitova, M.; Iodice, C.; Paya, M.; DeRosa, S. *J. Nat. Prod.* **2004**, *67*, 1459–63. c) Lau, W. M.; Ng, K. W.; White, A. W.; Heard, C. M. *Mol. Pharmaceutics* **2011**, *8*, 2398–2407.

(44) Lainson, J. C.; Daly, S. M.; Triplett, K.; Johnston, S. A.; Hall, P. R.; Diehnelt, C. W. *ACS Med. Chem. Lett.* **2017**, *8*, 853−857.

(45) Mohammad, H.; Younis, W.; Chen, L.; Peters, C. E.; Pogliano, J.; Pogliano, K.; Cooper, B.; Zhang, J.; Mayhoub, A.; Oldfield, E.; Cushman, M.; Seleem, M. N. *J. Med. Chem.* **2017**, *60*, 2425−2438.

(46) Abee, T.; Kovacs, A. T.; Kuipers, O. P.; van der Veen, S. *Curr. Opin. Biotechnol.* **2011**, *22*, 172–179.

(47) Donlan, R. M.; Costerton, J. W. *Clin. Microbiol. Rev.* **2002**, *15*, 167–193.

(48) Kamaruzzaman, N. F.; Chong, S. Q. Y.; Edmondson-Brown, K. M.; Ntow-Boahene, W.; Bardiau, M.; Good, L. *Front. Microbiol.* **2017**, *8*, 1518–1527.

(49) Zhao, Y.; Tian, Y.; Cui, Y.; Liu, W.; Ma, W.; Jiang, X. *J. Am. Chem. Soc.* **2010**, *132*, 12349–12356.

(50) Hoque, J.; Akkapeddi, P.; Yadav, V.; Manjunath, G. B.; Uppu, D. S. S. M.; Konai, M. M.; Yarlagadda, V.; Sanyal, K.; Haldar, J. *ACS Appl. Mater. Interfaces* **2015**, *7*, 1804−1815.

(51) Malanovic, N.; Lohner, K. *Biochim. Biophys. Acta* **2016**, *1858*, 936–946.

Chapter 7

Conclusions and Future Work

The aims of the PhD project are mainly divided into two sections:

i) Design and synthesis of more efficient and stable Ru^{II} ethylenediamine complexes for the catalytic TH reduction of cell coenzyme nicotinamide adenine nucleotide (NAD^+) using sodium formate as hydride source, and use of Ru catalysed TH reduction of NAD^+ to NADH in antiproliferative study against various cancer cell lines.

ii) Synthesis and characterization of novel organo Ir^{III} complexes using biguanide molecules as bidentate ligands, and determination of their antimicrobial activity against Gram-positive and Gram-negative bacteria, including some nosocomial pathogens, *e.g. S. aureus* and *P. aeruginosa*; and fungii.

7.1 The Role of Substituents on Ethylenediamine in Catalytic Efficiency of TH Reduction of NAD^+ (Chapter 3)

Initially, $[(\eta^6\text{-arene})Ru(en)Cl]^+$ complexes (**Figure 7.1**) were synthesized as potent anticancer agents,[1] however, Ru^{II}-en complexes are poor TH catalysts in TH reduction of NAD^+ to NADH (TOF, 0.1 h^{-1}).[2] Given the success of Noyori type complexes and their potent catalytic activity in TH reduction of aromatic ketones, Soldevila-Barreda *et al.* introduced sulfonyl substituents in the ethylenediamine ligand to achieve to achiral Ru^{II} complexes $[(\eta^6\text{-arene})Ru(TsEn)Cl]$ (**Figure 7.1**).[3] As expected, these complexes are more potent than Ru^{II}-en complexes in TH catalysis of NAD^+ to NADH with formate as hydride source; the TOF increased up to 2.8 h^{-1}.[3]

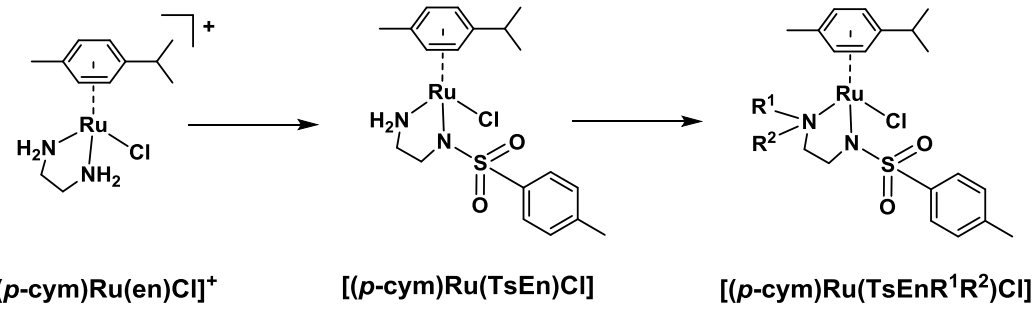

Figure 7.1 Chemical structures of complexes $[(\eta^6\text{-}p\text{-cym})Ru(en)Cl]^+$, $[(\eta^6\text{-}p\text{-cym})Ru(TsEn)Cl]$ and substituted $[(\eta^6\text{-}p\text{-cym})Ru(TsEn(R^1,R^2))Cl]$.

In Chapter 3, to improve the efficiency of TH reduction of NAD^+ to NADH, Ru^{II}-TsEn complexes were modified to obtain a series of new Ru^{II} toluenesulfonyl ethylenediamine complexes **1**-**6** of the type $[(\eta^6\text{-}p\text{-cym})Ru(TsEn(R^1,R^2))Cl]$, where R^1,R^2 are aliphatic or aromatic substituents on a terminal N of ethylenediamine (**Figure 7.1**). Interestingly, with the enhancement of bulkiness of substituents, the catalytic activity of TH reduction of NAD^+ to NADH significantly increased, giving TOFs up to 7.4 h^{-1} for complex **4** (R^1 is benzyl). Meanwhile, complex **4** was also shown to have the best antiproliferative activity towards A2780 human ovarian cancer cells among these new complexes, with IC_{50} as low as 1.0 μM (comparable to clinical used drug cisplatin, IC_{50}, 1.2 μM). Co-incubation of Ru^{II} complexes **1**-**6** (**Chart 3.1** in Chapter 3 for structure details) with cell-tolerable amounts of sodium formate can improve the antiproliferative activity by up to 36% (complex **6**, R^1 is napthyl, R^2 is H in **Figure 7.1**) against A2780 cancer cells. Also, complex **4** can bind rapidly to 9-ethylguanine in aqueous solution; however, DNA is unlikely to be the target of those complexes, as no significant binding to either calf thymus or plasmid DNA was observed. DFT calculations revealed that the hydride transfer and release of carbon dioxide are costly in energy, perhaps the rate-limiting steps in the transfer hydrogenation cycle.

7.2 High Affinity of Ru^{II} Sulfonyl Ethylenediamine Complexes with Glutathione (Chapter 4)

Ru^{II} complex [(η^6-*p*-cym)Ru(TsEnBz)Cl] (complex **4**, **Chart 3.1** in Chapetr 3) achieved both high catalytic activity in TH reduction of NAD^+ to NADH and high potency in anticancer activity against A2780 human ovarian cancer cells. As an extension of complex **4**, to improve the catalytic efficiency, a series of Ru^{II} (Os^{II}, complex **10**) sulfonyl ethylenediamine complexes **7-15** [(η^6-arene)Ru(BzEnR)Cl], where arene is *p*-cymene, biph or $HO(CH_2)_2OPh$, R is phenylsulfonyl (PhSul), 4-F-PhSul, or 4-NO_2-PhSul, were synthesized in Chapter 4 (**Table 4.1** for details), those complexes also exhibited potent catalytic activity in TH reaction of NAD^+ to NADH using sodium formate as hydride donor, with TOFs in the range of 2.5-12.9 h^{-1}. The interaction of complex **8** [(η^6-biph)Ru(TsEnBz)Cl] with thiol-containing molecules, glutathione (GSH) and N-acetyl-L-cysteine (NAC) was studied via NMR, HPLC and LC-MS. The adducts were identified as $[(\eta^6\text{-biph})_2Ru_2(GS)_3]^{2+}$ and $[(\eta^6\text{-biph})_2Ru_2(NAC)_3]^+$ dimers. Such reactions can liberate free ethylenediamine ligands which can retrigger the fluorescence of complex **15** which has dansyl substituent. The catalytic activity of complex **8** for TH reaction of NAD^+ to NADH is hampered in the presence of GSH.

These new complexes have variable antiproliferative activity against A2780 human ovarian and A549 human lung cancer cells, and the levels of reactive oxygen species and anticancer activity decreased with increase of GSH concentration. The rapid reaction of Ru sulfonyl ethylenediamine complexes with thiol-containing molecules may appears to introduce a potential metabolic pathway for complexes entering cancer cells.

7.3 Tethered Ru^{II} Sulfonyl Ethylenediamine Complexes in Anticancer Research (Chapter 5)

Four achiral tethered Ru^{II} sulfonyl ethylenediamine complexes [Ru(η^6-Ph$(CH_2)_3$-ethylenediamine-*N*-R)Cl], where R is Ms, Ts, Tf and Nb (complexes **16-19**, respectively, in **Scheme 5.1**) were synthesized and their structures confirmed by X-ray crystallography in Chapter 5. Tethered Ru^{II} complex **17** [Ru(η^6-Ph$(CH_2)_3$-ethylenediamine-*N*-Ts)Cl] can react rapidly with GSH to form **17**-SG adduct, however, the **17**-SG adduct degraded slowly to release free ligand [η^6-Ph$(CH_2)_3$-ethylenediamine-*N*(H)-Ts] after 24 h at 310 K. Such interaction of **17** with GSH can block the catalytic TH reaction of NAD^+ to NADH with TOF decreasing from 4.7 h^{-1} (no GSH) to 4.27 h^{-1} (0.5 mol equiv of GSH), until the complete inhibition of the TH reaction (with 1 mol equiv of GSH).

These complexes exhibited moderate to good anticancer activity towards A2780 human ovarian, A2780 cisplatin resistant human ovarian, A549 human lung, MCF7 human breast and HEPG2 human liver cancer cell lines, with IC_{50} values as low as 7.3 μM. Complex **17** [Ru(η^6-Ph$(CH_2)_3$-ethylenediamine-*N*-Ts)Cl] showed better selectivity than cisplatin against A2780 cancer cells and MRC 5 human fibroblast normal cells. Also, complex **17** is less likely to be cross resistant with cisplatin against A2780 cancer cells. Co-incubation of these tethered Ru^{II} complexes with non-toxic amounts of sodium formate gave up to 22% of enhancement (complex **16**) in antiproliferative activity against A2780 cancer cells. The good antiproliferative activity of **17** against A2780 cancer cells probably arises from to the high intracellular ROS levels induced, which may provide a basis for killing cancer cells.

Complex **17** can induce G1 cell cycle arrest at IC_{50} concentration in A2780 cancer cells. However, no obvious binding was observed to calf thymus (ct) DNA, bacterial plasmid DNA and short single- or double-stranded oligonucleotides, suggesting that these complexes do not

target DNA in cells. Together with a DNA study of complex **4** [(*p*-cym)Ru(TsEnBz)Cl], the conclusion can be drawn that Ru^{II} ethylenediamine complexes with sulfonyl substituents are unlikely to target DNA or RNA in cells.

7.4 Novel Ir^{III} Biguanide Complexes with Potent Antimicrobial Activity and Bio-compatibility (Chapter 6)

In Chapter 6, a library of Ru^{II}, Os^{II} or Ir^{III} biguanide complexes [(arene/Cp^{X})M(Big)X]Y (complexes **20-37**, where arene = η^5-Cp*, η^6-*p*-cymene or η^6-biph, M = Ru, Os or Ir, X, Y = halides, Big = biguanide ligands or functional sulfonyl substituted biguanide ligands) was synthesized (**Chart 6.1** for details). The structures of metformin and phenylbiguanide complexes **22** (Os(cym)Metf), **23** (Os(biph)Metf), **24** (Ir(Cp*)Metf) and **27** (Ir(Cp^{Xbiph})PhBig) were confirmed by X-ray crystallographic analysis. Complexes **20-24** with high hydrophilic property exhibited poor antibacterial activity, while complexes **27-35** display moderate to good antibacterial activity towards Gram-negative bacteria (including multidrug resistant pathogens, with MICs as low as 4 μg/mL, shown in **Table 6.5**), and excellent antimicrobial activity against Gram-positive bacteria (MICs as low as 0.125 μg/mL) and fungii (MICs as low as 0.5 μg/mL); but low toxicity towards human mammalian cells (embryonic kidney cells, keratinocytes and red blood cells, shown in **Table 6.6**).

Interestingly, the potency of biguanide Ir^{III} complexes towards both microorganisms and human mammalian cells can be tuned by modifying the chelated bidentate biguanide ligands and the monodentate halido ligands. These complexes are highly stable in culture medium and mutation studies of selected active complexes **27** [(Cp^{Xbiph})Ir(PhBig)]Cl, **28** [(Cp^{Xbiph})Ir(4-F-PhBig)]Cl and **30** [(Cp^{Xbiph})Ir(TolBig)Cl]Cl against *S. aureus* suggested that these novel complexes are less likely to generate any mutation (over 24 passages).

Also these complexes (*e.g.* complex **27** [(Cp^{Xbiph})Ir(PhBig)]Cl) exhibit a synergistic effect with the clinical drug vancomycin against vancomycin-resistant Enterococci, with MIC decreasing significantly from 64 μg/mL to 0.25 μg/mL. Reactivation of vancomycin makes these Ir^{III} biguanide complexes promising potentiators and may provide an alternative strategy to treat multidrug resistance. Such Ir^{III} complexes also can effectively disrupt biofilms in the model of *S. aureus* at 10× MIC concentration. The primary mode of action study by DEAD/LIVE staining and TEM reveals that those novel complexes are less likely to target cell walls, but may interfere in the intracellular metabolism of bacteria cells.

7.5 Future Work

7.5.1 Design and Synthesis of Novel Half-sandwich Ru^{II} Complexes

The interesting reaction of complex **8** [(η^6-biph)Ru(TsEnBz)Cl] with thiol-containing molecules to form Ru-S bridged dimers in Chapter 4 may open the possibility for enhancement of antiproliferative activity, upon modification of arene or bidentate ligands with biologically active anticancer drugs or scaffolds in Ru ethylenediamine complexes in future research.

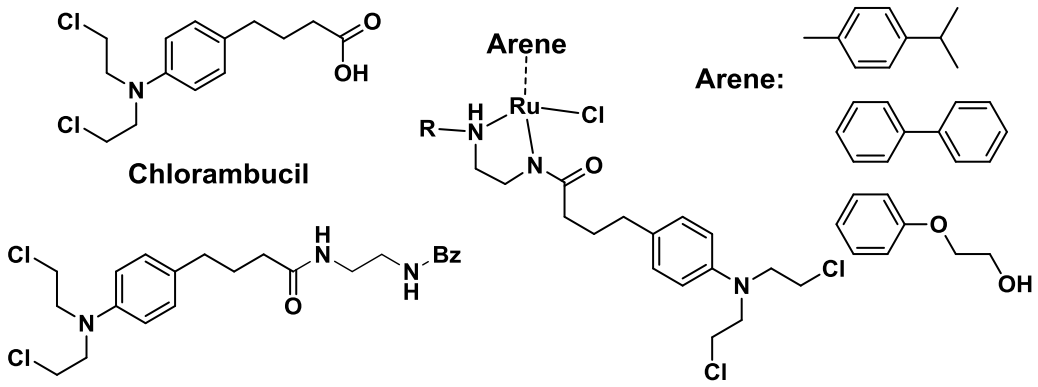

Figure 7.2 Structures of Chlorambucil, a new ligand and Ru^{II} ethylenediamine complexes.

Chlorambucil is a chemotherapeutic agent initially synthesized and reported by Everett *et al.* in 1950s (**Figure 7.2**),[4] in combination with other drugs for the treatment of lymphocytic leukemia.[5,6] Ru-en complex $[(\eta^6\text{-}p\text{-cym})Ru(en)Cl]^+$ (**Figure 7.1**) preferentially binds to nucleobase versus GSH;[7] however, complex $[(\eta^6\text{-}p\text{-cym})Ru(TsEnBz)Cl]$ becomes more thiophilic when the electron distribution in ethylenediamine changes (introduction of electron withdrawing sulfonyl functional groups). Given the labile property of Ru^{II} complex $[(\eta^6\text{-arene})Ru(TsEnBz)Cl]$ in the presence of cell-abundant GSH, the novel Ru complex $[(\eta^6\text{-arene})Ru(BzEnChlo)Cl]$ (**Figure 7.2**) could be synthesized and characterized, the interaction of these novel complexes with GSH can be fully investigated (new complex may decompose in the presence of GSH similar to sulfonyl substituted complexes); the amide bond may hydrolyse in the acidic envirvoment in cancer cells to release the biologically active anticancer drug Chlorambucil and $[(\eta^6\text{-arene})Ru(REn)Cl]$, which may work synergistically in cancer cells.

7.5.2 Mode of Action Study of Potent Antimicrobial Ir Biguanide Agents

Based on a wealth of preliminary screening for antimicrobial study. The mode of action for the Ir^{III} biguanide complexes (Chapter 6) in Gram-positive bacteria can be determined.

Initially, the time- and dose-dependence of accumulation of metalloantibiotcs in bacteria (uptake/efflux)) can be determined by cell fractionation and ICP-MS to determine metal (iridium) concentrations.

The localisation of the complexes (Ir) in bacteria can be investigated by nanofocussed synchrotron X-ray fluorescence (at Diamond and ESRF synchrotrons).[8]

The metalation of proteins in bacteria (initially *S. aureus*) can be studied using continuous flow gel electrophoresis combined with ICP-MS and MS/MS for metal detection and protein identification.[9] The changes in proteins in bacteria before and after metalloantibiotic treatment can be studied by using ultra high resolution mass spectrometry (FTICR-MS).[10]

7.6 References

(1) Aird, R. E.; Cummings, J.; Ritchie, A. A.; Muir, M.; Morris, R. E.; Chen, H.; Sadler, P. J.; Jodrell, D. I. *Br. J. Cancer* **2002**, *86*, 1652–1657.

(2) Yan, Y. K.; Melchart, M.; Habtemariam, A.; Peacock, A. F. A.; Sadler, P. J. *J. Biol. Inorg. Chem.* **2006**, *11*, 483−488.

(3) Soldevila-Barreda, J. J.; Bruijnincx, P. C. A.; Habtemariam, A.; Clarkson, G. J.; Deeth, R. J.; Sadler, P. J. *Organometallics* **2012**, *31*, 5958−5967.

(4) Everett, J. L.; Roberts, J. J.; Ross, W. C. J. *J. Chem. Soc.* **1953**, 2386–2392.

(5) Montserrat, E.; Rozman, C. *Blood ReV.* **1993**, *7*, 164–175.

(6) Pedersen, P. J.; Christensen, M. S.; Ruysschaert, T.; Linderoth, L.; Andresen, T. L.; Melander, F.; Mouritsen, O. G.; Madsen, R.; Clausen, M. H. *J. Med. Chem.* **2009**, *52*, 3408–3415.

(7) Wang, F.; Xu, J.; Habtemariam, A.; Bella, J.; Sadler, P. J. *J. Am. Chem. Soc.* **2005**, *127*, 17734–17743.

(8) Sanchez-Cano, C.; Romero-Caneljn, I.; Yang, Y.; Hands-Portman, I. J.; Bohic, S.; Cloetens, P.; Sadler, P.J. *Chem. Eur. J.* **2017**, *23*, 2512 – 2516.

(9)Wang, Y.; Hu, L.; Xu, F.; Quan, Q.; Lai, Y. T.; Xia, W.; Yang, Y.; Chang, Y. Y.; Yang, X.; Chai, Z.; Wang, J.; Chu, I. K.; Li, H.; Sun. H. *Chem. Sci.* **2017**, *8*, 4626–4633.

(10) Wootton, C. A.; Sanchez-Cano, C.; Lopez-Clavijo, A. F.; Shaili, E.; Barrow, M. P.; Sadler, P. J.; O'Connor, P. B. *Chem. Sci.* **2018**, *9*, 2733–2739.

Complexes in This Thesis

Chapter 3

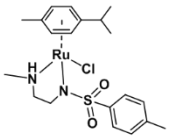

1

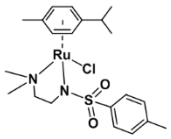

2

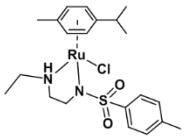

3

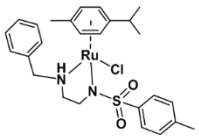

4

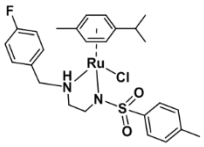

5

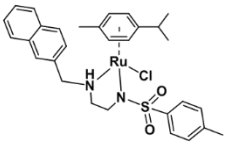

6

Chapter 4

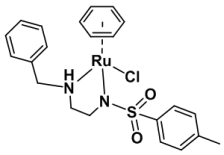

7

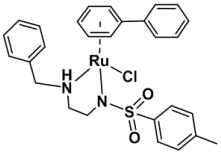

8

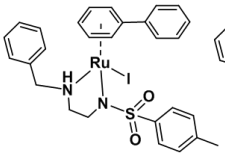

9

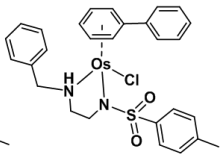

10

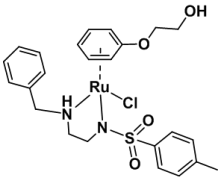

11

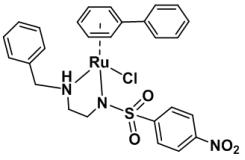

12

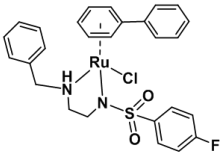

13

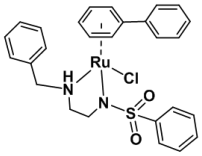

14

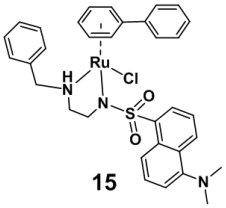

15

Chapter 5

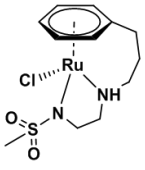

16

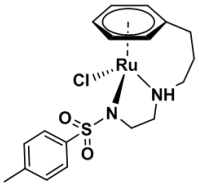

17

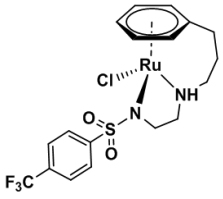

18

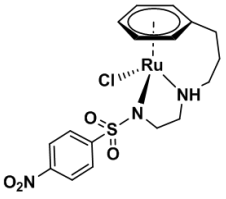

19

Chapter 6

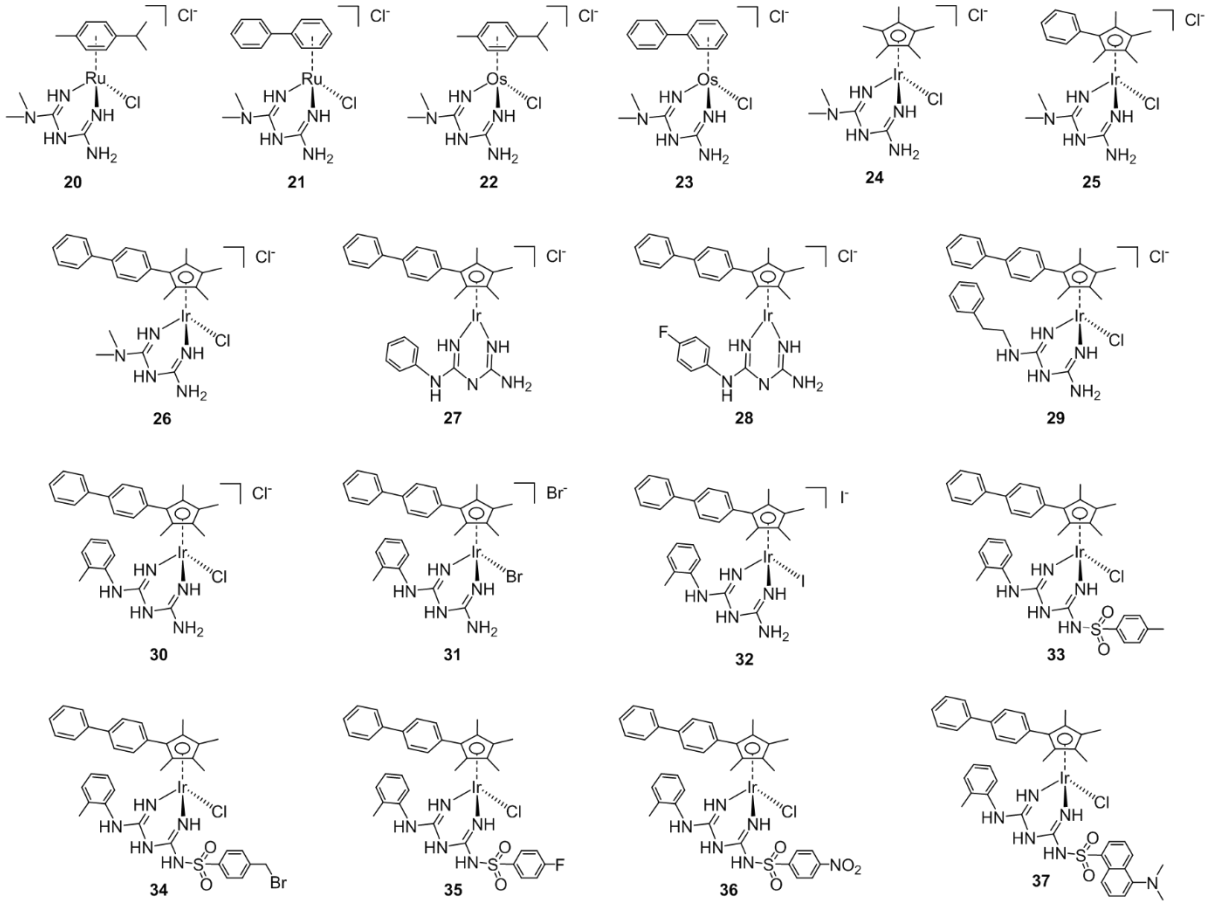

Conferences and Meetings Attended

1. **2017.06** 'National Bridging the Gaps Symposium', University of Warwick, UK. Oral presentation.

2. **2016.09** '8th International Symposium on Bioorganometallic Chemistry (ISBOMC)', Moscow, Russia. Poster and oral presentation.

3. **2016.05** 'Dalton 2016, Joint Interest Groups Meeting of Royal Society of Chemistry', University of Warwick, UK. Poster.

4. **2015.11** 'Sadler's Symposium on Metals in Life Processes', Sun Yat Sen University, China. Oral presentation.

Appendix

NAD^+ Model Compounds

In order to study the mechanism of TH reduction of NAD^+ to NADH, a series of NAD^+ model compounds were synthesized, and the purity was confirmed by their ^1H NMR spectra (**Figure A1**).

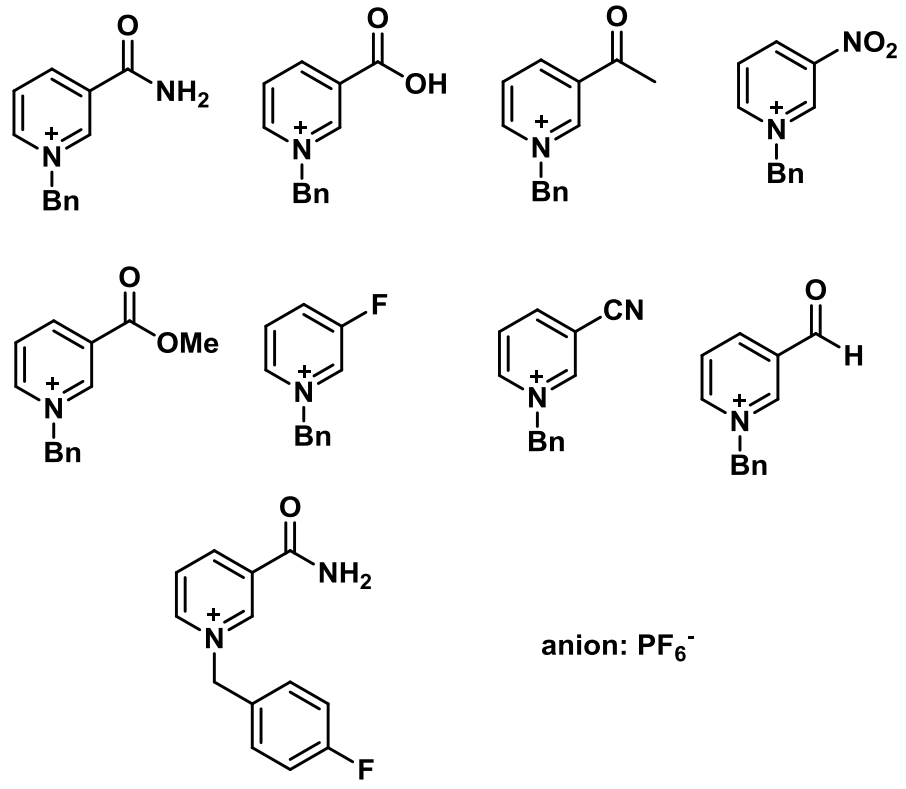

Figure A1 Structures of synthesized NAD^+ model compounds with various substituents.

The TH reduction was initially monitored by UV-vis spectroscopy using complex **4** [(η^6-*p*-cym)Ru(TsEnBz)Cl] as catalyst and formate as hydride source (**Figure A2**). Complex **4** (84 µM) was dissolved in MeOH/H_2O (1:4 v/v) in a glass vial. Solutions of NAD^+ models (510 µM) and sodium formate (102 mM) were made in H_2O. An aliquot of 330 µL from each solution was added to a 1 mL cuvette bringing the total volume to 1 mL and complex **4**, NAD^+ models and formate in molar ratio of 1:6:1200 (final concentrations: **4** 28 µM; NAD^+ models 170 µM; formate 34 mM;). The pH was adjusted to 7.2 before the sample was introduced and

UV spectra were recorded every 5 min until completion of the reaction. The spectrum was monitored by following the absorbance in the range of 350-450 nm.

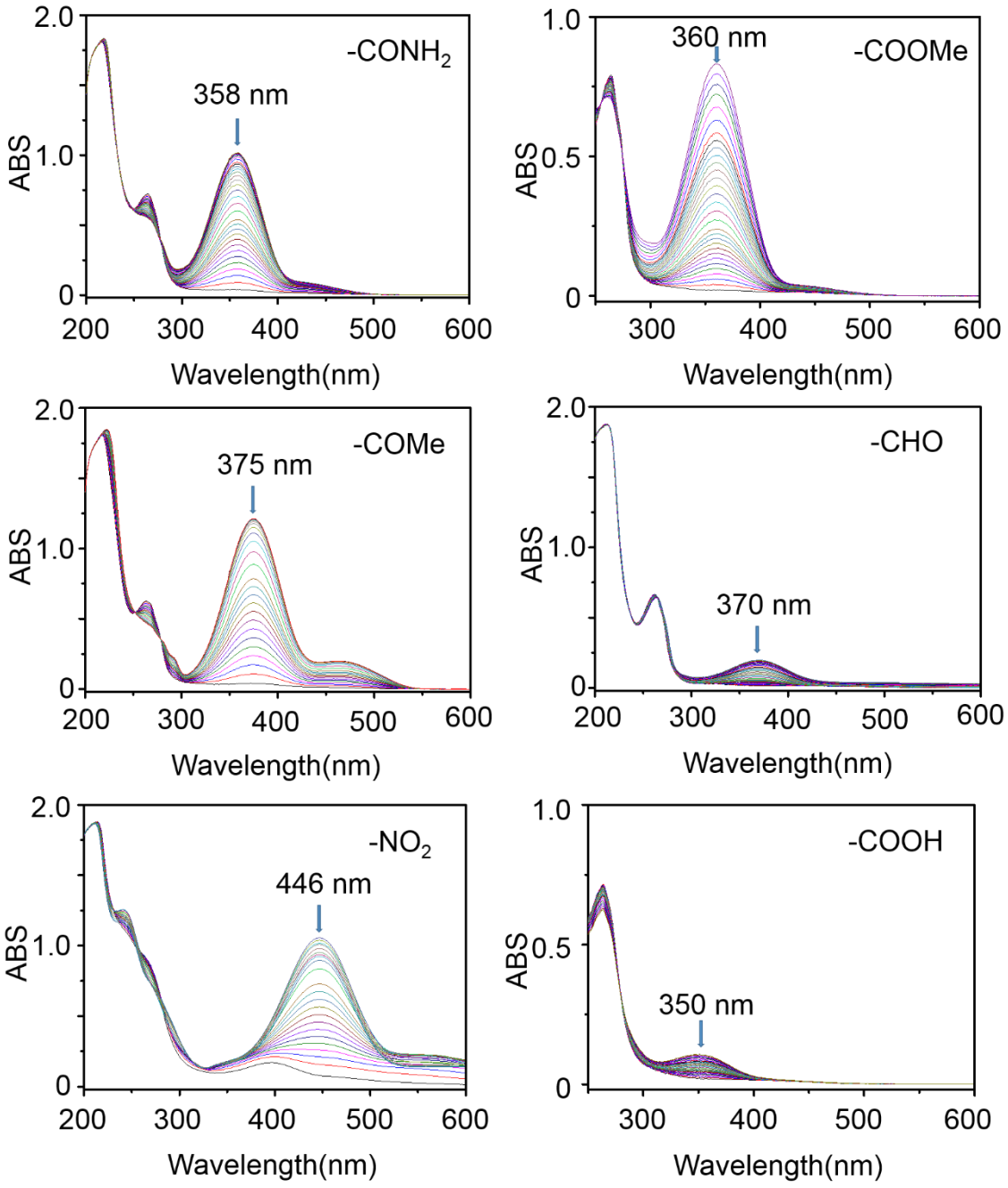

Figure A2 Monitoring of TH reduction of NAD^+ model compounds by UV-vis spectroscopy using complex **4** as catalyst and formate as hydride donor. Complex **4**, NAD^+ models and formate were in the ratio of 1: 6: 1200. The pH was adjusted to 7.1 ± 0.1, 310 K.

Next, the catalytic rate of TH reduction of NAD^+ model compounds by complex **4** was determined by 600 MHz NMR using formate as hydride donor (**Table A1**). Solutions of complex **4** (1.4 mM, MeOD-d_4/D_2O 1:4 v/v), sodium formate (35 mM, D_2O) and NAD^+ models (5.6 mM, D_2O) were prepared. An aliquot of 200 μL from each solution was added into a 5 mm NMR tube, to give the final volume to 0.64 mL (**4** 0.44 mM; NAD^+ models 1.75 mM; $NaHCO_2$ 10.94 mM; in molar ratio of 1:4:25). The pH^* was adjusted to 7.2 ± 0.1. The ^1H NMR spectrum were recorded at 310 K every 162 s until the completion of the reaction. The TOFs were calculated following the precedures decribed in **Section 3.2.4** in Chapter 3, giving values in the range of 2.3-7.2 h^{-1}.

Table A1 Catalytic Activity of Complex **4** as Catalyst in the TH Reduction of NAD^+ Model Compounds Monitored on NMR (600 MHz) Using Formate as Hydride Source.

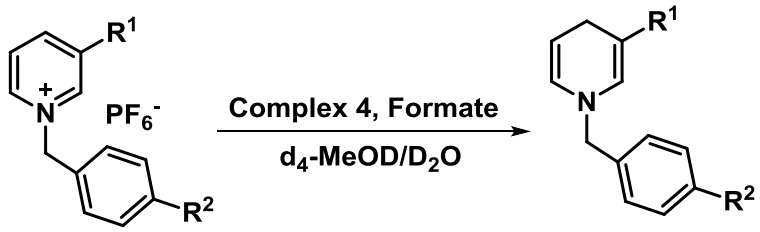

R^1	R^2	TOF
-$CONH_2$	H	5.45±0.25
-$COOCH_3$	H	7.16±0.15
-$COCH_3$	H	7.0±0.1
-CN	H	2.17±0.12
-COOH	H	2.36±0.32
-NO_2	H	7.2±0.2
-CHO	H	5.54±0.08
-$CONH_2$	F	4.87±0.12
F	H	No Reaction

Discussion

It is evident from **Table A1**, that substitutions on the C4 position of pyridine influence the TH activity more significantly than that on the pyridine nitrogen. The reaction rate for hydride transfer is greatly affected by electronic effects form the substituents. Strong electron withdrawing groups, *e.g.* ester and nitro groups (TOFs *ca.* 7.2 h^{-1}), facilitate hydride transfer. No TH reaction was observed with F as the R^1 substituent on the pyridine ring (structure in **Figure A1**), which is highly consistent with the observations of Fish *et al.* (*Angew. Chem. Int. Ed.* **1999**, *38*, 1429-1432), indicating that the electronic properties of substituents on C4 of the pyridine ring are very important for the formation of the metal-NAD^+ six-membered intermediate (proposed mechanisms and structures are shown in **Figure 1.18** in Chapter 1) which is essential for hydride transfer.